JOURNAL OF THE AERONAUTICAL SCIENCES

VOLUME 21 DECEMBER, 1954 NUMBER 12

CONTENTS

The Story of Shimmy.....WILLIAM J. MORELAND 793

Development of Charts for Downwash Coefficients of Oscillating Wings of Finite Span and Arbitrary Plan Form.....MAX A. DENGLER 809

A Method for Analyzing the Heat Insulating Properties of the Laminar Compressible Boundary Layer.....PAUL A. LIBBY AND ADRIAN PALLONE 825

Three-Dimensional Laminar Boundary Layer with Small Cross-Flow..ARTUR MAGER 835

Readers' Forum: "Note on Photoelastic Study of a Swept-Wing Model," by George Gerard and Ralph Papiruo; "Rectangular Plates with Stringers and Ribs," by J. Irving and N. Mullineux; "On Motion of Submerged Cylinder," by H. S. Tan; "Note on the Propagation of Infinitesimal Disturbances in Gases According to the Navier-Stokes Equations," by M. Lessen; "The Effect of Heat Transfer on the Behavior of a Compressible Laminar Boundary Layer Under Favorable and Adverse Pressure Gradients," by Ting-Yi Li and H. T. Nagamatsu; "Second-Order Methods in Inviscid Supersonic Theory," by J. Fell and D. C. M. Leslie; "Buckling Stress of Thin Cylindrical Clamped Shells Subject to Hydrostatic Pressure," by P. P. Bijlaard; "A Supplementary Note on the Spanwise Loadings over Slender Airfoils," by Hsien K. Cheng; "A Semiempirical Method for Determining Delta-Wing Pressure Distributions in an Incompressible Flow," by William R. Laidlaw and P. T. Hsu; "Addendum—'Characteristic Solution for Axially Symmetric Transonic Flow,'" by Erik Mollo-Christensen; "Shock-Wave Yaw for 9½° Semiapex Cone," by Eugene D. Boyer; "Effect of Spin in Aerodynamic Properties of Bodies of Revolution," by L. E. Schmidt and C. H. Murphy; "Tip or Leading-Edge Temperatures on Pointed Heat Conducting Bodies at High Supersonic Speeds," by M. Richard Denison; "On Panel Flutter in Supersonic Flow," by W. C. Randels; "Throat Station Concept in Transonic Flow over Two-Dimensional Wedges," by Robert Wesley Truitt; "Effect of Helicopter Blade Stall on Blade Flapping," by K. H. Hohenemser....846–861

Index to Volume 21..... 862

DEC 13 PUBLIC LIBRARY

Published by

INSTITUTE OF THE AERONAUTICAL SCIENCES, INC.

JOURNAL OF THE AERONAUTICAL SCIENCES

Editor: HUGH L. DRYDEN, *Director, NACA*

Associate Editor: ROBERT R. DEXTER *Managing Editor:* BERNEICE H. JARCK

Editorial Committee

Aerodynamics

Dean R. Chapman
Francis H. Clauser
Antonio Ferri
Alexander Flax
R. Paul Harrington
R. T. Jones
Carl Kaplan
H. W. Liepmann
C. C. Lin
H. F. Ludloff
Harold Luskin
John R. Markham
Clark B. Millikan
Shatswell Ober
W. Bailey Oswald
C. D. Perkins
Elliott G. Reid
H. J. E. Reid
Russell Robinson
George S. Schairer
G. B. Schubauer
W. R. Sears
John Stack
Theodore Theodorsen
Th. von Kármán

Air Transport

Charles Froesch
J. A. Herlihy
R. D. Kelly
Otto E. Kirchner
Jerome Lederer
John C. Leslie
R. Dixon Speas

Flight Testing

R. R. Gilruth
Melvin N. Gough
W. L. Howland
W. F. Milliken, Jr.
E. G. Stout

Structures and Materials

W. B. Bleakney
E. W. Conlon
John E. Duberg
E. C. Hartmann
N. J. Hoff
Samuel Levy
J. F. McBrearty
Alfred S. Niles
W. Ramberg
F. R. Shanley
C. R. Strang
S. Timoshenko
H. S. Tsien
Chi-Teh Wang

Rotating Wing Aircraft

F. B. Gustafson
K. H. Hohenemser
Bartram Kelley
R. B. Maloy
Ralph McClarren
R. H. Miller
R. H. Prewitt
Igor I. Sikorsky

Vibration and Flutter

Lee Arnold
M. A. Biot
R. L. Bisplinghoff
William Bollay
Chieh-Chien Chang
J. P. Den Hartog
I. E. Garrick
Martin Goland
Theodore Theodorsen

Aircraft Design

W. E. Beall
E. H. Heinemann
Hall L. Hibbard
Richard Hutton
C. L. Johnson
A. A. Kartveli
E. G. Stout
F. K. Teichmann
Robert J. Woods

Electronics in Aviation

Welcome W. Bender
K. C. Black
M. V. Kiebert, Jr.
David S. Little
S. B. Rogers
Paul Rosenberg
L. M. Sherer

Physiologic Problems

H. G. Armstrong
Louis H. Bauer
Robert J. Benford
W. Randolph Lovelace, II
Ross A. MacFarland

Fuels and Oils

D. P. Barnard
J. H. Doolittle
Graham Edgar
R. T. Goodwin
A. M. Rothrock

Flight Propulsion

George W. Brady
Frank W. Caldwell
L. S. Hobbs
E. E. Johnson
Joseph Keenan
R. P. Kroon
Hans Reissner
Abe Silverstein
C. Fayette Taylor
E. S. Taylor
P. B. Taylor
E. S. Thompson
H. S. Tsien

Instruments

Allan G. Binnie
Charles H. Colvin
Frank R. Cook
C. S. Draper
S. G. Eskin
O. E. Esval
C. F. Savage
R. C. Sylvander

Meteorology

C. F. Brooks
D. M. Little
F. W. Reichelderfer
K. C. Spengler

SUBSCRIPTION RATES

JOURNAL OF THE AERONAUTICAL SCIENCES, Published Monthly.—United States and Possessions: 1 Year, $12.00; Single Copies, $1.50. Foreign Countries Including Canada (American Currency Rates): 1 Year, $13.00; Single Copies, $1.50.

AERONAUTICAL ENGINEERING REVIEW, Published Monthly.—United States and Possessions: 1 Year, $3.00; Single Copies, $0.50. Foreign Countries Including Canada (American Currency Rates): 1 Year, $3.50; Single Copies, $0.50.

Notices of change of address should be sent to the Institute at least 30 days prior to actual change of address.

Manuscripts for publication, proofs, and all correspondence should be addressed to the Editorial Office of the JOURNAL.

Correspondence regarding subscriptions may be addressed to Publication Office, 20th and Northampton Sts., Easton, Pa., or to the Editorial Office of the JOURNAL OF THE AERONAUTICAL SCIENCES, 2 East 64th Street, New York 21, N.Y.

Copyright, 1954, by the Institute of the Aeronautical Sciences, Inc.

Entered as Second Class Matter at the Post Office, Easton, Pa., May 1, 1937. Acceptance for mailing at a special rate of Postage provided for in the Act of August 24, 1912. Authorized April 29, 1937.

JOURNAL OF THE AERONAUTICAL SCIENCES

VOLUME 21 DECEMBER, 1954 NUMBER 12

The Story of Shimmy*

WILLIAM J. MORELAND†

Wright Air Development Center

SUMMARY

A theory of landing-gear shimmy is developed in which the basic assumptions involving the part played by the tire, the air frame, and the gear proper have been individually submitted to direct test.

Analysis and analog studies of the theory are used to establish a design procedure for obtaining a stable gear with a minimum of artificial damping.

The predictions of the theory have been tested on a model whose parameters can be varied to simulate nosegear structures of light high-speed fighters, as well as heavy bombers. A complete description of the model and a summary of the test results are presented.

Full-scale field test results are given for instrumented fighter, bomber, and cargo-type aircraft.

INTRODUCTION

SHIMMY IS THE term used to describe the self-induced swiveling of the nosegear of an airplane. Its appearance is unmistakable, and is characterized by the rapid build-up of a high-frequency oscillation accompanied by a shudder which progresses along the aircraft from the nose to the tail surface. In some instances the action is too rapid to permit the pilot to take the necessary corrective measures and the destruction of part of the plane may result.

The problem has been studied intensively for more than 20 years, yet, even since 1950, millions of dollars have been spent because of shimmy troubles. There is an interesting paradox about shimmy. It is one of the most widely known of dynamic phenomena. Even aside from the esthetic meaning of the term it is almost a household word because of its common occurrence in automobiles, trailers and tea carts. But as recently as 1952, three mutually contradictory theories on this subject have appeared. True, means for controlling shimmy are available but they are restricted in their application and provide little toward an understanding of its cause. The explanation for this anomalous situation is not that insufficient attention has been focused on the problem. Some 300 papers[3] bearing directly or indirectly on this subject have been published since 1922, and important contributions have been made by the French workers, Lavaud and Broulhiét; by the Germans, von Schlippe, Dietrich, Dietz, Harling and Fromm; and by the British and Americans, Lanchester, Temple, Bull, and Evans. The primary purpose of this paper is to describe the program which was pursued at the Wright Air Development Center to study the problem of shimmy. In addition, some attention will be given to learning the cause of the inadequacy of earlier efforts. The program was initiated in 1951, following a series of accidents traceable to landing gears. The work was planned to cover four distinct areas:

(1) Development of a theory of shimmy.
(2) Electronic computer studies of the theory.
(3) Experimental research on laboratory model.
(4) Full-scale field testing of fighter, bomber, and cargo-type aircraft.

DEVELOPMENT OF THE THEORY OF SHIMMY

Earlier Efforts

In 1925, Broulhiét in France, published a paper in which he succeeded in showing that the mechanical properties of the pneumatic tire could account for a sustained oscillation in a swivelling structure. Following this work the notion became widespread that the problem of achieving stability in a castering wheel depended in great measure on the properties of the tire. This viewpoint is still adhered to by the majority of analytical workers in the subject.[3] The philosophy

Presented at the Aeroelasticity Session, Twenty-Second Annual Meeting, IAS, January 25-29, 1954.

* The following individuals gave valuable assistance in the several phases of the program: computations—T. G. Sanborn and W. C. Bennewitz; analogue studies—W. L. Cyrus, J. G. Clarke, and R. T. Harnett; model tests—N. W. Carlson, P. E. Gies, and K. A. Erfurth; field tests—L. T. Waterman and D. W. Weller, Fairchild Engine and Aircraft Company, and F. C. Minch.

† Chief, Mechanics Research Branch, Aeronautical Research Laboratory.

of this school is expressed in the paper by Bourcier de Carbon (translated from the French and published 1952 by NACA, TM 1337). It will be helpful to briefly review the main points of this paper in order to obtain a clearer understanding of the reasons for the radically different conclusions obtained from the WADC approach. The mathematical model, Fig. 1, chosen by de Carbon to represent the nosegear system, consists of a rubber-tired wheel whose axle is carried in a fork which in turn is permitted to swivel in a fixed vertical pivot after the fashion of an ordinary furniture caster. The significant property of this simple system is based on the observation that a rolling wheel which has no force acting normal to its plane will describe a straight line over the ground parallel to its plane. But, if a steady force is applied normal to the wheel, it will drift sidewise while rolling and thus trace out a line on the ground which makes an angle (called the drift angle) with the wheel plane. This angle is directly proportional to the applied force. The action is still one of pure rolling—i.e., does not involve skidding. A theoretical explanation of the phenomenon is given by von Schlippe.[3] Employing this experimental law, the simple two-degree-of-freedom system is readily described by a third order differential equation which yields the stability criterion[2]

$$aD > T \tag{1}$$

where

a = trail distance, in.
D = drift angle divided by the force causing the drift, rad./lb.
T = the lateral deflection of the tire per pound of force. (Found by measuring the sidewise deflection of the nonrolling wheel under the action of a side force)

Eq. (1) states that if the trail a is made sufficiently large so that the product of trail times drift coefficient exceeds the lateral compressibility of the tire, then the wheel will not experience a self-excited vibration. This law is, of course, rigorously true *for the system under discussion*. But, this simple rule does not apply, even qualitatively, to an aircraft structure. The reasons for this will be discussed in detail in the remainder of the article. However, the most convincing explanation is quite simple. Suppose the model, Fig. 1, is assumed to have a rigid tire for which T is zero while D has a value approaching zero. The system would then be stable according to Eq. (1). However, if instead of assuming that the pivot is fixed laterally, it is permitted to have a lateral degree of freedom against a restoring force whose coefficient of elasticity is K_1, then, as shown in reference 1, page 9, this undamped system is inherently unstable no matter how large the lateral rigidy (K_1) may be. The assumption that the rigidity of the pivot is sufficiently great to permit describing it as "fixed" is tempting, but untenable. Even if we permit ourselves the luxury of assuming a heavily reinforced structure, the "fixed" pivot theory will not apply.

Fig. 2 may be used to illustrate this point. Suppose it is required to determine the stiffness of the spring, one end of which is attached to the finite mass m. If point A is moved slowly 1 in. toward the right, no resistance is felt at point A as m slides over the frictionless support. Under these circumstances, it must be concluded that the rigidity of the system is zero since a 1-in. deflection was obtained without force. This result is quite independent of the K of the spring itself. If point A is caused to move with simple harmonic motion of 1-in. amplitude, it will be found that, at low frequencies, when A has moved 1 in. to the right the mass m will actually have traveled more than one inch in the same direction. The spring will be stretched and in tension, and the force at A will be directed toward the *left*. Hence, since a 1-in. motion to the right, instead of requiring a push, actually demands a pull, it must be concluded that the rigidity of the system is negative. Stiffening the spring itself will not change this result. Next, if the frequency of oscillation of point A is gradually increased, the negative rigidity will increase until the natural frequency of the system is reached. Beyond this frequency it will be found that when point A is at the extreme right of its travel, the mass m will be at the extreme left of its excursion with a resulting high-compression in the spring and a positive value for the rigidity of the system. As the frequency is further increased, the mass will approach a condition of rest and under these circumstances the rigidity of the system will approach the K of the spring itself.

If the above experiment is repeated while another spring and mass are attached on the right-hand side of m, the variations in the apparent rigidity of the system will be found even more significant. In fact, a frequency will always be found at which the motion of m will be exactly the same as that of A. Under these circumstances, the rigidity of the system is actually zero regardless of the stiffness K of the spring itself. This same conclusion applies to the airplane. Even when the strut itself is made quite rigid the effective rigidity of the system may be small.

Fig. 3 shows the relationship between the effective rigidity and frequency for this idealized model. The relevance of this discussion to the problem of determining the "true rigidity" of the nosegear structure is obvious—it cannot be found by static deflection of the strut. As shown by instrumented taxi tests on a shimmying airplane, stiffening the strut cannot suppress the lateral motion of the pivot. Hence, a theory of shimmy based on the elastic properties of the tire alone is inadequate. A nosegear structure designed on the basis of the rule $aD > T$ would, if not otherwise stabilized, be destroyed on its first taxi run. But this is not all. An even more significant degree of freedom than the lateral motion of the pivot is that due to the finite

torsional elasticity of the damper system. During a shimmy, the wheel will swivel in its pivot and by means of linkage this motion forces a damper piston to drive oil through an orifice which offers sufficient resistance to cause the oscillation to attenuate. If the orifice size is reduced, the damping action is increased and the system becomes still more stable. However, if the finite elasticity of the linkage is taken into account, this conclusion may be reversed. It can be shown[1] that below a certain critical value of the linkage elasticity, no orifice size can be found that will stabilize the system. This critical elastic coefficient is disclosed by the nondimensional number composed of the torsional and lateral rigidities, the wheel moment of inertia, and the strut weight. The method for calculating this number will be given later.

This does not imply that the influence of the tire on stability may not be important. Only by analysis of fairly complete models of the whole structure can the part played by the tire be properly evaluated.

This is the key to the long controversy; no degree of freedom can be neglected until numerical analysis and experiment have demonstrated the part it plays in determining the system stability. Over two thousand such analyses of various types of aircraft have been made at the Wright Air Development Center. In one of these, using experimentally determined data from a fighter-type aircraft and published[4] tire data, it was shown that in order for the stability criterion given by Eq. (1) to apply, the lateral rigidity of the pivot would have to be increased threefold—a physical impossibility.

The author next examines the effect of transient drift in the tire and from this study obtains a modified form of the original stability criterion:

$$(IRV^2 - a)\,(aD - T) > 0 \qquad (2)$$

where

I = moment of inertia of the oscillating system about the pivot
V = velocity of the aircraft

Since stability exists if both terms are positive, the inescapable conclusions to be drawn from Eq. (2) are:

(1) Increasing the system inertia, I, is stabilizing.
(2) Increasing the taxi speed, V, is stabilizing.
(3) Sufficiently great trail, a, is destabilizing.

In each of the above conditions the opposite conclusion is predicted by WADC Theory and the latter is supported by both model and full-scale tests to be described later. The erroneous conclusions are due in part to the assumption of a "fixed" pivot. With this restriction removed, the above rules are actually reversed as shown in reference 1. (Because of a misinterpretation of the "law of turning," reference 2, p. 23, the relation $S\epsilon = D$ is obtained, where $S = \delta/M$ is the coefficient of torsional elasticity of the tire, and $\epsilon = M/F$ is the pneumatic trail. In what appeared to be a check of this equation, some experimental data were substituted in what closer examination reveals to be a mere identity, viz., $(\delta/M)\,(M/F) = (\delta/F)$. Of course, substitution of any arbitrary numbers will give an exact "check." Published data[4] giving independent measurements of S, ϵ, and D do not verify the given equation.)

Comments on the Wright Air Development Center Theory of Shimmy

Details of the mathematical development of the WADC theory of shimmy[1] will not be repeated here. The basic assumptions employed, the experimental evidence in support of these, and the significant conclusions are discussed.

Degrees of Freedom.—The degrees of freedom of the mathematical model used in the development of the theory are (1) the lateral displacement of the wheel while the tire footprint remains fixed on the ground. This is due to the lateral flexing of the tire; (2) the swiveling motion of the wheel about the strut axis; (3) the lateral displacement of the pivot or strut against the elastic restraint of the strut and airframe; (4) the relative motion between the swiveling of the wheel and the movement of the damper piston. This relative motion is due to the elasticity of the damper linkage; (5) the relative motion between the strut and the airframe. (The airframe itself is in turn represented by a lumped-parameter system of one or more degrees of freedom.)

Taxi tests on instrumented bomber and cargo-type aircraft have been conducted to obtain quantitative data on the relative magnitudes of the motions in the various degrees of freedom. Velocity and acceleration type instruments were placed on the nosewheel, along the fuselage, in the wings and stabilizers. Oscillograph records of the instrument readings were taken for various taxi speeds and for shimmy conditions which varied from mild to severe. These records disclose the frequency, amplitude, and phase of the several parts of the airframe. Instruments located as far as 50 feet from the nosegear recorded vigorous vibrations of shimmy frequency usually within one second of the onset of the disturbance at the gear. The lateral motion of the pivot (or projected strut) is always present and frequently exceeds the lateral movement of the wheel.

Lateral Rigidity.—As previously indicated the lateral rigidity of the strut is frequency-sensitive. Experimentally, this quantity is obtained by applying a harmonic force at the axle in a direction perpendicular to the axis of the airplane and, with the wheel removed, record the lateral deflection as a function of the frequency of the vibration. A fighter-type aircraft under test at WADC and Cornell Aeronautical Laboratory showed a variation in lateral rigidity from 500 lbs./in. to 12,000 lbs./in.—a ratio of 24 to 1—as the frequency was varied from below to above normal shimmy ranges. Hence, the lateral rigidity cannot be known until the shimmy frequency is given, and the shimmy frequency

is itself dependent on the lateral rigidity. A graphical solution of these simultaneous functions is described in Reference 1.

How the Tire Influences Shimmy.—One of the most controversial subjects in the problem of shimmy concerns the part played by the pneumatic tire. The approach taken in the WADC report is based on assumptions which individually can be submitted to direct test. The theory is as follows: A wheel rolling over the ground with a forward velocity V (Fig. 4) will, when acted upon by a force F *from* the ground, travel along the path V' making the yaw angle ψ with its plane. Thus the wheel center has a velocity $V_n = V\psi$ normal to its plane and directed against the ground force. But the force F does not instantly create the yaw angle ψ. A measurable time delay follows the application of the force before a steady yaw angle is established and this condition can be described by the equation

$$\psi + C_1\dot{\psi} = CF \tag{3}$$

where

C = the coefficient of yaw, rad./lb.
C_1 = the time constant, sec.

Due to the lateral compressibility of the tire, the center of the wheel will be displaced relative to the ground contact point whenever a force F acts between the ground and tire. This force is transmitted through the rubber from the ground to the wheel. The accompanying strain in the rubber is

$$\Delta = pF \tag{4}$$

where

p = the lateral coefficient of compressibility of the tire, in./lb.

Hence, the total normal velocity of the wheel due to the combined effects of yaw and tire stretch is $V\psi + \dot{\Delta}$. A third source of normal velocity exists when the wheel is trailing the pivot at an angle θ with the direction of forward velocity of the airplane. This is most easily pictured by assuming the pivot at rest and the ground moving under it toward the left. As shown in Fig. 5, this creates a velocity normal to the wheel plane equal to $-V\theta$.

Combining the three effects, the total normal velocity becomes

$$V_n = V\psi + \dot{\Delta} - V\theta$$

and the angular velocity of the wheel about the pivot is thus

$$\frac{V_n}{L} = \dot{\theta} = \frac{V\psi + \Delta - V\theta}{L} \tag{5}$$

This equation defines the coupling between the two degrees of freedom, θ and Δ, and may be combined with the dynamic equations of the system, including the lateral motion of the pivot, as described in reference 1. In this way (as discussed under computer studies) a true perspective of the part played by the tire in the dynamics of the overall system is obtained. (Both the present theory and that of de Carbon employ the same basic law of tire yaw. Hence, the former must contain the stability criterion given by de Carbon. This can be seen by combining Eqs. (B1) and (5) of reference 1 and omitting the term that describes the lateral motion of the pivot.) In the derivation of Eq. (5) above, the critical assumption is that expressed by Eq. (3) and this may be subjected to direct test in the following way: Place the wheel and pivot assembly in a fixture that will permit free swivelling of the wheel while the latter is pressed against a rotating drum. A force applied to the axle normal to the wheel plane will cause the trail arm to swing about the pivot and assume a fixed angular position with the direction of free trail. This fixed angle is the yaw created by the normal force. The coefficient of yaw C is the ratio of the angular displacement to the applied force. In addition, if an oscillograph record is made of the angular motion following the application of a step input force, it will be found that the wheel will oscillate about its equilibrium position of steady state yaw with a decaying amplitude. The logarithmic decrement of this motion defines the time constant C_1 of the tire. Thus, a single simple setup provides the means for determining C and C_1 simultaneously. Tests conducted at the Wright Air Development Center have fixed this latter quantity at about 0.01 sec. for the tire used on the model nosegear. The significant point to observe here is that direct dynamic measurements involving no unsubstantiated assumptions have established the coefficients of Eq. (3). It is important that a theory of shimmy provide for the concept of the time constant C_1. This is apparent when it is recalled that for shimmy frequencies encountered in practice, the yaw angle is built up from zero to its maximum value in about $^1/_{60}$ of a second. For this reason, a theory of shimmy which assumes that the full steady state yaw is associated with a given side force will be considerably in error.

Replacing the airframe by a two-mass lumped parameter system, the complete mathematical model will contain six degrees of freedom. From the set of simultaneous equations that express the dynamics of the parts of the model a single tenth-order differential equation for the complete system is obtained. Details of the process differ according to the coordinate system used to describe the motion of the strut. If the strut is assumed to oscillate laterally about a fixed point, polar coordinates apply; but if the point about which the oscillation occurs is taken infinitely far above the wheel axis, rectangular coordinates may be used. The choice is not arbitrary and its significance will be brought out when discussing the theory of the experimental model. Rectangular coordinates are employed in presenting the theory in reference 1, while polar coordinates are used to describe the experimental model.

THE STRUT MOVES FORWARD IN A STRAIGHT LINE WITH NO LATERAL VIBRATION (FIXED PIVOT). THE WHEEL SWIVELS AROUND THE STRUT BY VIRTUE OF THE ELASTIC PROPERTIES OF THE TIRE.

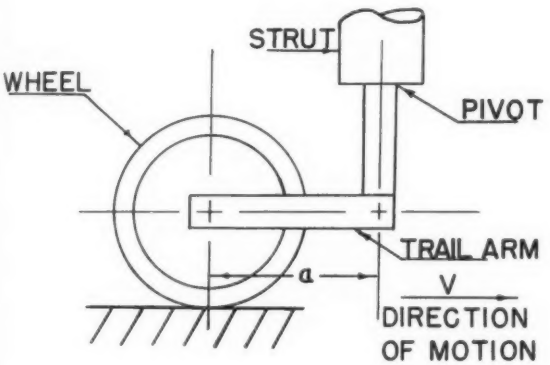

FIG. 1. Simplest nosegear system capable of self-excited vibration.

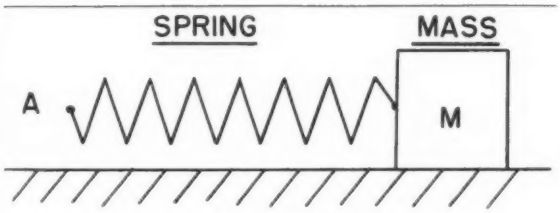

FIG. 2. Model to illustrate effective rigidity.

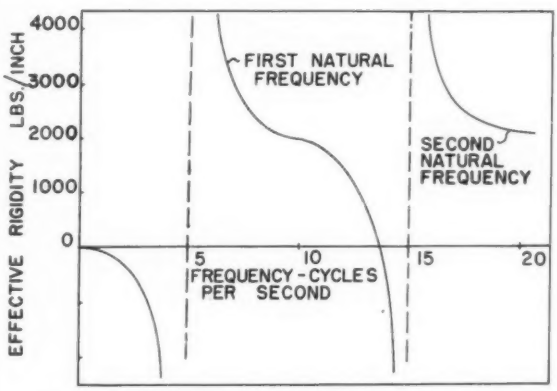

FIG. 3. Variation of rigidity due to frequency change.

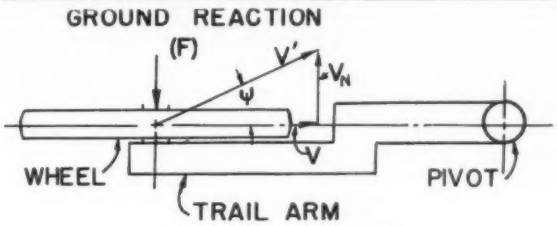

FIG. 4. Normal velocity due to tire yaw.

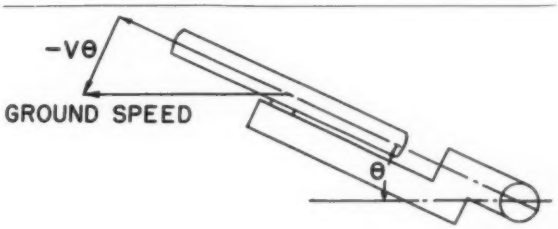

FIG. 5. Normal velocity due to trail angle θ.

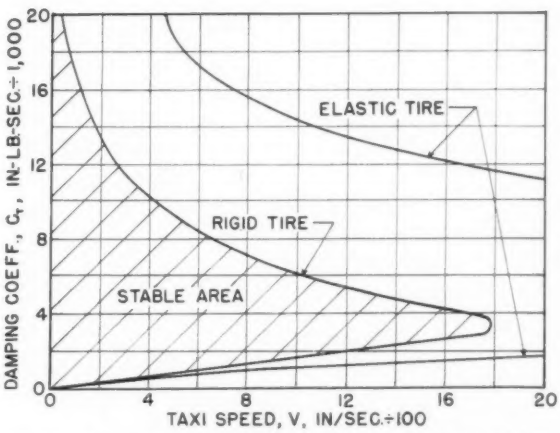

FIG. 6. Comparison of stability of nosegear with and without a rubber tire.

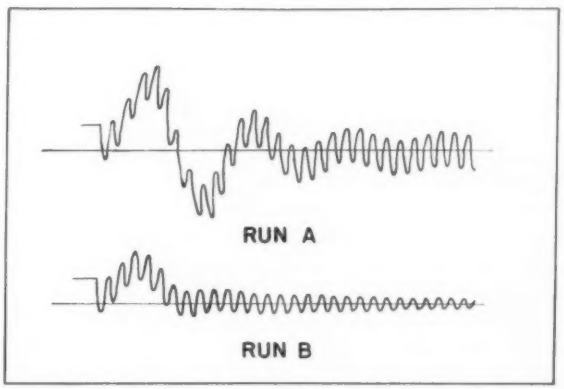

FIG. 7. Combined tire and strut vibration modes.

The problem now at hand is to determine whether regions of stability for the nosegear can be mapped from the dynamic equations. The problem is considerably simplified if the system is assumed divided at the junction of the self-excited portion with the passive airframe. Analysis of the two parts may be carried out separately and a simultaneous solution obtained by an impedance match at the junction. In this way the search for stability criteria is directed to the portion of the system which contains the most significant parameters. In addition, since normal ranges of tire parameters have been found to have remarkably little influence on the damping required for stability, the tire may at first be taken as rigid. This simplified system can now be completely described by using only four nondimensional parameters.[5] As shown below, the ratio of two of these numbers, called the inertia ratio, is a useful index of stability. This number does not contain the trail—the parameter which plays so prominent a part in tire mode theories. The principal conclusions from the analysis, applicable to the design of a stable nosegear structure, are repeated here. Let

Q = nondimensional velocity = $V2\sqrt{I_{\bar{w}}}/L\sqrt{K_t}$
R = nondimensional damping = $C_t/2\sqrt{K_t I_{\bar{w}}}$
S = nondimensional strut mass = $NL^2/I_{\bar{w}}$
T = nondimensional trail = $L/\sqrt{K_t/K_1}$
T^2/S = nondimensional "inertia ratio"
C_t = coefficient of viscous damping, lb. in. sec.
$I_{\bar{w}}$ = moment of inertia of nosewheel about a diameter plus moment of inertia of spindle about its axis, lb. in. sec.^{2}
K_1 = lateral rigidity of strut, lb./in.
K_t = torsional elastic coefficient of the damper linkage (obtained by applying a couple in a horizontal plane to the wheel while the damper piston is locked), lb. in./rad.
L = trail, in.
N = equivalent mass of strut (the lateral moment of inertia of the strut about its nodal point divided by the square of the distance between this point and the ground), lb. sec.^{2}/in.
V = ground speed, in./sec.

(1) The complete stability criterion for the fourth order rigid tire system is

$$QS(1 - T^2/S)R^3 + [1 + S(2 - T^2/S)]R^2 + [(1 + S)/Q - QS/4]R - (1 + S)/4 > 0 \quad (6)$$

Examination of this inequality will reveal all of the essential phenomena pertaining to the dynamics of the fourth order system, and, as shown below, will give the damping required to stabilize the complete seventh order system for all normal parameter ranges. It should be particularly noted that only three numbers, Q, S, and T are required for analysis of any given airplane. Families of curves can be constructed[1] from this expression to portray the effects of variation of any one of 9 system parameters. However, simple inspection of Eq. (6) yields significant information. For example, it is apparent from the first term of Eq. (6) that if T^2/S exceeds unity, then sufficiently large values of damping (R) will cause the system to become unstable. In effect, the main gear has infinite damping since it is not permitted to swivel, and in this case the system cannot tolerate any advance of T^2/S (the "inertia ratio") beyond unity. Hence, the condition that must be satisfied to insure stability without the danger of overdamping is that the inertia ratio

$$\frac{T^2}{S} = \frac{I_{\bar{w}}K_1}{NK_t} < 1 \quad (7)$$

For example, measurements of a fighter-type jet nosegear gave $I_{\bar{w}} = 3$; $K_t = 0.5 \times 10^6$; $N = 0.033$. Hence,

$$\frac{T^2}{S} = \frac{I_{\bar{w}}K_1}{NK_t} = \frac{3 \times K_1}{0.033 \times 0.5 \times 10^6} < 1$$

or K_1 must not exceed 5,500 lbs./in. when measured at the shimmy frequency of the nosegear. If K_1 is larger than this amount, the first term of Eq. (6) becomes negative and, for large values of R, the left side of the inequality is negative indicating instability.

(2) The damping required to maintain neutral stability when $T^2/S = 1$ is found from Eq. (6):

$$R = \frac{\frac{QS}{4(1+S)} - \frac{1}{Q} \pm \sqrt{\left|\frac{QS}{4(1+S)} - \frac{1}{Q}\right|^2 + 1}}{2} \quad (6A)$$

Eq. (6A) applies quite closely for all values of T^2/S from 1 to zero. Ample attenuation of wheel disturbance is provided when C_t is given a value between two and two and one-half times that found from Eq. (6A). It is significant to observe the values of C_t required for stability when extreme values of the parameters are substituted in the above equations. For example, when

$V = 0$, $\quad C_t = 0$

$V = \infty$, $\quad C_t = \sqrt{\dfrac{K_t I_{\bar{w}}}{1 - T^2/S}}$ [from Eq. (6)]

Hence, C_t must always be made greater as V increases, yet will remain finite if $T^2/S < 1$. (Gyroscopic effects reduce the required damping at high speeds but this favorable result is approximately cancelled by tire yaw and flexibility.)

$L = 0$, $\quad C_t = \sqrt{K_t I_{\bar{w}}}$, i.e., stability is possible with zero trail
$L = \infty$, $\quad C_t = 0$
$K_t = \infty$, $\quad C_t = VI_{\bar{w}}/L$
$I_{\bar{w}} = 0$, $\quad C_t = 0$
$I_{\bar{w}} = \infty$, $\quad C_t = \infty$

It is apparent that $I_{\bar{w}}$ is the most important factor in determining C_t. It should be noted that increasing $I_{\bar{w}}$

is here predicted to have the opposite effect to that found on the basis of tire effects alone. As will be shown later, both model and full-scale tests support the conclusion that increasing the wheel moment of inertia is destabilizing. Returning to Eq. (6), it can be seen that for $T^2/S < 1$, the first two terms are positive, the third may be positive or negative, while the fourth is negative. That is, there is only one change in sign and hence no more than one positive root. All values of R greater than this root are stabilizing. But if $T^2/S > 1$, there can be two changes in sign indicating a possibility of two values of R for neutral stability between which the system is stable. Hence, stability may exist for values of the inertia ratio greater than unity. But for this to be a practical solution the two roots must be spread sufficiently far apart so that intermediate values of R will provide sufficient attenuation and also so that the risk of accidental overdamping will be avoided. Analog studies of the system have shown that if the larger root R is taken as 2.5, satisfactory stability can be obtained over the complete range of system parameters. If this value of R is substituted in Eq. (6) and the inequality solved for T^2/S, it can be shown that when T^2/S is less than $(1 + S)/2.5\,QS$ the stability will be satisfactory. Substituting for the dimensionless terms gives

$$K_1 < \frac{[1 + (NL^2/I_{\bar{w}})]\,K_t^{3/2}}{5VL\sqrt{I_{\bar{w}}}} \qquad (8)$$

K_1 should be computed from Eq. (7) and Eq. (8) and the larger value retained. Further analysis of Eq. (6) shows that when the inertia ratio is continuously increased beyond unity the two real roots approach each other and finally coalesce and beyond this point stability is impossible regardless of the amount of damping employed.

(3) "Middle" values of trail are destabilizing. This conclusion was reached by a number of experimenters (Tonnies and Gollung, *German View of Tricycle Undercarriage*, Aircr. Engrg., May, 1947). Also (Seifert, *Stability in Taxiing*, ME-GE 1940) and (Fairchild C-119 Taxi Tests 1953). No explanation had been given for these observations, but as shown in reference 1, page 32, this phenomenon has a simple theoretical explanation due directly to an excessive value of the inertia ratio.

(4) For the values of strut mass and trail commonly encountered, stability is impossible if the inertia ratio exceeds a calculable upper limit. This conclusion is valid regardless of the amount of viscous damping employed. (See Fig. 7a, reference 1).

(5) The above conclusions apply strictly to the case of a rigid tire with negligible gyroscopic effects, but remain valid when normal tire parameters[4] are inserted in the general equations of the system (see Appendix B, reference 1). Pneumatic trail—i.e., the additional trail induced by the shifting aft of the center of pressure in the tire footprint, has little effect on the damping requirement.

(6) No theory of shimmy can be complete. Factors such as nonlinearity of parameters, backlash, fore-and-aft strut motion and extreme tire parameters play a part in the phenomenon. Results of studies to date at the Wright Air Development Center indicate that under normal conditions these effects are not predominant.

Electronic Computer Studies

The purpose of these studies was to examine the effects on stability due to the pneumatic tire. A system of four degrees of freedom containing 15 parameters was selected. Twelve of the 15 parameters were obtained by direct measurements from a fighter-type aircraft. The tire characteristics C and p were obtained from published data[4] and C_1 was determined from model tests at the Wright Air Development Center. The following procedure was used in setting the problem on the machine: All of the tire parameters were set equal to zero (simulating a rigid tire) and the wheel was given an initial displacement corresponding to a lateral shock. The damping coefficient C_t was then adjusted by trial until a neutrally stable shimmy was obtained. The same procedure was repeated with different taxi speeds and a graph of C_t vs. speed was plotted. Next, with the same structural parameters, a combination of tire parameters, C, C_1, p, were selected so that according to the stability rule obtained from the fixed pivot theory,[2] the system should be strongly unstable—i.e., $LC < p$. The complete system was then placed in the computer and data were again obtained to plot C_t for neutral stability vs. taxi speed. The results are shown in Fig. 6.

It is to be particularly noted that at every point the system that included the elastic tire is more stable, i.e., a greater region of stability is enclosed by the graph, despite the fact that the tire system by itself is unstable. It might be reasoned that although the tire system by itself is unstable, the presence of C_t serves to hold it stable. But this does not explain the fact that the combination of the two unstable systems required less damping than that demanded by the original system. Fig. 6 is typical of the results obtained over a wide range of system parameters. Only for abnormally large values of tire parameters does the destabilizing influence of the rubber become comparable to that of the structural parameters.

A second series of studies was made using a combination of tire parameters that would be stable on the fixed pivot theory[2] —i.e., $LC > p$ (or, in de Carbon's notation, $aD > T$). In every case, this system was unstable for normal ranges of structural parameters unless artificial damping was employed. Moreover, when the lateral rigidity of the strut was increased from its normal value of 7×10^6 lbs./in. to $10 \times 7 \times 10^6$ lbs./in., the system was still unstable, again demon-

strating the impracticality of attempting to base a stability criterion on the mechanical properties of the tire alone.

Fig. 7A is an oscillograph record of the lateral movement of the wheel during a neutrally stable shimmy. The system is composed of a laterally soft (unstable) tire and an abnormally rigid strut. Following the initial displacement, about three oscillations of low frequency (the tire mode) can be observed, while the high-frequency strut mode is sustained. With the damping increased (Fig. 7B) to slightly attenuate the strut mode, the tire component is strongly attenuated. In a sense, these diagrams visibly portray the grounds on which the opinions of the two schools of thought are based. Both modes of motion—that due to the tire and that due to the structure—are ever present and inextricably interwoven. In this particular case where sufficient damping is provided to control the tire mode, it is obviously not sufficient to give stability to the entire structure. This again demonstrates that generalizations from particular cases may be misleading especially if the system is oversimplified.

The Experimental Model

Few problems in the field of experimental dynamics present greater difficulty than that of devising a suitable procedure for testing a theory of stability of a mechanical system. If the theory predicts stable operation for a given configuration and observation shows that an initial disturbance will die out, this is merely agreement with—not confirmation of—the theory. Again, if the tests are conducted at a condition of neutral stability, this delicate balance may be disproportionately affected by the ever present nonlinearities and other unknowns. For example, a 1 per cent error in the measured damping might well correspond to a 20 per cent error in the neutrally stable speed. A summary of possible test procedures follows:

(1) Measure all the system parameters and, applying the Hurwitz[6] criterion to the characteristic equation, determine whether the system is stable or not. Observation will agree or disagree with the theory. At best, this method provides only a rough qualitative check on the theory.

(2) Plot a graph showing the relation between the theoretical damping coefficient C_t and the taxi speed V for *neutral* stability. Then, with the damper adjusted for a given value of C_t, adjust the speed V until a sustained oscillation is developed. This method supplies a quantitative check on the theory.

(3) A method presently under investigation at the Wright Air Development Center is analogous to the frequency response technique employed in servomechanism research. With the system parameters adjusted for *stable* operation, a harmonic excitation supplied by a mass attached to the rotating wheel induces a steady harmonic response at each speed which may then be compared with the corresponding theoretical value.

Most of the tests on the WADC model were made using the second method. In order to reduce the effects of possible compensating errors in observing stability, precise measurements of the sustained frequencies were obtained and compared with the theoretical values. In addition, the phase relation between the wheel motion and the latteral motion of the pivot provides an exacting check on the theory.

As shown in Fig. 8, the model consists of a wheel and rubber tire on an axle which in turn is supported by a trail arm. This assembly is carried on a vertical spindle which passes through two ball bearings. The lower bearing is fastened to the spindle and transmits a spring load to the wheel forcing it against the driving drum, thus simulating the airplane weight. The upper bearing is fixed to a sleeve (the airplane strut) which in turn is pivoted to the frame of the machine. The lateral rigidity of the nosegear is created by means of helical springs between the frame and the sleeve. These springs are carried on a collar which surrounds the sleeve and which can be adjusted relative to the sleeve pivot. In this way the lateral rigidity K_1 can be adjusted to any predetermined value by simply selecting the appropriate position of the collar relative to the pivot. The spindle passes up through the sleeve and

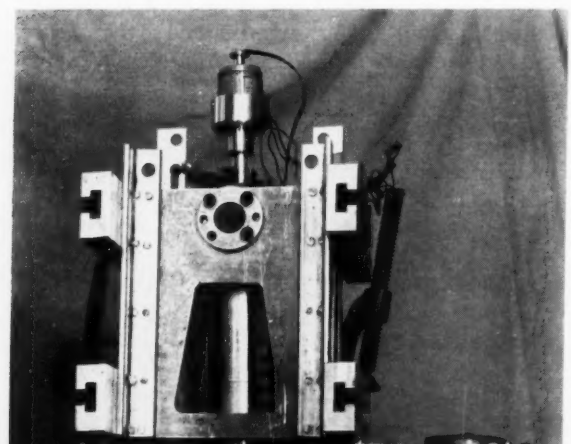

FIG. 8. Landing gear model.

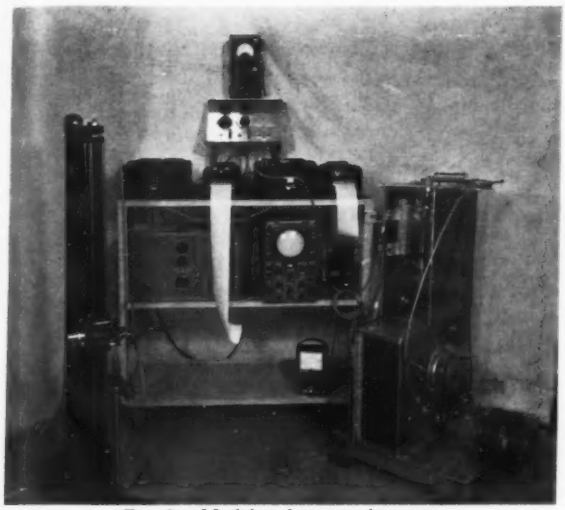

FIG. 9. Model and test equipment.

is attached by means of a spring to a viscous damper. This spring supplies the necessary degree of freedom in torsion. The base of the damper is mounted rigidly to the oscillating strut, thus permitting damping action only against the swivelling motion of the spindle. When in operation, the sleeve which supports the spindle oscillates on its pivot thus providing the degree of freedom corresponding to the lateral motion of the nosegear pivot. To simulate the airframe, the oscillating motion of the pivot drives a massive ring through an elastic shaft. Smaller masses, attached by flat springs to the main ring, simulate higher modes of motion in the airframe. Altogether, the model is provided with six selective degrees of freedom. Fig. 9 shows the complete test setup. Fig. 10 shows the two degree-of-freedom airframe simulator. Fig. 11 shows the accurately adjustable silicone-fluid viscous damper.

The following adjustments can be made: Various wheels and tires; 0- to 4-in. trail; vertical load; lateral pivot rigidity; spindle-damper torsional rigidity; damping from zero to several times critical; infinite damping coefficient; strut mass; drum speed from 0 to 400 in./sec.; airframe simulator modes. In addition, any of the degrees of freedom can be suppressed at will.

An autosyn attached to the top of the spindle is used to measure the swivelling motion of the wheel. A similar instrument attached to the sleeve pivot measures the lateral motion of the nosegear. These two readings are recorded on an oscillograph thus permitting accurate measurements of stability, frequency, amplitudes, and phase relations of the two principal motions. The drum speed is recorded separately.

Model Theory

A precise mathematical description of the model requires the use of polar coordinates to specify the lateral motion of the strut since this element is carried on a fixed pivot in the model. In addition, in order to permit accurate prediction of shimmy frequencies over the wide range of operating conditions for which the model can be adjusted, two parameters not included in the published report are given here—gyroscopic and vertical load effects.

Notation

C	=	coefficient of yaw, rad./lb.
C_1	=	tire time constant, sec.
C_f	=	coefficient of viscous damping, in.-lb. sec.
D	=	differential operator
F_n	=	ground reaction normal to wheel plane, lbs.
F_r	=	ground reaction parallel to strut, lbs.
H	=	distance from trunion to axle, in.
I	=	polar moment of inertia of rotating wheel, lb. in. sec.^{2}
I_f	=	moment of inertia of the system about the strut axis, lb. in. sec.^{2}
I_s	=	moment of inertia of the swivelling parts about the spindle, lb. in. sec.^{2}
K	=	torsional coefficient about the strut axis, in. lb./rad.
K_0	=	$K + W_0L_0 + W_1L_1 + W_2H$
K_t	=	torsional coefficient of the damper linkage, in. lb./rad.
L	=	trail length, in.
L_0	=	distance from strut axis to c.g. of strut, in.
L_1	=	distance from strut axis to c.g. of spindle, in.
m	=	wheel mass, lb. sec.^{2}/in.
p	=	lateral compliance of tire, in./lb.
r	=	wheel radius, in.
S	=	spring load, lbs.
V	=	taxi velocity, in./sec.
W	=	$S + W_1$

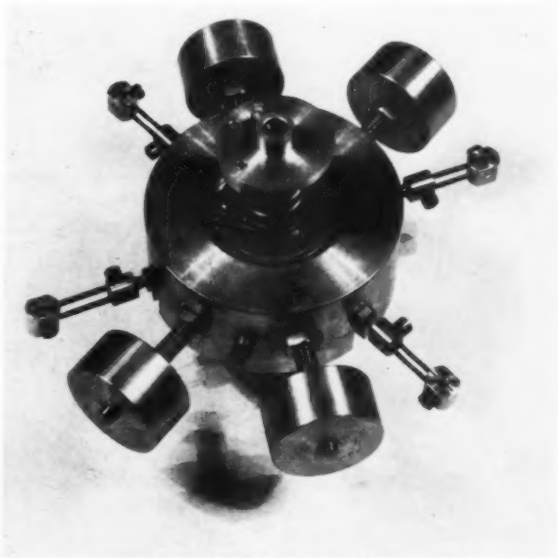

FIG. 10. Airframe simulator.

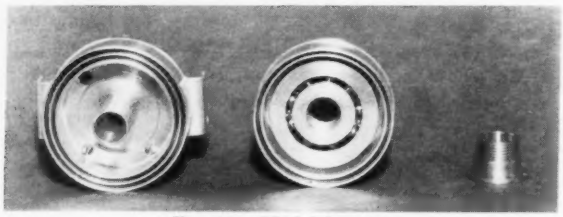

FIG. 11. Model damper.

W_0 = strut weight, lbs.
W_1 = spindle weight, lbs.
W_2 = wheel weight (mg.) lbs.
ω = angular velocity of wheel, rad./sec.
α = angular deflection of strut, rad.
Δ = lateral deflection of tire, in.
θ = angular position of trail arm, rad.
θ_1 = equivalent angular position of damper, rad.
$(\theta - \theta_1)$ = angular strain in damper linkage, rad.

Inspection of Fig. 12 reveals the presence of the following moments about the strut axis:

(1) $F_n(H + r)$, due to the ground reaction acting perpendicular to the wheel plane.

(2) $F_rL\theta$, F_r is in the wheel plane but does not pass through the strut axis because of the trail angle θ.

(3) $I_f\ddot{\alpha}$, the inertia torque of the whole system if the trail arm did not pivot about the spindle axis.

(4) $mLH\ddot{\theta}$, the c.g. of the wheel mass feels an acceleration due to $\ddot{\theta}$ equal to $L\ddot{\theta}$. The resulting inertia force acting on a moment arm H about the strut axis produces a torque superimposed on that due to $\ddot{\alpha}$.

(5) $I\omega\dot{\theta}$, due to the wheel spin axis precessing in the horizontal plane creating a gyroscopic couple in the vertical plane.

(6) $W_0L_0 + W_1L_1 + W_2(H\alpha + L\theta)$, the pendulous restoring moment due to the weight of the parts.

(7) $K\alpha$, the restoring moment due to the elasticity of the strut and its support.

Summation of these moments about the strut axis gives:

$$F_n(H + r) + F_rL\theta - I_f\ddot{\alpha} - mLH\ddot{\theta} - I\omega\dot{\theta} - (W_0L_0 + W_1L_1)\alpha - W_2(H\alpha + L\theta) - K\alpha = 0 \tag{9}$$

Summation of moments about the spindle axis gives:

$$F_nL - I_s\ddot{\theta} - mLH\ddot{\alpha} - C_t\dot{\theta}_1 + I\omega\dot{\alpha} - W_2L\alpha = 0 \tag{10}$$

Equating damper torque to damper strain times the torsional elastic coefficient:

$$C_t\dot{\theta}_1 = K_t(\theta - \theta_1) \tag{11}$$

In Eq. (5) above, replace ψ from (1) by

$$\psi = -CF_n/(1 + C_1D)$$

and with $\Delta = -pF_n$ obtain (see also reference 1):

$$(C_1pD^2 + pD + CV)F_n + [(H + r)C_1D^2 + (H + r)D]\alpha + [C_1LD^2 + (VC_1 + L)D + V]\theta = 0 \tag{12}$$

(It should be noted that this polar form of the system equations reduces to the coplaner form given in reference 1 when H approaches infinity. As previously remarked, the effect of this transformation is to eliminate the gyroscopic stabilizing action of the wheel. For normal configurations, and at low speeds, the gyroscopic action is negligible.)

The determinant of these four simultaneous equations yields the seventh-order characteristic equation of the model which may be written

$$A_7D^7\theta + A_6D^6\theta + A_5D^5\theta + A_4D^4\theta + A_3D^3\theta + A_2D^2\theta + A_1D\theta + A_0\theta = 0 \tag{13}$$

where, with $W_2 = 0$

$$A_0 = K_0K_tLV$$

$$A_1 = K_t[K_0L^2 + I\omega V(H + r) + WL^2(H + r)] + C_tK_0V(L + CK_t) - CWLI\omega VK_t + C_1K_0K_tLV$$

$$A_2 = K_tLV[I_f - mH(H + r)] + C_t[K_0L^2 + I\omega V(H + r) + WL^2(H + r) + K_t(H + r)^2] + p[C_tK_0K_t - WLI\omega K_t] + C_1[C_tK_0LV + K_0K_tL^2 + I\omega VK_t(H + r) + WL^2(H + r)K_t] + CV[K_t(I_sK_0 + I^2\omega^2 + mL^2WH) - C_tWLI\omega]$$

$$A_3 = K_t[I_s(H + r)^2 + I_fL^2 - 2mL^2H(H + r)] + (C_t + C_1K_t)[I_f - mH(H + r)]LV + C_tCV(I_fK_t + I_sK_0 + I^2\omega^2) + C_tC_1[K_0L^2 + K_t(H + r)^2 + I\omega V(H + r) + pK_0K_t] + pK_t(I_sK_0 + I^2\omega^2) + WL^2[pK_tmH + C_tCmHV + C_tC_1(H + r)] - (C_t + C_1K_t)WLI\omega p$$

$$A_4 = (C_t + C_1K_t)[I_s(H + r)^2 + I_fL^2 - 2mL^2H(H + r)] + CK_tV(I_fI_s - m^2H^2L^2) + C_tpI_fK_t + (C_t + C_1K_t)p[I_sK_0 + I^2\omega^2 + mL^2HW] - C_tC_1I\omega pWL + C_tC_1LV[I_f - mH(H + r)]$$

$$A_5 = C_tC_1[I_s(H + r)^2 + I_fL^2 - 2mL^2H(H + r) + p(I_sK_0 + I_fK_t + I^2\omega^2 + mL^2WH)] + (C_tCV + pK_t)(I_fI_s - m^2H^2L^2)$$

$$A_6 = (C_t + C_1K_t)p(I_fI_s - m^2H^2L^2)$$

$$A_7 = C_tC_1p(I_fI_s - m^2H^2L^2)$$

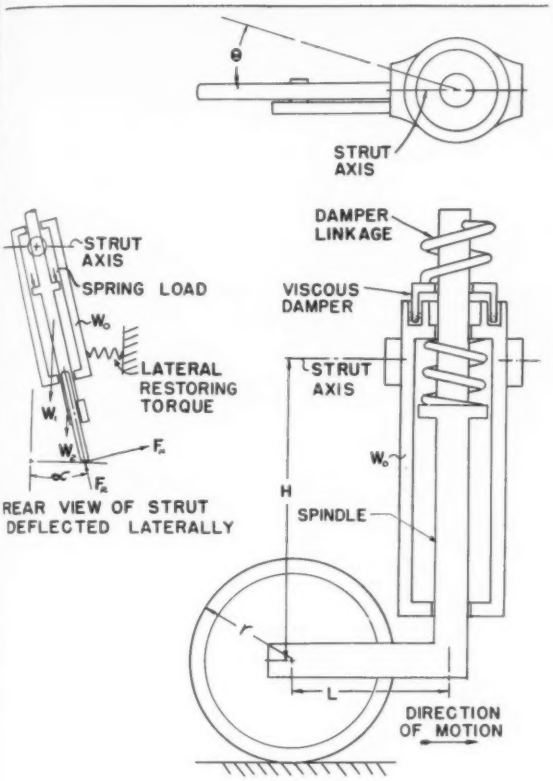

FIG. 12. Test model schematic.

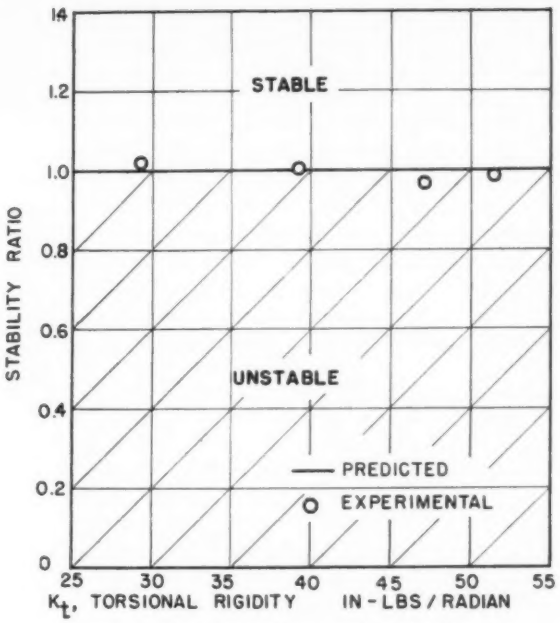

FIG. 14. Stability ratio vs. torsional rigidity.

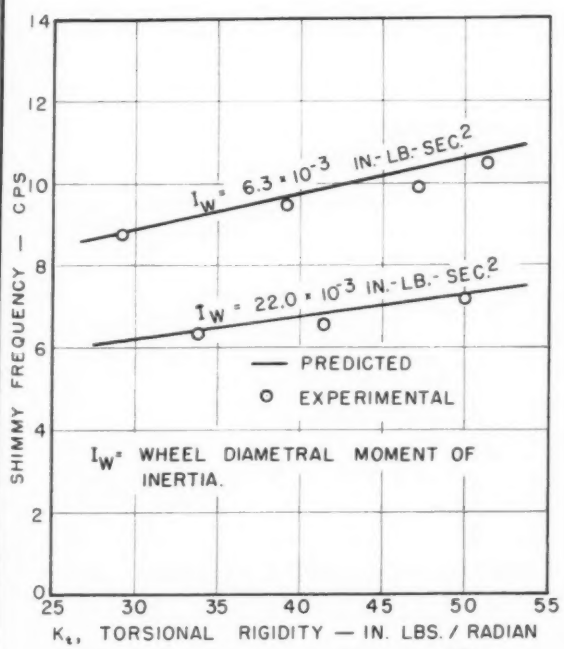
SHIMMY FREQUENCY — CPS
$I_W = 6.3 \times 10^{-3}$ IN.-LB.-SEC.^{2}
$I_W = 22.0 \times 10^{-3}$ IN.-LB.-SEC.^{2}
PREDICTED
EXPERIMENTAL
I_W = WHEEL DIAMETRAL MOMENT OF INERTIA.
K_t, TORSIONAL RIGIDITY — IN. LBS./RADIAN

FIG. 13. Shimmy frequency vs. torsional rigidity.

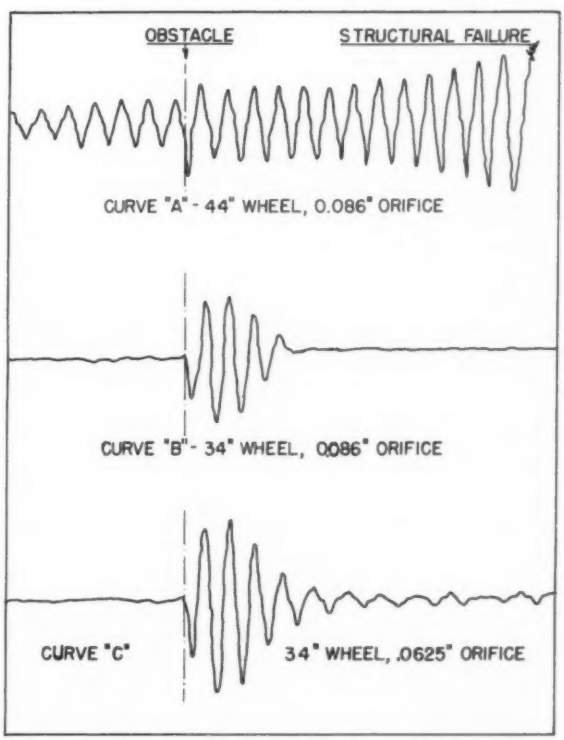

FIG. 15. Vibration of C-119 shimmy damper link assembly.

Eq. (13) describes the nuances in the performance of the model with precision over the widest ranges of system parameters. It contains the stability criterion found by assuming a "fixed" pivot; yet shows that the conclusions reached for this case are actually reversed with more realistic configurations. For all normal ranges of parameters the damping coefficient computed by Eq. (6A) will stabilize the system represented by Eq. (13). For each value of the lateral rigidity used in this equation there will be associated a sustained natural frequency provided the damping is adjusted to maintain neutral stability. A graph of this frequency vs. the lateral rigidity of the strut may be superimposed on a similar graph of frequency vs. rigidity for the airframe. The points of intersection represent neutrally stable operating points for the complete system as described in reference 1, p. 47. In order to determine whether the coefficients in Eq. (13) will provide stable operation, Routh's criterion[6] (as given by Hurwitz) should be used.

For the purpose of electronic analog studies, it is simpler to use the four simultaneous equations rather than the single Eq. (13). But the latter is more suited to the study of particular cases. For example, the particular case in which p approaches zero and the motion of the damper piston is suppressed, ($C_t = \infty$) is described by

$$A_0 = A_6 = A_7 = 0$$
$$A_1 = CVK_0K_t + K_0LV$$
$$A_2 = K_0L^2 + K_t(H + r)^2 + WL^2(H + r) + I\omega V(H + r) - CVWI\omega L + C_1LVK_0$$
$$A_3 = LV[I_f - mH(H + r)] + CV[I_fK_t + I_sK_0 + I^2\omega^2 + WHmL^2] + C_1[K_0L^2 + K_t(H + r)^2 + WL^2(H + r) + I\omega V(H + r)]$$
$$A_4 = I_s(H + r)^2 + I_fL^2 - 2mL^2H(H + r) + C_1LV[I_f - mH(H + r)]$$
$$A_5 = CV[I_fI_s - m^2H^2L^2] + C_1[I_s(H + r)^2 + I_fL^2 - 2mL^2H(H + r)]$$

where $W = S + W_1$

NOTE: These equations now describe the physical system of the main landing gear because in this case the torsional motion of the wheel is opposed by the torsional elasticity of the strut. There is no damper. It is important to note that the main gear, although not freely swivelling, may shimmy if the stability criterion is not satisfied.

The criterion for neutral stability for this case is[1]

$$A_2A_3A_4 = A_1A_4^2 + A_2^2A_5 \tag{14}$$

and the associated sustained frequency becomes[1]

$$\omega^2 = A_2/A_4 \tag{15}$$

With the model damper locked and the surface speed adjusted until a neutrally stable oscillation is established, these expressions can be used to obtain two separate checks on the accuracy of the theory. Other special cases may be tested in a similar manner.

Table 1 contains a summary of the various nose-gear configurations for which over 2,000 analog studies and 100 model runs have been completed. For example, Case 1 describes a structure for which the torsional rigidity is infinite and the lateral motion of the strut is completely suppressed. Only the degrees of freedom described by the spindle swivel (θ) and the tire deflection (Δ) are present. For this simple case the coefficients of the general Eq. (13) reduce it to a third order equation,

$$pI_s\ddot{\theta} + CVI_s\dot{\theta} + L^2\dot{\theta} + LV\theta = 0$$

and for stability the product of the coefficients of the middle terms must exceed the product of the end terms, i.e., $LC > p$. This is the stability criterion advocated by Riekert and also by de Carbon. Case 2 differs from Case 1 only in the presence of the tire time delay factor C_1. It is obvious that the stability criterion for this system may upset the predictions for the simpler system. In Case 6 the pivot is allowed to have lateral motion (α) while the tire is assumed rigid ($p = 0$). The stability criterion is now markedly different from that given for Case 1. In particular, it is sensitive to changes in K_0, $I_{\bar{w}}$, and V, factors which do not appear in the simpler criteria. The influence of these factors can be demonstrated by model tests. Case 13 is a close approximation to the main gear structure. The stability criterion may be readily formed from the general equation by substitution of $p = 0$ and retaining only those terms which contain C_t.

TEST RESULTS

Since the equations given in the report[1] are expressed in nondimensional form, the problem of selecting the model parameters to represent any given prototype gear is simple. For example, the proper operating speed for the model is found by equating its nondimensional speed to that of the prototype. As shown on p. 17, reference 1, speed is nondimensionalized by multiplying it by C_c/K_tL. If the prototype and model dimensions are, respectively, $L = 5$ in. and 2 in., $K_t = 0.5 \times 10^6$ and 50, $I_{\bar{w}} = 3$ and 0.005, then for a prototype speed of 3,000 in./sec., the model speed is 295 in./sec. In this way over 100 model configurations simulating various airplane gears were tested. Typical results are shown in Figs. 13 and 14.

Fig. 13 compares the predicted values of shimmy frequency, Eq. (15), with the measured values on the model for several values of the torsional rigidity. It should be noted that the close agreement between the two extends over a range of parameters several times greater than that covered from the lightest type fighter

CASE	TORSIONAL RIGIDITY	LATERAL RIGIDITY	GYROSCOPIC EFFECT	TIRE YAW	TIRE COMPLIANCE	TIRE TIME-CONSTANT	VISCOUS DAMPING	DEGREES OF FREEDOM	ORDER OF EQUATION	STABILITY CRITERION $A_1A_2A_3 > A_0A_3^2 + A_1^2A_4$
1	∞	FIXED PIVOT	0	C	P	0	0	$\theta\ \Delta$	3	$LC > p$
2	∞	FIXED PIVOT	0	C	P	C_1	0	$\theta\ \Delta$	4	$LC > p + \frac{C_\alpha^2 L^2}{I_\theta}\left[1+\frac{C_1 V}{L}\right] - CC_1V$
3	∞	0	0	C	0	0	0	$\theta\ \alpha$	3	$\frac{I_\varpi}{L^2} + \frac{mr}{H+r} < 0$
6	∞	K_α	I	C	0	C_1	C_T	$\theta\ \alpha$	4	$A_0 = \frac{K_\alpha LV}{(H+r)^2}$ $A_1 = \frac{K_\alpha L^2}{(H+r)^2} + \frac{WL^2}{H+r} + \frac{IV^2WL}{r(H+r)^2}\left(\frac{H+r}{WL} - C\right) + \frac{K_\alpha LV}{(H+r)^2}\left(\frac{CC_T}{L} + C_1\right)$ $A_2 = VL\left[\frac{I_\theta}{(H+r)^2} - \frac{mH}{H+r}\right] + VC\left[\frac{(IV)^2}{r^2(H+r)^2} + \frac{WL^2mH}{(H+r)^2} + \frac{K_\alpha I_\theta}{(H+r)^2}\right] + C_1\left[\frac{IV^2}{r(H+r)} + \frac{WL^2}{H+r} + \frac{K_\alpha L^2}{(H+r)^2}\right] + C_T$ $A_3 = I_\varpi + \frac{I_\theta L^2}{(H+r)^2} - \frac{2mL^2H}{H+r} + \frac{CC_TVI_\theta}{(H+r)^2} + C_1\left[VL\left(\frac{I_\theta}{(H+r)^2} - \frac{mH}{H+r}\right) + C_T\right]$ $A_4 = \frac{VC(I_\theta I_\varpi - m^2L^2H^2)}{(H+r)^2} + C_1\left[I_\varpi + \frac{I_\theta L^2}{(H+r)^2} - \frac{2mL^2H}{H+r}\right]$
14	∞	K_α	I	0	0	0	C_T	$\theta\ \alpha$	3	$C_T > \frac{VI_\varpi}{L}\left[\frac{\frac{L^2}{I_\theta}\left(I_\theta + \frac{I_\theta L^2}{(H+r)^2} - 2\frac{mHL^2}{H+r}\right)\left(K_\alpha - \beta\frac{H+r}{L}\right)}{K_\alpha L^2 + (H+r)I\omega'V + (WL-\beta)(H+r)L} - \frac{I_\theta L^2}{I_\varpi(H+r)^2} + \frac{mHL^2}{I_\varpi(H+r)}\right]$
15	K_T	K_α	I	0	0	0	C_T	$\theta\ \theta_1\ \alpha$	4	USE HURWITZ CRITERION
13	K_T	K_α	I	C	0	C_1	LOCKED DAMPER	$\theta\ \alpha$	4	$A_1 = K_\alpha V(L+CK_T)$ $A_2 = K_\alpha L^2 + K_T(H+r)^2 + WL^2(H+r) + I(V^2/r)(H+r-WLC) + C_1K_\alpha LV$ $A_3 = LV(I_\theta - mH(H+r)) + VC(I_\theta K_T + I_\theta K_\alpha + I^2V^2/r^2) + C_1(K_\alpha L^2 + K_T(H+r)^2 + (H+r)IV^2/r) + CWL^2HmV + C_1WL^2(H+r)$ $A_4 = (H+r)^2I_\theta + I_\theta L^2 - 2mL^2H(H+r) + C_1LV(I_\theta - mH(H+r))$ $A_5 = CV(I_\theta I_\varpi - m^2L^2H^2) + C_1[(H+r)^2I_\varpi + I_\theta L^2 - 2mL^2H(H+r)]$
7	∞	K_α	I	C	P	0	0	$\theta\alpha\ \Delta$	5	ALL NORMAL CONFIGURATIONS UNSTABLE. "FIXED PIVOT" CRITERION APPLICABLE WHEN K_α EXCEEDS VALUE GIVEN BY HURWITZ CRITERION.
9	∞	K_α	I	C	P	C_1	C_T	$\theta\alpha\ \Delta$	6	USE HURWITZ CRITERION
12	K_T	K_α	I	C	P	C_1	C_T	$\theta\theta_1\alpha\ \Delta$	7	USE HURWITZ CRITERION

TABLE 1. Stability Criteria for Various Nosegear Configurations.

to the heaviest cargo planes (Runs 55, 111, 113, 114, 117, 118).

An even more searching test of the theory is its capacity to predict whether a given combination of parameters will produce a stable system. The ordinate of the plotted point of Fig. 14 is the ratio of the left to the right side of the stability equation, Eq. (14). The test was made by adjusting the drum speed of the model until a neutrally stable vibration was established. The measured model parameters were then used to compute the stability ratio. If both the theory and measurements were exact, this ratio would be unity. The absolute size of the error carries no meaning unless it is related to some significant parameter. For example, in Fig. 14, if a plotted point shows a stability ratio of 1.01, this 1 per cent error corresponds approximately to an error in damping of 1 per cent of the critical damping—i.e., the error could be corrected by a relatively small change in the measured damping. Equally accurate results have been obtained with the variation of other parameters such as trail, wheel mass, strut mass, and wheel load for both rigid wheels and rubber-tired wheels.

When the results shown in Fig. 13 and Fig. 14 are considered together, they provide conclusive evidence that the theoretical equations describe the model with satisfactory precision.

The Four-Degree-of-Freedom System

When an analog or digital computer is available, the complete 15-parameter nosegear system should be examined. Table 2 contains all the parameters for nine airplane configurations tested on the model. For each test the coefficient of damping (C_t) was held constant and the drum speed adjusted until a precisely neutral oscillation was established. The coefficients of Eq. (13) were then computed on an IBM Card Programmed Calculator by causing it to search automatically for the value of C_t which would satisfy Routh's criterion for neutral stability. As a further check on the accuracy of Eq. (13), the roots of the characteristic equation were computed, and from them the neutrally stable frequencies were found. The agreement between the experimental values and the theoretical values is within the limits of accuracy of the measurements.

By assigning various velocities and computing C_t, a complete graph similar to Fig. 6 can be constructed for each configuration. In this way, the most desirable proportions for the gear to achieve any degree of stability may be readily determined.

Following is a summary of the model test results:

(1) A nosegear can be made to operate in a completely stable manner with no artificial damping. This result was achieved with both the rubber-tired wheel and an aluminum wheel without a tire in complete accord with the theory. The stabilizing action is due to the gyroscopic and vertical load effects. Friction plays no measurable part in this remarkable action since both the spindle and pivot are mounted in nearly friction-free ball bearings. To further test this theory, the gyroscopic effect was increased by mounting a small high-speed gyro on the spindle with the result that the stability became greater as the speed of the auxiliary gyro was increased. The effect was even more dramatically demonstrated when, with no other changes in the system, the direction of rotation of the gyro was reversed resulting in an instantaneous and violent instability. Possible applications are being explored.

(2) Stabilizing effects are obtained by each of the following parameter changes: Decreasing the wheel moment of inertia; decreasing the lateral rigidity of the pivot; increasing the mass of the strut; increasing the torsional rigidity of the damper-system elasticity;

TABLE 2

Comparison of Observed and Theoretical Damping and Frequency for Nine Nosewheel Configurations

Parameter	Run Number								
	10	11	12	13	14	15	16	17	18
C	0.01								
P	0.006								
C_1	0.025								
W	20								
I	0.01	constant for all runs							
H	15.3								
r	2.7								
K_t	2,700								
L	0.5								
I_f	1.45	2.06	2.68	2.68	2.06	1.45	1.45	2.06	2.68
I_s	0.0169	0.0245	0.0322	0.0322	0.0245	0.0169	0.0169	0.0245	0.0322
m	0.0035	0.0061	0.0087	0.0087	0.0061	0.0035	0.0035	0.0061	0.0087
K_0	12,200	12,200	12,200	9,680	9,680	9,680	5,830	5,830	5,830
V	(stable)	59	38	30	50	127	187	63	40
C_t[1]	0.84	0.84	0.84	0.84	0.84	0.84	0.84	0.84	0.84
C_t[2]		0.88	0.88	0.83	0.85	0.91	0.88	0.88	0.91
f[3]	6.6	5.0	4.0	3.5	4.5	7.2	6.5	3.8	3.0
f[4]	6.8	5.0	3.9	3.3	4.3	6.8	6.4	3.7	2.9

[1] Measured damping coefficient.
[2] Theoretical damping coefficient given by Eq. (13).
[3] Measured shimmy frequency, cycles per sec.
[4] Theoretical shimmy frequency given by Eq. (13).

and by increasing the vertical load. Finally, increasing the drum speed is destabilizing except for artificially high gyroscopic parameters. All of these results are in accord with the theory.

(3) Qualitative check runs on de Carbon's stability criterion

$$(IRV^2 - a)(aD - T) > 0$$

were made as follows:

A wheel and tire combination for which $aD = 8T$ and $IRV^2 > a$ were placed on the model, and the system proved to be strongly stable in complete accord with de Carbon's rule. Then with no other changes in the system except a slight increase in the lateral rigidity of the pivot, the operation became unstable. This observation cannot be explained by the above stability criterion since it does not contain the lateral rigidity. Next, the lateral rigidity was adjusted to its original stable value, whereupon it was found that by *increasing* either I or V the oscillations became divergent in direct contradiction to the given stability criterion. These observations have been accepted by the research people who have witnessed them as proof of the inadequacy of a theory of shimmy based on the properties of the pneumatic tire alone.

Full-Scale Field Tests

The aircraft selected for these tests was the Fairchild C-119 cargo plane. Cumulative operating experience with this aircraft has demonstrated that its nosegear, though structurally sound, is only marginally stable. The particular plane on which the tests were conducted was susceptible to shimmy at speeds above 60 knots, and sustained oscillations could be readily induced at lower speeds by striking a $2^1/_2$-in. obstruction placed at a 45° angle to the runway. Examination of the hydraulic damping and steering system and a systematic check for backlash failed to reveal any abnormal conditions. An analysis of the C-119 gear on the basis of the WADC theory of shimmy indicated that the cause of the poor performance of this gear was to be found in the unfavorable proportions of four structural features, the most severe of which was the excessive diametral moment of inertia of the wheel proper. The nondimensional inertia ratio—which, in general, should not exceed unity—is approximately 6 for the C-119. This high value together with the unfavorable trail ratio describes, as shown on p. 32, reference 1, a system which cannot be stabilized regardless of the amount of viscous damping employed. In practice, of course, the presence of Coulomb damping does permit stable, but generally undependable, operation.

The experimental program was planned to provide a series of modifications to the gear and to conduct instrumented taxi runs to determine the influence on stability and frequency of each of the alterations. The first instrumented run was made with the normal configuration and resulted in an accident. The oscillograph records, however, were intact. The divergent oscillations began at a speed of 60 knots. The runway obstacle was struck two seconds later, resulting in an increased rate of divergence. In less than two additional seconds, the amplitude built up sufficiently to shear off the damper anchor bolts. The entire airplane then shook violently until its forward motion was arrested. As indicated above, theoretical analysis shows that the most significant factor in determining stability is the diametral moment of inertia of the wheel. To test this point a 34-in. wheel was substituted for the original 44-in. wheel which represented a reduction in moment of inertia of 65 per cent. The first run was made at a speed of 60 knots and when no shimmy was observed the speed was increased to 120 knots with no tendency toward instability. The next series of runs was made striking the runway obstacle at speeds up to 100 knots. Shimmy could not be induced, and the oscillograph records showed a rapid attenuation of the oscillation following the impact.

The actual trail on the C-119 is 5.5 in. Its nondimensional value is 0.41. Under these circumstances increasing the trail should be destabilizing [p. 32, Ref. (1)]. The results of tests conducted with a 7.91-in. trail showed shimmy starting at lower taxi speeds and rapidly reaching greater amplitudes than with the 5.5-in. trail. (It may be noted that these results are again in conflict with the predictions based on the rule given by de Carbon which indicate greater stability for moderate increase in trail.)

When the inertia ratio is high, it is predicted that the system will be unstable for very large values of C_t as well as for values below a given amount. To examine this point a series of tests were conducted using damper orifice sizes of 0.042 in., 0.0625 in., 0.086 in., 0.125 in., 0.156 in., and 0.188 in. For both the smallest orifice (high damping) and largest the shimmy was uncontrollable; it occurred at lower taxi speeds and diverged more rapidly, even without striking the obstacle, than was the case with the intermediate sizes.

A nosegear structure which is unstable because of a high inertia ratio can be stabilized by increasing the torsional rigidity (K_t) of the damper system. This is not the most efficient method because on an existing structure it is accompanied by an increase in weight and, as shown by Eq. (6A) above, requires somewhat greater damping. For the C-119 tests, a 20% increase in torsional rigidity was obtained by replacing the production scissors links with links of considerably greater weight and cross section. Results showed a slight but definite improvement in stability indicated by the higher speeds reached before the onset of self-sustained oscillations and greater attenuation of shock disturbances below these speeds.

No attempt was made to decrease the lateral rigidity of the strut to improve the stability as indicated by the theory. But in one test, the lateral rigidity was increased by restraining the motion of the top of the strut

by angle irons riveted to a crossbeam. This structure was destroyed during the first taxi run. Whether this was due to the added vigor of the shimmy or to structural weakness is not known. However, it was felt that it would be unsafe to pursue this particular type of test on an already unstable structure. (A 1948 Boeing investigation (D-9361) confirms in considerable detail the conclusion that stability is increased by decreasing the lateral rigidity.)

Fig. 15A (Run 4) is a trace of the oscillograph record taken at the damper link during the first of the tests described above. The nosegear configuration is normal, with its inertia ratio of approximately six. The system is obviously unstable and, in fact, the motion was divergent before striking the runway obstacle. Failure occurred shortly beyond this point.

Fig. 15B (Runs 17, 18, 19) is the oscillograph record taken at the same point as in 15A, but here the inertia ratio has been reduced to two. In this case, the runway obstacle was struck in an attempt to induce shimmy but the displacement was rapidly attenuated thus demonstrating the strong influence of the inertia ratio on stability.

Fig. 15C (Run 21) is the record obtained for the same configuration as in Fig. 15B but with the damping coefficient *increased* by reducing the damper orifice diameter. This is in accord with the theory wherein it is shown that for inertia ratios in excess of unity there is an upper limit of damping coefficient beyond which stability is not possible. As this condition is approached, stability is reduced as is apparent from the record.

Conclusions

(1) A stable landing gear that will show satisfactory attenuation of disturbances, without the risk of overdamping, can be obtained provided that the inertia ratio $I_w K_1/NK_t$ does not exceed unity.

(2) When the above condition is satisfied, the damping ratio required for neutral stability is closely approximated over a wide range of system parameters by

$$R = \frac{\dfrac{QS}{4(1+S)} - \dfrac{1}{Q} \pm \sqrt{\left[\dfrac{QS}{4(1+S)} - \dfrac{1}{Q}\right]^2 + 1}}{2} \qquad (6A)$$

(3) A precise description of all the essential phenomena of shimmy requires a mathematical model of 5 degrees of freedom, namely, tire deflection, swivel angle, strut deflection, damper-linkage strain, and airframe motion. Eq. (13) is the most accurate representation of the dynamics of this system that can be expressed in linear coefficients. It establishes a generalized concept of inertia ratio and supports the conclusions given in (1) and (2). This latter result is due in part to the cancellation of the stabilizing gyroscopic action by the yawing action of the pneumatic tire.

(4) Eq. (13) predicts the conditions under which corotating dual wheels are inherently stable. Although not usually susceptible to large-angle shimmy[7] this construction suffers severe fatigue loading due to wheel unbalance when the stability is marginal.

(5) A completely stable free-swivelling landing gear can be designed with no artificial damping when provided with sufficient gyroscopic momentum. Whether this goal is important, or even desirable, depends on the application. For example, if power steering is to be used, very high damping is a simple adjunct and the gear will be stable provided its inertia ratio can be made sufficiently small. For this case and also for the main gear, Eq. (13) should be used to check the stability of high-inertia systems, using an analog computer or Hurwitz criterion.

(6) The stability of a landing gear is influenced in varying degrees by 15 parameters. Eq. (13) predicts, and experiment confirms, the quantitative influence of each of these parameters.

References

[1] Moreland, W. J., *Landing Gear Vibration*, Air Force Tech. Rept. 6590, 1951.

[2] Bourcier de Carbon, C., *A Theoretical Study of the Shimmy of Airplane Wheels* (translated from the French), 1952, NACA TM 1337.

[3] Dengler, M., Goland, M., and Herrman, G., *A Bibliographic Survey of Automobile and Aircraft Wheel Shimmy*, WADC Tech. Rept. 52-141, 1951.

[4] Hadekel, R., *The Mechanical Characteristics of Pneumatic Tires: A Digest of Present Knowledge*, Brit. Min. Supply Tech. Info. Bur. TPA 3, March, 1950.

[5] Langhoar, H. L., *Dimensional Analysis and Theory of Models;* John Wiley & Sons, Inc., New York, 1951.

[6] Gardner and Barnes, *Transients in Linear Systems* (Hurwitz Form of Routh's Criterion, p. 197), John Wiley & Sons, Inc., New York, 1942.

[7] Maier, E., and Renz, M., *Shimmying Tests on Dual Wheels I: Model Tests* (in German), ZWB-FB-RE 1728, ATI No. 22381, January, 1943.

Development of Charts for Downwash Coefficients of Oscillating Wings of Finite Span and Arbitrary Plan Form

MAX A. DENGLER*
Northrop Aircraft, Inc.

SUMMARY

An outline is given for the development of downwash coefficient charts to be used for the theoretical prediction of circulatory spanwise loadings of oscillating wings of finite span. The charts are based on lifting line considerations which could be thought of as the logical extensions and generalizations of the Prandtl and Weissinger lifting line theories to unsteady state. The use of the charts should greatly simplify and facilitate the amount of computational effort generally involved in a flutter analysis. They seem to be fit for routine calculations in the hand of the aircraft engineer.

A brief outline of the determination of lift and moment coefficients of a finite span wing oscillating in bending and twist as well as of the complete flutter analysis is added to illustrate the practical use of the charts.

DISCUSSION

THE FUNDAMENTAL ideas of the present investigation are based on the nonsteady state lifting line theory for wings of finite span developed in reference 1. It is thought that this theory, which is restricted to incompressible flow and subsonic speeds, may be considered as the logical extension and generalization of the Prandtl and Weissinger lifting line theories from steady state to oscillatory wing motions. The basic aim of the theory is the prediction of spanwise circulatory loadings for wings of general form, specifically for tapered wings of high sweep and low aspect ratio as are of great interest in present-day aircraft design.

Spanwise variations of circulation are needed for calculations concerned with stability and flutter. The present analysis is an extension and modification of the aerodynamic theory of reference 1. It is a modification in the sense that some of the underlying aerodynamic principles of the wing vorticity model employed there have been radically changed. It is believed that this change constitutes a substantial improvement of the theory, as seen both from the mathematical and physical point of view. The most directly apparent effect of this modification is the absence of any bound vorticity correction factor in the new version. It is the intuition of the writer that the new vorticity model, designated as "alternative (1),"† is aerodynamically superior over the original version as contained in reference 1, designated as "alternative (2)"† from now on.

This should not mean that the latter one should now be completely abandoned. On the contrary, as derived from past investigations concerned with agreement between theory and experiment (Ref. 2) the conclusion must be drawn that alternative (2) yields values of satisfactory accuracy for flutter frequency and flutter speed. No numerical results for alternative (1), on the other hand, are as yet available. The present paper is concerned with both these alternatives.

The present investigation is an extension of the earlier work on the subject in two different respects. First, it is one of the inherent characteristics of A(1) that it is in no way restricted to the use of one single lifting line for the total wing vorticity, but permits equally well the use of any finite number of lifting lines spread out over the wing surface. A(2) is restricted to the use of one single lifting line by fundamental reasons. One of the outstanding consequences of these circumstances is the fact that A(1) may be applied to wings of very low aspect ratio, A(2) not.

The other aspect which distinguishes the present work from the contents of reference 1 is situated in a change of general perspective. This study is no more limited to purely theoretical considerations of aerodynamic character but intends to pursue the theory all the way down to the numerical ends. The aim was to overbridge the gap between the theory itself and its application and to open the problem of the oscillating wing of finite span to the aircraft engineer. Seen from the practical side the heart of a flutter analysis is the determination of the spanwise variations of circulation due to the various modes present in the actual wing motion. The circulation is directly related to the distribution of downwash and the downwash velocities result from the vorticity of the flow. It becomes apparent at this point that it is the determination of the vorticity which should be systematized and simplified to the greatest possible extent. Downwash coefficients hence play a predominant role in any flutter analysis.

This should justify the main objective of the present study which is concerned with the preparation of charts and tables for downwash coefficients of an oscillating lifting surface corresponding to any assumed type of vibration. The fundamental idea underlying such a

Received January 19, 1954.

* Senior Aerodynamicist, Boundary Layer Research Department.

† Designated also as "A(1)" and "A(2)."

procedure is not new. The presently developed method has certain basic features in common with the principles of F. W. Diederich (Ref. 3) with regard to downwash coefficient charts for finite span wings in steady state.

The fundamental concept of the Diederich method is the use of a finite number of discrete rectangular horseshoe vortices arranged along the forward quarter-chord line, having distinct intensities and vortex trails extending downward to infinity, parallel to the direction of flow. The downwash induced by the vortex system is to be equal to the geometrical downwash of the wing motion assumed. This condition, called downwash condition from here on, should be satisfied at all points of a lifting surface. An approximative solution of reasonable accuracy is obtained if the criterion is satisfied at a selected sequence of wing points only, the latter to be called downwash points. It follows from theoretical arguments of Weissinger, Pistolesi and others that favorable approximations should be obtained if only a few discrete points at the rear quarter-chord line are taken as downwash points.

It was analyzed in reference 1 that these same three-quarter chord points should yield good approximations to the solution of the underlying integro-differential equation for the circulation also in the corresponding case of oscillatory motion if at the same time rectangular horseshoe vortices of oscillatory intensity are aligned along the forward quarter-chord of the wing. A(2) is based on this scheme. There is, on the other hand, no reason why the total wing vorticity should be represented by a single lifting line only. A(1) accordingly permits the use of a finite number of elementary vortices arranged along lifting lines (vortex lines) extending in spanwise direction over the surface. Downwash points have now to be specified at more than one line, the number of downwash lines being equal to the number of vortex lines and the total number of downwash points being equal to the total number of vortices. There are reasons that also in this case the $(c/4)$-line should be retained as one of the vortex lines (the principal one) and that the $(3c/4)$-line should be kept as one of the downwash lines (the principal one). The question where to place the others is difficult to answer. The specific choice should not matter too much, but further theoretical clarification of this point would seem desirable. The basic intuition of the present theory is that the validity of the results must increase with the number of vortex lines and the number of vortices composing them as long as the $(c/4)$-line is maintained as the principal vortex line and the $(3c/4)$-line is retained as the principal downwash line.

The total induced downwash due to the whole system of vortices is to be equal to the geometrical downwash corresponding to the assumed wing oscillations, at any of the downwash points. If the idea of narrow-span horseshoe vortices is applied to harmonic oscillations, a new parameter related to the reduced frequency of the oscillation enters the picture. While one single chart is sufficient to represent downwash coefficients in steady state (Ref. 3), a number of charts for different values of the frequency parameter is needed to serve the same purpose in unsteady state. How this may be done in the perspective of efficient design procedures in the hand of the flutter engineer will be shown. It will become apparent then that the advantages of the rectangular short-span horseshoe vortices which are characteristic for steady state calculations are even more pronounced in unsteady state considerations. These advantages are linked to the fact that such vortices may be employed in case of low aspect ratio wings (e.g., delta wings) just as well as in the case of high aspect ratio wings (e.g., the "Scorpion" and other low drag airfoils). The feature that all of the elementary vortices do have the same span permits a scheme of nondimensionalization which makes them applicable to wings of any actual dimensions.

The bound vortex sections of the vortices are directed normally to the direction of flow and hence approximate the lifting lines in a staircase-like manner. Errors from this source introduced into the numerics should be of minor importance only in the light of other more severe simplifications of the theory as a whole as are the assumptions of prevailing potential flow and the neglect of all viscous effects in general. The use of one or two vortex lines, each carrying eleven vortices, should be sufficient in most cases. Increase of the number of vortex lines and the number of elementary vortices will increase the accuracy of the solution but, of course, the computational labor at the same time. Symmetrical wing oscillations may be analyzed as well as nonsymmetrical ones.

The vortex schemes according to both alternatives are shown in Figs. 2 and 6. Local semichord is b, root semichord is b_0, and wing tip semichord is b_T. Wing semispan is s and aspect ratio is $AR = (\text{span } 2s)^2/\text{planform area}$. Wing and wake points are referred to a Cartesian coordinate system (x, y) with center at point of intersection of forward quarter-chord and wing axis of symmetry, the x-axis extending downstream and the y-axis being directed normally to direction of flow. A dimensionless spanwise coordinate is introduced according to $y = \eta \cdot s$. The angle of sweep φ is supposed to be defined by the inclination of the local tangent on the $(c/4)$-line. Sweep is constant in case of a tapered wing. As seen from Figs. 2 and 6, all elementary vortices have the same span, $2r$. Middle points of the bound-vortex sections will be called vortex centers. They are located at the same spanwise wing stations as the downwash points. Vortices are numbered by $n_{1,i}, n_{2,i}, \ldots$, downwash points by $m_{1,i}, m_{2,i}, \ldots$. Coordinates of the forward quarter-chord line measured at the specified wing stations are denoted by p_i and q_i.

The theory of the oscillating airfoil requires that the wake of any of the elementary vortices building up the wing vorticity distribution starts at the trailing edge point. The theory of reference 1 deliberately intro-

duces the assumption that the wakes of the vortices start at the respective quarter-chord points. This simplification considerably reduces the mathematical complexity. It was reasoned, on the other hand, that the inaccuracy or "error" introduced from this source could be compensated satisfactorily by introduction of a bound-vorticity correction factor $n(k)$ which would be independent of the specific wing motion and dependent only on the reduced frequency k of the oscillation. Numerical results deduced on this basis (Ref. 2) seem to justify this hypothesis. However, any "correction term" whatsoever should be eliminated from a theory if possible. This idea was the guiding thought for the formulation of an alternative vorticity model (A(1)) which will be developed now.

According to the theory of the oscillating airfoil in two-dimensional motion developed by Cicala, Glauert, Küssner, Reissner, and Theodorsen the velocity distribution of an airfoil in incompressible flow may be conceived as being induced by a system of vorticity spread out over the lifting surface and its wake. The vorticity moving with the surface is called bound vor-

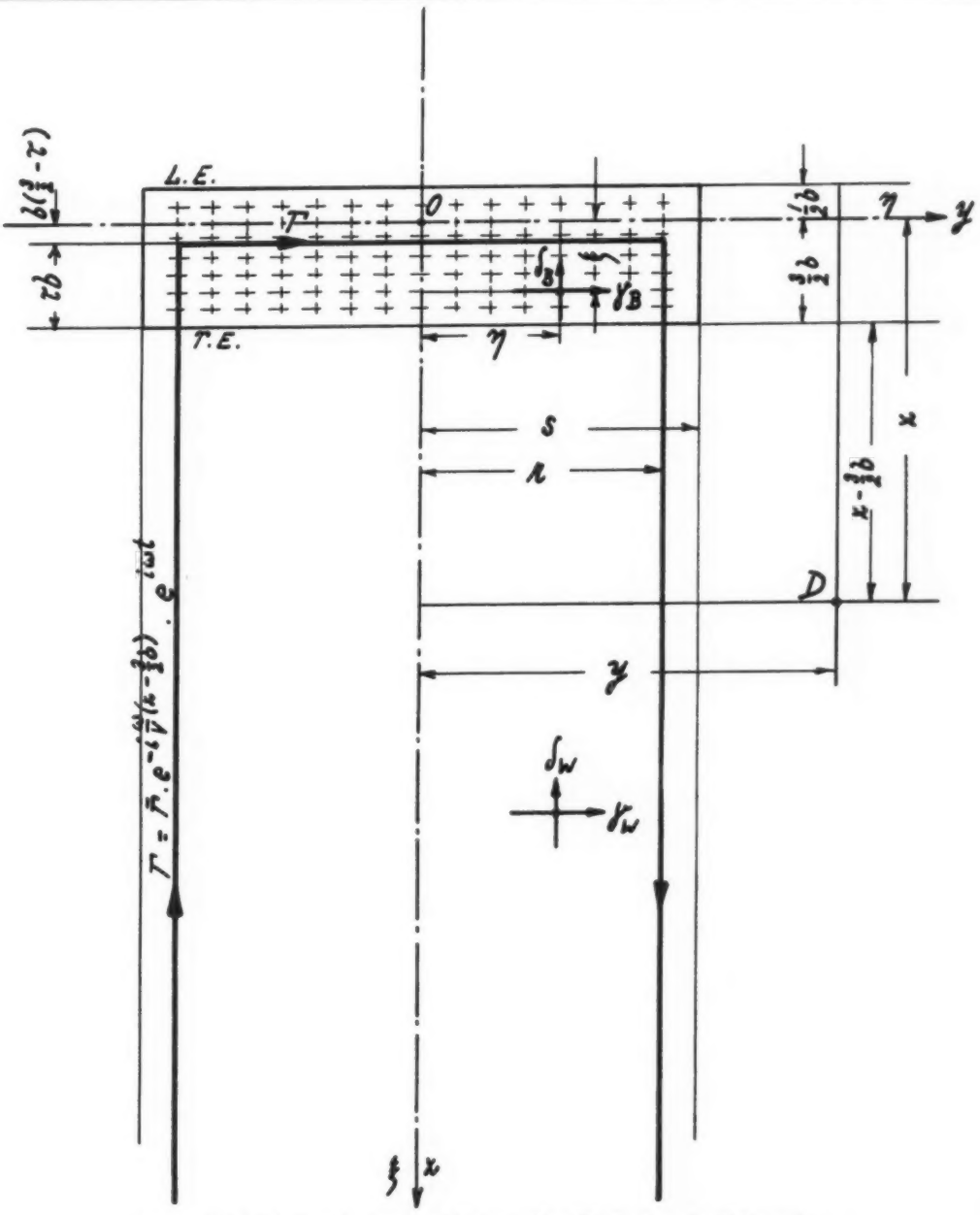

FIG. 1. The fundamental properties of the vorticity distribution of a lifting surface.

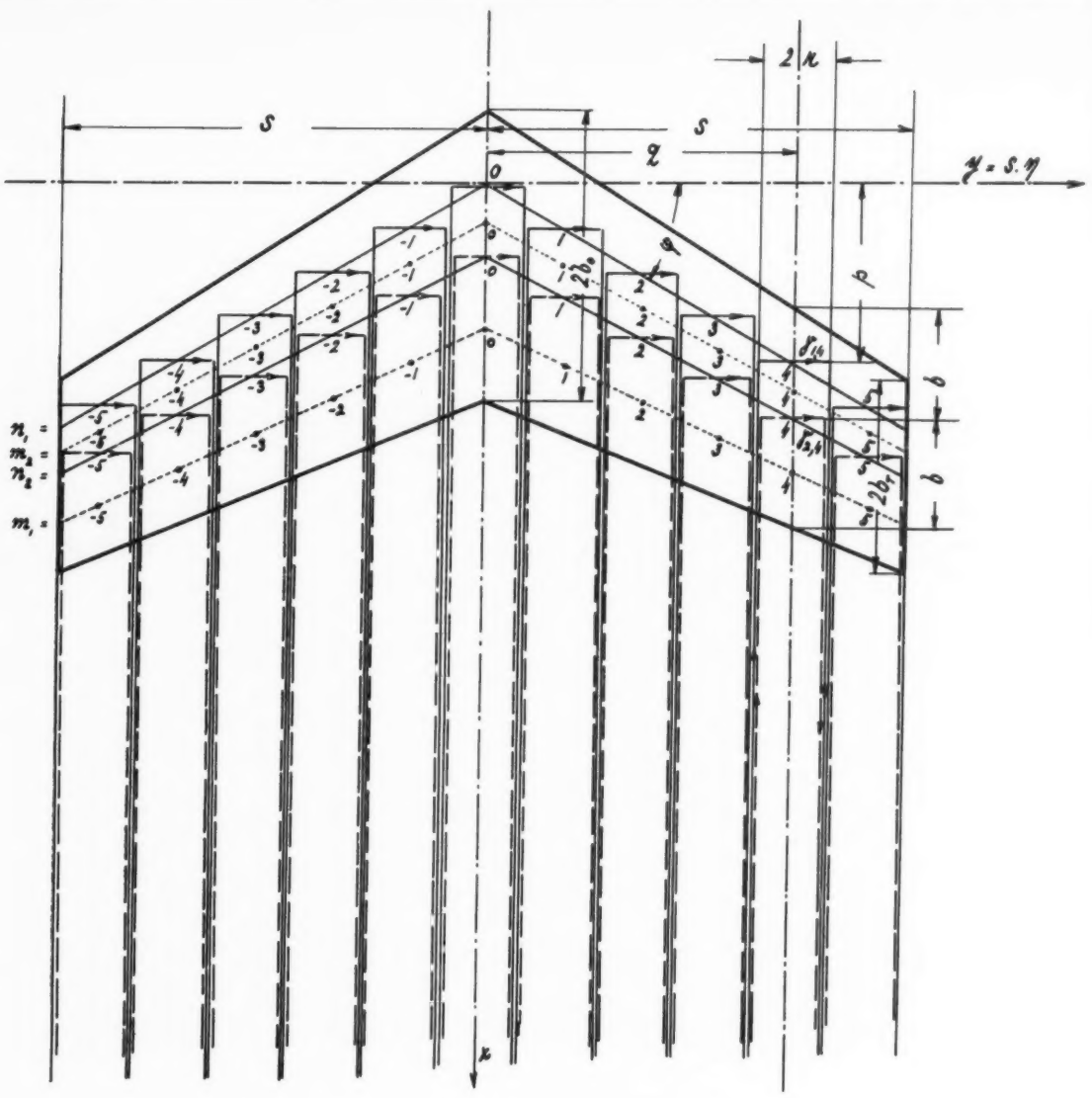

FIG. 2. Wing vorticity diagram corresponding to two lifting lines, based on alternative (1).

ticity; the vorticity which is shed periodically at the trailing edge and is not participating in the wing motion is called wake vorticity. If components of the vorticity normal to and parallel to the direction of forward motion are denoted by $\gamma = \bar{\gamma} \cdot e^{i\omega t}$ and $\delta = \bar{\delta} \cdot e^{i\omega t}$, ξ and η designating Cartesian coordinates as in Fig. 1, they obey the relation

$$\partial \bar{\gamma}(\xi, \eta)/\partial \eta = \partial \bar{\delta}(\xi, \eta)/\partial \xi \tag{1}$$

at any point of the lifting surface and any point of the wake. The subscript B standing for bound vorticity and the subscript W for wake vorticity, the distribution of $\bar{\delta}_B(\xi, \eta)$ follows immediately once the distribution of $\bar{\gamma}_B(\xi, \eta)$ is known:

$$\bar{\delta}_B(\xi, \eta) = \int_{-b_0/2}^{\xi} \{\partial \bar{\gamma}_B(\xi, \eta)/\partial \eta\}\, d\xi \tag{2}$$

The wing circulation Γ on the other hand is

$$\Gamma = \bar{\Gamma} \cdot e^{i\omega t} = \int_{-b_0/2}^{3b_0/2} \bar{\gamma}_B(\xi, \eta)\, d\xi \cdot e^{i\omega t} = b\Omega \cdot e^{-i\omega b_0/V} \tag{3}$$

where Ω, as usual, is the circulation function. The analysis of the mechanism of vorticity shed at the trailing edge leads to the further relations

$$\bar{\gamma}_W = -i\,\frac{\omega}{V}\,\bar{\Gamma} \cdot e^{-i(\omega/V)[\xi - 3(b_0/2)]} \tag{4}$$

$$\bar{\delta}_W = \frac{\partial \bar{\Gamma}(\eta)}{\partial \eta} \cdot e^{-i(\omega/V)[\xi - 3(b_0/2)]} \tag{5}$$

and it is seen that also the wake vorticity components satisfy relation (1). Due to the absolute analogy between the magnetic field induced by an electric current flowing in a closed wire on the one hand and the velocity distribution induced by a field of a three-dimensional line vortex on the other, the induced downwash is determined by the law of Biot and Savart and for a rectangular wing is therefore given by

$$4\pi \cdot V \cdot w^{(i)}(x, y) \cdot e^{i\omega t} = \int_{-s}^{s} \left\{ \int_{-b_0/2}^{3b_0/2} \frac{\tilde{\gamma}_B(\xi, \eta)\,(x - \xi) + \tilde{\delta}_B(\xi, \eta)\,(y - \eta)}{\left\{(x - \xi)^2 + (y - \eta)^2\right\}^{3/2}}\, d\xi \right\} d\eta \cdot e^{i\omega t} + \int_{-s}^{s} \left\{ \int_{3b_0/2}^{\infty} e^{-i(\omega/V)[\xi - (3/2)b_0]} \cdot \frac{(-i\omega/V)\bar{\Gamma}(\eta)\,(x - \xi) + \left\{d\bar{\Gamma}(\eta)/d\eta\right\}\,(y - \eta)}{\left\{(x - \xi)^2 + (y - \eta)^2\right\}^{3/2}}\, d\xi \right\} d\eta \cdot e^{i\omega t} \tag{6}$$

Assume now the wing vorticity consists of a single horseshoe vortex as indicated in Fig. 1 and that, accordingly, the bound vorticity components are

$$\tilde{\gamma}_B(\xi, \eta) = \begin{cases} b_0 V\,\gamma/\epsilon \ldots . & -r < \eta < +r \\ & b_0[(3/2) - \tau] < \xi < b_0[(3/2) - \tau] + \epsilon \\ 0 \quad \ldots . & \text{at all other points of the wing} \end{cases} \tag{7}$$

$$\tilde{\delta}_B(\xi, \eta) = \begin{cases} b_0 V\,\gamma/\epsilon \quad \ldots . & -r < \eta < -r + \epsilon,\ b_0[(3/2) - \tau] < \xi < b_0(3/2) \\ 0 \quad \ldots . & \text{at all other points of the wing} \\ -b_0 V\gamma/\epsilon \ldots . & r < \eta < r + \epsilon,\ b_0[(3/2) - \tau] < \xi < b_0(3/2) \end{cases} \tag{8}$$

The contribution to the total induced downwash velocity $4\pi \cdot V \cdot e^{i\omega t} \cdot w^{(i)}(x, y)$ arising in the bound vorticity then becomes, for $\epsilon \to 0$,

$$\frac{4\pi \cdot V \cdot e^{i\omega t} \cdot w_B{}^{(i)}(x, y)}{(b_0 V\gamma)} = e^{i\omega t} \left[\int_{-r}^{r} \left\{ (1/\epsilon) \int_{b_0[(3/2) - \tau]}^{b_0[(3/2) - \tau] + \epsilon} \frac{(x - \xi)}{\left\{(x - \xi)^2 + (y - \eta)^2\right\}^{3/2}}\, d\xi \right\} d\eta + \int_{-r}^{-r + \epsilon} \left\{ (1/\epsilon) \int_{b_0[(3/2) - \tau]}^{b_0(3/2)} \frac{(y + r)}{\left\{(x - \xi)^2 + (y + r)^2\right\}^{3/2}}\, d\xi \right\} d\eta + \int_{r}^{r + \epsilon} \left\{ (1/\epsilon) \int_{b_0[(3/2) - \tau]}^{(b_0(3/2)} \frac{(-1) \cdot (y - r)}{\left\{(x - \xi)^2 + (y - r)^2\right\}^{3/2}}\, d\xi \right\} d\eta \right] \tag{9}$$

or

$$4\pi \cdot V \cdot w_B{}^{(i)}(x, y)/b_0 V\gamma = \int_{-r}^{r} \frac{\left\{x - b_0[(3/2) - \tau]\right\}}{<\left\{x - b_0[(3/2) - \tau]\right\}^2 + (y - \eta)^2>^{3/2}}\, d\eta + \int_{b_0[(3/2) - r]}^{3b_0/2} \frac{(y + r)}{<(x - \xi)^2 + (y + r)^2>^{3/2}}\, d\xi - \int_{b_0[(3/2) - r)]}^{3b_0/2} \frac{(y - r)}{<(x - \xi)^2 + (y - r)^2>^{3/2}}\, d\xi \tag{10}$$

$$4\pi \cdot V \cdot w_B{}^{(i)}(x, y)/b_0 V\gamma = \frac{1}{x - z} \left\{ \frac{(y + r)}{\sqrt{(x - z)^2 + (y + r)^2}} - \frac{(y - r)}{\sqrt{(x - z)^2 + (y - r)^2}} \right\} - \frac{1}{y + r} \left\{ \frac{(x - 3b_0/2)}{\sqrt{(x - 3b_0/2)^2 + (y + r)^2}} - \frac{(x - z)}{\sqrt{(x - z)^2 + (y + r)^2}} \right\} + \frac{1}{y - r} \left\{ \frac{(x - 3b_0/2)}{\sqrt{(x - 3b_0/2)^2 + (y - r)^2}} - \frac{(x - z)}{\sqrt{(x - z)^2 + (y - r)^2}} \right\} \tag{11}$$

where

$$z = b_0[(3/2) - \tau] \tag{12}$$

The downwash contribution due to the wake vorticity is of the form

$$4\pi \cdot V \cdot w_W{}^{(i)}(x, y)/b_0 V\gamma = \int_0^{\infty} e^{-i\omega\lambda/V} \frac{(y + r)}{\left\{(x - 3b_0/2 - \lambda)^2 + (y + r)^2\right\}^{3/2}}\, d\lambda - \int_0^{\infty} e^{-i\omega\lambda/V} \frac{(y - r)}{\left\{(x - 3b_0/2 - \lambda)^2 + (y - r)^2\right\}^{3/2}}\, d\lambda - (i\omega/V) \int_{-r}^{r} \left\{ \int_0^{\infty} e^{-i\omega\lambda/V} \frac{(x - 3b_0/2 - \lambda)}{\left\{(x - 3b_0/2 - \lambda)^2 + (y - \eta)^2\right\}^{3/2}}\, d\lambda \right\} d\eta \tag{13}$$

$$4\pi \cdot V \cdot w_W^{(i)}(x, y)/b_0 V\gamma = \left\{ \frac{(x - 3b_0/2)}{(y + r)\sqrt{(x - 3b_0/2)^2 + (y + r)^2}} - \frac{(x - 3b_0/2)}{(y - r)\sqrt{(x - 3b_0/2)^2 + (y - r)^2}} \right\} -$$
$$\left\{2r/(y^2 - r^2)\right\} \cdot e^{-i(\omega/V)\,[x\,-\,(3b_0/2)]} - \frac{i\omega}{V} \cdot e^{-i(\omega/V)\,[x\,-\,(3b_0/2)]} \left(\left\{ \frac{(y + r)}{|y + r|} - \frac{(y - r)}{|y - r|} \right\} \cdot \right.$$
$$\left\langle i\pi/2 + i \cdot Si\left\{ \frac{\omega}{V}(x - 3b_0/2) \right\} + Ci\left\{ \frac{\omega}{V}(x - 3b_0/2) \right\} \right\rangle + \left\langle \frac{(y + r)}{|y + r|} \cdot F\left\{ \frac{\omega}{V}|y + r| \right\} - \right.$$
$$\frac{(y - r)}{y - r} \cdot F\left\{ \frac{\omega}{V}|y - r| \right\} \Big\rangle + \left\langle \frac{(y + r)}{|y + r|} \cdot S\left\{ \frac{x - 3b_0/2}{|y + r|}, \frac{\omega}{V}|y + r| \right\} - \right.$$
$$\left. \left. \frac{(y - r)}{|y - r|} \cdot S\left\{ \frac{x - 3b_0/2}{|y - r|}, \frac{\omega}{V}|y - r| \right\} \right\rangle \right) \quad (14)$$

where $Si(t)$ and $Ci(t)$ are the familiar functions "Sinus Integralis" and "Cosinus Integralis," $F(t)$ is the Cicala Function

$$F(t) = (1/t) \int_0^\infty e^{-is} \left\{1 - (\sqrt{s^2 + t^2} - t)/s\right\} ds \quad (15)$$

and S is defined by

$$S(a, t) = \int_0^a e^{its} \left(\left\{\sqrt{(s^2 + 1)} - 1\right\}/s\right) ds \quad (16)$$

Assume now that new variables u, v, μ, and σ are introduced according to

$$(x - 3b/2) = r \cdot u + p, \qquad y = r \cdot v + q \quad (17)^*$$

$$\mu = (r/b)k = \omega r/V, \qquad \sigma = (b/r)\tau \quad (18)^*$$

The total induced downwash, obtained by combination of wing and wake contributions, may then be written in the form

$$\frac{4\pi}{\gamma} \cdot \frac{r}{b_0} \cdot w^{(i)}(x, y) = \frac{1}{(u + \sigma)} \left\{ \frac{\sqrt{(u + \sigma)^2 + (v + 1)^2}}{(v + 1)} - \frac{\sqrt{(u + \sigma)^2 + (v - 1)^2}}{(v - 1)} \right\} -$$
$$i\mu \cdot e^{-i\mu u} \left(\frac{-i}{\mu} \frac{2}{(v^2 - 1)} + \left\{ \frac{(v + 1)}{|v + 1|} - \frac{(v - 1)}{|v - 1|} \right\} \left\{ i\pi/2 + i \cdot Si(\mu u) + Ci(\mu u) \right\} + \right.$$
$$\left\{ \frac{(v + 1)}{|v + 1|} \cdot F(\mu|v + 1|) - \frac{(v - 1)}{|v - 1|} \cdot F(\mu|v - 1|) \right\} + \left\langle \frac{(v + 1)}{|v + 1|} \cdot S\left\{ \frac{u}{|v + 1|}, |v + 1|\mu \right\} - \right.$$
$$\left. \left. \frac{(v - 1)}{|v - 1|} \cdot S\left\{ \frac{u}{|v - 1|}, (v - 1|\mu \right\} \right\rangle \right) = w^*(\sigma, \mu, u, v) \quad (19)$$

After a few more algebraic transformations the induced downwash appears as

$$\frac{4\pi}{\gamma} \cdot \frac{r}{b_0} \cdot w^{(i)}(x, y) = \frac{1}{(u + \sigma)} \cdot \left\{ \frac{\sqrt{(u + \sigma)^2 + (v + 1)^2}}{(v + 1)} - \frac{\sqrt{(u + \sigma)^2 + (v - 1)^2}}{(v - 1)} \right\} + D^*(\mu, u, v) \quad (20)$$

where

$$D^*(\mu, u, v) = \frac{1}{(v + 1)} \left[e^{-ib_1 g_1} \left(1 - \frac{ib_1}{2} \log \left\{ \frac{g_1}{1 + \sqrt{(1 + g_1^2)}} \right\}^2 \right) - iD(g_1, b_1) \right] -$$
$$\frac{1}{(v - 1)} \left[e^{-ib_2 g_2} \left(1 - \frac{ib_2}{2} \log \frac{g_2}{1 + \sqrt{(1 + g_2^2)}} \right\}^2 \right) - iD(g_2, b_2) \right] \quad (21)$$

$$D(g, b) = e^{-ibg} \left\{ < b\pi/2 + b \cdot Im\left\{F(b)\right\} + B(gb, b) > i + < b\sqrt{(1 + g^2)} + b[Re\left\{F(b)\right\} + \right.$$
$$\left. \log(2b) + \psi - 1] - A(gb, b) > \right\} \quad (22)$$

$$A(gb, b) = \int_0^{gb} (1 - \cos u) \left\{\sqrt{(u^2 + b^2)}/u\right\} du \quad (23)$$

$$B(gb, b) = \int_0^{gb} (\sin u) \left\{\sqrt{(u^2 + b^2)}/u\right\} du \quad (24)$$

* The b appears here the first time as compared to the b_0, p and q are the coordinates of the vortex center, and k is the local reduced frequency.

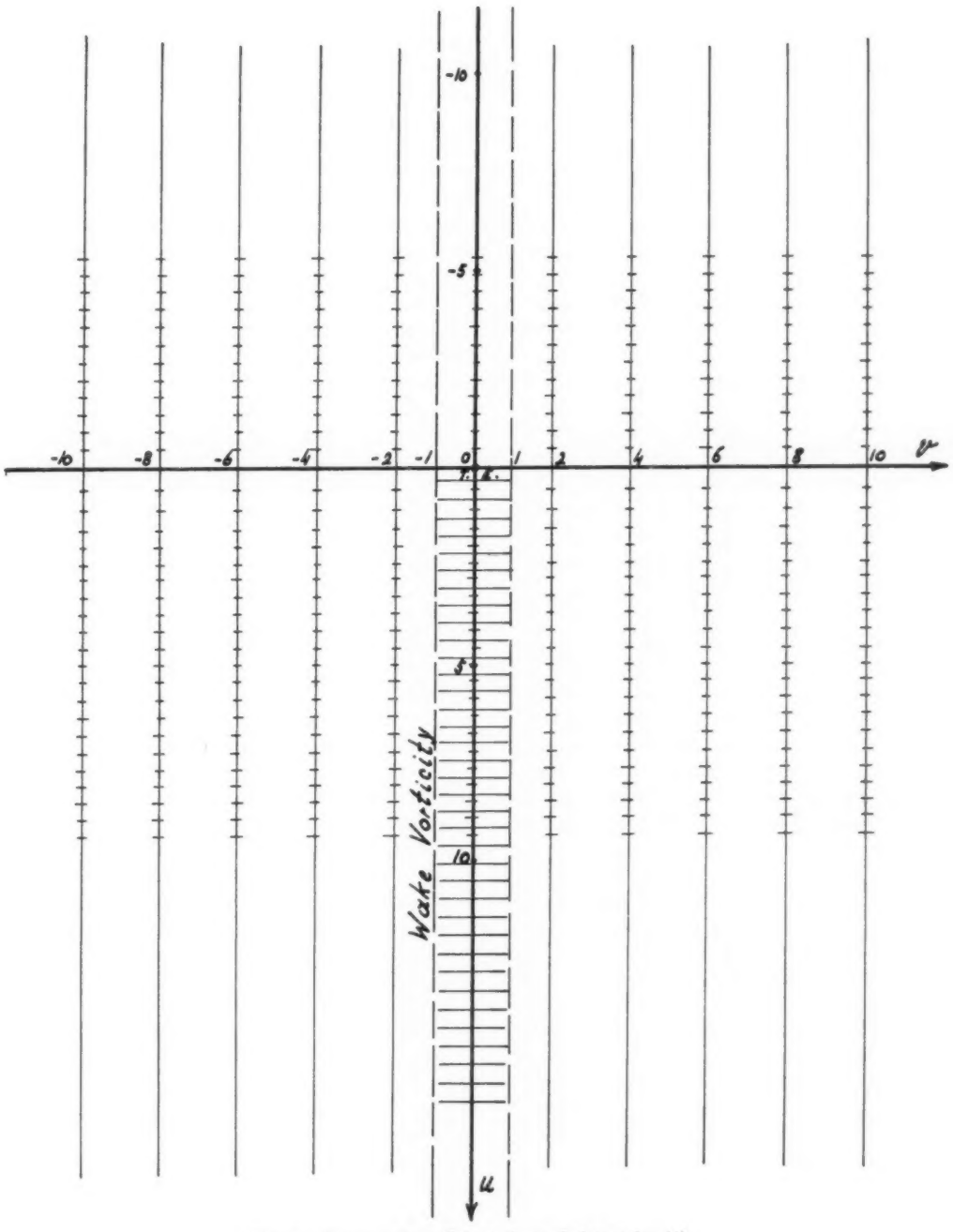

FIG. 3. Downwash coefficient chart of alternative (1).

$$Re\{F(b)\} \text{ and } Im\{F(b)\} \ldots \text{real and imaginary parts of the Cicala Function, Eq. (15)} \quad (25)$$

$$\psi = 0.5772157 \ldots \text{ Euler's Constant} \quad (26)$$

$$b_1 = \mu|v + 1|; \qquad b_2 = \mu|v - 1| \quad (27)$$

$$g_1 = u/|v + 1|; \qquad g_2 = u/|v - 1| \quad (28)$$

The Cicala Function has been tabulated by various authors (Ref. 5). Tables of the functions $A(gb, b)$ and $B(gb, b)$ are found in reference 4. The reasons for these purely mathematical transformations are evident: the "D-Function $D(g, b)$" comprises all the principal transcendental terms of the downwash expressions. It is a function of two parameters only while covering the range of the three independent parameters μ, u, and v. And finally, it does not possess any singularity.

Based on the foregoing mathematical developments downwash coefficient charts may now be developed for alternative (1) as follows.

Consider the vorticity distribution of a tapered swept wing as shown in Fig. 2. There are two vortex lines, located at $(c/4)$ and $(c/2)$, each carrying eleven elementary vortices. There are two downwash lines located at $(3c/4)$ and $(3c/8)$. Assume there is a chart (Fig. 3) prepared for a specific value of the frequency parameter $\mu = kr/b$, containing numerous entries of $D^*(\mu, u, v)$ for various positive and negative values of u and $v = \ldots, -10, -8, -6, -4, -2, 0, +2, +4, +6, +8, +10, \ldots$, the numbers $D^*(\mu, u, v)$ being located exactly at the geometrical points (u, v). Assume the transparent chart is placed above the wing vorticity diagram (Fig. 2) in such a manner that the origin of the chart ($u = v = 0$) coincides with the trailing edge point of the wing station of the vortex considered (Fig. 4). If r was chosen as the unit of length in both diagrams and if the μ of the chart is the μ of the wing station considered, the major elements (i.e., D^*) of the induced downwash due to vortices of this wing station may be read off the chart, directly and for all wing downwash points. Adding the few more terms of Eq. (20) the complete downwash expressions are obtained. If the μ is not exactly the μ of the station, interpolation is to be employed.

It is evident from this that a great number for different values of μ are to be prepared in order to render the process efficient. There are needed so many charts that linear interpolation will yield results of satisfactory accuracy. After the procedure is completed for one of the wing stations (and all vortices of this station) it is to be repeated for all other stations. It will be noted that the coefficients $D^*(\mu, u, v)$ are independent of σ and hence identical for all vortices of one and the same wing station. This is a necessary consequence of the fact that they represent wake contributions. Adding up terms belonging together, the total induced downwash at each of the downwash points is obtained. Equating induced downwash and geometrical downwash, the latter being a mere consequence of the geometry of the wing motion, the as yet unknown vortex intensities are found and from there the spanwise circulation distributions. Magnitudes and positions of the local circulatory lift forces may be deduced from there according to known relations of the two-dimensional airfoil theory. The total aerodynamic forces and moments are obtained by adding the noncirculatory terms ("apparent mass and inertia terms") to the circulatory terms. Combining the aerodynamic characteristics of the wing with the geometrical and mechanical parameters the flutter analysis of the wing may now be developed along conventional lines, finally leading to the flutter frequency and flutter speed for incompressible flow. If the Mach Number of the flow is of moderate magnitude, results of satisfactory accuracy may be deduced from there by application of the Prandtl-Glauert Rule or other adequate compressibility corrections. The computational effort thus seems to be reduced to a minimum, the advantages of the downwash coefficient charts are evident and it is felt that they will be welcomed by the general aircraft engineer.

The development of the downwash coefficient charts for alternative (1) may now be considered as completed. The analysis will be continued by a brief discussion of the principal aerodynamic characteristics of the vorticity model of alternative (2) which was developed in reference 1 and successfully applied in a set of extensive flutter calculations aimed at comparisons between theory and experiment as are reported in reference 2. Of course only these few aspects will be analyzed where the vorticity model of A(2) differs basically from the model of A(1).

As was studied earlier it is an inherent property of the flow around an oscillating lifting surface that vorticity will be shed periodically at the trailing edge. In consequence, if a system of short-span horseshoe vortices is used to represent the wing vorticity, the wake of any of these vortices is to start at the trailing edge point of its station. This causes mathematical complications and it would be of computational advantage to shift the point where the wake is to start to the vortex center, i.e., to the forward quarter-chord point if a single lifting line located there is employed. The vorticity model thus obtained would not be adequate without further modifications compensating for the arbitrary change. The theory of reference 1 arrives at the conclusion that such a compensating modification may be accomplished along the lines of the following two principles:

(a) As far as wake vorticity contributions are concerned the arbitrary shift of the origin of the wake may be compensated by a multiplication of all wake terms by a factor $e^{(3/2)ik}$ (*a posteriori*, i.e., "outside the integrals").

(*b*) The bound vorticity terms should be multiplied (*a posteriori*) by a correction factor $n(k) \cdot e^{(3/2)ik}$ corresponding to the requirement that the downwash due to a three-dimensional vortex of strength γ at the three-

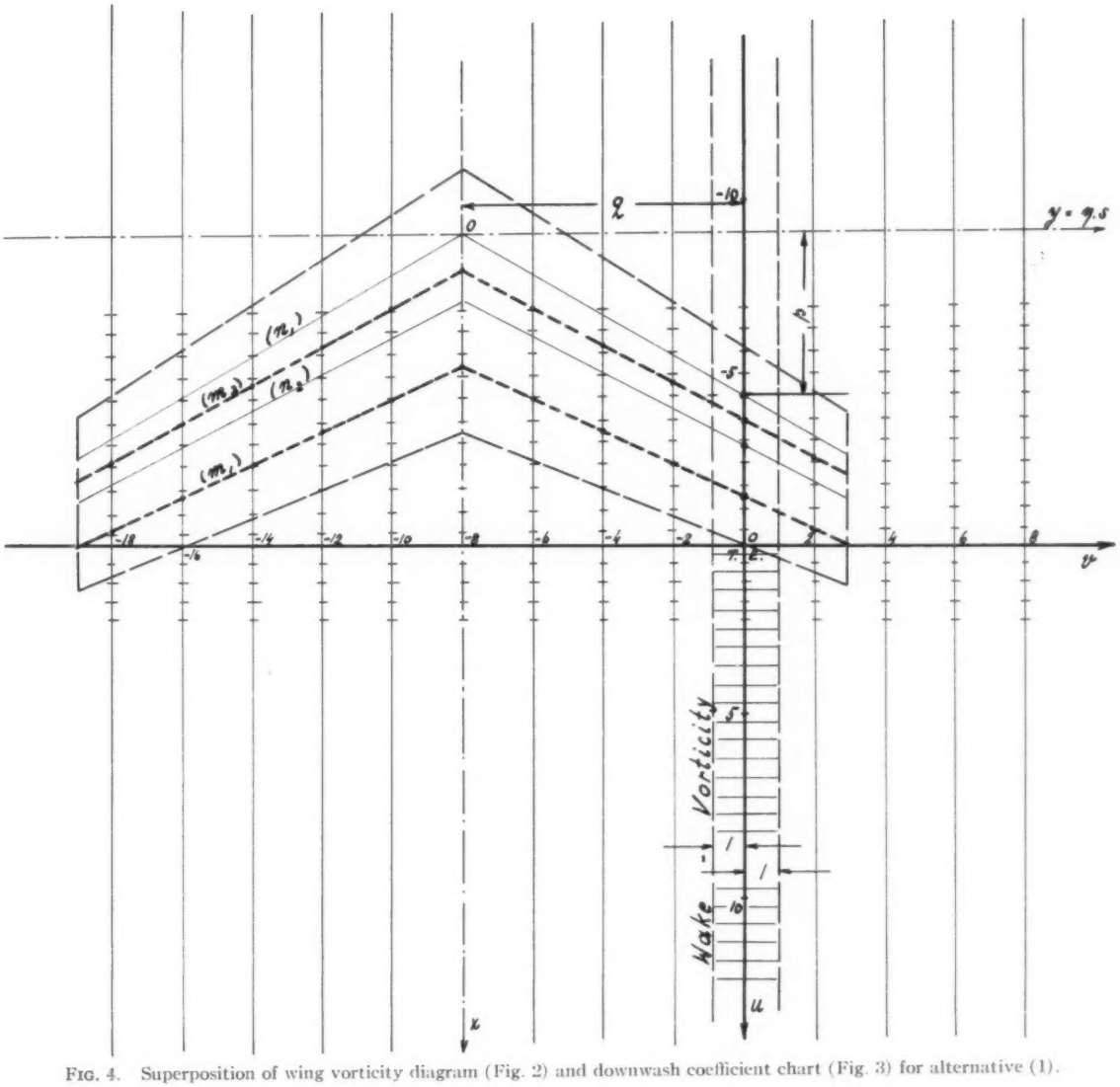

FIG. 4. Superposition of wing vorticity diagram (Fig. 2) and downwash coefficient chart (Fig. 3) for alternative (1).

quarter chord point of its station should be equal to the downwash due to a two-dimensional vortex of same strength induced at the same point.

One concludes then on the basis of known principles of the two-dimensional theory that

$$n(k) = e^{-ik/2} \cdot \frac{1}{2}\,\pi k \cdot \left\{H_0^{(2)}(k) - iH_1^{(2)}(k)\right\} + ike^{-ik}\left\{\frac{i\pi}{2} + i \cdot Si(k) + Ci(k)\right\} \quad (29)$$

Assume now that the two relations (17) defining dimensionless quantities u and v are changed into

$$x - p = u \cdot r; \qquad y - q = v \cdot r \quad (30)$$

while Eqs. (15) and (16) and Eqs. (22) to (28) remain unchanged. It can then be shown that the induced downwash of the vorticity model of alternative (2) becomes

$$(4\pi/\gamma)w^{(i)}(x, y)\ (r/b_0) = \left\langle \frac{1}{(v+1)}\left\{\frac{n(k)}{g_1\sqrt{(1+g_1^2)}}\right\} - \frac{1}{(v-1)}\left\{\frac{n(k)}{g_2\sqrt{(1+g_2^2)}}\right\}\right\rangle e^{3ik/2} + \left[\frac{1}{(v+1)} \cdot \left\langle \frac{g_1}{\sqrt{(1+g_1^2)}} + e^{-ib_1g_1}\left(1 - \frac{ib_1}{2}\log\left\{\frac{g_1}{1+\sqrt{(1+g_1^2)}}\right\}^2\right) - iD(g_1, b_1)\right\rangle - \frac{1}{(v-1)} \cdot \left\langle \frac{g_2}{\sqrt{(1+g_2^2)}} + e^{-ib_2g_2}\left(1 - \frac{ib_2}{2}\log\left\{\frac{g_2}{1+\sqrt{(1+g_2^2)}}\right\}^2\right) - iD(g_2, b_2)\right\rangle\right] e^{3ik/2} = n(k) \cdot e^{3ik/2} \cdot P(\mu, u, v) + e^{3ik/2} \cdot Q(\mu, u, v) \quad (31)$$

Downwash coefficient charts for the vorticity model of alternative (2) could now be developed along lines rather similar to the basic principles of the charts for alternative (1). The charts would now have to be prepared for the coefficients $Q(\mu, u, v)$ and, again, for various values of the frequency parameter μ. Assume now that a chart as shown in Fig. 7 contains numerous entries for $Q(\mu, u, v)$ placed along the "v-lines," i.e., for various values of u and even values of v. The vorticity diagram of the wing, on the other hand, should be as shown in Fig. 6. The transparent chart corresponding to a certain value of μ is now placed on top of the wing vorticity diagram in such a manner that the origin of the chart ($u = v = 0$) coincides with the forward quarter-chord point of the wing station of the considered vortex, i.e., with the point ($x = p$, $y = q$) (Fig. 8).

The downwash velocities due to this specific vortex induced at all the different downwash points (which are located at the rear quarter-chord line) may now be established by reading from the chart the coefficients $Q(\mu, u, v)$, adding $n(k) \cdot P(\mu, u, v)$ and multiplying the two terms by $e^{3ik/2}$ in line with relation (31). In most cases linear interpolation with respect to μ will be needed and many charts are to be prepared to render the method accurate and efficient.

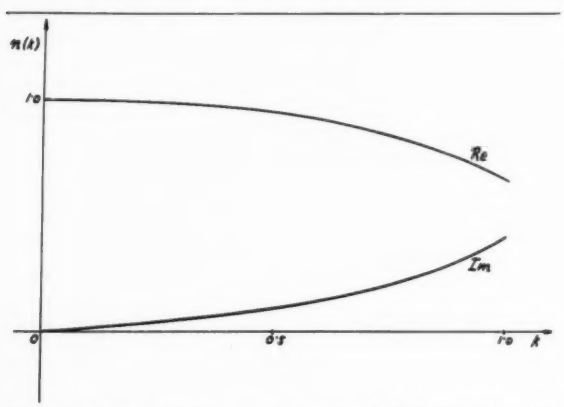

FIG. 5. Bound vorticity correction factor $n(k)$ of alternative (2).

The development of the downwash coefficient charts has now been completed. The next two paragraphs are to contain a brief outline of the derivation of lift and moment coefficients for a wing of finite span oscillating in bending and twist, as well as a complete flutter analysis based on these developments.

Consider a swept wing of a geometry as shown in Fig. 9. There are two Cartesian coordinate systems, (x, y) and (x_φ, y_φ). The origin of the first is located at forward quarter-chord, the origin of the latter at the point of intersection between elastic axis "*e.a.*" (which does not have to be straight) and wing plane of symmetry. The actual wing oscillation may be thought of as superposition of bending oscillations about the hypothetical axis ($A_\varphi B_\varphi$) and pure torsional oscillations about the elastic axis and may approximatively be represented by the first normal modes of a cantilever beam in bending and in twist. Thus we have:

(a) *Bending about hypothetical axis* ($A_\varphi B_\varphi$)

$$\left.\begin{aligned} z(\eta_\varphi) &= p(t) \cdot b_0 \cdot f_p(\eta_\varphi) \quad \ldots \eta_\varphi > 0 \\ z(\eta_\varphi) &= 0 \quad \ldots \eta_\varphi < 0 \end{aligned}\right\} \quad (32)$$

(b) *Twist about elastic axis* (*e.a.*)

$$\left.\begin{aligned} \theta(\eta_\varphi) &= q(t) \cdot f_q(\eta_\varphi) \quad \ldots \eta_\varphi > 0 \\ \theta(\eta_\varphi) &= 0 \quad \ldots \eta_\varphi < 0 \end{aligned}\right\} \quad (33)$$

The nondimensional distances η and η_φ are related to each other by

$$\eta_\varphi = \eta - (d \cdot b/s) \sin\varphi \cdot \cos\varphi \quad (34)$$

while the coordinates x, y and x_φ, y_φ are satisfying the equations

$$\left.\begin{aligned} x &= y_\varphi \cdot \sin\varphi + x_\varphi \cdot \cos\varphi + d_0 \cdot b_0 \\ y &= y_\varphi \cdot \cos\varphi - x_\varphi \cdot \sin\varphi \end{aligned}\right\} \tag{35}$$

d_0 stands for the value of $d(\eta)$ at wing root. In case of a tapered wing of straight elastic axis $d(\eta)$ is constant over the span. The first normal modes of a cantilever beam are

$$\text{(Bending)} \ldots f_p(\eta_\varphi) = 0.5\,(\cosh \sigma\eta_\varphi - \cos \sigma\eta_\varphi) - 0.367\,(\sinh \sigma\eta_\varphi - \sin \sigma\eta_\varphi) \tag{36}$$

$$\text{(Torsion)} \ldots f_q(\eta_\varphi) = \sin\{(n/2)\eta_\varphi\} \tag{37}$$

where $\sigma = 1.8751$.

Translatory and angular displacements of a wing element PQ at the forward quarter-chord point R will be denoted by $h(\eta)$ and $\alpha(\eta)$. h is positive when directed downward, α is positive when nose-up. Introducing the amplitude functions

$$p(t) = p_0 \cdot e^{i\omega t}; \qquad q(t) = q_0 \cdot e^{i\omega t} \tag{38}$$

and the mode functions

$$g_p(\eta) = f_p(\eta_\varphi)_R = f_p\{\eta - (db/s)\sin\varphi \cdot \cos\varphi\} \tag{39}$$

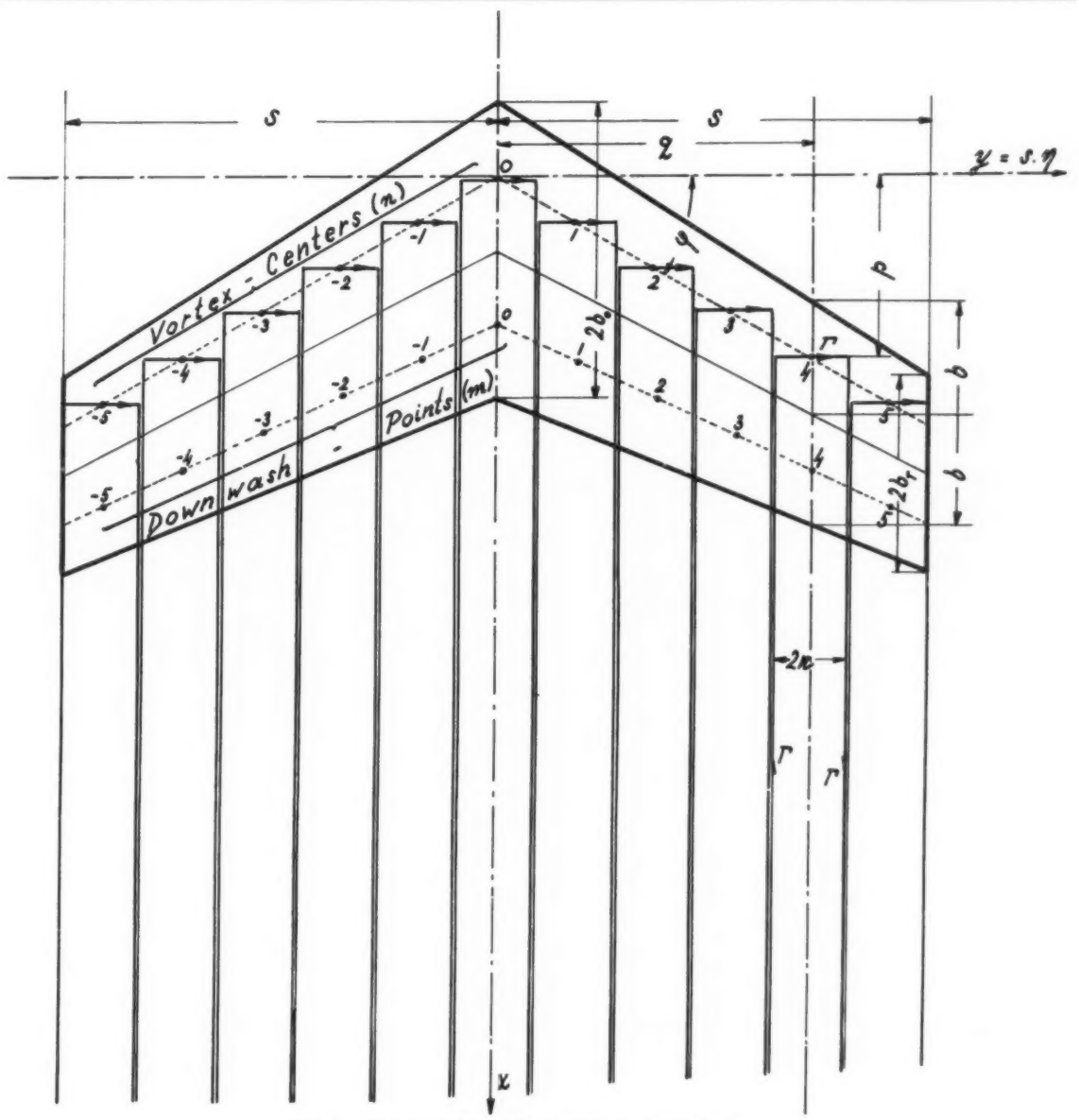

FIG. 6. Wing vorticity diagram based on alternative (2).

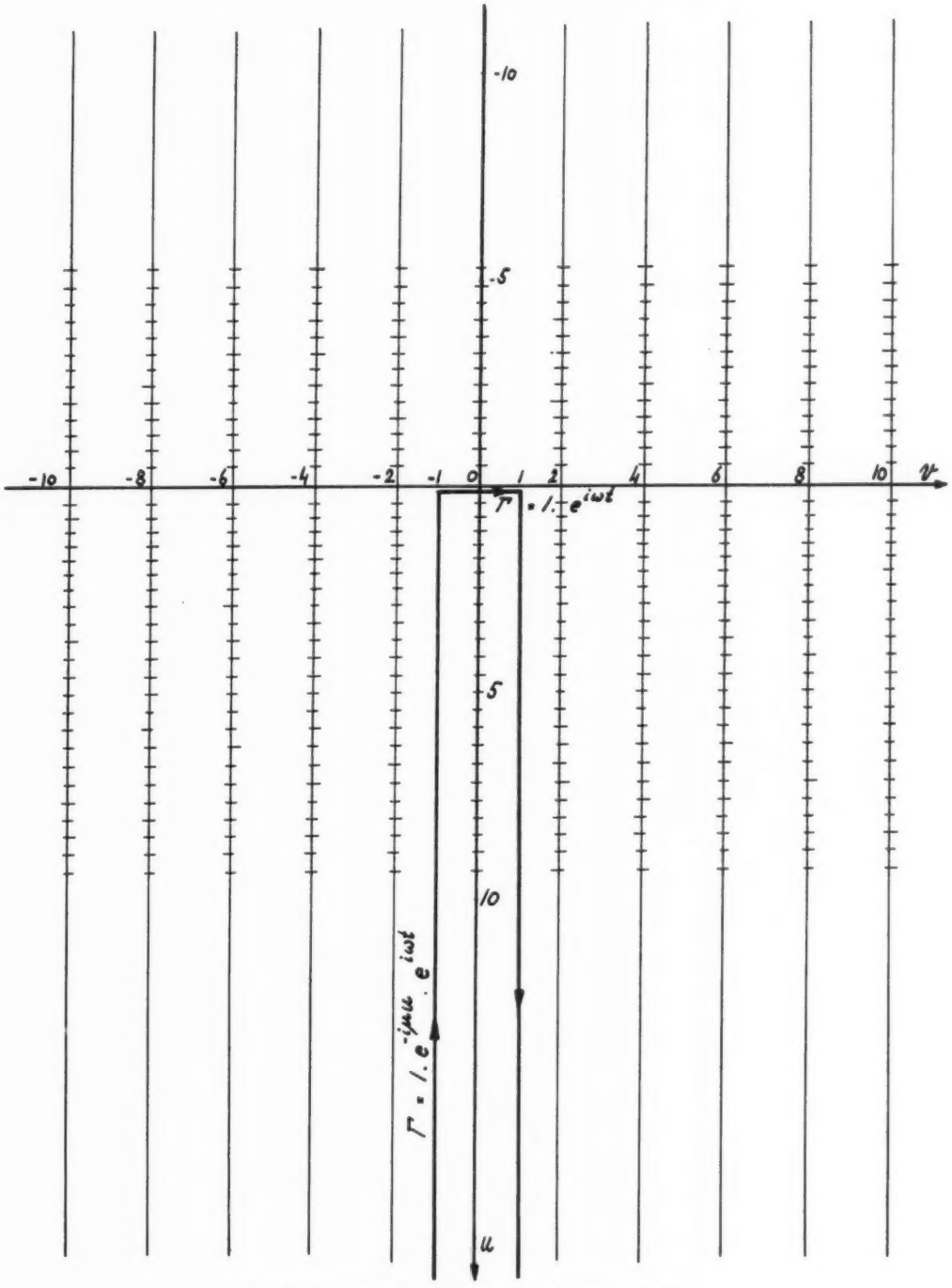

FIG. 7. Downwash coefficient chart of alternative (2).

$$g_q(\eta) = f_q(\eta_\varphi)_R = f_q\{\eta - (db/s) \sin \varphi \cdot \cos \varphi\} \quad (40)$$

the displacements $h(\eta)$ and $\alpha(\eta)$ are found to be

$$h(\eta) = p(t)b_0 \cdot g_p(\eta) - q(t)db \cdot \cos \varphi \cdot g_q(\eta) \quad (41)$$

$$\alpha(\eta) = p(t)\,(b_0/s) \sin \varphi \cdot \cos \varphi \cdot g_p'(\eta) + q(t) \cos \varphi \cdot g_q(\eta) \quad (42)$$

where $g_p'(\eta) = dg_p(\eta)/d\eta = d\{f_p(\eta_\varphi)\}/d\eta_\varphi$. According to Eqs. (41) and (42) the total wing oscillations may be conceived as superposition of four partial oscillations corresponding to translatory displacements $h_p(\eta)$ and $h_q(\eta)$ and rotatory displacements $\alpha_p(\eta)$ and $\alpha_q(\eta)$. Designating the geometrical downwash corresponding to a wing oscillation $z(x, y, t)$ by

$$V \cdot e^{i\omega t} \cdot w^{(g)}(x, y) = \partial z/\partial t + V(\partial z/\partial x) \quad (43)$$

and employing adequate subscripts, there are the following basic relations.

(a) Translatory oscillations corresponding to a linear vertical displacement $h_p(\eta) = p_0 b_0 g_p(\eta) e^{i\omega t}$, caused by wing bending about axis $(A_\varphi B_\varphi)$:

$$\text{Geometrical downwash } w_{hp}^{(g)}(x, y) = p_0 i k_0 \cdot g_p(\eta), \quad \text{(independent of chordwise coordinate x)} \quad (44)$$

(b) Translatory oscillations corresponding to a linear vertical displacement $h_q(\eta) = -q_0 db \cos \varphi \cdot g_q(\eta) e^{i\omega t}$, caused by wing twist about elastic axis:

$$\text{Geometrical downwash } w_{hq}^{(g)}(x, y) = -q_0 d(b/b_0) \cos \varphi \cdot i k_0 \cdot g_q(\eta) \quad \text{(independent of chordwise coordinate } x) \quad (45)$$

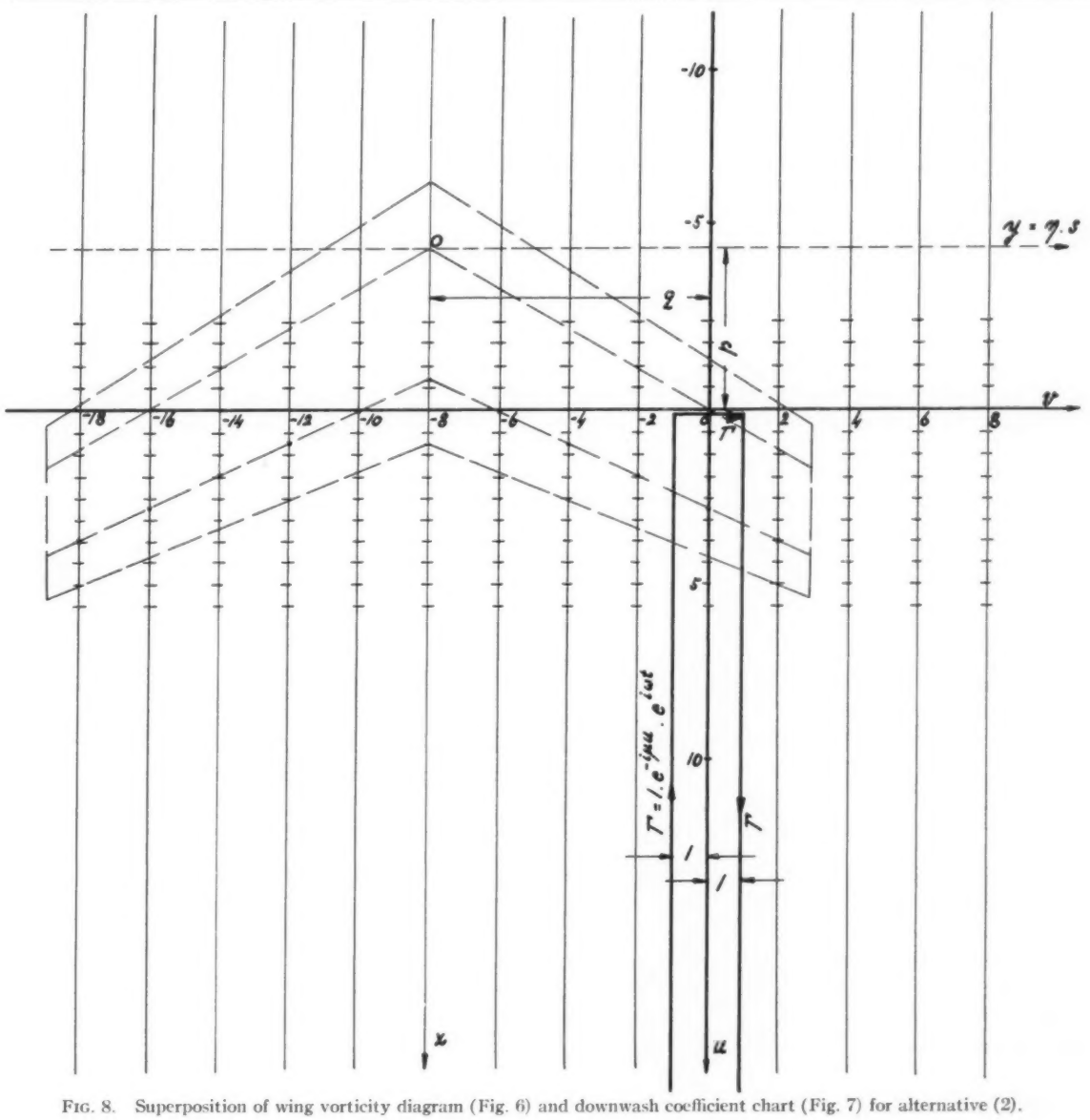

FIG. 8. Superposition of wing vorticity diagram (Fig. 6) and downwash coefficient chart (Fig. 7) for alternative (2).

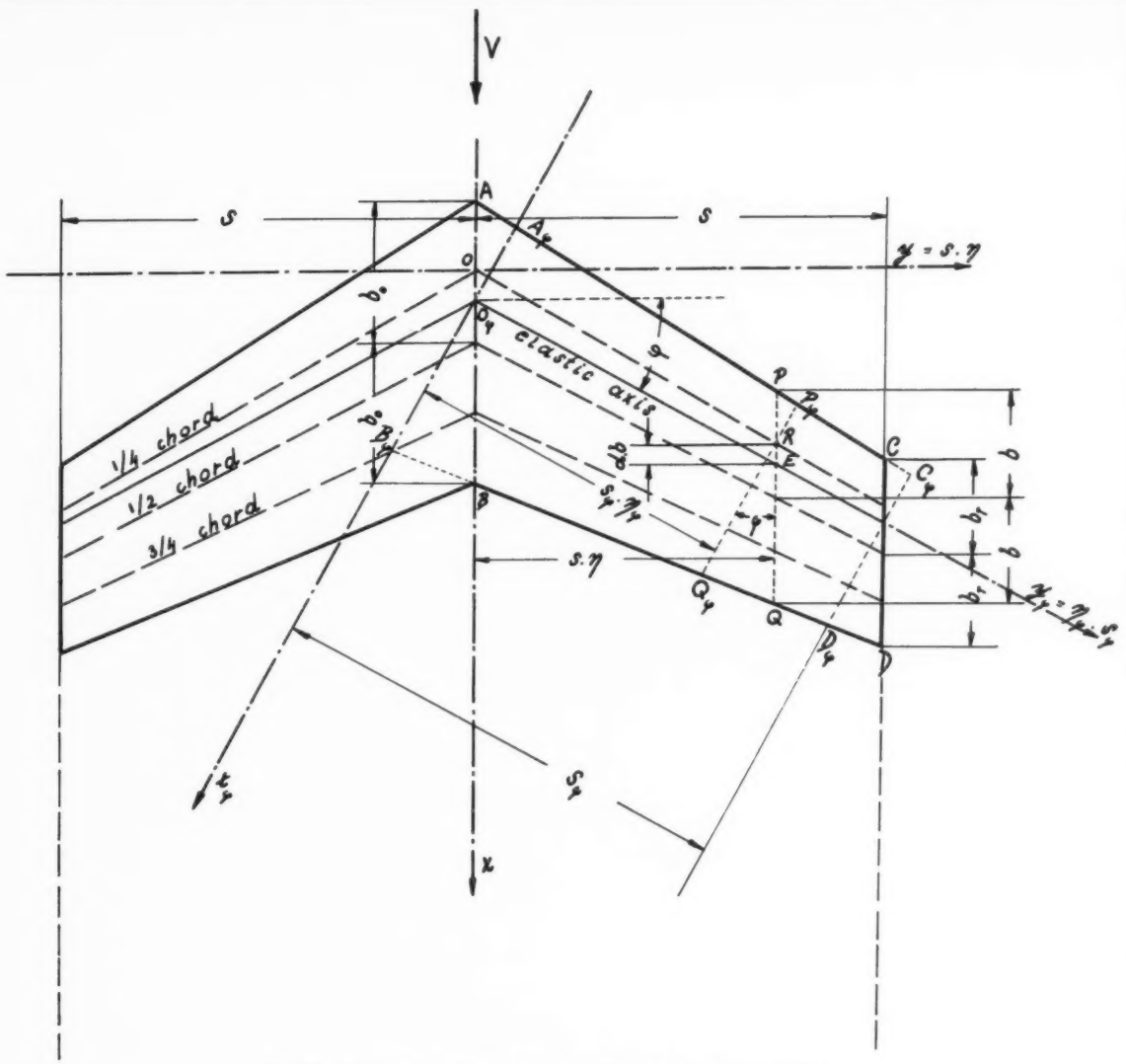

FIG. 9. Geometry of a swept wing oscillating in bending and twist.

(c) Rotational oscillations corresponding to an angular displacement $\alpha_p(\eta) = p_0(b_0/s) \sin \varphi \cdot \cos \varphi \cdot g_p'(\eta) e^{i\omega t}$, caused by wing bending about hypothetical axis $(A_\varphi B_\varphi)$:

Geometrical downwash

$$w_{\alpha p}^{(g)}(x, y) = p_0(b_0/s) \sin \varphi \cdot \cos \varphi \cdot \{ik_0(x - y \cdot \tan \varphi)/b_0 + 1\} \cdot g_p'(\eta) \quad (46)$$

Geometrical downwash at rear quarter-chord point

$$w_{\alpha p}^{(g)}(y \tan \varphi + b, y) = p_0(b_0/s) \sin \varphi \cdot \cos \varphi \cdot (ik + 1) \cdot g_p'(\eta) \quad (46a)$$

(d) Rotational oscillations corresponding to an angular displacement $\alpha_q(\eta) = q_0 \cos \varphi \cdot g_q(\eta) e^{i\omega t}$, caused by wing twist about elastic axis:

Geometrical downwash

$$w_{\alpha q}^{(g)}(x, y) = q_0 \cdot \cos \varphi \cdot \{ik_0(x - y \tan \varphi)/b_0 + 1\} \cdot g_q(\eta) \quad (47)$$

Geometrical downwash at rear quarter-chord point

$$w_{\alpha q}^{(g)}(y \tan \varphi + b, y) = q_0 \cdot \cos \varphi \cdot (ik + 1) \cdot g_q(\eta) \quad (47a)$$

If it is assumed for simplicity that a single lifting line located at forward quarter-chord represents the total wing vorticity, both the alternatives (1) and (2) apply directly to the present case. The downwash conditions then are to be satisfied at selected points of the rear quarter-chord line only. The distributions of geometrical downwash are given in Eqs. (44) to (47a). The distributions of induced downwash are found from Eqs. (20) or (31). Equating geometrical and induced downwash at all of the downwash points, the vortex intensities γ_{hp}, γ_{hq}, $\gamma_{\alpha p}$, and $\gamma_{\alpha q}$ are found. Using the general symbol γ_{ij} for these intensities, the wing circulation $\Gamma_{ij}(\eta)$ in each case is found from

$$\Gamma_{tj}(\eta) = b_0 \cdot V \cdot e^{i\omega t} \cdot \gamma_{tj}(\eta) \tag{48}$$

As known from the two-dimensional theory of the oscillating airfoil, on the other hand, circulatory lift $L_{ctre}(\eta)$ and circulation $\Gamma(\eta)$ are related to each other according to

$$L_{ctre}(\eta) = -ik \cdot e^{ik} \cdot K_1(ik) \rho V \cdot \Gamma(\eta) \tag{49}$$

where K_1 stands for the modified Bessel Function of the second kind. The total lift and moment distributions are obtained by adding the two-dimensional noncirculatory contributions to the circulatory terms. The lift acts at the forward quarter-chord and is counted positive upward. The pitching moment is counted positive when nose-up. Total lift and moment per unit span (measured normal to direction of flow), referred to the forward quarter-chord point, may be written

$$L(\eta) = \pi\rho b^2\omega^2 < h_p(\eta)L_{hp}(\eta) + h_q(\eta)L_{hq}(\eta) + b\{\alpha_p(\eta)L_{\alpha p}(\eta) + \alpha_q(\eta)L_{\alpha q}(\eta)\} > \tag{50}$$

$$M(\eta) = \pi\rho b^3\omega^2 < h_p(\eta)M_{hp}(\eta) + h_q(\eta)M_{hq}(\eta) + b\cdot\{\alpha_p(\eta)M_{\alpha p}(\eta) + \alpha_q(\eta)M_{\alpha q}(\eta)\} > \tag{51}$$

where lift-and-moment coefficients are determined by

$$h_p(\eta)\cdot L_{hp}(\eta) = p_0 b_0\{g_p(\eta) - (i/\pi k)e^{ik}K_1(ik)\ (\gamma_{hp}/p_0)\}e^{i\omega t} \tag{52}$$

$$h_q(\eta)\cdot L_{hq}(\eta) = q_0 b_0\{-d(\eta)b(\eta)/b_0 \cdot \cos\varphi \cdot g_q(\eta) - (i/\pi k)e^{ik}K_1(ik)\ (\gamma_{hq}/q_0)\}e^{i\omega t} \tag{53}$$

$$\alpha_p(\eta)\cdot L_{\alpha p}(\eta) = p_0\{(1/2 - i/k)\ (b_0/s)\ \sin\varphi \cdot \cos\varphi \cdot g_p'(\eta) - (i/\pi k)e^{ik}K_1(ik)\ (b_0/b)\ (\gamma_{\alpha p}/p_0)\}e^{i\omega t} \tag{54}$$

$$\alpha_q(\eta)\cdot L_{\alpha q}(\eta) = q_0\{(1/2 - i/k)\cos\varphi \cdot g_q(\eta) - (i/\pi k)e^{ik}K_1(ik)\ (b_0/b)\ (\gamma_{\alpha q}/q_0)\}e^{i\omega t} \tag{55}$$

$$h_p(\eta)\cdot M_{hp}(n) = p_0 b_0(1/2)\cdot g_p(\eta)\cdot e^{i\omega t} \tag{56}$$

$$h_q(\eta)\cdot M_{hq}(\eta) = -q_0 d(\eta)b(\eta)\ (1/2)\cos\varphi \cdot g_q(\eta)\cdot e^{i\omega t} \tag{57}$$

$$\alpha_p(\eta)\cdot M_{\alpha p}(\eta) = p_0(b_0/s)\ (3/8 - i/k)\ \sin\varphi \cdot \cos\varphi \cdot g_p'(\eta)\cdot e^{i\omega t} \tag{58}$$

$$\alpha_q(\eta)\cdot M_{\alpha q}(\eta) = q_0(3/8 - i/k)g_q(\eta)\cdot e^{i\omega t}\cdot \cos\varphi \tag{59}$$

The motion of the oscillating wing follows the Lagrange equations of motion

$$\frac{d}{dt}\left\{\frac{\partial T}{\partial \dot{u}}\right\} + \left\{\frac{\partial U}{\partial u}\right\} - \left\{\frac{\partial T}{\partial u}\right\} = F_u, \qquad u = p, q \tag{60}$$

where p and q are the general coordinates, T and U the kinetic and potential energies and F_p and F_q the generalized forces of the system.

Using the definitions

(a) $M(\eta_\varphi)$ . . . wing mass per unit span, measured parallel to elastic axis

(b) $S(\eta_\varphi)$ . . . wing static unbalance per unit span about elastic axis

(c) $I(\eta_\varphi)$ . . . wing moment of inertia per unit span about elastic axis

(d) ω_p . . . fundamental uncoupled bending frequency (bending about axis $A_\varphi B_\varphi$)

(e) ω_q . . . fundamental uncoupled torsion frequency (twist about elastic axis)

(f) $g^{(p)}$, $g^{(q)}$ . . . structural damping coefficients associated with the two degrees of freedom

one has the fundamental relations

$$T = (1/2)\{\dot{p}(t)\}^2\{sb_0^2/\cos\varphi\}\int_0^1 M(\eta_\varphi)\{f_p(\eta_\varphi)\}^2 d\eta_\varphi + \{\dot{p}(t)\}\{\dot{q}(t)\}\cdot\{sb_0/\cos\varphi\}\times \int_0^1 S(\eta_\varphi)f_p(\eta_\varphi)f_q(\eta_\varphi)d\eta_\varphi + (1/2)\{\dot{q}(t)\}^2\{s/\cos\varphi\}\int_0^1 I(\eta_\varphi)\{f_q(\eta_\varphi)\}^2 d\eta_\varphi \tag{61}$$

$$U = (1 + ig^{(p)})(\omega_p^2/2)\{p(t)\}^2\{b_0^2 s/\cos\varphi\}\int_0^1 M(\eta_\varphi)\{f_p(\eta_\varphi)\}^2 d\eta_\varphi + (1 + ig^{(q)})(\omega_q^2/2)\{q(t)\}^2\{s/\cos\varphi\}\int_0^1 I(\eta_\varphi)\{f_q(\eta_\varphi)\}^2 d\eta_\varphi \tag{62}$$

$$F_p = s\int_0^1 \left\langle \frac{d}{dp}h_p(\eta)L(\eta) + \frac{d}{dp}\alpha_p(\eta)M(\eta)\right\rangle d\eta \tag{63}$$

$$F_q = s\int_0^1 \left\langle \frac{d}{dq}h_q(\eta)L(\eta) + \frac{d}{dq}\alpha_q(\eta)\ M(\eta)\right\rangle d\eta \tag{64}$$

But

$$d\{h_p(\eta)\}/dp = b_0\cdot g_p(\eta) \tag{65}$$

$$d\{h_q(\eta)\}/dq = -d(\eta)b(\eta)\cos\varphi\cdot g_q(\eta) \tag{66}$$

$$d\{\alpha_p(\eta)\}/dp = (b_0/s)\sin\varphi\cdot\cos\varphi\ g_p'(\eta) \tag{67}$$

$$d\{\alpha_q(\eta)\}/dq = \cos\varphi\cdot g_q(\eta) \tag{68}$$

and hence

$$F_p = \pi\rho\omega^2 s b_0 \int_0^1 g_p(\eta)\left\{b^2 h_p L_{hp} + b^2 h_q L_{hq} + b^3\alpha_p L_{\alpha p} + b^3\alpha_q L_{\alpha q}\right\} d\eta + \pi\rho\omega^2\, b_0 \sin\varphi\cos\varphi \int_0^1 g_p'(\eta)\left\{b^3 h_p M_{hp} + b^3 h_q M_{hq} + b^4\alpha_p M_{\alpha p} + b^4\alpha_q M_{\alpha q}\right\} d\eta \quad (69)$$

$$F_q = -\pi\rho\omega^2 s\cdot\cos\varphi \int_0^1 d(\eta)b(\eta)g_q(\eta)\left\{b^2 h_p L_{hp} + b^2 h_q L_{hq} + b^3\alpha_p L_{\alpha p} + b^3\alpha_q L_{\alpha q}\right\} d\eta + \pi\rho\omega^2 s\cdot\cos\varphi \int_0^1 g_q(\eta)\left\{b^3 h_p M_{hp} + b^3 h_q M_{hq} + b^4\alpha_p M_{\alpha p} + b^4\alpha_q M_{\alpha q}\right\} d\eta \quad (70)$$

After expressions for the generalized forces are combined with the terms derived from the kinetic and potential energies, a homogeneous system of two linear equations in the two unknowns p and q results. These may be written

$$A\cdot p + B\cdot q = 0 \quad (71)$$

$$D\cdot p + E\cdot q = 0 \quad (72)$$

where

$$A\cdot\cos\varphi\cdot\pi\rho b_0^2 = \left\{1 - (1 + ig^{(p)})\right\}(\omega_p/\omega)^2 \int_0^1 M(\eta)f_p(\eta)f_p(\eta)\,d\eta + \int_0^1 (b/b_0)^2 L_{hp}(\eta)g_p(\eta)g_p(\eta)\,d\eta + \sin\varphi\cdot\cos\varphi\cdot\int_0^1 (b/b_0)^2(b/s)L_{\alpha p}(\eta)g_p(\eta)g_p'(\eta)\,d\eta + \sin\varphi/\cos\varphi\cdot\int_0^1 (b/b_0)^2(b/s)M_{hp}(\eta)g_p(\eta)g_p'(\eta)\,d\eta + \sin^2\varphi\cdot\cos^2\varphi\int_0^1 (b/b_0)^2(b/s)^2 M_{\alpha p}(\eta)g_p'(\eta)g_p'(\eta)\,d\eta \quad (73)$$

$$B\cdot\cos\varphi\cdot\pi\rho b_0^3 = \int_0^1 S(\eta)f_p(\eta)f_q(\eta)\,d\eta - \cos\varphi\cdot\int_0^1 (b/b_0)^3 d(\eta)L_{hq}(\eta)g_p(\eta)g_q(\eta)\,d\eta + \cos\varphi\cdot\int_0^1 (b/b_0)^3 L_{\alpha q}(\eta)g_p(\eta)g_q(\eta)\,d\eta - \sin\varphi\cdot\cos^2\varphi\cdot\int_0^1 (b/b_0)^3(b/s)d(\eta)M_{hq}(\eta)g_q(\eta)g_p'(\eta)\,d\eta + \sin\varphi\cdot\cos^2\varphi\cdot\int_0^1 (b/b_0)^3(b/s)M_{\alpha q}(\eta)g_q(\eta)g_p'(\eta)\,d\eta \quad (74)$$

$$D\cdot\cos\varphi\cdot\pi\rho b_0^3 = \int_0^1 S(\eta)f_p(\eta)f_q(\eta)\,d\eta - \cos\varphi\cdot\int_0^1 (b/b_0)^3 d(\eta)L_{hp}(\eta)g_p(\eta)g_q(\eta)\,d\eta + \cos\varphi\cdot\int_0^1 (b/b_0)^3 M_{hp}(\eta)g_p(\eta)g_q(\eta)\,d\eta - \sin\varphi\cdot\cos^2\varphi\cdot\int_0^1 (b/b_0)^3(b/s)d(\eta)L_{\alpha p}(\eta)g_q(\eta)g_p'(\eta)\,d\eta + \sin\varphi\cdot\cos^2\varphi\cdot\int_0^1 (b/b_0)^3(b/s)M_{\alpha p}(\eta)g_q(\eta)g_p'(\eta)\,d\eta \quad (75)$$

$$E\cdot\cos\varphi\cdot\pi\rho b_0^4 = \left\{1 - (1 + ig^{(q)})(\omega_q/\omega)^2\right\}\int_0^1 I(\eta)f_q(\eta)f_q(\eta)\,d\eta - \cos^2\varphi\int_0^1 (b/b_0)^4 d(\eta)L_{\alpha q}(\eta)g_q(\eta)g_q(\eta) + \cos^2\varphi\int_0^1 (b/b_0)^4\{d(\eta)\}^2 L_{hq}(\eta)g_q(\eta)g_q(\eta)\,d\eta - \cos^2\varphi\int_0^1 (b/b_0)^4\{d(\eta)\}M_{hq}(\eta)g_q(\eta)g_q(\eta)\,d\eta + \cos^2\varphi\cdot\int_0^1 (b/b_0)^4 M_{\alpha q}(\eta)g_q(\eta)g_q(\eta)\,d\eta \quad (76)$$

The system (71), (72) can have a nontrivial solution only if its determinant, the flutter frequency determinant, vanishes:

$$A.E - B.D = 0 \quad (77)$$

One may put, within certain limits of accuracy, $g^{(p)} = g^{(q)} = g$, introduce the symbol

$$\Omega = (1 + ig)(\omega_q/\omega)^2 \quad (78)$$

and write the flutter frequency equation in the form

$$\Omega^2 + P\cdot\Omega + Q = 0 \quad (79)$$

Eq. 79 is a function of the wing root reduced frequency $k_0 = b_0\omega/V$ and may now be solved assigning different numerical values to k_0. In this manner the root Ω corresponding to the preassumed value of g may be found. Eq. 78 then yields the flutter frequency ω and the flutter speed V is found from $V = k_0/\omega b_0$. This speed, of course, refers to incompressible flow and would have to be corrected by the Prandtl-Glauert Rule, V (compr.) $= (1 - (\text{Mach})^2)^{1/4}\cdot V$ (incompr.), if it is considered necessary to account for compressibility effects. Eq. 79 has two different roots for each specific value of k_0

(*Continued on page 834*)

A Method for Analyzing the Heat Insulating Properties of the Laminar Compressible Boundary Layer*

PAUL A. LIBBY† AND ADRIAN PALLONE‡

Polytechnic Institute of Brooklyn

SUMMARY

In some cooling problems associated with high energy flows it may be convenient to localize strongly the cooling, as for example by injecting a coolant through an upstream porous strip, and to depend on the insulating properties of the boundary layer to reduce, or to eliminate completely the need for further cooling on the surface downstream of the highly cooled section. This upstream cooling technique may be of interest in connection with optical windows in hypersonic wind tunnels, and on radomes, wings, and bodies of high-speed aircraft and missiles.

In this paper a method for investigating the insulating properties of a laminar compressible boundary layer on a two-dimensional surface with zero heat transfer is presented. The physical situation considered thus corresponds to the case in which the heat transfer downstream of the strongly cooled section is completely eliminated. Of practical concern is how the temperature of the uncooled surface varies in the downstream direction from its low initial value and thus how the low energy layer established by the upstream cooling insulates the downstream surface.

The Kármán integral method extended to both the momentum and energy partial differential equations of the boundary layer has been used. The station, at which cooling and/or injection ceases, corresponds to a discontinuity in boundary conditions and thus in solutions. At this point the flux of mass, momentum, and energy within the boundary layer has been made continuous by the introduction of three additional parameters in the velocity and stagnation enthalpy profiles. Thus the velocity and stagnation enthalpy profiles have both been taken as sixth degree polynomials. The resulting two integral-differential equations are then solved for two unknown functions of the distance along the wall. These two functions are related to the boundary-layer thickness and to the wall temperature. Initial conditions corresponding to a given initial wall temperature and an initial boundary-layer thickness are prescribed. Exact closed-form solutions for the case of zero axial pressure gradient are obtained. For flows with significant pressure gradients, numerical solutions are required in general. Several numerical examples of practical interest are presented.

SYMBOLS

$F_{1,2,3}$ = integrals defined after Eq. (14)
G = function of M_0 and M_1 [cf. Eq. (34)]
H = stagnation enthalpy $\equiv (u^2/2) + c_pT$
M = Mach Number
p = static pressure
R = gas constant
S = Sutherland constant, 216°R. for air
$\bar{T}$ = an average temperature
T = absolute temperature
t = transformed variable [cf. Eq. (11)]
u = velocity component in x direction
U = potential flow velocity parallel to the surface
v = velocity component in the y direction
W = ratio of stagnation enthalpy at the wall and in potential flow
x = coordinate along the surface
y = coordinate normal to the surface
Z = pressure gradient parameter; [cf. Eqs. (19) and (43)].
γ = ratio of specific heats
δ = boundary-layer thickness
λ = nondimensional boundary-layer thickness ratio ($\lambda \equiv \Lambda/\Lambda_0$)
μ = coefficient of viscosity
ξ = nondimensional space coordinate ($\xi = \rho_0 U_0 x/\mu_0$)
ρ = mass density
Λ = nondimensional boundary-layer thickness parameter ($\Lambda = \rho_1 U_1 \rho_0 U_0 \delta_t^2/\mu_1\mu_0$)
τ = t/δ_t
ψ = $(\rho_w v_w/\rho_0 U_0)\Lambda^{1/2}$

Subscripts

$()_w$ = value at the surface, $y = 0$, for any value of x
$()_1$ = value at the outer edge of the boundary layer
$()_0$ = value at $x = 0$
$()_t$ = value in the x-t or ξ-τ plane
$()_s$ = stagnation values

Received January 21, 1954.

* This research was conducted under the auspices of Project Squid, jointly sponsored by the Office of Naval Research and the Office of Air Research under Contract N6ori-105 TO III. This paper in abbreviated and considerably modified form was read by the first author at the Eighth International Congress of Theoretical and Applied Mechanics in Istanbul, Turkey, August 20–28, 1952.

† Associate Professor of Aeronautical Engineering.

‡ Research Assistant, Department of Aeronautical Engineering and Applied Mechanics.

INTRODUCTION

SOME OF THE MOST important current problems in the aeronautical engineering field are those connected with preventing critical components of aircraft, propulsion units, and test equipment from being heated to temperatures greater than those permitted by structural, functional, or life considerations. While improved materials can give some temporary relief, it appears that only by appropriate cooling can most of these heat transfer problems be solved.

In many practical cases involving cooling, it may be convenient or even necessary from a functional or economic point of view to localize the cooling in a restricted region. For example, the sweat cooling technique (cf. for example references 1 and 2), which is of considerable interest, requires the use of porous mate-

rials which are expensive and which have, at the present, reduced strength properties. It may thus be desirable to localize their use. Another example is provided by the radome on high-speed missiles; the radiation requirements make cooling difficult and may even dictate the use of special materials, which have poor strength properties at elevated temperatures and which, therefore, increase the complexity of the heat transfer problem. Finally, the optical windows in hypersonic wind tunnels operating at elevated stagnation temperatures are difficult to cool without seriously affecting their use in connection with schlieren and shadowgraph systems.

A method of preventing excessive temperatures from being reached or of realizing the advantages of localized cooling may be to cool the upstream portions of the critical section and to depend on the insulating properties of the boundary layer to protect the downstream surface from the high-energy outside flow. The upstream cooling results in the establishment of a continuously replaced, low-energy layer of gas within the boundary layer and between the exposed surface and the high-energy flow. It might be mentioned that film cooling, which has been used in protecting rocket motor liners for some time, depends in a similar manner on the insulating and heat absorbing properties of an evaporating liquid layer. The efficacy of upstream cooling for any particular application is determined by whether the surface temperature does or does not increase from its initial low value at the upstream edge to above an acceptable value within the length of the critical section with reduced or no heat transfer.

In this paper a method is presented for obtaining an indication of this variation of wall temperature when the boundary layer is laminar and two-dimensional and when there is no heat transfer downstream of the highly cooled section. The flow is assumed to be two-dimensional, steady and to be describable by the Prandtl boundary-layer equations. The fluid is assumed to be a perfect gas with a constant Prandtl Number of unity and with a linear viscosity-temperature relation. The heat conductivity of the surface material is assumed negligibly small. It is pointed out that these assumptions have all been used extensively in boundary-layer theory in the past and have been considered satisfactory for many engineering analyses.

The investigation is carried out along the following lines: It is assumed that the boundary-layer characteristics at the downstream edge of the cooled portion of the surface are known.* This edge represents a discontinuity in the solution to the boundary-layer equations since the boundary conditions are discontinuous there and, therefore, requires special treatment as will be discussed presently. The momentum and energy equations of the laminar boundary layer are formulated as two integral-differential equations for the case of axial pressure gradient with no heat transfer. After the method of von Kármán profiles for the local velocity and local stagnation enthalpy in terms of the distance normal to the wall are assumed. These profiles satisfy certain boundary conditions at the wall and at the outer edge of the boundary layer. In addition three parameters are introduced into these profiles and are determined by conditions at the leading edge discontinuity where the flux of the mass, momentum, and energy within the boundary layer are made continuous. It is shown that the discontinuities in the local velocity and local stagnation enthalpy profiles are comparatively small when the overall conditions are imposed. The downstream length in which an adjustment of the boundary-layer flow takes place can, therefore, be expected to be small compared to the length of interest in examining the efficacy of the insulating ability of the boundary layer.

With the assumption of these profiles the two integral-differential equations can be converted to ordinary differential equations which give essentially the downstream variation of the boundary-layer thickness and the wall stagnation enthalpy from some prescribed initial values. For the case of zero axial pressure gradient these two equations can be solved in closed form. However, for the general pressure gradient case a numerical solution of the differential equations must be employed.

At first thought it may be disturbing that the results of this analysis indicate zero heat transfer on a surface with variable wall temperature. Ordinarily for Prandtl Number of unity the surface temperature for zero heat transfer is constant and equal to the stagnation temperature of the flow. However, most boundary-layer analyses assume an isoenergetic flow at the leading edge whereas here the effect of the upstream cooling is to provide an energy variation at the leading edge of the surface under consideration. It is of interest to point out that Levy[5] has obtained from an exact numerical integration of the constant gas properties, laminar flow equations, zero heat transfer, variable wall temperature solutions. As pointed out by Eckert[6] these solutions involve an infinite temperature difference at the leading edge of the surface and thus mathematically although not physically are analogous to those obtained here.

The authors are pleased to acknowledge that Professor Antonio Ferri suggested in private conversations the upstream cooling technique analyzed here and has been a source of helpful discussion throughout the research.

Basic Equations

The following equations describe the two-dimensional, steady laminar boundary-layer flow over a slightly curved surface of a perfect gas with a Prandtl Number

* The methods of analysis of references 2, 3, and 4 may be of value in determining these characteristics. For completeness, in the Appendix, the case of cooling by injection over a constant pressure surface has been treated in terms of the variables used here.

of unity and with constant coefficients of specific heat—

Equation of motion in x direction:

$$\rho u u_x + \rho v u_y = -p_x + (\mu u_y)_y \quad (1)$$

Equation of motion in y direction:

$$p_y = 0; \quad -p_x = \rho_1 U_1 (dU_1/dx) \quad (2)$$

Equation of mass conservation:

$$(\rho u)_x + (\rho v)_y = 0 \quad (3)$$

Equation of energy conservation:

$$\rho u H_x + \rho v H_y = (\mu H_y)_y \quad (4)$$

Equation of state: $p = \rho R T$ (5)

Viscosity-temperature relation: $\mu = C\mu_0(T/T_0)$ (6)

where

ρ = mass density of gas
u = velocity component in x direction
v = velocity component in y direction
p = static pressure
μ = coefficient of viscosity
$H \equiv (u^2/2) + c_p T$, local stagnation enthalpy
R = gas constant
T = static temperature
$C = (\bar{T}_w/T_0)^{1/2}\,(T_0 + S)/(\bar{T}_w + S)$
S = Sutherland constant, 216°R. for air

where the subscript 0 denotes conditions outside the boundary layer at $x = 0$, the subscript 1 conditions outside the boundary layer at any value of x, and the subscript w conditions at the surface ($y \equiv 0$), and where $\bar{T}_w$ is some average wall temperature used to modify the linear viscosity-temperature relation so that the exact Sutherland relation is closely approximated at the average wall temperature in the region of x of interest. This modified linear viscosity-temperature relation was first suggested by Chapman[7] and has since been used extensively.

Eqs. (1), (3), (4), and (5) with the accompanying equations and definitions may be considered to be four equations giving ρ, u, v, and H as functions of x and y for certain boundary and initial conditions. As is usual in boundary-layer analyses, the pressure and/or the potential velocity distribution in the x direction is assumed known from potential flow considerations and the required fluid constants R, S, and c_p specified.

For the investigation of the insulating properties of the laminar boundary layer given here, the following boundary and initial conditions are prescribed: The origin of the x axis is located at the upstream edge of the critical, uncooled section. At $x = 0$, in particular, the boundary layer thickness and wall temperature are known while more generally the u velocity and stagnation enthalpy distributions determined from an analysis of the upstream boundary layer are prescribed. Along the positive x axis the velocity components u and v are as usual assumed zero, and the heat transfer is assumed zero corresponding to the assumption that the critical section of the surface ($x > 0$) is thermally insulated. At the outer edge of the boundary layer or $y \to \infty$, the u velocity takes on prescribed values denoted by U_1, the density by ρ_1 and the stagnation enthalpy the constant value H_1. It is required to find in particular for this investigation the distribution of stagnation enthalpy along the surface ($x > 0$), since from this the distribution of wall temperature can immediately be found.

A convenient way to solve approximately the above formulated problem is to use the integral methods due to von Kármán. Eqs. (1) and (4) are multiplied by dy integrated from $y = 0$ to $y = \delta(x)$ where δ is the boundary layer thickness, an unknown function of x, and in this analysis is the value of y in which both the u velocity and the stagnation enthalpy H are equal to their potential flow values.* Applying the boundary conditions,

$$\text{at } y = 0, \qquad \left.\begin{aligned} u &= v = 0 \\ H_y &= 0 \end{aligned}\right\} \quad (7)$$

and at $y = \delta(x)$,

$$\left.\begin{aligned} u &= U_1, \qquad u_y = 0 \\ H &= H_1, \qquad H_y = 0 \end{aligned}\right\} \quad (8)$$

and using Eq. (3), one can convert Eqs. (1) and (4) into the following integral-differential equations:

$$(d/dx)\left\{\rho_1 U_1^2 \int_0^\delta (\rho/\rho_1)\,(u/U_1)\,[1 - (u/U_1)]\,dy\right\} + \rho_1 U_1 (dU_1/dx) \int_0^\delta (\rho/\rho_1)\,[(\rho_1/\rho) - (u/U_1)] \times dy = (\mu u_y)_w \quad (9)$$

$$(d/dx)\left\{\rho_1 U_1 \int_0^\delta (\rho/\rho_1)\,(u/U_1)\,[1 - (H/H_1)]\,dy\right\} = 0 \quad (10)$$

Eqs. (9) and (10) can be handled more conveniently if the Dorodnitzyn transformation is introduced. A new variable t is defined such that for a given value of x

$$dt = (\rho/\rho_1)\,dy \quad (11)$$

This implies the introduction of a new boundary-layer thickness in the x-t plane defined most conveniently by the inverse transformation

$$\delta = \int_0^{\delta_t} (\rho_1/\rho)\,dt \quad (12)$$

If Eqs. (11) and (12) are applied, Eqs. (9) and (10) can

* For the case of isoenergetic flow and Prandtl Number of unity the frequently distinguished thermal and velocity thicknesses are exactly equal. For the flow with variable stagnation enthalpy treated here the two thicknesses cannot be expected to be greatly different. Moreover, in the integral method there appear to be good mathematical reasons for adopting the point of view of one thickness within which all fluid properties change from their wall values to their local potential flow values. (Cf. reference 4.)

be nondimensionalized and put in the following form:*

$$(F_1/2)\Lambda' + F_1\Lambda[\ln (F_1G)]' + F_2\Lambda[\ln (U_1/U_0)]' = [(u/U_1)_\tau]_w \quad (13)$$

$$(G\Lambda^{1/2}F_2)' = 0 \quad (14)$$

where

$$F_1 \equiv \int_0^1 (u/U_1)\,[1 - (u/U_1)]\,d\tau$$

$$F_2 \equiv [1 + (\gamma - 1)\,(M_1^2/2)] \int_0^1 [(H/H_1) - (u/U_1)^2]\,d\tau$$

$$F_3 \equiv \int_0^1 (u/U_1)\,[1 - (H/H_1)]\,d\tau$$

$$\Lambda \equiv \rho_1 U_1 \rho_0 U_0 \delta_t^2/\mu_1\mu_0$$

$$G^2 \equiv (\rho_1/\rho_0)\,(U_1/U_0)\,(\mu_1/\mu_0)$$

$$\tau \equiv t/\delta_t$$

γ = ratio of specific heats

M_1 = potential flow Mach Number

and where $(\ )'$ denotes differentiation with respect to $\xi \equiv \rho_0 U_0 x/\mu_0$. Eqs. (13) and (14) are in a form for approximate solution following the method of von Kármán. Polynomials in τ are assumed for u/U_1 and H/H_1; the coefficients of these polynomials are selected so that the boundary conditions in the $\xi - \tau$ plane corresponding to those given by Eqs. (7) and (8) in the $x - y$ plane are satisfied for any value of δ_t and in this application of the method for any value of the wall temperature. Additional accuracy can be realized if the polynomials are taken of sufficiently high order so that they satisfy several additional boundary conditions corresponding to those which an exact solution of the partial differential equations would automatically satisfy. Moreover, three additional parameters that are independent of x and which are determined from conditions at the discontinuity existing at $x = 0$ are introduced.†

Sufficient accuracy for the purpose of the present investigation can be realized if sixth degree polynomials in the velocity and stagnation profiles are assumed. It may be noted that since three of the parameters are determined from leading edge conditions this corresponds to assuming fourth and fifth degree polynomials for the velocity and stagnation enthalpy profiles respectively; such profiles have been found satisfactory for heat transfer and skin friction determination (cf. references 4 and 8). Thus

$$u/U_1 = \sum_{j=0}^{6} a_j \tau^j \quad (15)$$

and

$$H/H_1 = \sum_{j=0}^{6} b_j \tau^j \quad (16)$$

The boundary conditions on u/U_1 and H/H_1 in the ξ-τ plane corresponding to those in the x-y plane given by Eqs. (7) and (8) are:

$$\text{at } \tau = 0, \quad \left.\begin{matrix} u/U_1 = 0 \\ (H/H_1)_\tau = 0 \end{matrix}\right\} \quad (17)$$

$$\text{and at } \tau = 1, \quad \left.\begin{matrix} u/U_1 = H/H_1 = 1 \\ (u/U_1)_\tau = (H/H_1)_\tau = 0 \end{matrix}\right\} \quad (18)$$

Additional boundary conditions at $y = 0$ can be obtained from Eqs. (1) and (4) with $u = v = 0$; they are

$$-p_x = \rho_1 U_1 (dU_1/dx) = -(\mu u_y)_y$$

$$(\mu H_y)_y = 0$$

which in the ξ-τ plane and in terms of Λ and ξ are at $\tau = 0$,

$$\left.\begin{matrix} (u/U_1)_{\tau\tau} = -[1 + (\gamma - 1)\,(M_1^2/2)]W\Lambda[\ln (U_1/U_0)]' \\ \qquad\qquad = -2Z \\ (H/H_1)_{\tau\tau} = 0 \end{matrix}\right\} \quad (19)$$

where $W = H_w/H_1$, at this point in the analysis an unknown function of ξ, and where Z is evidently defined.

Similarly, additional boundary conditions at $y = \delta(x)$ can be obtained from Eqs. (1) and (4) with $u_y = H_y = 0$; they are in the ξ-τ plane:

$$\text{at } \tau = 1, \qquad (u/U_1)_{\tau\tau} = (H/H_1)_{\tau\tau} = 0 \quad (20)$$

At the leading edge corresponding to $x = 0$ a discontinuity in solution exists because the boundary conditions are not continuous. Indeed, it is possible that in the immediate neighborhood thereof the boundary-layer equations themselves may not be valid since the discontinuity corresponds to an abrupt change of the flow variables in the x direction; fundamentally the boundary-layer hypothesis precludes such changes. However, here the discontinuity has been handled in the customary manner; namely, the equations have been taken to be valid on either side of the discontinuity and finite conditions corresponding to conservation of mass, momentum, and energy across the discontinuity have been imposed. This approach can be expected to be valid provided the discontinuities of the local velocity and stagnation enthalpy within the boundary layer are relatively small since then it could be expected that a readjustment zone on the order of only several boundary-layer thicknesses would be required for the description of the boundary-layer properties presented here to be valid. It might be mentioned that in the past such discontinuities have been treated by making either the boundary-layer thickness or the momentum thickness continuous; both of these conditions are contained in the more complete treatment used here.

The conditions at $x = 0$ will now be discussed explicitly; the notation superscript $(+)$ and $(-)$ will be

* Although there are many possible choices of variables and methods of nondimensionalizing, the ones selected here seem especially convenient.

† Professor Martin H. Bloom suggested the possibility of these additional parameters to the first author in a private conversation.

used to denote values on the sides $x > 0$ and $x < 0$ of the discontinuity respectively. The finite potential flow quantities are taken to be continuous although dU_1/dx may be discontinuous. Moreover, the boundary-layer thickness in the x-y plane is taken to be continuous; to do otherwise would be physically unappealing. Along with the other conditions of continuity of mass, momentum, and energy within the boundary layer imposed, the boundary-layer thickness in the x-t plane and thus Λ also are made continuous. Thus

$$\Lambda^{(-)} = \Lambda^{(+)} \tag{21}$$

$$F_4^{(-)} = F_4^{(+)} \tag{22}$$

$$F_1^{(-)} = F_1^{(+)} \tag{23}$$

$$F_3^{(-)} = F_3^{(+)} \tag{24}$$

where $F_4 \equiv \int_0^1 (u/U_1)\, d\tau$. Eq. (21) has been discussed above; Eqs. (22), (23), and (24) result from making the mass, momentum, and energy, respectively, continuous and from Eq. (21).

It is pointed out that Z defined by Eq. (19) is continuous if dU_1/dx is continuous at $x = 0$ but with injection upstream this is not the same as making $(u/U_1)_{\tau\tau}$ continuous. Actually, $(u/U_1)_{\tau\tau}$ is discontinuous at $x = 0$ if injection exists upstream, or if a discontinuity in dU_1/dx exists at $x = 0$. It is pointed out that this latter can occur frequently in supersonic flow since only a discontinuity in surface curvature is required to lead to a discontinuity in $dM_1/d\xi$.

With Eqs. (17) through (20) and (22) through (24), the 14 coefficients of the velocity and stagnation enthalpy profiles can be evaluated in terms of Z, W, and of the jumps in the three parameters determined by the discontinuity conditions. These have been taken to be a_5, a_6, and b_6, parameters which are zero for $x < 0$; thus the jumps are represented solely by $a_5^{(+)}$, $a_6^{(+)}$, and $b_6^{(+)}$, and can be expressed in terms of the parameter; $a_1^{(-)}$, $a_2^{(-)}$, $a_2^{(+)} \equiv -Z(0)$, $b_1^{(-)}$, $b_2^{(-)}$, $b_0^{(-)}$, and $b_0^{(+)} \equiv b_0^{(-)}$, which are determinable from initial conditions. Thus

$$a_5^{(+)} = (1/2)\,[a_2^{(-)} - a_2^{(+)}] - (45/14)\, a_6^{(+)} \tag{25}$$

while $a_6^{(+)}$ is determined from the equation

$$\begin{aligned} a_6^{(+)}\,[(3a_1^{(+)}/1540) + (a_2^{(+)}/2772) - (a_6^{(+)}/12012)] &= (8/231)\,[a_1^{(-)} - a_1^{(+)}] + (1/277)\,[a_2^{(-)} - a_2^{(+)}] + (23/4620) \times \\ [a_1^{(+)}a_2^{(+)} - a_1^{(-)}a_2^{(-)}] + (52/3465)\,[(a_1^{(+)})^2 - (a_1^{(-)})^2] &+ (1/2310)\,[(a_2^{(+)})^2 - (a_2^{(-)})^2] \end{aligned} \tag{26}$$

where

$$a_1^{(+)} = 2 - (1/6)\,[a_2^{(-)} + a_2^{(+)}] + (a_6^{(+)}/14) \tag{27}$$

Finally $b_6^{(+)}$ is determined from the equation

$$\begin{aligned} b_6^{(+)}\,[(11/3080) + (3a_1^{(+)}/3080) + (a_2^{(+)}/5544) - (a_6^{(+)}/12012)] &= (1 - W_0)\,[(311/4620) \times (a_1^{(-)} - a_1^{(+)}) + (281/27720)\,(a_2^{(-)} - a_2^{(+)}) + (11a_6^{(+)}/3080)] - b_1^{(-)}\,[(131/4620) + (52\,a_1^{(-)}/3465) + (23a_2^{(-)}/9240)] - \\ b_2^{(-)}\,[(181/27720) + (23a_1^{(-)}/9240) &+ (a_2^{(-)}/2310)] \end{aligned} \tag{28}$$

In summary then, at the discontinuity ($\xi = 0$) one has at his disposal from the analysis of the boundary layer upstream ($x < 0$), $a_1^{(-)}$, $a_2^{(-)}$, $b_1^{(-)}$, $b_2^{(-)}$. Moreover, if Λ and W are made continuous across the discontinuity, $Z(0) = -a_2^{(+)}$ and $b_0^{(-)} = b_0^{(+)} = W_0$ are known. From Eqs. (25) through (28) the constants $a_5^{(+)}$, $a_6^{(+)}$, and $b_6^{(+)}$ are computed. Thus the velocity and stagnation enthalpy profiles for $x > 0$ are specified except for Z and W, which are determined by the solutions of Eqs. (13) and (14).

Explicitly, the velocity and stagnation enthalpy profiles are:

$$\begin{aligned} u/U_1 = [2\tau - 2\tau^3 + \tau^4] &+ Z[(\tau/3) - \tau^2 + \tau^3 - (\tau^4/3)] + a_5^{(+)}\,[-(\tau/3) + 2\tau^3 - (8\tau^4/3) + \tau^5] + a_6^{(+)}\,[-\tau + 5\tau^3 - 5\tau^4 + \tau^6] \end{aligned} \tag{29}$$

and

$$H/H_1 = 1 - (1 - W)\,[1 - 10\tau^3 + 15\tau^4 - 6\tau^5] + b_6^{(+)}\,[-\tau^3 + 3\tau^4 - 3\tau^5 + \tau^6] \tag{30}$$

Henceforth, the superscript $(+)$ on $a_5^{(+)}$, $a_6^{(+)}$, $b_6^{(+)}$ will be dropped since it is understood that $a_5^{(-)} \equiv a_6^{(-)} \equiv b_6^{(-)} \equiv 0$. It will be noted that Eqs. (29) and (30) reduce to the customary profiles of fourth and fifth degree, respectively, if $a_5 \equiv a_6 \equiv b_6 \equiv 0$ (cf. reference 4).

The F integrals become with these profiles

$$\begin{aligned} F_1 = (37/315) &+ (Z/124740) \times [-264 + 211a_5 + 663a_6] + (a_5/41580)\,(352 - 443a_6) + (203a_6/6930) - (z^2/2268) - (52\,a_5^2/31185) - (1417\,a_6^2/83160) \end{aligned} \tag{31}$$

$$\begin{aligned} F_2 = \{[1 + (\gamma - 1)\,(M_1^2/2)]/27720\}\, &\{11570 - 13860(1 - W) + (1159 - 259a_6)a_5 + 3783a_6 - (395\,b_6/2) - 46a_5^2 - 472\,a_6^2 + (-521 + 147a_6 + 46a_5)Z - (110\,9)Z^2\} \end{aligned} \tag{32}$$

$$F_3 = (1 - W)\,[(17/70) - (311a_5/13860) + (31Z/2520) - (131a_6/1848)] + b_6[(17/3080) - (a_5/3080) - (127a_6/120120) + (Z/6930)] \tag{33}$$

The solution of Eqs. (13) and (14) may now be conveniently discussed. It will be assumed that the potential flow quantities (denoted here by the subscript 1) are expressed in terms of M_1 and that M_1 is a known function of ξ. There is no loss in generality in making

this assumption, since if, for example, the potential flow characteristics are known in terms of U_1/U_0 as a function of ξ, U_1/U_0 can be expressed in terms of M_1 and the discussion presented here then applied. Applying Eq. (6) and the usual isentropic relations in the potential flow, one finds

$$\left.\begin{aligned} G^2 &= C(M_1/M_0)\left\{[1+(\gamma-1)(M_0^2/2)]\div[1+(\gamma-1)(M_1^2/2)]\right\}^{(3\gamma-1)/2(\gamma-1)} \\ U_1/U_0 &= (M_1/M_0)\left\{[1+(\gamma-1)(M_0^2/2)]\div[1+(\gamma-1)(M_1^2/2)]\right\}^{1/2} \end{aligned}\right\} \quad (34)$$

where M_0 is the potential flow Mach Number at $\xi = 0$.

Eq. (14) can be integrated directly; if the initial conditions that $\Lambda = \Lambda_0$ and $W = W_0$ at $\xi = 0$ are imposed, one obtains the following algebraic relation which relates implicitly Λ and W:

$$G_0\Lambda_0^{1/2}(F_3)_0 = G\Lambda^{1/2}F_3 \quad (35)$$

Note that $G_0 \equiv C$ and thus that Eq. (35) is independent of C. Finally Eq. (13) can be written symbolically as

$$\Lambda' = f(\Lambda, W, Z, M_1, a_5, a_6, b_6) \quad (36)$$

With Eqs. (35) and (19) relating W and Z, respectively, to Λ, with $M_1 = M_1(\xi)$ known, and with a_5, a_6, and b_6 determined by Eqs. (25) through (28), Eq. (36) can be integrated numerically to give $\Lambda = \Lambda(\xi)$ subject to the initial condition $\Lambda = \Lambda_0$ when $\xi = 0$. The wall temperature which is of prime interest here can be found from the equation

$$T_w/T_{w_0} = W/W_0 \quad (37)$$

where T_{w_0} is the initial wall temperature and where W is found as a function of ξ from Eq. (35) and from the solution to Eq. (36).

The solution of Eq. (36) for the case of zero pressure gradient is of interest for the insulation of the walls of hypersonic wind tunnel test sections and on wedge-shaped airfoil profiles and will be discussed first.

Zero Pressure Gradient

For the case with $Z \equiv 0$, Eq. (36) becomes explicitly

$$(F_1/2)\Lambda' = a_1^{(+)} = 2 - (a_5/3) - a_6 \quad (38)$$

as may be seen from Eqs. (13) and (29). Eq. (38) can be integrated directly; the solution with $\Lambda = \Lambda_0$ at $\xi = 0$ is:

$$\Lambda/\Lambda_0 = 1 + (2/F_1)[2 - (a_5/3) - a_6](\xi/\Lambda_0) \quad (39)$$

Thus for this case $T_w = T_w(\xi)$ can be found readily since from Eq. (35), $W = W(\xi)$ can be found upon substitution of Eq. (39) and finally T_w is determined directly from Eq. (37).

Flows with Axial Pressure Gradients

In the general case, in which M_1 is a prescribed function of ξ, solution of Eq. (36) involves a numerical integration. However, the numerical work is reduced if a new dependent variable

$$\lambda = \Lambda/\Lambda_0 \quad (40)$$

is introduced and if M_1 is considered the independent variable. Eq. (13) becomes with these changes and with the right-hand side expressed in terms of Z by Eq. (29)

$$(F_1/2)(d\lambda/dM_1) + \lambda\{F_1[(d/dM_1)\ln(F_1G)] + F_2[(d/dM_1)\ln(U_1/U_0)]\} = [2 + Z/3 - (a_5/3) - a_6][dM_1/d(\xi/\Lambda_0)]^{-1} \quad (41)$$

If now the W variable appearing in F_2 and implicitly given as a function of Λ by Eq. (35) is eliminated from Eq. (41), the final equation for numerical integration is obtained; it is

$$(F_1/2)(d\lambda/dM_1) + (\lambda/M_1)[m + z_1] - (\lambda^{1/2}/M_1G)z_2 = [2 - (a_5/3) - a_6] \times [dM_1/d(\xi/\Lambda_0)]^{-1} \quad (42)$$

where

$$m = m(M_1) = (1 - \gamma M_1^2)/2[1 + (\gamma-1)(M_1^2/2)]$$

$$z_1 = z_1(Z) = (1/27720)[6952 + a_5(1159 - 295a_6) + (3783a_6) - (395b_6/2) - (46a_5^2) - (472a_6^2) + Z(-521 + 147a_6 + 46a_5)] - (Z^2/2268) + (b_6/3)[(17/3080) - (a_5/3080) - (127a_6 \div 120120) + (Z/6930)][(17/70) - (311a_5 \div 13860) + (31Z/2520) - (131a_6/1848)]^{-1}$$

$$z_2 = z_2(Z) = [(F_3)_0/3][(17/70) - (311a_5/13860) + (31Z/2520) - (131a_6/1848)]$$

and where $G = G(M_1)$ is given explicitly by Eq. (34).

Eq. (42) can be integrated numerically by any of the standard techniques for first order, ordinary differential equations, as for example Adam's method (reference 9), from the initial condition $\lambda = 1$ at $M_1 = M_0$. The only auxiliary equation required is

$$Z = (W\lambda/2M_1)[dM_1/d(\xi/\Lambda_0)] \quad (43)$$

along with $[dM_1/d(\xi/\Lambda_0)]$ which must be determined from $M_1 = M_1(\xi)$ and Λ_0. With $\Lambda = \Lambda(M_1) = \Lambda(\xi)$ given by Eq. (42) $W = W(\xi)$ and $T_w = T_w(\xi)$ are found from Eqs. (35) and (37), respectively.

Numerical Examples

In this section several numerical examples based on the above analysis have been carried out.

Example (1): Optical windows in hypersonic wind tunnel walls. As a numerical example of the zero axial pressure gradient analysis the protection of wind tunnel optical windows by coolant injected upstream according to the sweat cooling technique is considered. The following conditions are assumed: stagnation pressure, $p_s = 500$ psia, stagnation temperature, $T_s =$

2000°R., $M_0 = 4.0$, $W_0 = 0.30$, the tunnel half-height $h = 1$ ft., and the coolant temperature $T_c = 500$°R.

The wall temperature distribution was computed for the two methods of injection as indicated by the discussion of Eq. (A-14) in the Appendix: namely, constant injection with variable surface temperature, and constant surface temperature with nonuniform injection. In both methods the injection was distributed over a 0.5-ft. length upstream of the region to be protected and the mass flow was adjusted so that $W_0 \approx 0.3$ in the first method and so that $W \equiv 0.3$ for $-\xi_t \leq \xi \leq 0$ in the second method. It is pointed out that the values of a_5, a_6, and b_6 were 9.69, -2.38, -14.89, respectively, for constant injection and 9.04, -3.35, and -8.29 for constant wall temperature.

In Fig. 1 the variation of surface temperature with x is shown. Also shown are the total amounts of coolant mass flow in terms of the mass flowing per unit length per unit time in the nozzle half-height. The significant insulating effect of small amounts of injection is evident. It is pointed out that with $\rho_w v_w / \rho_0 U_0$ on the order of 10^{-3} throughout most of the length over which the injection is distributed and with the effect of cooling considered, laminar layers could be expected provided of course that the boundary layer is thin and laminar at $\xi = -\xi_t$. It will be noted that the boundary-layer thickness at this point has implicitly been assumed negligibly small compared to the boundary-layer thickness at $\xi = 0$. Undoubtedly, it would be of interest to study the insulating ability of the turbulent boundary-layer since circumstances wherein the boundary layer is already turbulent at $\xi = -\xi_t$ or becomes turbulent due to large rates of injection will arise. However, at the present time not enough is known about turbulent boundary layers with injection to make this investigation possible. It is furthermore pointed out that the singularities at $\xi = -\xi_t$ for both methods of injection, the first yielding a singularity in that $W = 1$ and the second in that $\rho_w v_w / \rho_0 U_0 \to \infty$, are typical of the singularities encountered at the leading edge in boundary-layer theory.

It is of interest to compare the velocity and stagnation enthalpy profiles on either side of the discontinuity at $\xi = 0$. This has been done for the first method in injection; that is, with $\rho_w v_w / \rho_0 U_0$ constant; the results are shown in Figs. 2 and 3. It will be seen that the velocity profiles on either side are almost identical indicating an insensitivity in the ξ-τ plane to the change in heat transfer at the wall but that, as might be expected, the stagnation enthalpy profile is modified somewhat by the discontinuity in wall heat transfer. Thus an adjustment zone downstream of $\xi = 0$ wherein the flow description given here may not be quite accurate for determination of local quantities away from the boundaries, $y = 0$ and $y = \delta$, is indicated. However, since the correct boundary conditions are prescribed it is believed that the existence of this zone does not alter significantly the distribution of wall temperature which is based on the integrated values of the profiles and on the boundary conditions, both of which are correct.

Example (2). Biconvex Airfoil: The insulating ability of the laminar boundary layer over a biconvex airfoil was studied by numerically integrating Eq. (42). The airfoil was taken as 4 per cent thick with a chord of 4 ft. It was assumed to be in steady flight at a Mach Number of 6 at 50,000 ft. The local Mach Number distribution over the surfaces was determined by the shock wave expansion method neglecting reflected waves (cf. reference 10). The leading 10 per cent of each surface was considered porous and cooling air at 800°R. assumed available. The coolant was injected, at a nonuniform rate, so as to give a constant wall temperature of $0.3T_s$ along the leading 10 per cent of each surface. The average rate of coolant injection was $1.1 \times 10^{-3}\, \rho_0 U_0$. The initial conditions were found by the method described in the Appendix. The parameters a_5, a_6, b_6 were 13.77, -3.695, and -7.39, respectively.

Fig. 4 shows the distribution of surface temperature, in terms of stagnation temperature, on the surface of the airfoil. Also shown in Fig. 4, for purpose of comparison is the temperature distribution, as computed by neglecting the pressure gradient and using Eqs. (38) and (39) along a flat plate subject to the free-stream conditions used for the airfoil. It appears from a comparison of these two results that the influence of the favorable pressure gradient with its concomitant expansion of the outside flow is to keep the surface temperature lower than the equivalent constant pressure surface.

From Fig. 4 the significant insulating ability of the laminar layer under these conditions may be seen. It may be pointed out that the actual surface temperature may be somewhat less than those indicated by this analysis since even at the altitude assumed in these computations radiation will remove some heat and the equilibrium temperature is actually somewhat less than the stagnation temperature because the actual Prandtl Number for air is less than unity.

Conclusions

A method for analyzing the insulating ability of a laminar compressible boundary layer has been developed. The flow situation studied involves an upstream section which is cooled either by convective or sweat cooling; downstream of this section the surface is uncooled, that is adiabatic. Because of the insulating ability of the laminar layer, the wall temperature is less than adiabatic and varies in the downstream direction.

The method is based on the integral approach. At the discontinuity where cooling and/or injection ceases the conditions of continuity of mass, momentum, energy, and of boundary-layer thickness are imposed

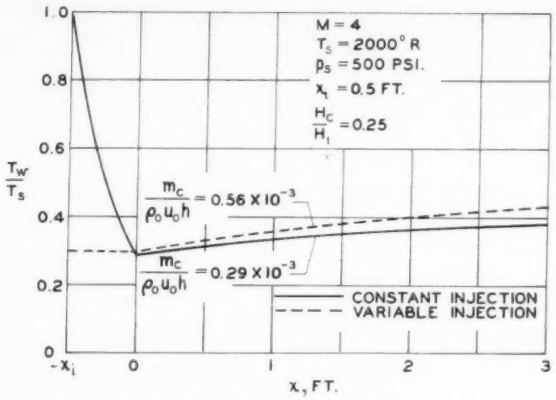

FIG. 1. Surface temperature distribution on a flat plate.

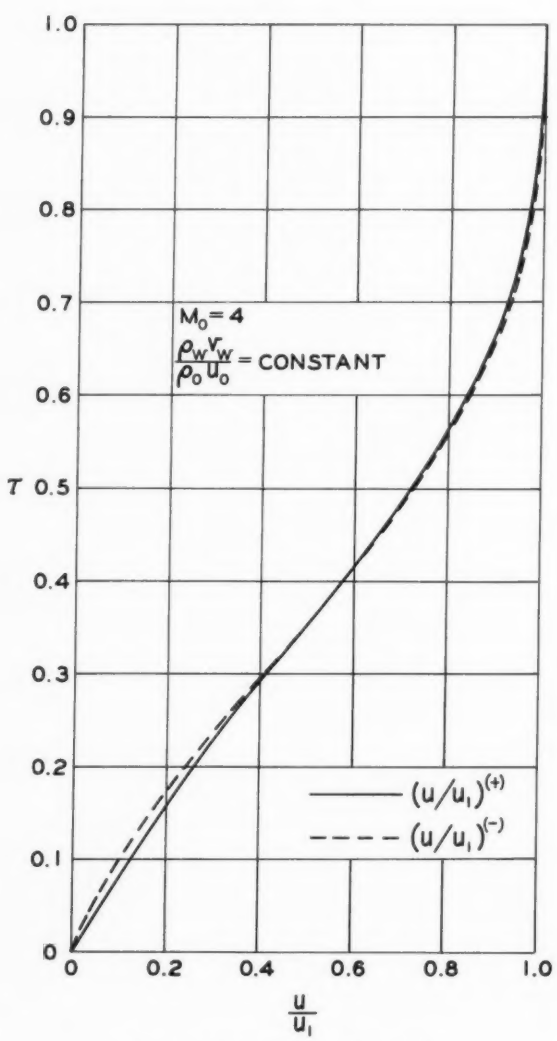

FIG. 2. Velocity profile for flat plate.

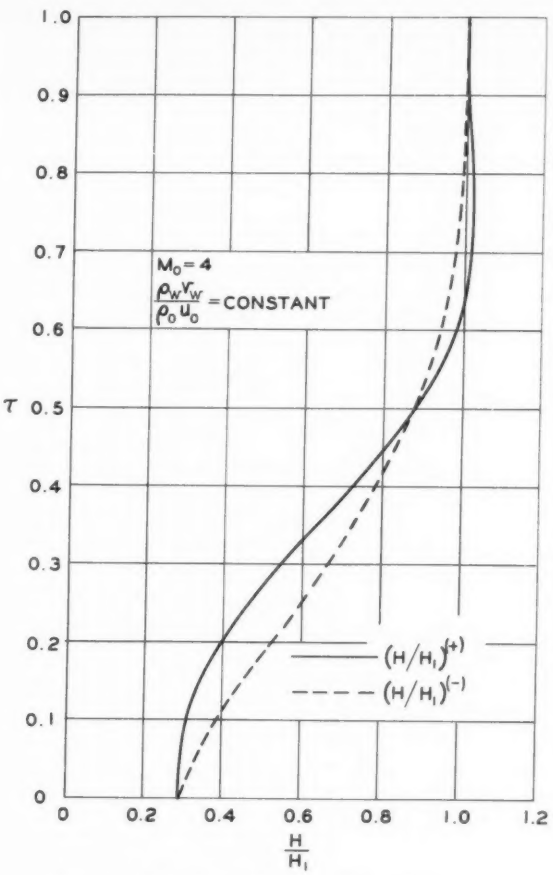

FIG. 3. Stagnation enthalpy profile for flat plate.

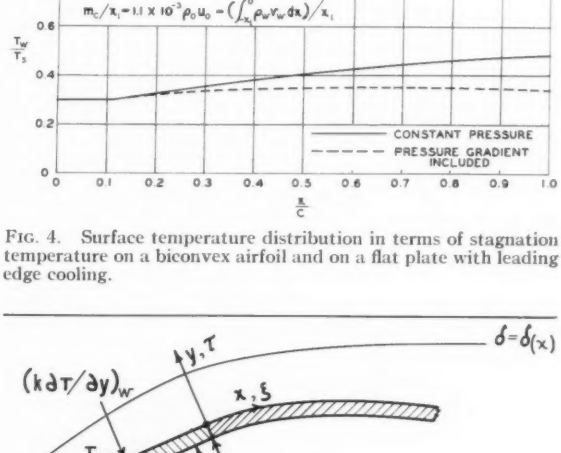

FIG. 4. Surface temperature distribution in terms of stagnation temperature on a biconvex airfoil and on a flat plate with leading edge cooling.

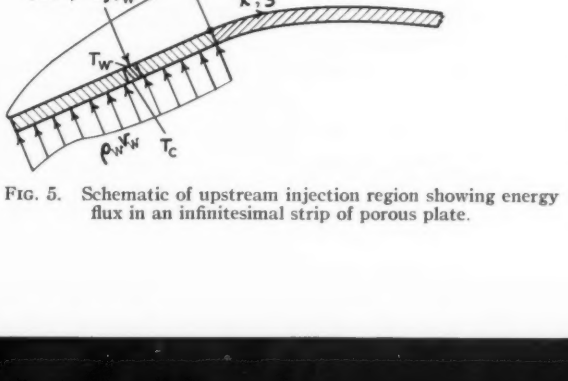

FIG. 5. Schematic of upstream injection region showing energy flux in an infinitesimal strip of porous plate.

by the addition of several parameters in the velocity and stagnation enthalpy profiles.

Two numerical examples indicate strong insulating ability of the laminar layer when cooling upstream is accomplished by injection. The required rates of injection are so small that laminar layers may exist despite the destabilizing effect of injection.

References

[1] Duwez, P., and Wheeler, H. L., Jr., *Experimental Study of Cooling by Injection of a Fluid through a Porous Material*, Journal of the Aeronautical Sciences, Vol. 16, No. 12, p. 727, December, 1949.

[2] Morduchow, M., *On Heat Transfer Over a Sweat Cooled Surface in Laminar Compressible Flow with Pressure Gradient*, Journal of Aeronautical Sciences, Vol. 19, No. 10, p. 705, October, 1952.

[3] Kalikhman, L. E., *Heat Transmission in the Boundary Layer*, NACA TM 1229, 1949.

[4] Libby, Paul A., and Morduchow, M., *A Method for the Calculation of the Compressible Laminar Boundary Layer with Axial Pressure Gradient and Heat Transfer*, NACA TN 3157, 1954.

[5] Levy, Solomon, *Heat Transfer to Constant-Property Laminar Boundary-Layer Flows with Power-Function Free-Stream Velocity and Wall-Temperature Variation*, Journal of the Aeronautical Sciences, Vol. 19, No. 5, p. 341, May, 1952.

[6] Eckert, E. R. G., *Developments in Convective Heat-Transfer Research*, Proceedings of the Second Midwestern Conference on Fluid Mechanics, p. 309, 1952.

[7] Chapman, Dean R., *Laminar Mixing of a Compressible Fluid*, NACA Rep. 958, 1950.

[8] Libby, Paul A., Morduchow, M., and Bloom, Martin H., *Critical Study of Integral Methods in Compressible Laminar Boundary Layers*, NACA TN 2655, 1952.

[9] Kármán and Biot, *Mathematical Methods in Engineering*, p. 16; McGraw-Hill Book Company, Inc., New York, 1940.

[10] Ferri, Antonio, *Elements of Aerodynamics of Supersonic Flows*, p. 122; The Macmillan Company, New York, 1949.

Appendix

For completeness and convenience an analysis of the laminar boundary layer with injection is presented in terms of the variables used in the downstream ($x > 0$)-region. The injection is assumed to occur on a constant pressure strip and thus the equations corresponding to Eqs. (13) and (14) for the case of constant pressure but with injection are*

$$(F_1/2)\Lambda' + \Lambda F_1' - (\rho_w v_w/\rho_0 U_0)\Lambda = [(u/U_1)_\tau]_w \quad \text{(A-1)}$$

$$(F_3/2)\Lambda' + \Lambda F_3' - (\rho_w v_w/\rho_0 U_0)\Lambda(1 - W) = [(H/H_1)_\tau]_w \quad \text{(A-2)}$$

It should be noted that $(\rho_w v_w/\rho_0 U_0)$ is the ratio of masses injected and flowing in the potential stream per unit time and per unit area and may be a function of x.

If fourth and fifth degree polynomials for the velocity and stagnation enthalpy profiles are assumed then

$$u/U_1 = \sum_{j=0}^{4} a_j \tau^j \quad \text{(A-3)}$$

and

$$H/H_1 = \sum_{j=0}^{5} b_j \tau^j \quad \text{(A-4)}$$

The boundary conditions on u/U_1 and H/H_1 in the ξ-τ plane are at $\tau = 0$,

$$\left.\begin{aligned} u/U_1 &= 0 \\ H/H_1 &= w \end{aligned}\right\} \quad \text{(A-5)}$$

and at $\tau = 1$,

$$\left.\begin{aligned} u/U_1 &= H/H_1 = 1 \\ (u/U_1)_\tau &= (H/H_1)_\tau = 0 \end{aligned}\right\} \quad \text{(A-6)}$$

Additional boundary conditions at $\tau = 0$ can be obtained from Eqs. (1) and (4) with $y = 0$; in terms of Λ and $\rho_w v_w/\rho_0 U_0$; they are

$$\left.\begin{aligned} (u/U_1)_{\tau\tau} &= (\rho_w v_w/\rho_0 U_0)\Lambda^{1/2}(u/U_1)_\tau \\ (H/H_1)_{\tau\tau} &= (\rho_w v_w/\rho_0 U_0)\Lambda^{1/2}(H/H_1)_\tau \end{aligned}\right\} \quad \text{(A-7)}$$

Similarly, additional boundary conditions at $y = \delta(x)$ or $\tau = 1$ can be obtained from Eqs. (1) and (4) with $u_y = H_y = 0$; they are in the ξ-τ plane

$$(u/U_1)_{\tau\tau} = (H/H_1)_{\tau\tau} = 0 \quad \text{(A-8)}$$

With Eqs. (A-5)–(A-8) the coefficients for the velocity and stagnation enthalpy profiles can be evaluated in terms of a_2, b_1 W, and an injection parameter. They are

$$u/U_1 = (2\tau - 2\tau^3 + \tau^4) + a_2[-(\tau/3) + \tau^2 - \tau^3 + (\tau^4/3)] \quad \text{(A-9)}$$

$$H/H_1 = 1 - (1 - W)[1 - 10\tau^3 + 15\tau^4 - 6\tau^5] + b_1[\tau - 6\tau^3 + 8\tau^4 - 3\tau^5] + (\psi b_1/2) \times [\tau^2 - 3\tau^3 + 3\tau^4 - \tau^5] \quad \text{(A-10)}$$

where

$$\begin{aligned} b_1 &= [(H/H_1)_\tau]_w \\ a_2 &= \psi/[1 + (\psi/6)] \\ a_1 &= 2 - (a_2/3) \\ \psi &\equiv (\rho_w v_w/\rho_0 U_0)\Lambda^{1/2} \end{aligned}$$

With Eqs. (A-9) and (A-10) the F integrals can be evaluated; they are

$$F_1 = (37/315) + (2a_2/945) - (a_2^2/2268) \quad \text{(A-11)}$$

$$F_3 = (1 - W)[(17/70) - (31a_2/2520)] + b_1[-(79/1260) + (19a_2/7560)] + (\psi b_1/2)[-(29/2520) + (a_2/2520)] \quad \text{(A-12)}$$

In a practical application of sweat cooling the local heat transfer which is proportional to b_1 and the rate of injection $\rho_w v_w/\rho_0 U_0$ are not independent but are related through a local heat balance within the porous plate. This introduces a coolant temperature T_c which is realistically taken constant. Fig. 5 indicates the upstream injection zone being considered with the energy flux in an infinitesimal strip of porous plate. The heat balance of this element neglecting axial heat

* Reference 2 contains an analysis of the case with axial pressure gradient, variable injection and constant wall temperature but the method differs from that used here in some details.

conduction along the plate is

$$(k\,dT/dy)_w = c_p\rho_w v_w(T_w - T_c) \qquad \text{(A-13)}$$

which in terms of the variables here becomes

$$\psi = b_1/(W - H_c/H_1) \qquad \text{(A-14)}$$

where $H_c \equiv c_p T_c$. It is pertinent to point out here that for constant static pressure $G \equiv 1$.

In practice with a homogeneous porous plate of constant thickness and with a constant pressure difference, $\rho_w v_w$ is constant, and thus Eq. (A-14) is satisfied by having W vary in the x direction. On the other hand if, as may well be, it is desired to have W constant, Eq. (A-14) is satisfied by a variable $\rho_w v_w$ which can be achieved in practice by either a nonhomogeneous porous plate or by a porous plate of variable thickness. These two different methods of sweat cooling require different solutions of Eqs. (A-1) and (A-2) and are discussed now.

With $\rho_w v_w$ constant and with Eq. (A-14) substituted into Eqs. (A-1) and (A-2) one obtains

$$\Lambda^{1/2}(d/d\xi)\,(F_1\Lambda^{1/2}) = 2 + \psi[(4 + \psi)/(6 + \psi)] \qquad \text{(A-15)}$$

$$\Lambda^{1/2}(d/d\xi)\,(F_3\Lambda^{1/2}) = \psi[1 - (H_c/H_1)] \qquad \text{(A-16)}$$

which define Λ and W as functions of x. Eq. (A-16) can be integrated directly; the solution with $\Lambda = 0$ at $\xi = -\xi_i$ is

$$F_3\Lambda = \psi(\xi + \xi_i)\,[1 - (H_c/H_1)] \qquad \text{(A-17)}$$

with the restriction $-\xi_i \leq \xi \leq 0$. Eqs. (A-12) and (A-17) give $W = W(\Lambda, \xi)$. The integration of Eq. (A-15) gives $\xi = \xi(\Lambda)$ in the form

$$(\rho_w v_w/\rho_0 U_0)^2(\xi + \xi_i) = 2.518 + 0.1143\psi - 0.888/(1 + \psi/6) + 0.3336 \ln (1 + \psi/6) + 0.1903 \ln (1 + \psi/6)^2 - 0.4475 \ln (\psi^2 + 6\psi + 12) - 0.49498 \tan^{-1}[(2\psi + 6)(12)^{-1/2}] \qquad \text{(A-18)}$$

Thus Eqs. (A-17) and (A-18) along with the equations for F_3 and ψ complete the solution for Λ and W as functions of x.

For the case of W constant, $\rho_w v_w$ variable, the differential equations and initial conditions are satisfied by taking ψ and b_1 constant, in which case Eqs. (A-1) and (A-2) become

$$d\Lambda/d\xi = \{2\psi\,[(4 + \psi)/(6 + \psi)] + 4\}/F_1 = 2\psi[1 - (H_c/H_1)]/F_3 \qquad \text{(A-19)}$$

Eqs. (A-19) and (A-14) permit the determination from two algebraic equations of the constant values of ψ and b_1 for given values of W and (H_c/H_1). With these values Eq. (A-19) can be integrated immediately to give $\Lambda = \Lambda(\xi)$. It is pointed out that this solution results in $\rho_w v_w$ proportional to $x^{-1/2}$ and corresponds to the well-known exact solutions of the laminar boundary-layer equations with such a distribution of injection.

Development of Charts for Downwash Coefficients of Oscillating Wings of Finite Span and Arbitrary Plan Form

(*Continued from page 824*)

and hence two branches of roots. In most cases only one of the two branches has a root within the narrow permissible variation of g. If both branches yield roots of physical validity, the one with the lower flutter speed determines flutter conditions.

References

[1] Dengler, M. A., and Goland, M., *The Subsonic Calculation of Circulatory Spanwise Loadings for Oscillating Airfoils by Lifting-Line Techniques*, Journal of the Aeronautical Sciences, Vol. 19, pp. 751–759, November, 1952.

[2] Dengler, M. A., Goland, M., and Luke, Y. L., *Theoretical Studies of the Effects of Aspect Ratio on Flutter*, WADC Report 5429, 1954.

[3] Diederich, F. W., *Charts and Tables for Use in Calculations of Downwash of Wings of Arbitrary Planform*, NACA TN 2535, May, 1951.

[4] Dengler, M. A., Goland, M., and Luke, Y. L., *Tables of the Functions* $\int_0^y (e^{iu} - 1)\sqrt{(u^2 + b^2)}\,du/u$, Mathematical Tables and Other Aids to Computation, Vol. VII, No. 41, January, 1953, Washington, D.C.

[5] Luke, Y. L., and Ufford, D., *A Table of the Complete Cicala Function*, Journal of the Aeronautical Sciences, Vol. 20, pp. 511–512, July, 1953.

[6] Biot, M. A., and Boehnlein, H., *Aerodynamic Theory of the Oscillating Wing of Finite Span*, GALCIT Rep. 5, September, 1942.

[7] Reissner, E., *Effect of Finite Span on the Airload Distribution for Oscillating Wings—I, Aerodynamic Theory of Oscillating Wings of Finite Span*, NACA TN 1194, March, 1947.

[8] Reissner, E., *Investigation of Oscillating Lifting Surfaces of Finite Span in Incompressible Flow*, Air Research and Development Command, Tech. Rep., October, 1951.

Three-Dimensional Laminar Boundary Layer with Small Cross-Flow*

ARTUR MAGER†

California Institute of Technology

ABSTRACT

Important problems involving three-dimensional boundary layer occur in almost all internal and external aerodynamic configurations. For many of these, the flow outside the boundary layer may be resolved into a large principal component and a small crosswise velocity. In this paper, three-dimensional laminar boundary-layer flows over flat and curved surfaces are treated under such a simplification. For flat surfaces, the solutions demonstrate the effect of the free stream turning on the velocity profiles in the crosswise and primary flow directions. When the surface curvature is large and varies so as to resemble a corner, the computed examples show the manner in which the asymmetric behavior of the boundary layer results from the cross-flow. The detailed examples are chosen to illustrate flows occurring on the casing and in the blade fillets of turbomachinery.

SYMBOLS

a	= cylinder radius
A_m; B_n; E_r	= functions of z
$\boldsymbol{b}$	= vector position
c	= curvature
d_i; $l_{n,i}$; $t_{n,i}(i = 0, 1, 2, \ldots)$	= functions of η
D, H	= constants
f_m; f_n; f_r; $f_{m,c}$; g_n; g_r	= functions of η
F	= Blasius function
$G_i(i = 1, 2, 3)$	= body forces
$h_i(i = 1, 2, 3)$	= length stretching factors
L	= length of duct
m, n, r	= exponents of x
M	= Mach Number
p	= pressure
$\boldsymbol{q}$	= vector velocity
$\bar{\boldsymbol{q}}$	= vector velocity at $y = \delta$
R	= cylinder path radius
Re	= Reynolds Number $U^0\xi/\nu$
s	= width of duct
u, v, w	= velocities in the boundary layer
U, V, W	= velocities of external flow
x, y, z	= Cartesian coordinates
X, Y, Z	= coordinates in compressible flow
α	= yaw angle
β	= angle between tangent to ζ axis and z axis
γ	= ratio of specific heats
δ	= boundary-layer thickness
ξ, λ, ζ	= curvilinear coordinates
η	= similarity variable $y[U^0/\nu x]^{1/2}$ also $y[U^0/\nu\xi]^{1/2}$
θ	= cylindrical coordinate
$\bar{\vartheta}$	= average turning at $x/L = 0.5$
κ	= curvature parameter $c(\nu\xi/U^0)$
ν	= kinematic viscosity
ρ	= density
χ	= perpendicular distance from axis of rotation
ψ; φ	= functions satisfying continuity
ω	= vector angular velocity
$\omega_i(i = 1, 2, 3)$	= components of angular velocity
$\Omega_i(i = 1, 2)$	= angular velocity components for cylinder
∇	= differential operator

Superscripts

0	= basic flow also standard quantity
*	= total value (basic + perturbation)
′	= differentiation with respect to η
—	= compressible flow

Subscripts

δ = at $y = \delta$

Coordinates indicate partial differentiation

(I) INTRODUCTION

THE IMPORTANT PROBLEM of three-dimensional boundary-layer flow occurs in almost any real, external or internal, aerodynamic configuration. Because of its complexity, this problem is generally avoided, and either a two-dimensional boundary-layer flow analysis is made as an approximation, or none at all. Such procedure is usually satisfactory as long as the design is conservative and the fluid is asked to perform but moderate tasks. When, however, one attempts to increase the performance by requiring the fluid to flow against stronger pressure gradients, then the available theories completely break down, with rather undesirable results. This is particularly well illustrated by the design of turbomachinery, which is successful, provided the stages of these machines operate at extremely moderate pressure ratios, far below those obtainable in cascades and single-stage experiments. However, when high pressure ratio per stage machine is attempted, the real fluid effects become so

Presented at the Aerodynamics Session, Twenty-Second Annual Meeting, IAS, New York, January 25–29, 1954.

* This paper is partly based on a Doctoral Thesis at the California Institute of Technology and is sponsored by the Air Research and Development Command under Contract No. AF 18(600)-178. Special acknowledgment is due to Profs. F. E. Marble and H. S. Tsien for their valuable advice and constructive criticism.

† Formerly, Research Fellow in Jet Propulsion; now, Engineering Specialist, Marquardt Aircraft Co.

important that they overshadow the aims of the newly incorporated features and the designed performance cannot be realized. Consequently, the important engineering problem of increase in power output, per unit weight of the machinery, remains unsolved.

The real fluid effects demonstrate themselves primarily in the so-called secondary flow and in the three-dimensional boundary-layer flow. The term secondary flow is currently used to designate flows arising from nonuniform total pressure or enthalpy, in regions not bordering on physical boundaries, where the effect of viscosity may be neglected. Such flows usually occur in internal aerodynamic configurations. On the other hand, by the term three-dimensional boundary-layer flow, we understand similar flows in the relatively thin regions, next to solid walls, where the viscosity plays an important part. Three-dimensional boundary-layer flows occur for both the internal, as well as external, aerodynamic configurations, differing in the nature of the flow outside the boundary layer. In internal aerodynamic configurations, the flow outside the boundary layer may be secondary and thus rotational, while in the external aerodynamic configurations that flow is potential.

A critical review of the three-dimensional boundary-layer literature reveals a definite division into three separate groups. The first group consists of the investigations of the forms of the boundary-layer equations and discussion of boundary-layer behavior as inferred from these forms, without actual solution of the equations. Here significant work has been done by Howarth,[1] Hayes,[2] and Moore.[3] The second group consists of general, but approximate, treatment of three-dimensional boundary-layer flow by the momentum-integral method. The laminar case in this group has been investigated by Timman,[4] and the turbulent one by Mager.[5] The validity of these methods depends to a large extent on the choice of the velocity distributions in the boundary layer, and since the experimental information is meager, attempts have been made to study the velocity distributions analytically. This leads us to the third group, which consists of solutions of some specialized cases of three-dimensional laminar boundary-layer flow. These specialized cases fall into two categories: (a) where the changes with respect to one of the independent coordinates are zero, or where there exists some sort of symmetry, and (b) where there is some characteristic parameter that is small. In the first category belongs the work of Sears,[6] Bödewart,[7] Howarth,[8] Loos,[9] and Carrier,[10] while in the second one the publications of Moore[11,12] and Fogarty[13] may be mentioned.

The general treatment of three-dimensional boundary-layer flow is extremely difficult in view of the complexity of the equations. However, for many important problems involving three-dimensional boundary layer, the flow outside the boundary layer may be resolved into a large principal component and a small cross-wise velocity. Since the pressure variation in the direction normal to the wall is usually negligible in the boundary layer, the flow there is affected by pressures existing outside the layer—that is, those governing the external flow. Consequently, the velocities in the boundary layer will have the order of magnitude of their values in the external flow. When the cross-wise velocity is small as compared with the principal velocity, but otherwise not specified, the boundary layer will be only slightly three-dimensional, and the small perturbation procedure will be applicable to a great variety of external flows. The object of this paper is to treat the three-dimensional laminar boundary-layer flows over flat and sharply curved surfaces under just such simplification.

(II) Boundary-Layer Flow over Flat Surface

Boundary-Layer Approximation

The motion of an incompressible steady viscous fluid, flowing relative to a coordinate system rotating with a uniform angular velocity is described by the momentum equations,

$$-\boldsymbol{q}\times(\boldsymbol{\nabla}\times\boldsymbol{q}) + \boldsymbol{\omega}\times(\boldsymbol{\omega}\times\boldsymbol{b}) + 2\boldsymbol{\omega}\times\boldsymbol{q} = -\boldsymbol{\nabla}\left(\frac{1}{\rho}p + \frac{1}{2}\boldsymbol{q}^2\right) + \nu[\boldsymbol{\nabla}(\boldsymbol{\nabla}\cdot\boldsymbol{q}) - \boldsymbol{\nabla}\times(\boldsymbol{\nabla}\times\boldsymbol{q})] \quad (1)$$

and the equation of continuity,

$$\boldsymbol{\nabla}\cdot\boldsymbol{q} = 0 \quad (2)$$

Making the usual boundary-layer simplifications—that is, neglecting all terms of $0(\delta)$ as compared with those of $0(1)$,—one obtains from Eqs. (1) and (2) the boundary layer equations,

$$\left.\begin{aligned} u^*u_x^* + v^*u_y^* + w^*u_z^* + 2\omega_2 w^* - \omega^2\chi\chi_x &= -\frac{1}{\rho}p_x + \nu u_{yy}^* \\ 2(\omega_3 u^* - \omega_1 w^*) - \omega^2\chi\chi_y &= -\frac{1}{\rho}p_y \\ u^*w_x^* + v^*w_y^* + w^*w_z^* - 2\omega_2 u^* - \omega^2\chi\chi_z &= -\frac{1}{\rho}p_z + \nu w_{yy}^* \end{aligned}\right\} \quad (1a)$$

and

$$u_x^* + v_y^* + w_z^* = 0 \quad (2a)$$

These equations differ from those used in two-dimensional theory, not only by the presence of an additional equation in the z direction (for notation see Fig. 1) but also by p_y being of $0(1)$ instead of $0(\delta)$. This occurs because a pressure gradient is necessary to balance the effect of the centripetal and Coriolis forces. But the total change of pressure throughout the boundary layer along a normal to the wall is still of $0(\delta)$, and although this is larger than on a nonrotating flat plate [where it is of $0(\delta^2)$], it may still be neglected. A reasonable as-

sumption, therefore, is to consider p as a function of x and z only.

External Flow

The external flow is defined as the flow where the effects of viscosity may be neglected, regardless of its character, which may be rotational or irrotational. This definition is different from that used in the conventional mechanics of the boundary-layer flow, and it implies a division of the total flow field into a region where the effects of viscosity are neglected and a (still thinner) region where such effects are considered. If the external flow is rotational, the Eulerian equations must be used (instead of the conventional Bernoulli's relation) for the variation of pressure,

$$-\bar{q}\times(\nabla\times\bar{q}) + \omega\times(\omega\times b) + 2\omega\times q = -\nabla\left(\frac{1}{\rho}p + \frac{1}{2}q^2\right) \tag{3}$$

In the present analysis it will be assumed that the external flow may be only slightly rotational, so that the derivatives U_y^* and W_y^* are small as compared with U_x^*. This simplification permits one to specify the pressure in terms of U^*, W^*, and ω alone, even if V^* is of $0(\delta)$. The external flow components U^*, W^*, and the angular velocity ω are assumed known. In particular one takes:

$$\left.\begin{aligned} &U^* = U^0 + U(x, z); \quad W^* = W(x, z);\\ &\omega = i\omega_1 + j\omega_2 + k\omega_3\\ &U \ll U^0; \qquad W \ll U^0; \qquad \omega_2 \ll \omega_1, \omega_3 \end{aligned}\right\} \tag{4}$$

as describing the external flow and the angular velocity. The velocity U^0 and the angular velocity ω are assumed constant. The component ω_2 is taken of the same order when compared to ω_1 as U when compared with U^0.

Perturbed Flow Equations

Corresponding to Eqs. (4), the flow in the boundary layer is expressed by

$$\left.\begin{aligned} u^* &= u^0(x, y) + u(x, y, z)\\ v^* &= v^0(x, y) + v(x, y, z)\\ w^* &= w(x, y, z) \end{aligned}\right\} \tag{5}$$

where again the perturbation terms u, v, w are assumed small, when compared with the basic flow terms u^0 and v^0. It is clear from the expressions (4) and (5), that, since U^0 is a constant, the substitution into Eqs. (1a) and (2a) must result in the zeroth-order terms forming the Blasius "flat-plate" equations. The first-order terms then give the relations, for the perturbation velocities u, v, w,

$$\left.\begin{aligned} &u^0u_x + uu_x{}^0 + v^0u_y + vu_y{}^0 = U^0U_x + \nu u_{yy}\\ &u^0w_x + v^0w_y + 2\omega_2(U^0 - u^0) = U^0W_x + \nu w_{yy}\\ &u_x + v_y + w_z = 0 \end{aligned}\right\} \tag{6}$$

The solution for the basic flow is known: $u^0 = U^0F'$, $v^0 = (1/2)\sqrt{\nu U^0/x}\,(\eta F' - F)$, $\eta = y\sqrt{U^0/\nu x}$, with $F(\eta)$ being the usual Blasius function tabulated in reference 14. Furthermore, proceeding in the manner of reference 3, the equation of continuity may be identically satisfied by introduction of two functions ψ and φ,

$$u \equiv \psi_y; \quad w \equiv \varphi_y; \quad v \equiv -(\psi_x + \varphi_z) \tag{7}$$

One now assumes that the external flow velocity components and ω_2 are expressible as power functions of the x coordinate: $U = \sum_m A_m(z)x^m$, $W = \sum_n B_n(z)x^n$, $\omega_2 = \sum_r E_r(z)x^r$, and puts the functions φ and ψ in a form that will later prove convenient,

$$\left.\begin{aligned} \psi &= \sqrt{\frac{\nu x}{U^0}}\left[\sum_m A_m x^m f_m + \sum_n \frac{\partial B_n}{\partial z}x^{n+1}f_n + 2\sum_r \frac{\partial E_r}{\partial z}x^{r+2}f_r\right]\\ \varphi &= \sqrt{\frac{\nu x}{U^0}}\left[\sum_n B_n x^n g_n + 2\sum_r E_r x^{r+1} g_r\right] \end{aligned}\right\} \tag{8}$$

Here f_m, f_n, f_r, g_n, and g_r are functions of η only. Using Eqs. (8) and the expressions for the basic flow velocities, Eqs. (6) become

$$\left.\begin{aligned} &\left\{\sum_m A_m x^m\left[f_m''' + \frac{F}{2}f_m'' - mF'f_m' + \left(m + \frac{1}{2}\right)F''f_m + m\right]\right\} +\\ &\quad\left\{\sum_n \frac{\partial B_n}{\partial z}x^{n+1}\left[f_n''' + \frac{F}{2}f_n'' - (n+1)F'f_n' + \left(n + \frac{3}{2}\right)F''f_n + F''g_n\right]\right\} +\\ &\quad\left\{2\sum_r \frac{\partial E_r}{\partial z}x^{r+2}\left[f_r''' + \frac{F}{2}f_r'' - (r+2)F'f_r' + \left(r + \frac{5}{2}\right)F''f_r + F''g_r\right]\right\} = 0\\ &\left\{\sum_n B_n x^n\left[g_n''' + \frac{F}{2}g_n'' - nF'g_n' + n\right]\right\} +\\ &\quad\left\{2\sum_r E_r x^{r+1}\left[g_r''' + \frac{F}{2}g_r'' - (r+1)F'g_r' - (1 - F')\right]\right\} = 0 \end{aligned}\right\} \tag{9}$$

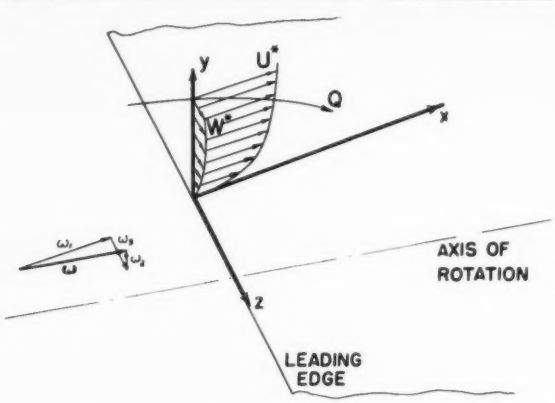

FIG. 1. Notation for flow over flat surface.

Since U, W, and ω_2 will, in general, be different functions of x and z, to satisfy Eqs. (9) for all values of these variables, it is necessary that the quantities in braces vanish separately. This is possible if all the coefficients of various powers of x vanish independently, or in other words, all the expressions in brackets in Eqs. (9), when set equal to zero, become the differential equations which functions f_m, f_n, f_r, g_n, and g_r must satisfy to make this true. Since the perturbation velocities (relative to the surface) are now given by

$$\left.\begin{aligned} u &= \sum_m A_m x^m f_m' + \sum_n \frac{\partial B_n}{\partial z} x^{n+1} f_n' + 2\sum_r \frac{\partial E_r}{\partial z} x^{r+2} f_r' \\ w &= \sum_n B_n x^n g_n' + 2\sum_r E_r x^{r+1} g_r' \\ v &= \frac{1}{2}\sqrt{\frac{\nu}{U^0 x}} \times \left\{ \sum_m A_m x^m [(1+2m) f_m - f_m' \eta] + \sum_n \frac{\partial B_n}{\partial z} x^{n+1} [(2n+3) f_n + 2g_n - f_n' \eta] + 2\sum_r \frac{\partial E_r}{\partial z} x^{r+2} [(2r+5) f_r + 2g_r - f_r' \eta] \right\} \end{aligned}\right\} \quad (10)$$

the appropriate boundary conditions are:

$$\left.\begin{aligned} f_m(0) &= f_m'(0) = f_n(0) = f_n'(0) = f_r(0) = \\ f_r'(0) &= g_n(0) = g_n'(0) = g_r(0) = g_r'(0) = 0 \\ {}_m'(\infty) &= g_n'(\infty) = 1; \quad f_n'(\infty) = f_r'(\infty) = \\ & g_r'(\infty) = 0 \end{aligned}\right\} \quad (11)$$

As may be seen from Eqs. (9), the functions g are completely independent of the functions f, which means that, to the first order of approximation, the cross-wise flow w is completely independent of the principal flow perturbation u and is affected only by the gradients of the external flow W and the component of the angular velocity normal to the surface ω_2. When the cross-wise velocity w is not a function of the z coordinate, the equations for the principal flow perturbation and the cross-wise flow perturbation are completely uncoupled. This means, that according to first-order theory, the changes in the principal flow velocity profile, and in particular the tendency toward the separation, are completely independent of the existence of cross-flow and will occur as if the flow were quasi-two-dimensional. This result is similar to the one obtained by Sears[6] and applies even when the u velocity varies in the z direction. The cross-wise flow w brings about changes in the principal velocity distribution in the form of functions f_n' and f_r', but only if that cross-wise flow is a function of the cross-wise coordinate z.

Two types of body forces were considered originally in Eq. (1): the centripetal force, and the Coriolis force. Of these, the centripetal force was assumed independent of the y coordinate and consequently has been completely canceled out of the equations. The Coriolis force, which did depend on the y coordinate, remained in the equations, and its effect demonstrates itself through functions g_r' and f_r'. In internal aerodynamics, particularily in turbomachinery, it is often convenient to represent the external flow field as caused by some imaginary force field. It should be clear, from the above discussion, that such representation will have no effect on the boundary-layer flow except that caused by external flow velocities, provided the force field is not a function of the y coordinate.

Solutions of Eqs. (9) for the various functions f' and g' were obtained by the relaxation method and are shown in Figs. 2(a–d). The inspection of these figures and Eqs. (9) reveals that the first-order solution does not affect the total boundary-layer thickness, which remains the same as that determined by the basic flow solution. This, of course, is not true for the momentum and displacement thicknesses, which will change, because of changes in the velocity profiles. We note also, that the maximum values of the functions f_n', f_r', and g_r' are considerably lower than those of functions f_m' and g_n'. This indicates that the effect of the Coriolis acceleration and of the variation of the w velocity with z coordinate is small when compared with the changes in velocity distribution brought about by the gradients of the external flow in the x direction.

Effect of Compressibility

To estimate the effect of compressibility on three-dimensional boundary-layer flow, one considers all quantities relative to some standard quantities, the viscosity as varying linearly with temperature, no heat transfer at the surface, and Prandtl Number equal to unity. Using Howarth's transformation,

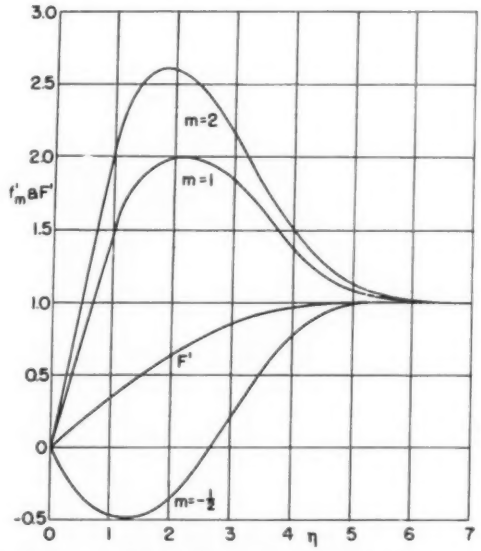

FIGURE 2.- PERTURBATION VELOCITY PROFILES
a) EFFECT OF PRESSURE GRADIENT IN PRINCIPAL DIRECTION

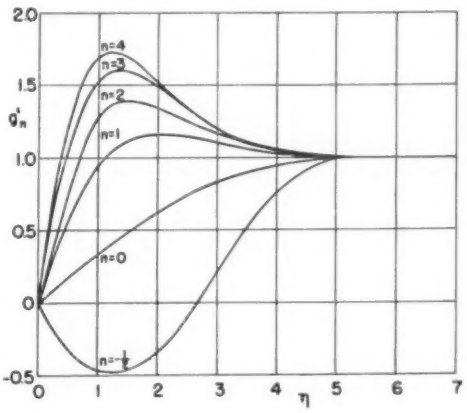

FIGURE 2.- CONT'D.
b) EFFECT OF PRESSURE GRADIENT IN CROSSWISE DIRECTION

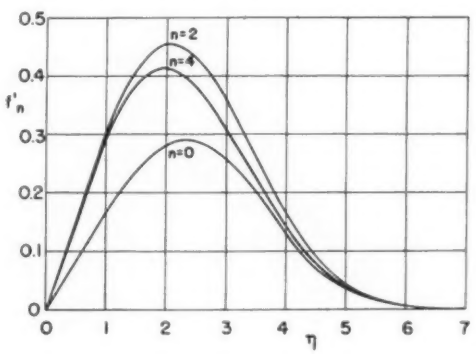

FIGURE 2.- CONT'D.
c) EFFECT OF CROSSWISE VARIATION OF THE CROSSWISE FLOW ON PRINCIPAL FLOW

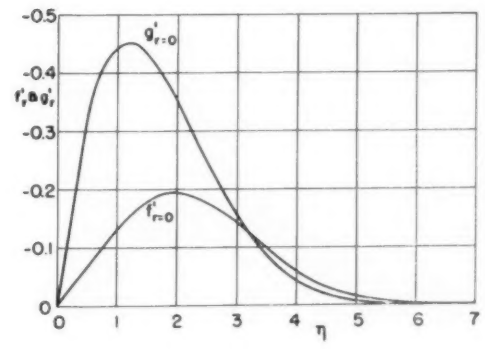

FIGURE 2.- CONT'D.
d) EFFECT OF SURFACE ROTATION (r = 0)

$$Y \equiv \left(\frac{p}{p^0}\right)^{-1/2} \int_0^y \frac{\rho}{\rho^0}\, dy; \quad X \equiv x; \quad Z \equiv z$$

$$\psi \equiv \left(\frac{p}{p^0}\right)^{1/2} \bar{\psi}; \quad \varphi \equiv \left(\frac{p}{p^0}\right)^{1/2} \bar{\varphi}; \quad \bar{\eta} \equiv Y\sqrt{\frac{U^0}{X}} \tag{12}$$

$$\bar{\psi} = \sqrt{U^0 X}\left[\bar{F} + \frac{1}{U^0}\sum_m A_m X^m \bar{f}_m + \frac{1}{U^0}\sum_n \frac{\partial B_n}{\partial Z} X^{n+1} \bar{f}_n\right]$$

$$\bar{\varphi} = \sqrt{\frac{X}{U^0}}\left[\sum_n B_n X^n \bar{g}_n\right]$$

The functions $\bar{\psi}$ and $\bar{\varphi}$ now written (for a nonrotating surface) as yield again the Blasius equation as the zeroth-order equation. The first-order equations now are

$$\left\{\sum_m A_m X^m \left\{\bar{f}_m''' + \frac{\bar{F}}{2}\bar{f}_m'' - m\bar{F}'\bar{f}_m' + \left(\frac{1}{2} + m\right)\bar{F}''\bar{f}_m + m \times \left[1 + \frac{\gamma - 1}{2} M^2(1 - \bar{F}'^2) - \frac{\gamma}{2} M^2 \bar{F}\bar{F}''\right]\right\}\right\} +$$
$$\left\{\sum_n \frac{\partial B_n}{\partial Z} X^{n+1}\left[\bar{f}_n'''' + \frac{\bar{F}}{2}\bar{f}_n'' - (n+1)\bar{F}'\bar{f}_n' + \left(\frac{3}{2} + n\right)\bar{F}''\bar{f}_n + \bar{F}''\bar{g}_n\right]\right\} = 0 \tag{13}$$
$$\sum_n B_n X^n \left\{\bar{g}_n''' + \frac{\bar{F}}{2}\bar{g}_n'' - n\bar{F}'\bar{g}_n' + n\left[1 + \frac{\gamma - 1}{2} M^2(1 - \bar{F}'^2)\right] = 0\right.$$

Defining a new auxiliary function satisfying

$$\bar{f}_{m,c}''' + \frac{\bar{F}}{2}\bar{f}''_{m,c} - m\bar{F}'\bar{f}_{m,c}' + \left(\frac{1}{2} + m\right)\bar{F}''\bar{f}_{m,c} + \bar{F}\bar{F}'' = 0 \tag{14}$$

with boundary conditions

$$\bar{f}_{m,c}'(0) = \bar{f}_{m,c}(0) = \bar{f}_{m,c}'(\infty) = 0$$

it is easy to show that the solution of the compressible equations is

$$\bar{f}_m = f_m(\bar{\eta}) + \frac{\gamma - 1}{2} M^2 [f_m(\bar{\eta}) - F(\bar{\eta})] - \frac{M^2}{2}\left[m(2\gamma - 1) + \frac{\gamma - 1}{2}\right]\bar{f}_{m,c}$$

$$\bar{f}_n = f_n(\bar{\eta}) + \frac{\gamma - 1}{2} M^2 [f_n(\bar{\eta}) - \bar{f}_{m,c}] \quad (\text{with } m = n + 1) \tag{15}$$

$$\bar{g}_n = g_n(\bar{\eta}) + \frac{\gamma - 1}{2} M^2 [g_n(\bar{\eta}) - F(\bar{\eta})]$$

The Mach Number is thus removed from the differential equations and the solutions for the cross-flow of compressible fluid are constructed from those of incompressible fluid [note also that: $\bar{f}_{m=1,c}' = f_{n=0}'(\bar{\eta})$]. From these solutions it is apparent that compressibility of the fluid causes not only the characteristic "stretching" of the y coordinate but also accentuates the cross-flow.

Examples

In order to illustrate how these results are applied to actual cases of three-dimensional boundary-layer flow, two examples were computed. The first is taken from external aerodynamics and concerns a thin cylindrical shell of circular cross section, flying at a small angle of yaw along a circular path, and simultaneously spinning about its own axis of revolution (Fig. 3). The problem is to compute the boundary-layer flow on such a body. As has been shown by Howarth,[1] all the results derived for a flat plate apply to the circular cylinder as well. For small angle of yaw, the external flow velocities are given by

$$U^0 = \Omega_1 R; \quad U = 0; \quad W = 2\alpha\Omega_1 R \sin\theta - \Omega_2 a$$

The angular velocity Ω_2 has no component in the direction normal to the surface of the cylinder, so that

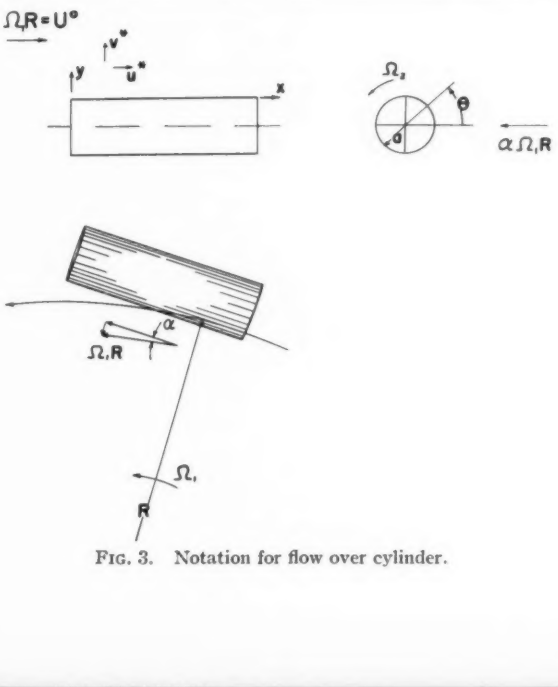

FIG. 3. Notation for flow over cylinder.

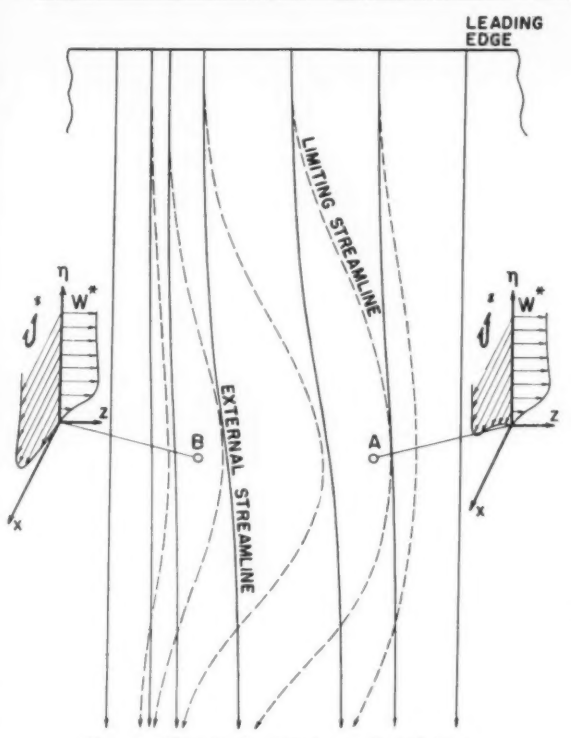

FIG. 4. Flow in simulated s = shaped duct.

$\omega_2 = \Omega_1 \sin\theta$. Remembering that $z = a\theta$ and that for this case $n = r = 0$, since W and ω_2 are independent of x, we write immediately, from Eqs. (10), the expressions for the u^* and w^* velocities in the boundary layer as

$$u^* = \Omega_1 R F' + 2\alpha\Omega_1 R \frac{x}{a} \cos\theta f_{n=0}' + 2x\Omega_1 \frac{x}{a} \cos\theta f_{r=0}'$$

$$w^* = (2\alpha\Omega_1 R \sin\theta - \Omega_2 a) g_{n=0}' + 2x\Omega_1 \sin\theta\, g_{r=0}'$$

The second example concerns the boundary-layer flow over a flat surface caused by a continuous force field simulating an s-shaped duct. Such flow is of interest, aside from the applications to internal ducting design, because it bears some resemblance to the flow over a casing of turbomachinery. In such machines, the successive rotor and stator stages serve to deflect the flow from the direction of the mean velocity, so that it oscillates about it in a periodic manner. In line with this analogy, the flow external to the boundary layer in this example is influenced by a body force in the crosswise direction, which is proportional to the square of the principal velocity, and the local curvature of the stream lines. This curvature, to simulate the double bend, is taken as

$$c \approx \left(1 - \cos 2\pi \frac{z}{s}\right)\left[2\left(\frac{x}{L}\right) - 6\left(\frac{x}{L}\right)^2 + 4\left(\frac{x}{L}\right)^3\right]$$

In addition, the velocity in the principal direction is assumed to be a constant. After cross differentiation, to eliminate the pressure, the Euler's equations yield

$$U^0(W_{xx} - U_{xz}) = (G_3)_x - (G_1)_z$$

so that (since $U = G_2 = 0$) the external velocity is given by

$$U^* = U^0; \quad W^* = W = 16 \tan\vartheta U^0 \times \left(1 - \cos 2\pi \frac{z}{s}\right)\left[\left(\frac{x}{I}\right)^2 - 2\left(\frac{x}{L}\right)^3 + \left(\frac{x}{L}\right)^4\right]$$

The integration constants determining the initial value of the body force and the inclination of the simulated duct have been arbitrarily set to zero. The picture of the stream lines (with the average deflection ϑ equal to 5°, and the width of duct s, equal to half its length I), is shown in Fig. 4.

Since the body force varies only in x and z direction, the boundary-layer velocities can be written, using Eqs. (10), as

$$u^* = U^0\left\{F' + 32\pi \tan\vartheta \sin\left(2\pi \frac{z}{s}\right)\left(\frac{L}{s}\right)\left(\frac{x}{L}\right)^3 \times \left[f_{n=2}' - 2\left(\frac{x}{L}\right) f_{n=3}' + \left(\frac{x}{L}\right)^2 f_{n=4}'\right]\right\}$$

$$w^* = 16 \tan\vartheta U^0 \left(1 - \cos 2\pi \frac{z}{s}\right)\left(\frac{x}{L}\right)^2 \times \left[g_{n=2}' - 2\left(\frac{x}{L}\right) g_{n=3}' + \left(\frac{x}{L}\right)^2 g_{n=4}'\right]$$

From the knowledge of the velocity distributions, one can compute the shape of the "limiting stream lines" at the wall ($y = 0$), and these are also shown in Fig. 4. It can be seen in this figure, that the boundary layer flows toward the "wall of the duct" nearest to the center of curvature. If the duct is to simulate two rows of blades, this means boundary layer flows toward the suction surface of the first row of the blades. By studying the velocity distributions at points A and B (in Fig.

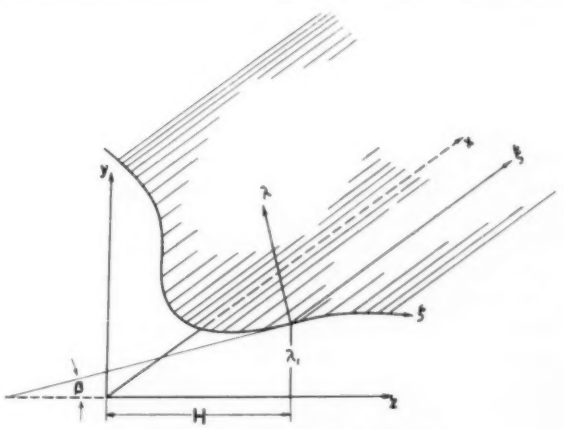

FIG. 5. Curvilinear coordinate system.

4 the scale of W^* is enlarged out of proportion), we note that the shift of the boundary-layer flow implies also a redistribution of the momentum of the principal flow, since the principal flow at point A slows down and tends toward separation, while that at point B accelerates. In fact, since in the vicinity of point A the crosswise flow also changes direction, somewhere near that point may occur a true separation of three-dimensional boundary layer—that is, all of the flow will leave the surface. The change of direction of the limiting stream lines occurs further downstream than the inflection point of the external flow. This means, that in the second row of blades the boundary layer will first continue toward the pressure surface (where it may separate) and only afterwards, deflect again toward the suction surface.

(III) Boundary-Layer Flow over Sharply Curved Surface

Perturbed Equations in Curvilinear System

In the last example, the "sidewalls" of the duct were straight, starting from the leading edge, and therefore, no cross-flow occurred there. In actuality, however, the sides would be curved, and, since the experimental evidence points strongly to the corners between these walls and the bottom of the duct as regions of high total pressure loss, the flow in such corners should also be studied. To simplify matters, one considers the corners as filleted, so that the boundary layer flows over a sharply (but continuously) curved surface.

For the purpose of this analysis it is convenient to use an orthogonal curvilinear coordinate system shown in Fig. 5. The transformation from the Cartesian system x, y, z to to the curvilinear system ξ, λ, ζ is given by

$$x \equiv \xi;\quad y \equiv \lambda_1 + \lambda \cos\beta;\quad \lambda_1 \equiv H - \int_0^\zeta \sin\beta\, d\zeta;$$
$$z \equiv \int_0^\zeta \cos\beta\, d\zeta + \lambda \sin\beta \qquad (16)$$

Restricting the analysis to curvature of the ζ axis $c = d\beta/d\zeta$, being a function of ζ coordinate only, the length stretching factors used in the transformation of the equations of motion become

$$h_1 = 1;\quad h_2 = 1;\quad h_3 = 1 + c\lambda \qquad (17)$$

It should be pointed out that in this coordinate system the ζ axis plays the role of a reference line and will be used to describe the shape of the wall over which the fluid is flowing. Coordinate λ will then measure the distance perpendicular to this wall, while the ξ axis is pointed in the direction of the principal flow, so that $\xi = \lambda = 0$ represent the leading edge of the configuration. Using the standard transformation formulas (velocities u^*, v^*, w^* are taken here in the ξ, λ, ζ directions, respectively) and applying the boundary-layer approximations—that is, considering v^* and λ of $0(\delta)$, c of $0(1/\delta)$ or larger, and neglecting all terms of $0(\delta)$—one obtains the boundary-layer momentum equations,

$$\left.\begin{aligned} &u^*u_\xi^* + v^*u_\lambda^* + \frac{1}{1+c\lambda}\,w^*u_\zeta^* = \\ &\qquad -\frac{1}{\rho}\,p_\xi + \nu\left(u_{\lambda\lambda}^* + \frac{c}{1+c\lambda}\,u_\lambda^*\right) \\ &[c/(1+c\lambda)]\,(w^*)^2 = -(1/\rho)p_\lambda \\ &u^*w_\xi + v^*w_\lambda^* + \frac{1}{1+c\lambda}\,w^*w_\zeta^* + \\ &\qquad \frac{c}{1+c\lambda}\,v^*w^* = -\frac{1}{\rho}\,\frac{1}{1+c\lambda}\,p_\zeta + \nu\times \\ &\qquad \left[w_{\lambda\lambda}^* + \frac{c}{1+c\lambda}\,w_\lambda^* - \left(\frac{c}{1+c\lambda}\right)^2 w^*\right] \end{aligned}\right\} \qquad (18)$$

and the equation of continuity,

$$u_\xi^* + v_\lambda^* + \frac{1}{1+c\lambda}\,w_\lambda^* + \frac{c}{1+c\lambda}\,v^* = 0 \qquad (19)$$

One now considers the flow as only slightly perturbed from the ξ direction, so that the zeroth-order terms yield again the basic flow equations,

$$\left.\begin{aligned} &u^0u_\xi^0 + v^0u_\lambda^0 = \nu\{u_{\lambda\lambda}^0 + [c/(1+c\lambda)]u_\lambda^0\} \\ &u_\xi^0 + v_\lambda^0 + [c/(1+c\lambda)]v^0 = 0 \end{aligned}\right\} \qquad (20)$$

and the first-order terms give the perturbation equations,

$$\left.\begin{aligned} &u^0u_\xi + uu_\xi^0 + v^0u_\lambda + vu_\lambda^0 + \frac{1}{1+c\lambda}\,wu_\zeta^0 = \\ &\qquad -\frac{1}{\rho}\,p_\xi + \nu\left(u_{\lambda\lambda} + \frac{c}{1+c\lambda}\,u_\lambda\right) \\ &u^0w_\xi + v^0w_\lambda + \frac{c}{1+c\lambda}\,v^0w = \\ &\qquad -\frac{1}{\rho}\,\frac{1}{1+c\lambda}\,p_\zeta + \nu\left[w_{\lambda\lambda} + \frac{c}{1+c\lambda}w_\lambda - \left(\frac{c}{1+c\lambda}\right)^2 w\right] \\ &p_\lambda = 0(w^2) \\ &u_\xi + v_\lambda + \frac{1}{1+c\lambda}\,w_\zeta + \frac{c}{1+c\lambda}\,v = 0 \end{aligned}\right\} \qquad (21)$$

Solution of Basic Flow Equations

The basic flow equations may be solved by defining a stream function $\psi^0(\xi, \lambda, \zeta)$, and an additional parameter $\kappa = c(\nu\xi/U^0)^{1/2}$ related to the local curvature of the wall. The stream function is first expanded,

$$\psi^0 = \sqrt{U^0\nu\xi}\,[F(\eta) + \kappa d(\eta) + \kappa^2 d_1(\eta) + \ldots] \qquad (22)$$

and introduced in this form into the equations of basic flow. Again, since the d's must be independent of ζ, the coefficients of the various powers of κ are set separately to zero. The maximum permissible value of κ will be small [of $0(1/\eta_\delta)$], otherwise the curvilinear system would lead to double values, and, consequently,

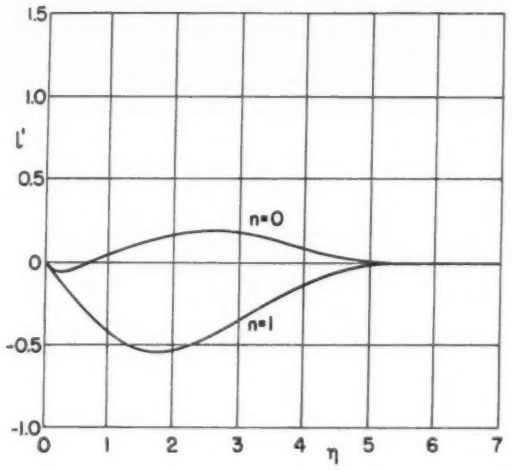

FIGURE 6.- VELOCITY PERTURBATION DUE TO WALL CURVATURE
a) IN THE PRINCIPAL DIRECTION

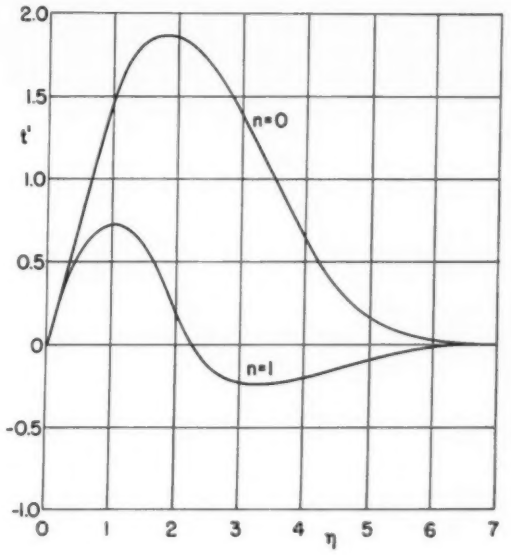

FIGURE 6.- CONT'D.
b) IN THE CROSSWISE DIRECTION

it is sufficient to consider only the first two terms in this expansion. One thus obtains the Blasius equation for $F(\eta)$ and an equation for d as follows:

$$2d''' + 2dd'' - (d')^2 + (\eta F - 2)F'' + F'(F'\eta - F) = 0 \quad (23)$$

Since the basic flow velocities, neglecting higher powers of κ, are:

$$\left.\begin{aligned} u^0 &\doteq [1/(1+\kappa\eta)]U^0\,(F' + \kappa d') \\ v^0 &\doteq -\frac{1}{2}\,\frac{1}{1+\kappa\eta}\sqrt{\frac{U^0\nu}{\xi}}\,[(F - F'\eta) + \kappa(2d - d'\eta)] \end{aligned}\right\} \quad (24)$$

d must satisfy $d(0) = d'(0) = 0$ and $d'(\infty) = \eta$. A numerical solution for d' (reference 15) shows that $d' \approx \eta$ everywhere, and therefore a fair approximation for the u^0 velocity is

$$u^0 \doteq U^0[(F' + \kappa\eta)/(1 + \kappa\eta)] \quad (25)$$

This approximation has been used subsequently. Since, for small values of η, F' may be approximated by $F' = 0.332\eta$, expression (25) shows that, for small values of η, $u^0 \doteq (0.332 + \kappa)\eta + 0(\eta^2)$. In other words, the slope of the velocity distribution near the surface depends to a great extent on the local curvature of this surface. On concave surfaces, κ will be negative, and thus the velocity profile will be nearer separation (will have a smaller slope), and on convex surfaces the basic flow velocity profile improves.

Solution of the Perturbed Equations

To solve the first-order equations, one proceeds in exactly the same manner[15] as for basic flow. To simplify matters but still retain a significant model, it is sufficient to consider the external flow to be of special type: $U = 0$, $W = D\xi^n$. The appropriate expressions for ψ and φ may now be written immediately, as a result of the flat surface investigation,

$$\left.\begin{aligned} \psi(\xi,\eta,\zeta) &= \xi\,\frac{\partial\kappa}{\partial\zeta}\,\frac{W}{U^0}\sqrt{\nu\xi U^0}\times [l_n(\eta) + \kappa l_{1,n}(\eta) + \dots] \\ \varphi(\xi,\eta,\zeta) &= \frac{W}{U^0}\sqrt{\nu\xi U^0}\,[g_n(\eta) + \kappa t_n(\eta) + \kappa^2 t_{1,n}(\eta) + \dots] \end{aligned}\right\} \quad (26)$$

It is clear that the equation for g_n must be the same as for the flat surface, and the equations for l_n and t_n become

$$\left.\begin{aligned} &l_n''' + \frac{F}{2}\,l_n'' - \left(\frac{3}{2} + n\right)F'l_n' + (2+n)F''l_n + F''t_n - (d' - F'\eta)g_n' = 0 \\ &t_n''' + \frac{F}{2}\,t_n'' - \left(\frac{1}{2} + n\right)F't_n' - \eta g_n''' + \left(d + \frac{F}{2}\eta + 1\right)g_n'' - \left[n(F'\eta + d') + \frac{1}{2}(F'\eta - F)\right]g_n' + 2n\eta + \frac{1}{2}\lim_{\eta\to\infty}(F'\eta - F) = 0 \end{aligned}\right\} \quad (27)$$

Since the perturbation velocity components are

$$u = W \frac{d(\log c)}{d\zeta} \frac{c\xi^2}{1 + c\lambda} \frac{1}{\sqrt{Re}} l_n'$$

$$w = W \left[g_n' + c\xi \frac{1}{\sqrt{Re}} t_n' \right] \qquad (28)$$

the appropriate boundary conditions are:

$$l_n(0) = l_n'(0) = l_n'(\infty) = t_n(0) = t_n'(0) = t_n'(\infty) = 0$$

Equations (27) were solved numerically for $n = 0$ and $n = 1$. These solutions are shown in Figs. 6a and 6b.

Example

To illustrate the manner in which the derived results are applied to an actual boundary-layer flow over a sharply curved wall, such flow has been computed for $U = 0$, $W = D\xi^n$, with $n = 0$ and $n = 1$. The wall was assumed to have a hyperbolic shape. Assuming $\eta_\delta = 8.0$, the maximum permissible value of κ has been set at 0.125, so that at any given Reynolds Number $U^0/\nu c_{max.}$, there exists a maximum value of $c\xi$:

$$c_{max.}\, \xi_{max.} = (0.125)^2 U^0/\nu c_{max.}$$

for which these considerations hold. In this example

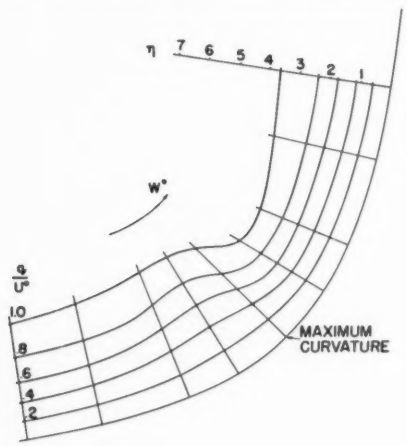

FIGURE 7- FLOW OVER A HYPERBOLICALLY SHAPED WALL
a) EXTERNAL FLOW: $U^\circ = U^\circ$; $W^\circ = D$
CONSTANT VELOCITY PROFILES

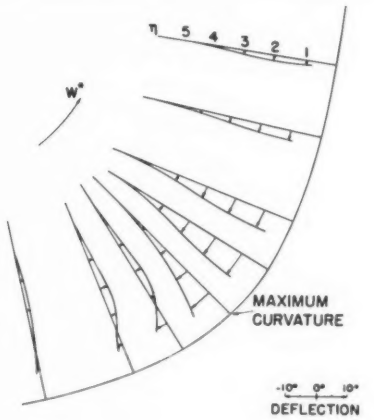

FIGURE 7.- CONT'D.
b) EXTERNAL FLOW: $U^\circ = U^\circ$; $W^\circ = D$
DEFLECTION FROM EXTERNAL FLOW DIRECTION

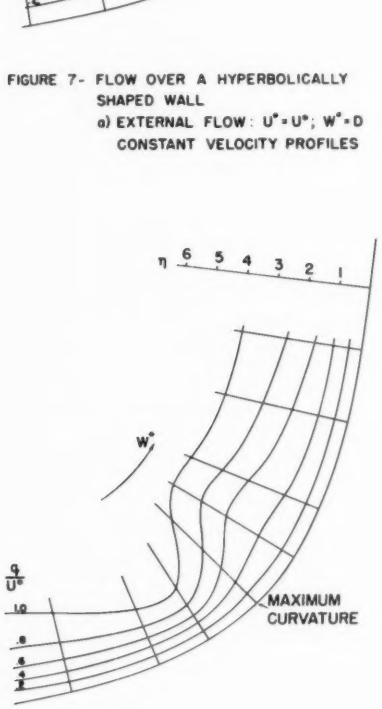

FIGURE 7.- CONT'D.
c) EXTERNAL FLOW: $U^\circ = U^\circ$; $W^\circ = D\xi$
CONSTANT VELOCITY PROFILES

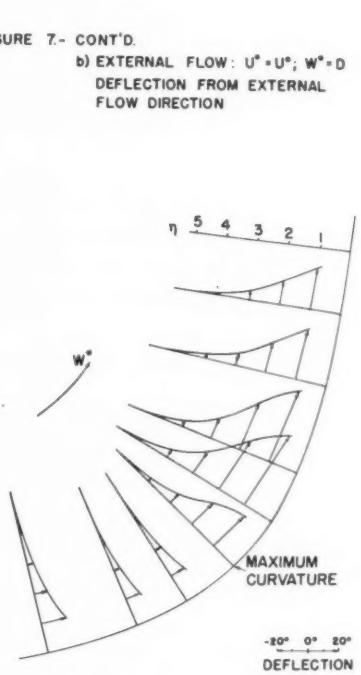

FIGURE 7.- CONT'D.
d) EXTERNAL FLOW: $U^\circ = U^\circ$; $W^\circ = D\xi$
DEFLECTION FROM EXTERNAL FLOW DIRECTION

$U^0/\nu c_{max.} = 634$, so that $\xi_{max.} = 10/c_{max.}$. The results of the computations are shown in Figs. 7 (a–d), where are plotted the velocity ratios, and the deflection from the external flow direction. It should be noted that at the computed position $\xi = \xi_{max.}$, the cross-wise component of the external flow W^* is the same in both cases, so that the differences can be traced directly to the cross-wise pressure gradient. Physically, such an external flow may be thought of as a vortex of constant strength for $n = 0$, and a vortex of an increasing strength for $n = 1.0$. Examination of Figs. 7a and 7b shows that, for $n = 0$, an accumulation of low momentum air occurs on the "upstream" wall of the corner. When $n = 1.0$, however, Figs. 7c and 7d reveal that now the large accumulation of the low momentum air occurs on the "downstream" wall, with corresponding large deflections in that region. We thus see that, when there is no pressure gradient in the external flow ($n = 0$), the wall curvature causes a weak secondary flow as shown in Fig. 7b. When, on the other hand, the external flow has a cross-wise pressure gradient ($n = 1$), the secondary flow due to that pressure gradient apparently (Fig. 7d) is in such a direction as to hinder the principal flow on the "downstream" wall, so that almost all of the flow "climbs" the wall in that region.

(IV) Concluding Remarks

The analysis of three-dimensional, steady laminar boundary layer with small cross-flow has indicated that many important problems in this class can be solved with relatively little effort, thus affording a greater understanding of real fluid flow. Although the accurate determination of the separation point is certainly beyond the scope of small perturbation analysis (and also beyond the standard boundary-layer theory), the factors that affect the separation of three-dimensional boundary layers are clearly pointed out. Among these factors, the cross-wise variation of flow is indicated as important in affecting the separation. In particular, the examples show the strong tendency toward the separation as a result of cross-wise variation of cross-flow, both on a cylindrical shell and in a simulated s-shaped duct. Similarily, the sharp, laterally varying, concave curvature of the surface tends to separate even the basic flow profile.

References

[1] Howarth, L., *The Boundary Layer in Three-Dimensional Flow—Part I. Derivation of the Equations for Flow Along a General Curved Surface*, Philosophical Mag., Vol. XLII, pp. 239–243, March, 1951.

[2] Hayes, Wallace D., *The Three-Dimensional Boundary Layer*, NAVORD Rep. 1313, NOTS 384, U.S. Naval Ordnance Test Station (Inyokern), May 9, 1951.

[3] Moore, Franklin K., *Three-Dimensional Compressible Laminar Boundary Layer Flow*, NACA TN No. 2279, 1951.

[4] Timman, R., *A Calculation Method for Three-Dimensional Laminar Boundary Layers*, National Luchtvaartlab. Amsterdam, Rep. F. 66, 1951.

[5] Mager, A., *Generalization of Boundary-Layer Momentum-Integral Equations to Three-Dimensional Flows Including Those of Rotating System*, NACA TR 1067, 1952.

[6] Sears, W. R., *The Boundary Layer of Yawed Cylinders*, Journal of the Aeronautical Sciences, Vol. 16, No. 1, pp. 41–45, January, 1949.

[7] Bödewart, U. T., *Die Drehströmung über festem Grunde*, ZAMM, 20, 241, 1940.

[8] Howarth, L., *Note on the Boundary Layer on a Rotating Sphere*, Philosophical Mag., Ser. 7, Vol. XLII, pp. 1308–1315, November, 1951.

[9] Loos, H. G., *A Simple Laminar Boundary Layer with Secondary Flow*, Daniel and Florence Guggenheim Jet Propulsion Center, California Institute of Technology, Technical Report No. 1.

[10] Carrier, G. F., *The Boundary Layer in a Corner*, Quart. of Appl. Math., Vol. IV, No. 4, pp. 367–370, January, 1947.

[11] Moore, F. K., *Laminar Boundary Layer on a Circular Cone in Supersonic Flow at a Small Angle of Attack*, NACA TN No. 2521, 1951.

[12] Moore, F. K., *Three-Dimensional Boundary Layer Flow*, Journal of the Aeronautical Sciences, Vol. 20, No. 8, pp. 525–534, August, 1953.

[13] Fogarty, L. E., *The Laminar Boundary Layer on a Rotating Blade*, Journal of the Aeronautical Sciences, Vol. 18, No. 4, pp. 247–252, April, 1951.

[14] Schlichtling, H., *Lecture Series—Boundary Layer Theory—Part I—Laminar Flows*, NACA TM No. 1217, 1949.

[15] Mager, A., *Laminar Boundary Layer Problems Associated with Flow Through Turbomachines*, Doctoral Thesis, California Institute of Technology, 1953.

Changes of Address

Since the Post Office Department does not as a rule forward magazines to forwarding addresses, it is important that the Institute be notified of changes in address 30 days in advance of publishing date to ensure receipt of every issue of the Journal and Review.

Notices should be printed legibly and sent directly to:

Institute of the Aeronautical Sciences, Inc.

2 East 64th Street, New York 21, New York

Readers' Forum

BRIEF REPORTS of investigations in the aeronautical sciences and discussions of papers published in the JOURNAL are presented in this special department. Publication is completed as soon as possible after receipt of the material. The Editorial Committee does not hold itself responsible for the opinions expressed by the correspondents.

Note on Photoelastic Study of a Swept-Wing Model

George Gerard and Ralph Papirno
Research Division, College of Engineering, New York University
July 10, 1954

THE PURPOSE of this note is to report briefly on preliminary photoelastic results obtained on a cemented swept-wing model using a "back-silvering" technique.

The extension of photoelastic techniques to relatively complex built-up structures has been hampered until recently by the lack of suitable photoelastic materials which can be cemented without introducing stresses at the bond and are not subject to slip. Becker[1] used cemented models in an airframe bulkhead investigation but found that although the technique gave a satisfactory first approximation, creep of the cement under load was a serious problem. Recently, Williams[2] referred to the resin Paraplex which is suitable for photoelastic work and which can be satisfactorily bonded.

We have been intrigued by the possibility of investigating complex built-up structural components by use of cemented model techniques. With the availability of Paraplex, an exploratory investigation has been conducted on an idealized swept-wing model. Fig. 1 shows the cemented swept-wing model and Fig. 2 shows the model installed in a loading jig.

If this model were loaded and viewed in the usual transmission polariscope, no fringe pattern would be observed. Since the upper cover is in tension and the lower is in compression the respective fringes annul each other. To surmount this difficulty, the inside surfaces of the model have been silvered and a doubling polariscope arrangement has been used to determine the fringe patterns. By use of the silvering technique, it is thus possible to investigate selectively the areas of interest in the model in addition to obtaining the increased sensitivity of a doubling polariscope. In Fig. 3, the fringe pattern is shown for the complete tension cover of the model. Fig. 4 shows the progressive increase in fringe order with load for one half of the tension cover.

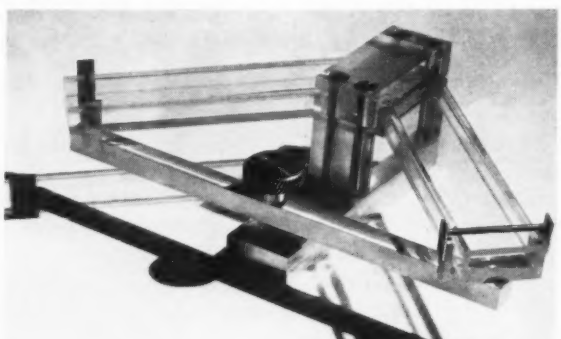

FIG. 2.

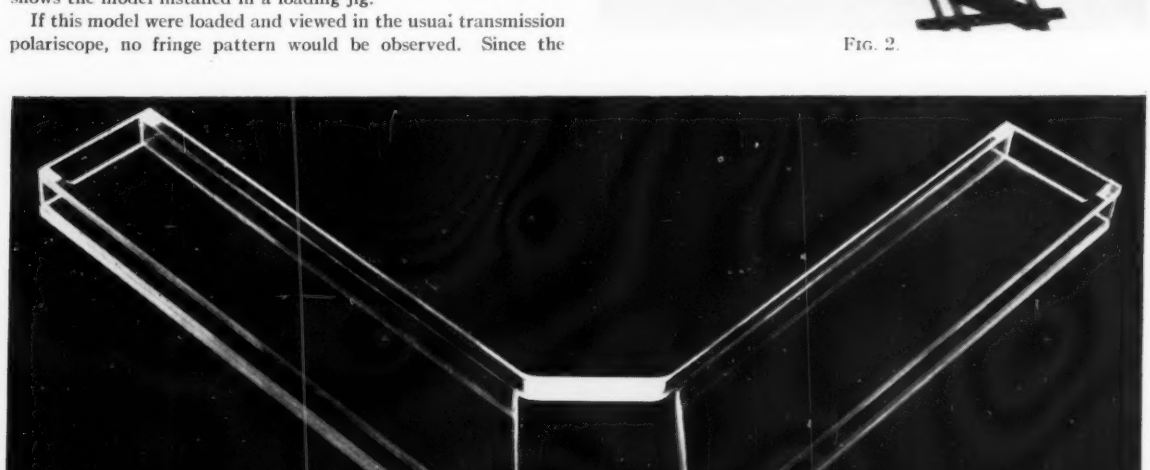

FIG. 1.

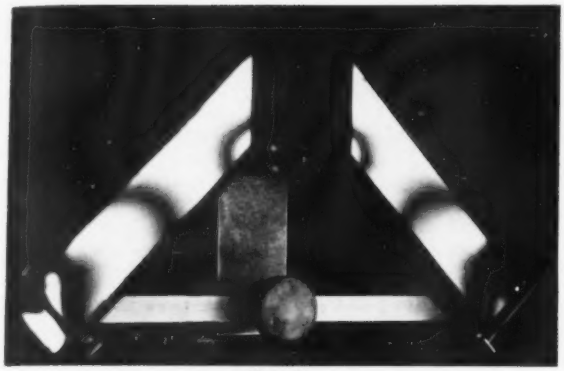

FIG. 3.

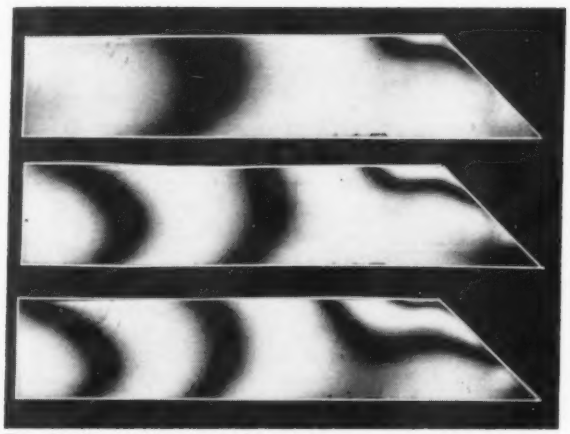

FIG. 4. Swept-wing model fringe photographs, light field reflection polariscope.

Further development of the techniques noted here can possibly lead to the widespread use of photoelastic analysis for complex built-up structural components.

REFERENCES

[1] Becker, H., *Photoelastic Analysis of a Spar Bulkhead in a Semi-monocoque Airplane Fuselage*, S.E.S.A. Proceedings, Vol. IV, No. 1, pp. 36–48, 1946.

[2] Williams, M. L., *A Review of Certain Analysis Methods for Swept-Wing Structures*, Journal of the Aeronautical Sciences, Vol. 19, No. 9, pp. 615–629, September, 1952.

Rectangular Plates with Stringers and Ribs

J. Irving and N. Mullineux

Senior Lecturer in Applied Mathematics and Lecturer in Mathematics, Respectively, Department of Mathematics, The University, Southampton, England

July 11, 1954

NOTATION

a, b	=	dimensions of plate
h	=	thickness of plate
x, y	=	coordinates
$q(x, y)$	=	intensity of lateral loading
$w(x, y)$	=	lateral deflection of plate
$\bar{w}(m, n)$	=	sine transform of lateral deflection
D	=	flexural rigidity of plate
x_i	=	position of rib
y_i	=	position of stringer
N_x, N_y	=	normal compressive forces per unit length of plate edge along the x- and y-axes, respectively
A	=	area of stringer
B	=	flexural stiffness of stringer
A'	=	area of rib
B'	=	flexural stiffness of rib
$P_i(x)$	=	effective force at point (x, y_i) due to stringer
$Q_j(y)$	=	effective force at point (x_j, y) due to rib
$\delta(x - x_j), \delta(y - y_i)$	=	Dirac delta functions
ν	=	Poisson's ratio

(1) INTRODUCTION

THE USE OF THE DIRAC DELTA function in conjunction with the finite sine transform simplifies the treatment of problems involving the loading of rectangular plates, for which at least one pair of opposite edges are simply supported.[1] Recently Radok[2] has discussed the problem of a simply supported rectangular plate strengthened with ribs and stringers by the usual tentative methods.[3] Moreover, he considers a stringer or rib as being equivalent to the limit of a certain triangular loading along a strip of finite width. It is, however, more direct to represent the forces due to the stringer (or rib) by a Dirac delta function and to carry out the subsequent analysis by means of sine transforms as described in the following paragraphs.

(2) ISOTROPIC PLATE WITH ONE STRINGER OR RIB

The deflection $w(x, y)$ of a simply supported rectangular plate, subject to uniform compressions N_x and N_y in the x- and y-directions, respectively, which are taken along adjacent edges of lengths a and b, satisfies the equation

$$\nabla^4 w + (N_x/D)\frac{\partial^2 w}{\partial x^2} + (N_y/D)\frac{\partial^2 w}{\partial y^2} = q/D + P_i(x)\delta(y - y_i)/D \quad (2.1)$$

where $q(x, y)$ is the intensity of the applied lateral load and $P_i(x)$ is the effective load at the point (x, y_i) due to the stringer at $y = y_i$.

Using the double finite sine transform[1] (or Sneddon[4]), and taking account of the boundary conditions for a simply supported plate, Eq. (2.1) becomes

$$\left[\pi^4\left\{\frac{m^2}{a^2} + \frac{n^2}{b^2}\right\}^2 - \frac{m^2\pi^2 N_x}{a^2 D} - \frac{n^2\pi^2 N_y}{b^2 D}\right]\bar{w}(m, n) = \left[\int_0^a\int_0^b q(x, y)\sin\frac{m\pi x}{a}\sin\frac{n\pi y}{b}\,dx dy + \sin\frac{n\pi y_i}{b}\int_0^a P_i(x)\sin\frac{m\pi x}{a}\,dx\right] \quad (2.2)$$

where

$$\bar{w}(m, n) \equiv \int_0^a\int_0^b w(x, y)\sin\frac{m\pi x}{a}\sin\frac{n\pi y}{b}\,dx\,dy$$

The well-known property of the delta-function,

$$\int_0^b \sin\frac{n\pi y}{b}\,\delta(y - y_i)dy = \sin\frac{n\pi y_i}{b}$$

has been assumed in deriving Eq. (2.2). Eq. (2.2) determines $\bar{w}(m, n)$ for any lateral load $q(x, y)$. By the usual inversion formula, the deflection is given directly by

$$w(x, y) = \frac{4}{ab}\sum_{m=1}^{\infty}\sum_{n=1}^{\infty}\bar{w}(m, n)\sin\frac{m\pi x}{a}\sin\frac{n\pi y}{b} \quad (2.3)$$

For $q(x, y) = 0$, $N_y = 0$, $\bar{w}(m, n)$ from Eq. (2.2) is equivalent to $C_{mn}^{\ t}$ as given by Radok[2] [Eq. (2.3.1)].

The case of a rib is treated in a similar way.

(3) Discrete Stringers

Consider now the case of stringers at y_i where $i = 1, 2, \ldots, f$. For comparison with Radok's results,[2] we take $q(x, y)$ and N_y to be zero.

The generalization of Eq. (2.2) for f stringers involves the unknown quantities

$$\int_0^a P_i(x) \sin \frac{m\pi x}{a}\, dx, \qquad (i = 1, 2, \ldots, f)$$

which are required to satisfy the internal boundary conditions at $y = y_i$. These are simply

$$\left[B_k \frac{\partial^4 w}{\partial x^4} + \frac{A_k N_x}{h} \frac{\partial^2 w}{\partial x^2} = -DP_k(x) \right]_{y=y_k} \tag{3.1}$$

$k = 1, 2, \ldots, f$. This form of the boundary condition avoids the analytical difficulties of Radok.[2] From Eqs. (2.2) and (2.3) generalized for f stringers

$$w(x, y) = \frac{4}{ab} \sum_{m=1}^{\infty} \sum_{n=1}^{\infty} \sum_{i=1}^{f} \times \frac{\sin \dfrac{n\pi y_i}{b} \displaystyle\int_0^a P_i(x') \sin \frac{m\pi x'}{a}\, dx'}{\left[\pi^4 \left(\frac{m^2}{a^2} + \frac{n^2}{b^2} \right)^2 - \frac{m^2\pi^2}{a^2} \frac{N_x}{D} \right]} \sin \frac{m\pi x}{a} \sin \frac{n\pi y}{b} \tag{3.2}$$

Substituting Eq. (3.2) in Eq. (3.1), multiplying by $\sin \dfrac{m\pi x}{a}$ and integrating from 0 to a

$$\frac{2}{b} \left\{ \left(\frac{m\pi}{a} \right)^4 B_k - \frac{A_k N_x}{h} \left(\frac{m\pi}{a} \right)^2 \right\} \left[\sum_{i=1} \left\{ \sum_{n=1}^{\infty} \times \right. \right.$$

$$\sin \frac{n\pi y_i}{b} \sin \frac{n\pi y_k}{b} \left[\pi^4 \left(\frac{m^2}{a^2} + \frac{n^2}{b^2} \right)^2 - \frac{m^2\pi^2 N_x}{a^2 D} \right] \int_0^a P_i(x') \sin \frac{m\pi x'}{a}\, dx' =$$

$$- D \int_0^a P_k(x) \sin \frac{m\pi x'}{a}\, dx', \qquad k = 1, 2, \ldots, f$$

This is a system of f homogeneous linear equations in the f variables $\displaystyle\int_0^a P_i(x') \sin \frac{m\pi x'}{a}\, dx'$, $i = 1, 2, \ldots, f$. The eliminant is identical with Eq. (3.1.3) of Radok.

Eq. (3.2.1) of Radok's paper is readily obtained by the above methods in the case of discrete stringers and ribs.

The case of distributed stringers which is equivalent to an orthotropic plate may be treated in the same way whether or not ribs are present. The internal boundary condition for a rib at $x = x_l$ is

$$\left[B'_l \frac{\partial^4 w}{\partial y^4} + \frac{A'_l N_y}{h} \frac{\partial^2 w}{\partial y^2} = -DQ_l(y) \right]_{x = x_l} (l = 1, 2, \ldots, g)$$

and the right-hand side of Eq. (2.1) contains the term $Q_l(y)\delta(x - x_l)/D$ for each rib.

The above calculations illustrate the concise and constructive nature of the transform approach in conjunction with the δ-function technique.

References

[1] Irving, J., and Mullineux, N., *The Bending and Oscillation of Thin Rectangular Plates* (to be published).

[2] Radok, J. R. M., *General Instability of Simply Supported Rectangular Plates*, Journal of the Aeronautical Sciences, Vol. 21, No. 2, p. 109, February, 1954.

[3] Timoshenko, S., *Theory of Plates and Shells*, McGraw-Hill Book Company, Inc., New York, 1940.

[4] Sneddon, I. N., *Fourier Transforms*, McGraw-Hill Book Company, Inc., New York, 1951.

On Motion of Submerged Cylinder

H. S. Tan

Department of Engineering Mechanics, University of Notre Dame, Notre Dame, Ind.

July 17, 1954

The two-dimensional problem of a submerged cylinder moving with constant forward speed c, under the assumption of irrotationality of fluid motion, and in coordinate system moving with the cylinder, reduces to the determination of a velocity potential $\phi(x, y)$, satisfying the differential equation:

$$\phi_{xx} + \phi_{yy} = 0 \tag{1}$$

with boundary conditions:

(I) on free surface, $y = 0$ $\qquad c^2\phi_{xx} + g\phi_y = 0$ (2)

(II) on surface of cylinder $\qquad \phi_n = 0$ (3)

and the physical limitation that the upstream disturbance must vanish at infinity—i.e.,

$$\lim_{x \to \infty} [\phi_x^2 + \phi_y^2] = 0 \tag{4}$$

The solution for a deeply submerged circular cylinder was first obtained by Lamb[1] in 1913, in the form:

$$\phi = -cx(1 + a^2/r^2) + \chi(x, y) \tag{5}$$

where a denotes the radius of cylinder, h the depth of submersion; $a \ll h$, and $r = [x^2 + (y + h)^2]^{1/2}$. The effect of χ on the surface of cylinder was neglected. Lamb's solution is accordingly a first approximation in the sense that the cylinder was replaced by a single doublet. Later, in 1936, Havelock[2] solved the same problem exactly. He expressed the solution in the form of an infinite series, the coefficients of which can be so determined that both boundary conditions are taken care of. Havelock's solution amounts to replacing the submerged cylinder by a system of distributed sources and sinks of zero total strength inside the cylinder, and replacing the free surface by a properly adjusted image system.

In 1935 Keldish,[3] by introducing the complex velocity potential

$$w = \phi + i\psi, \qquad (z = x + iy) \tag{6}$$

and rewriting the boundary condition (I) in the form:

$$\text{(Ia)}\ y = 0: \qquad I\left[i \frac{d^2w}{dz^2} - \nu \frac{dw}{dz} \right] = 0, \qquad (\nu = g/c^2) \tag{7}$$

was able to utilize Schwarz's reflection principle for constructing solutions involving free surface. Indeed, he obtained in this way the solution for a submerged moving eddy. Generalizing Keldish's result, and making extensive use of Cauchy's integral theorem, Kotchin,[4] in 1937 was then able to establish an exact solution for submerged cylinder of arbitrary shape in the form of an integral equation. A close examination of Kotchin's solution reveals that here the cylinder was replaced by a distribution of sources, sinks, and vortices. Thus in addition to drag force, the lifting force due to circulation can also be calculated.

An entirely different approach to the solution of the problem of submerged circular cylinder was given in 1938 by Sretensky.[5] Here the disturbance stream function ψ was considered. On taking account of the facts that: (1) upstream disturbance vanishes at infinity, (2) free surface is given by vanishing stream function $\psi = 0$, (3) cylinder surface is given by constant streamline $\Psi = \alpha$, and (4) the relation $\Psi = -cy + \psi$ holds; the two boundary conditions can be put in integrated form as follows:

(I′) free surface, $y = 0$ $\qquad \psi_y = (g/c)\psi$ (8)

(II′) surface of cylinder $\qquad \psi = \alpha + cy$ (9)

Sretensky further succeeded in transforming the entire flow field into a region enclosed between two concentric circles in ζ

plane by a transformation:

$$\zeta = \frac{z - \lambda i}{z + \lambda i}, \qquad \lambda = -[h^2 - a^2]^{1/2} < 0 \tag{10}$$

where $|\zeta| = 1$ corresponds to the free surface, and $|\zeta| = [(h + \lambda)/a] = \rho$ the surface of cylinder. The corresponding transformed boundary conditions expressed in polar coordinates r, ω of ζ are

$$[\psi_r = \mu\psi/(1 - \cos\omega)]_{r=1}, \qquad (\mu = -\lambda g/c^2) \tag{11}$$

$$[\psi]_{r=\rho} = \alpha + c\lambda(1 - \rho^2)/(1 - 2\rho\cos\omega + \rho^2) \tag{12}$$

These, upon further introducing the complex potential w, take on following form:

$$(\mathrm{I}'') \qquad I[2\mu w + w_\zeta (1 - \zeta)^2/\zeta] = 0, \qquad |\zeta| = 1 \tag{13}$$

$$(\mathrm{II}'') \qquad I[w - cz] = \alpha, \qquad |\zeta| = \rho \tag{14}$$

Although w here is a holomorphic function in the ring $\rho < |\zeta| < 1$, it is no longer single valued. Indeed, a solution was obtained by assuming following series form:

$$w = q \ln \zeta + \sum_{m=-\infty}^{\infty} p_m \zeta^m \tag{15}$$

where p_m are determined by substituting (15) into conditions (I″), (II″), and then equating to zero the coefficients of $\begin{matrix}\sin\\ \cos\end{matrix} m\omega$.

It is to be noted that Sretensky's solution as presented in reference 5 is not correct; this is because his boundary condition corresponding to (I″) was incorrectly transformed. Indeed, it will be valuable if a complete solution can be carried out with the correct boundary conditions (I″) and (II″) arrived at above.

References

[1] Lamb, H., *On Some Cases of Wave-Motion on Deep Water*, Ann. di Matematica (3), Vol. xxi, p. 237, 1913.

[2] Havelock, T. H., *The Forces on a Circular Cylinder Submerged in a Uniform Stream*, Proc. Roy. Soc. (London), Ser. A, Vol. 157, pp. 526–534, 1936.

[3] Keldish, *Notes on Some Motions of Heavy Fluid*, Technical Notes, ZAGI No. 52, pp. 5–9, 1935.

[4] Kotchin, N. E., *On the Wave-Making Resistance and Lift of Bodies Submerged in Water*, Trans. Conference on the Theory of Wave Resistance, USSR, Moscow, 1937. Translated as Tech. and Res. Bull. 1-8, Soc. of Naval Architects and Marine Eng., 1951.

[5] Sretensky, L. N., *Motion of a Cylinder under the Surface of a Heavy Fluid*, CAHI Rept. 346, 1938. Translated as NACA TM 1335.

Note on the Propagation of Infinitesimal Disturbances in Gases According to the Navier-Stokes Equations

M. Lessen

Professor of Applied Mechanics, University of Pennsylvania, Philadelphia, Pa.

July 14, 1954

In Truesdell's[1] comprehensive memoir on the propagation of plane sound waves according to the Navier-Stokes equations, the dispersion and damping of longitudinal waves is reviewed and studied. The analysis, however, may be generalized to any stress disturbance and the results presented in convenient form.

Nomenclature

x_i	=	space coordinate vector
t	=	time coordinate
u_i	=	velocity vector
ρ	=	density
p	=	pressure
τ_{ij}	=	stress tensor
T	=	temperature
K	=	thermal conductivity
$\mu_1; \mu_2$	=	viscosity coefficients (shear, bulk)
c_v	=	specific heat at constant volume
c_p	=	specific heat at constant pressure
γ	=	c_p/c_v
a	=	perfect adiabatic velocity of sound
$\dot{q}$	$\equiv$	dq/dt
q, k	$\equiv$	$\partial q/\partial x_k$

Repeated indices connote summation.

Analysis

The Navier-Stokes equations for the motion of a viscous fluid may be written as follows:

Continuity $$\frac{\dot{\rho}}{\rho} + u_{k,k} = 0$$

Momentum $$\rho\dot{u}_i = \tau_{ki,k}$$

Stress—Rate of Strain

$$\tau_{ki} + p\delta_{ki} = (^2/_3)(\mu_2 - \mu_1)u_{l,l}\,\delta_{ki} + \mu_1(u_{k,i} + u_{i,k})$$

Energy $$\rho c_v \dot{T} = (KT,_l),_l + \tau_{kl}\,u_{k,l}$$

State

$$\frac{p}{\rho} = RT$$
$$K = K(T)$$
$$\mu_1 = \mu_1(T)$$
$$\mu_2 = \mu_2(T)$$

The equations may be linearized by considering each of the dependent variables to be of the form

$$q = \bar{q} + q'(x_k, t)$$

where $q' \ll \bar{q}$ and $\bar{q}$ is a particular (constant in x_k and t) solution of the equations. Since it is assumed that the gas is grossly at rest,

$$\bar{u}_i \equiv 0$$

The linearized equations for the disturbance therefore are

Continuity $$\frac{1}{\bar{\rho}}\frac{\partial\rho'}{\partial t} + u_{k,k}' = 0$$

Momentum $$\bar{\rho}\frac{\partial u_i'}{\partial t} = \tau_{ki,k}'$$

Stress—Rate of Strain

$$\tau_{ki}' + p'\delta_{ki} = (^2/_3)(\bar{\mu}_2 - \bar{\mu}_1)u_{l,l}'\,\delta_{ki} + \bar{\mu}_1(u_{k,i}' + u_{i,k}')$$

Energy $$\bar{\rho}\,c_v\frac{\partial T'}{\partial t} = \bar{K}T,_{ll}' - \bar{p}\,u_{k,k}'$$

State $$\frac{p'}{\bar{p}} = \frac{\rho'}{\bar{\rho}} + \frac{T'}{\bar{T}}$$

If the stress—rate of strain equation is substituted into the momentum equation, the resulting equation differentiated by x_i and summed over the repeated "i" index, the resulting velocity divergence terms may then be eliminated from all the equations using the continuity equation. The temperature and pressure disturbance terms may be eliminated in combination with the energy and state equations. After rearranging, the resulting equation for the generalized density disturbance is

$$\frac{\partial}{\partial t}\left(\frac{\partial^2\rho'}{\partial t^2} - a^2\rho',_{kk}\right) = \frac{\bar{K}}{\bar{\rho}c_v}\left(\frac{\partial^2\rho'}{\partial t^2} - \frac{a^2}{\gamma}\rho',_{kk}\right),_{ll} + \frac{4\bar{\mu}_1 + 2\bar{\mu}_2}{3\bar{\rho}}\frac{\partial}{\partial t}\left(\frac{\partial\rho'}{\partial t} - \frac{\bar{K}}{\bar{\rho}c_v}\rho',_{kk}\right),_{ll}$$

where $a^2 \equiv \gamma R\bar{T}$.

The equation for the density disturbance may be put into dimensionless form by the following transformation and groupings.

$$x_i = \frac{a}{\omega} x_i^*$$

$$t = \frac{1}{\omega} t^*$$

$$Re = \frac{3\bar{\rho}}{(4\bar{\mu}_1 + 2\bar{\mu}_2)} \frac{a^2}{\omega} \qquad \text{"Reynolds Number"}$$

$$\sigma = \frac{(4\bar{\mu}_1 + 2\bar{\mu}_2)c_p}{3\bar{K}} \qquad \text{"Prandtl Number"}$$

where ω = characteristic disturbance circular frequency.

The resulting dimensionless equation for the density disturbance (with all primes and asterisks dropped) is

$$\frac{\partial}{\partial t}\left(\frac{\partial^2 \rho}{\partial t^2} - \rho_{,\,kk}\right) = \frac{\gamma}{\sigma Re}\left(\frac{\partial^2 \rho}{\partial t^2} - \frac{1}{\gamma}\rho_{,\,kk}\right)_{,\,ii} + \frac{1}{Re}\frac{\partial}{\partial t}\left(\frac{\partial \rho}{\partial t} - \frac{\gamma}{\sigma Re}\rho_{,\,kk}\right)_{,\,ii}$$

or in vector form

$$\frac{\partial}{\partial t}\left(\frac{\partial^2}{\partial t^2} - \nabla\cdot\nabla\right)\rho = \frac{\gamma}{\sigma Re}\nabla\cdot\nabla\left(\frac{\partial^2}{\partial t^2} - \frac{1}{\gamma}\nabla\cdot\nabla\right)\rho + \frac{1}{Re}\frac{\partial}{\partial t}\nabla\cdot\nabla\left(\frac{\partial}{\partial t} - \frac{\gamma}{\sigma Re}\nabla\cdot\nabla\right)\rho$$

The form of the final, dimensionless equation is of interest. For $\sigma \neq 0$ and $Re \to \infty$, the density disturbance is given by the three-dimensional wave equation where the velocity of propagation of a longitudinal wave is the usually considered "perfect" adiabatic velocity of sound.

$$\left(\frac{\partial^2}{\partial t^2} - \nabla\cdot\nabla\right)\rho = 0$$

The foregoing corresponds to the first correct calculation of the inviscid velocity of sound by Laplace[2] who assumed that the gas went through an isentropic state change.

For the case of $\sigma \to 0$ and $Re \to \infty$ such that $\sigma Re \to 0$, the density disturbance may be given by the three-dimensional wave equation wherein the velocity of propagation of a longitudinal wave is the frictionless, isothermal velocity of sound.

$$\left(\frac{\partial^2}{\partial t^2} - \frac{1}{\gamma}\nabla\cdot\nabla\right)\rho = 0$$

This case corresponds to the first calculation of the velocity of sound by Newton[3] who incorrectly assumed that the gas went through an isothermal state change.

All intermediate cases are given by the full equations and correspond to the investigation of Kirchhoff[4] for the plane, longitudinal wave. Detailed numerical results for the case of a plane longitudinal wave are given by Truesdell.[1]

It is interesting to note, from the linearized disturbance equations, that a pure shear (transverse) mode of disturbance does not interact with a longitudinal disturbance. This dilatation-free disturbance therefore behaves as if in an incompressible, viscous fluid, for which this problem has already been completely solved.

References

[1] Truesdell, *Hydrodynamical Theory of Ultrasonic Waves*, J. Rat. Mech. Anal., Vol. 2, pp. 643–742, 1953.

[2] Laplace, Ann. Phys. Chimie, Vol. 3, pp. 238–241, 1816.

[3] Newton, *Principia Math.*, Book II, Prop. XLVIII–L.

[4] Kirchhoff, Ann. Phys., Vol. 134, pp. 177–193, 1868.

The Effect of Heat Transfer on the Behavior of a Compressible Laminar Boundary Layer Under Favorable and Adverse Pressure Gradients

Ting-Yi Li and H. T. Nagamatsu
California Institute of Technology, Pasadena, Calif.

July 17, 1954

HARTREE[1] EMPLOYED the differential analyzer to evaluate solutions of the Falkner-Skan[2] equation

$$K''' = -KK'' + \beta[K'^2 - 1] \tag{1}$$

with boundary conditions $K = K' = 0$ at $\eta = 0$, $K' \to 1$ as $\eta \to \infty$. It was shown that to make the solutions for $\beta < 0$ unique and appropriate to the boundary-layer applications, the condition at infinity was replaced by

$$K' \to 1 \text{ from below, and as rapidly as possible, as } \eta \to \infty \tag{2}$$

The value of $K''(0)$, required to satisfy the above condition for β negative, was found to decrease for increasing $|\beta|$ and to become zero at a value $\beta = \beta_0 = -0.199$. The value of β_0 is significant because it determines the point at which an incompressible laminar boundary layer breaks away from the surface. The aim of the present note is to extend Hartree's computations into the compressible flow régime and to present some general results regarding the effects of heat transfer on the behavior of a laminar boundary layer with free-stream pressure gradient.

In a recent paper,[3, 3a] we have shown that if the free-stream velocity distribution satisfies a certain differential equation and if the surface temperature assumes a constant value, the compressible laminar boundary-layer equations can be reduced to

$$K''' = -KK'' + \beta[K'^2 - G] \tag{3}$$

$$G'' + KG' = 0 \tag{4}$$

with boundary conditions

$$\eta = 0, \qquad K = K' = 0 \qquad G = \frac{T_w}{T_0} \tag{5}$$

$$\eta \to \infty, \qquad K' \to 1 \qquad G \to 1 \tag{6}$$

Here $K' = u/u_1$, $G = H/H_1$, and η is the similarity variable (cf. reference 3). H and u denote, respectively, the specific total energy and the velocity component parallel to the surface. T denotes the absolute temperature. Subscript 1 refers to the free stream; subscript 0, the stagnation condition in the free stream; subscript w, the condition on the surface. In the deviation of Eqs. (3) and (4), the simplifying assumptions that (1) Prandtl Number is unity, (2) the viscosity coefficient is a linear function of the absolute temperature, and (3) the specific heats are constants, are used.

If the surface is insulated, we must have $G = 1$. Such a case corresponds exactly to the case analyzed by Hartree. The present formulation permits us to discuss the effect of heat transfer on the laminar separation in the sense that when G varies from 1—i.e., the surface is noninsulated—we can find the corresponding variation in β_0. If we specify that $K''(0)$ must change continuously with G, we can derive the following relation[3]

$$\Delta\beta = -\beta_0 \, \Delta G \tag{7}$$

In the deviation of the above equation we have assumed that (1) for $G = 1$, $K''(0)$ vanishes when $\beta = \beta_0 = -0.199$, (2) for $G = 1 + \Delta G$, $K''(0)$ would vanish when $\beta = \beta_0 + \Delta\beta$, where $\Delta G \ll 1$, and $\Delta\beta \ll |\beta_0| = 0(1)$. In other words, Eq. (7) strictly applies only to the case of a surface with a very small amount of heat transfer. It is seen from Eq. (7) that the boundary layer on a heated surface will separate under a comparatively weaker adverse pressure gradient than in the case of an insulated surface; and that the boundary layer on a cooled surface can sustain a

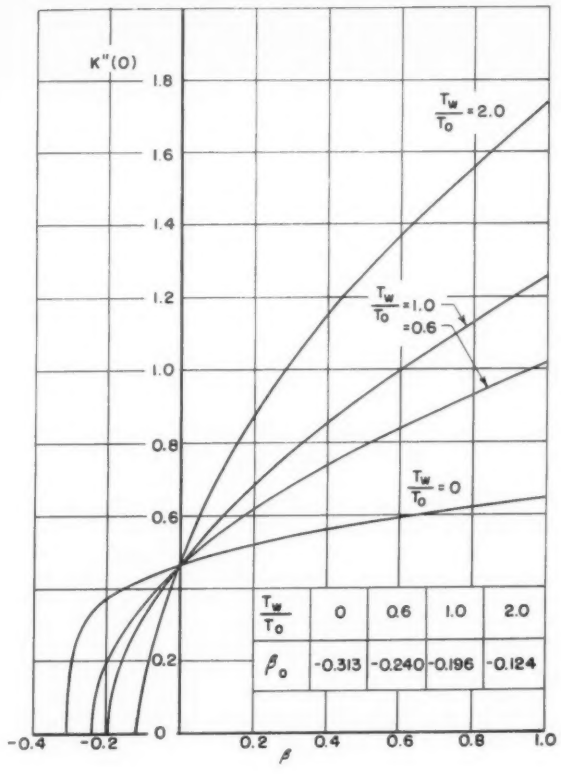

FIG. 1.

stronger adverse pressure gradient. Recent numerical analysis of Eqs. (3) and (4) on a REAC* confirms these deductions.

In Fig. 1, the values of $K''(0)$ of the numerical solutions obtained on the REAC are plotted against β for various T_w's. Since the local skin friction can be shown to be directly proportional to $K''(0)$, the following observations can be made with regard to the boundary layer under a favorable pressure gradient in the free stream:

(1) For a fixed $\beta > 0$ the value of $K''(0)$ decreases as T_w decreases; that is, in the presence of a favorable free-stream pressure gradient, cooling the surface tends to reduce the skin friction.

(2) For a fixed T_w, the value of $K''(0)$ increases with β and the rate of increase is higher at an elevated surface temperature. Therefore, on a surface with fixed temperature, a larger favorable pressure gradient tends to increase the skin friction.

Besides these interesting observations, we note that an increase in the adverse pressure gradient in the free stream tends to decrease the skin friction with $K''(0)$ eventually becoming zero as $\beta = \beta_0$. We have thus obtained four values of β_0's corresponding to the following cases:

(1) insulated surface, $\dfrac{T_w}{T_0} = 1, \quad \beta_0 = -0.196$

(2) cooled surface, $\dfrac{T_w}{T_0} = 0.6, \beta_0 = -0.240$

(3) heated surface, $\dfrac{T_w}{T_0} = 2, \quad \beta_0 = -0.124$

$\dfrac{T_w}{T_0} = 0, \quad \beta_0 = -0.313$

Therefore, we conclude the effect of surface cooling is to enable the boundary layer to sustain a stronger adverse pressure gradient. The effect of surface heating is just the opposite.

It is perhaps interesting to note that $K''(0) = 0.47$ for $\beta = 0$ with various T_w's.† This is significant because when $\beta = 0$, we have by Reynolds analogy

$$\frac{2C_{h_1}}{C_{f_1}} = -\frac{G'(0)}{[(T_w/T_0) - 1]K''(0)} = 1$$

where C_{h_1} and C_{f_1} represent, respectively, the local coefficients of heat transfer and skin friction based on the free-stream quantities. Therefore, we anticipate that the value of $G'(0)/[(T_w/T_0) - 1]$ for $\beta = 0$ should not be affected by changes in T_w. This fact is actually verified from our data obtained on the REAC, and can easily be proved analytically.

Illingworth[4] recently argued that when the surface is heated the fluid near it is lighter and is therefore more readily accelerated or retarded by a pressure gradient. In other words, *the effect of pressure gradient is enhanced when the surface is heated* and our data seem to substantiate this argument.

* Sincere thanks are due to Dr. C. Gazley, Jr. of the RAND Corporation for his kind help in obtaining these results.

† For such a case, Eq. (3) becomes the Blasius equation.

REFERENCES

[1] Hartree, D. R., Proc. Cambr. Phil. Soc., Vol. 33, p. 237, 1937.
[2] Falkner, V. M., and Skan, S. W., Phil. Mag., Vol. 12, p. 865, 1931.
[3] Li, T.-Y., and Nagamatsu, H. T., Proc. of Heat Transfer and Fluid Mech. Inst., p. 143, 1954.
[3a] Li, T.-Y., and Nagamatsu, H. T., Journal of the Aeronautical Sciences, Vol. 20, No. 9, p. 653, September, 1953.
[4] Illingworth, C. R., Quar. Jour. Mech. and Appl. Math., Vol. 7, p. 8, 1954.

Second-Order Methods in Inviscid Supersonic Theory

J. Fell and D. C. M. Leslie
Armaments Division, Sir W. G. Armstrong Whitworth Aircraft, Limited, Baginton, near Coventry, England
July 25, 1954

THE FULL EQUATION for the inviscid supersonic motion of a polytropic gas is very complex, and can only be solved for a few special cases. For general problems, the usual procedure is to assume the existence of a velocity potential

$$\Omega = U(x + \phi) \tag{1}$$

where U is the free stream velocity. If it is assumed that ϕ is so small that terms of order $\{\phi\}^2$ may be neglected, one arrives at the usual linearized equation of motion. In the second-order procedure associated with the name of Van Dyke,[1] one sets

$$\Omega = U(x + \phi + \varphi) \tag{2}$$

assumes that ϕ satisfies the linearized equation, and neglects terms of order $\{\varphi\}^2$. The resulting equation for φ is given by Van Dyke: it contains both double and triple products of ϕ. The triple products can be ignored in some problems, and treated approximately in others, so that we need only integrate precisely the equation involving the double products,

$$\Box^2\varphi = \varphi_{yy} + \varphi_{zz} - \beta^2\varphi_{xx} = 2M^2[(N-1)\beta^2\phi_x\phi_{xx} + \phi_y\phi_{xy} + \phi_z\phi_{xz}] \tag{3}$$

(the notation is the same as Van Dyke's).

The first step is to find a particular integral (p.i.) of this equation; the complementary function is then chosen to satisfy the

boundary conditions of the problem. Van Dyke has been able to do this for two-dimensional and axisymmetric flow; an extension of this work to the general case is obviously most desirable.

Now in all practical problems, the sources of ϕ will lie on some surface Σ, so that

$$\phi = -\frac{1}{\pi}\iint_{\Sigma} f(x_1, y_1)\,\frac{dx_1 dy_1}{|\boldsymbol{R} - \boldsymbol{R}_1|}$$

where we are using the "hyperbolic vector notation"

$$\boldsymbol{A}\cdot\boldsymbol{B} = A_x\beta_x - \beta^2(A_yB_y + A_zB_z)$$

The first step in the problem is to find a p.i. for

$$\Box^2\psi = \frac{1}{|\boldsymbol{R} - \boldsymbol{R}_1|\,|\boldsymbol{R} - \boldsymbol{R}_2|} \tag{4}$$

Using two different systematic procedures, the authors have found four related p.i.'s of Eq. (4)

$$\lambda = \pm\frac{1}{\beta^2}\log\left|\,|\boldsymbol{R}_1 - \boldsymbol{R}_2| \pm |\boldsymbol{R} - \boldsymbol{R}_1| \pm |\boldsymbol{R} - \boldsymbol{R}_2|\,\right|$$

Any combination of signs may be taken in the argument of the logarithm: it will then be obvious which sign should be taken for the whole expression. The most useful combination of these p.i.'s is

$$\lambda_r = \frac{1}{4\beta^2}\log\frac{|(\boldsymbol{R} - \boldsymbol{R}_1)\cdot(\boldsymbol{R} - \boldsymbol{R}_2) - |\boldsymbol{R} - \boldsymbol{R}_1|\,|\boldsymbol{R} - \boldsymbol{R}_2||}{(\boldsymbol{R} - \boldsymbol{R}_1)\cdot(\boldsymbol{R} - \boldsymbol{R}_2) + |\boldsymbol{R} - \boldsymbol{R}_1|\,|\boldsymbol{R} - \boldsymbol{R}_2|} \tag{5}$$

It will be noted that λ_r vanishes on the Mach cones $|\boldsymbol{R} - \boldsymbol{R}_1| = 0$; $|\boldsymbol{R} - \boldsymbol{R}_2| = 0$. Using this expression, one may obtain the known p.i.'s for axisymmetric, two-dimensional, and yawed conical flows.

Eq. (5) has been applied to the calculation of aerodynamic derivatives of wings of finite aspect ratio and thickness and the lift of bodies of revolution. Results and a full description of this work will be published later. This work forms part of the research program of the Armaments Division of Sir W. G. Armstrong Whitworth Aircraft, Limited, and is published with the permission of the firm.

References

[1] Van Dyke, M. D., *First- and Second-Order Theory of Supersonic Flow Past Bodies of Revolution*, Journal of the Aeronautical Sciences, Volume 18, No. 3, p. 161, March, 1951.

Buckling Stress of Thin Cylindrical Clamped Shells Subject to Hydrostatic Pressure

P. P. Bijlaard
Consultant, Bell Aircraft Corporation, and Professor, Cornell University, Ithaca, N.Y.

July 26, 1954

In a recent note[1] Professor W. A. Nash refers to the existing, rather involved methods for calculating the buckling stresses of cylindrical shells with various boundary conditions subjected to hydrostatic pressure. He then gives a rather simple derivation of an approximate formula for the buckling stress of a thin cylindrical shell that is clamped at the edges.

In this connection it may be of interest to present two other simple methods which lead to explicit formulas for the critical hydrostatic pressure of clamped cylindrical shells. These methods have also been worked out by the writer for the case of elastic end restraints.

In reference 2 the writer has considered the deflecting and restraining forces that act upon a longitudinal strip of a shell at the moment of incipient buckling. The deflecting forces are caused by the compressive membrane stresses in the shell due to the changes of curvature. The restraining forces are due to the excess membrane forces, transverse shear forces and twisting moments along the longitudinal edges of the strip. He proves that for shells where the ratio of the half wave length of buckles in the axial direction and that in the circumferential direction is sufficiently large, the resulting deflecting forces (deflecting minus restraining forces) acting on such a strip at any point are proportional to its deflection w. Hence, these resulting deflecting forces can be represented as Cw per unit length, where C is a constant for a given shell, dependent on the external pressure, but independent of the boundary conditions at $x = \pm c$ (Fig. 1a). These resulting deflecting forces, acting on an element of length dx of the strip, have to be in equilibrium with the restraining forces $-dQ_x$, where Q_x is the transverse shear force in the strip. Since $Q_x = -Nd^3w/dx^3$, where N is the flexural rigidity of the shell, the equilibrium equation $-dQ_x = Cw\,dx$ leads to the differential equation of the strip

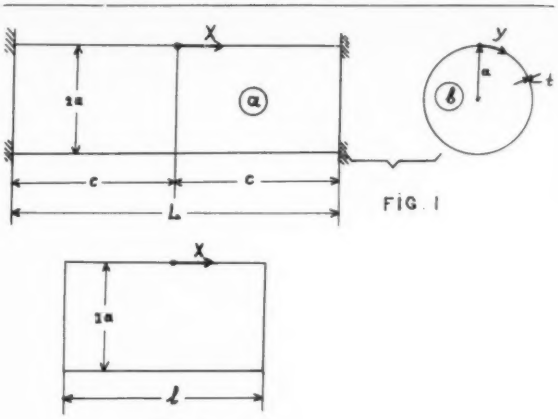

FIG. 1

FIG. 2

FIG. 1. Clamped Cylindrical Shell.
FIG. 2. Simply Supported Cylindrical Shell.

$$Nd^4w/dx^4 = Cw \tag{1}$$

This equation may also be obtained from Donnell's equation[3] for the present case, where $\sigma_x = {}^1/_2\sigma_y$ (Fig. 1),

$$N\nabla^8 w + \frac{Et}{a^2}\frac{\partial^4 w}{\partial x^4} + t\sigma_y\nabla^4\left(\frac{\partial^2 w}{\partial y^2} + \frac{1}{2}\frac{\partial^2 w}{\partial x^2}\right) = 0 \tag{2}$$

by taking into account that with the above assumption the derivatives in the axial direction can be neglected with respect to those in the circumferential direction, so that Eq. (2) reduces to

$$N\frac{\partial^8 w}{\partial y^8} + \frac{Et}{a^2}\frac{\partial^4 w}{\partial x^4} + t\sigma_y\frac{\partial^6 w}{\partial y^6} = 0 \tag{3}$$

With $w = w_0 \cos ny/a$, where w_0 is a function of x only, this becomes, with $N = Et^3/[12(1 - \nu^2)]$,

$$\frac{d^4 w_0}{dx^4} + n^6\left(\frac{n^2t^2}{12(1-\nu^2)a^6} - \frac{\sigma_y}{Ea^4}\right)w_0 = 0 \tag{4}$$

Equations similar to Eqs. (3) and (4) are derived in reference 4 from Flügge's three differential equations by order of magnitude considerations.

Since Eq. (1) also obtains for a simply supported shell, with length l (Fig. 2), which is known to buckle in lobes with only one half wave in the axial direction, in that case $w = w_0 \cos \pi x/l$, so that from Eq. (1) $C = \pi^4 N/l^4$. Hence Eq. (1) may be written as

$$d^4w/dx^4 = (\pi^4/l^4)w \tag{5}$$

where l is the length of the simply supported shell that buckles

at the same critical pressure as the clamped shell. For the latter case, owing to symmetry, the general solution of Eq. (5) is

$$w = A \cosh \pi x/l + B \cos \pi x/l \tag{6}$$

Inserting this equation into the boundary conditions, $w = 0$ and $dw/dx = 0$, at $x = \pm c$ (Fig. 1a), one obtains two homogeneous linear equations, which for deflections different from zero, are only satisfied if the determinant of the system is zero, yielding

$$\tanh \pi c/l + \tan \pi c/l = 0 \tag{7}$$

This condition is satisfied if $l = 1.33c = 0.665L \cong (2/3)L$. Hence, a fully clamped shell of length L has the same critical external pressure as a simply supported shell of length $(2/3)L$. As shown in reference 2, for steel shells and aluminum shells having L/a ratios larger than 1.5 and 2.25, respectively, that is, for shells having ratios of the half waves in the axial and circumferential direction that are sufficiently large (larger than about 4), excellent agreement exists with results obtained in reference 5. For shorter shells, reference 2 presents another solution.

From reference 6 the von Mises equation for the critical pressure p_{cr} of simply supported shells can be reduced to a formula which may be written in the form

$$p_{cr} = \frac{0.92E(t/a)^2}{(l/a)\ (a/t)^{1/2} - 0.636} \tag{8}$$

Hence, for clamped shells of length L, with $l = (2/3)L$,

$$p_{cr} = \frac{1.38E(t/a)^2}{(L/a)\ (a/t)^{1/2} - 0.954} \tag{9}$$

A practically similar equation to the subject problem can be derived using the method employed by Professor P. Lardy in reference 7 in calculating the bending moments in clamped slabs. Assume

$$w = \cos n\varphi \Sigma w_m u_m \tag{10}$$

where the functions

$$u_m = \frac{\cosh \alpha_m x}{\cosh \alpha_m c} - \frac{\cos \alpha_m x}{\cos \alpha_m c} \tag{11}$$

are the normal functions that automatically satisfy the boundary conditions, which for clamped shells require that

$$\tanh \alpha_m c + \tan \alpha_m c = 0 \tag{12}$$

For the symmetrical case the solutions of Eq. (12) are $\alpha_1 = 2.365/c$ and $\alpha_m = (4m - 1)\pi/(4c)$ for $m \geqslant 2$. As a matter of fact, for $m = 1$, Eqs. (11) and (12) are identical to Eqs. (6) and (7). The functions u_m are orthogonal. Further $\partial^4 u_m/\partial x^4 = \alpha_m{}^4 u_m$ and $\partial^2 u_m/\partial x^2 = \alpha_m{}^2 \tilde{u}_m$, where

$$\tilde{u}_m = \frac{\cosh \alpha_m x}{\cosh \alpha_m c} + \frac{\cos \alpha_m x}{\cos \alpha_m c} \tag{13}$$

However, due to the orthogonality of the functions u_m, $\tilde{u}_m$ can be developed into a series of u_m,

$$\tilde{u}_m = k_{1m}u_1 + k_{2m}u_2 + k_{3m}u_3 + \ldots \tag{14}$$

From reference 7, for example, $k_{11} = -0.54984$.

The solution converges rapidly. Using only the first terms of Eqs. (10) and (14) the writer found for a compressed plate that is clamped at the unloaded edges a buckling stress coefficient $k = 7.04$, which is in excellent agreement with the exact value $k = 7.00$. Also in the present case, due to the identity of Eqs. (6) and (11), the latter for $m = 1$, a good convergence may be expected. Insertion of Eq. (10) into Eq. (2) and using only the first terms of Eqs. (10) and (14) yields, after solution for σ_y and p_{cr},

$$p_{cr} = \frac{t\sigma_y}{a} = \frac{N(n^6\beta^6 + 12.3n^6\beta^6 + 188.4n^4\beta^4 + 386n^2\beta^2 + 985) + 31.4Et^3\gamma^2\beta^6}{\beta^2a^3(n^6\beta^6 + 7.70n^4\beta^4 + 62.8n^2\beta^2 + 48.34)} \tag{15}$$

where $\beta = c/a = L/2a$ and $\gamma = a/t$. With relatively small half waves $\lambda = \pi a/n$ in the circumferential direction the ratio $c/\lambda = nc/\pi a = n\beta/\pi$, and certainly $n^2\beta^2$, is large with respect to one, so that approximately

$$p_{cr} = \frac{Nn^6\beta^6 + 31.4Et^3\gamma^2\beta^6}{\beta^2a^3n^6\beta^6} = \left[\frac{n^2}{12(1 - \nu^2)} + \frac{31.4}{n^6\beta^4}\left(\frac{a}{t}\right)^2\right] E\left(\frac{t}{a}\right)^3 \tag{16}$$

The condition $\partial p_{cr}/\partial n = 0$ gives $n = 2.38\ (\gamma/\beta^2)^{1/4}$. Inserting this into Eq. (15) and dividing the numerator by the denominator, leads to

$$p_{cr} = [0.691\beta\gamma^{1/2} + 0.190 + 1.43/(\beta\gamma^{1/2}) - 1.40/(\beta\gamma^{1/2})^2 + \ldots]E/(\beta^2\gamma^2) \tag{17}$$

Taking only the first two terms of Eq. (17) gives

$$p_{cr} = \frac{1.382(t/a)^2 + 0.76(t/a)^{5/2}(a/L)}{(L/a)\ (a/t)^{1/2}} E \tag{18}$$

which is practically identical to Eq. (9).

For example, for Model 2 in Table 1 of reference 1, Eqs. (9), (17), and (18) give $p_{cr} = 32.5$, 32.4, and 32.3 psi, respectively, against $p_{cr} = 34.0$ and 35.2 in columns C and D of Table 1 in reference 1.

The writer wishes to thank the Bell Aircraft Corporation for permission to publish these results.

References

[1] Nash, W. A., *Buckling of Thin Cylindrical Shells Subject to Hydrostatic Pressure*, Journal of the Aeronautical Sciences, Vol. 21, No. 5, pp. 354–355, May, 1954.

[2] Bijlaard, P. P., *Buckling under External Pressure of Cylindrical Shells Evenly Stiffened by Rings Only*, Bell Aircraft Corporation Report 02-941-002, May 21, 1952.

[3] Donnell, L. H., *Stability of Thin-Walled Tubes under Torsion*, NACA Rep. 479, 1933.

[4] Biezeno, C. B., and Koch, J. J., *The Buckling of a Cylindrical Tank of Variable Thickness under External Pressure*, Proc. 5th Int. Congress for Applied Mechanics, pp. 34–39, 1938.

[5] Sturm, R. G., *A Study of the Collapsing Pressure of Thin-Walled Cylinders*, University of Illinois, Eng. Exp. Sta., Bull. Ser. 329, 1941.

[6] Windenburg, D. F., and Trilling, C., *Collapse by Instability of Thin Cylindrical Shells under External Pressure*, Trans. ASME, Vol. 56, pp. 819–825, 1934.

[7] Lardy, P., *Sur une Méthode Nouvelle de Résolution du Problème des Dalles Rectangulaires Encastrées*, Publ. Internat. Assoc. for Bridge and Struct. Engrg., Vol. 13, pp. 197–220, 1953.

A Supplementary Note on the Spanwise Loadings over Slender Airfoils

Hsien K. Cheng

Aerodynamicist, Aerodynamics Section, Bell Aircraft Corporation, Buffalo 5, N.Y.

July 30, 1954

THIS NOTE concerns mainly the aerodynamic load distribution over a slender lifting surface. It is written with the aim to generalize a seemingly obscure conclusion arrived from load prediction for a slender delta wing with *symmetrically linear* and parabolic twists.

At a distance sufficiently far downstream of the "leading edge" of a flat plate of low aspect ratio—i.e., $|M^2 - 1|^{1/2}(\text{A.R.}) \ll 1$,

the spanwise lift distribution or the potential difference across the wing surface $\Delta\varphi$, according to Jones's slender-wing theory, is

$$\Delta\varphi = 2U\alpha\sqrt{a^2 - y^2} \tag{1}$$

where U is the free stream velocity, $a = a(x)$ the local half-span, x and y the chordwise and the spanwise rectangular coordinates, and α the angle of attack. The cross-flow field of the lifting airfoil is thereby completely determined by the upwash distribution along the local span, it follows that the *spanwise lift distribution* or $\Delta\varphi$ for a cambered slender airfoil of zero twist, i.e., $\partial\alpha/\partial y = 0$, will also be *elliptic* and given by Eq. (1), in which both the angle of attack α and the span $2a$ are functions of x. This has been pointed out by Jones.[1]

For twisted slender airfoils with zero camber, i.e., $\partial\alpha/\partial x = 0$, a general feature in the load distribution somewhat analogous to the previous can be found. The cross-flow field in the neighborhood of a slender plane lifting surface is[2]

$$\frac{\partial\varphi}{\partial y} - i\frac{\partial\varphi}{\partial z} = g(\zeta) = -\frac{1}{\pi\sqrt{a^2 - \zeta^2}}\int_{-a}^{a}\frac{\sqrt{a^2 - s^2}w_0\,ds}{s - \zeta} \tag{2}$$

where $\zeta = y + iz$, $g(\zeta)$ the complex velocity in the cross-flow plane, i.e., ζ-plane, and w_0 the upwash distribution over the lifting surface at $z = 0$. For the airfoil surface with zero camber (assuming $\alpha(y)$ remains finite),

$$w_0 = -U\alpha(y), \quad -a < y < a, \tag{3}$$

the side-wash on the top surface of the wing, according to Eq. (2), is

$$\frac{\partial\varphi}{\partial y} = \frac{U}{\pi\sqrt{a^2 - y^2}}\int_{-a}^{a}\frac{\sqrt{a^2 - s^2}\,\alpha(s)\,dS}{s - y}, \quad -a < y < a \tag{4}$$

where the principal value of the integral is to be taken. The linearized pressure distribution or $\partial\varphi/\partial x$ on the top surface may be computed from Eq. (4) as follows:

$$\frac{\partial^2\varphi}{\partial y\partial x} = \frac{da}{dx}\cdot\frac{\partial\varphi}{\partial a} = \frac{Ua}{\pi}\cdot\frac{da}{dx}\cdot\int_{-a}^{a}\frac{\alpha(s)\,ds}{s - y}\times\left[-\frac{\sqrt{a^2 - s^2}}{(a^2 - y^2)^{3/2}} + \frac{1}{\sqrt{a^2 - y^2}\sqrt{a^2 - s^2}}\right]$$

which gives

$$\frac{\partial^2\varphi}{\partial y\partial x} = A(x)\cdot\frac{y}{(a^2 - y^2)^{3/2}} + B(x)\cdot\frac{1}{(a^2 - y^2)^{3/2}}, \quad -a < y < a \tag{5}$$

where

$$\left.\begin{aligned} A(x) &\equiv \frac{Ua}{\pi}\cdot\frac{da}{dx}\cdot\int_{-a}^{a}\frac{\alpha(y)\,dy}{\sqrt{a^2 - y^2}} \\ B(x) &\equiv \frac{Ua}{\pi}\cdot\frac{da}{dx}\int_{-a}^{a}\frac{y\alpha(y)\,dy}{\sqrt{a^2 - y^2}} \end{aligned}\right\} \tag{6}$$

Integrating Eq. (5) with respect to y along the top surface, one has

$$\frac{\partial\varphi}{\partial x} = A(x)\cdot\frac{1}{\sqrt{a^2 - y^2}} + \frac{B(x)}{a^2}\cdot\frac{y}{\sqrt{a^2 - y^2}} + F(x), \quad -a < y < a \tag{7}$$

But in approaching the leading edge—i.e., $|y| \to a$ the value of $\partial\varphi/\partial x$ or the linearized pressure difference should either tend to infinity as a *pure* inverse square root or vanish. In other words, the constant of integration appeared on the right-hand side of the above equation, $F(x)$, must be identically zero; otherwise, a logarithmic singularity in the upwash distribution will occur at the leading edges, which will certainly violate the boundary condition on the wing surface, namely, Eq. (3). Therefore, one arrives, under condition Eq. (3) at

$$\Delta\frac{\partial\varphi}{\partial x} = 2A(x)\cdot\frac{1}{\sqrt{a^2 - y^2}} + 2\frac{B(x)}{a^2}\cdot\frac{y}{\sqrt{a^2 - y^2}}, \quad -a < y < a \tag{8}$$

where $A(x)$ and $B(x)$ have been given by Eq. (6).

Hence, within the scope of the slender-airfoil theory, the following conclusions can be drawn:

(I) If the plane lifting surface has *no twist* at the station x, i.e., $\alpha = \alpha(x)$, the *spanwise distribution* of the *lift* ($\rho U\Delta\varphi$) at that station is the same as over a *flat plate* at angle of attack, which is the elliptic distribution given by Eq. (1), as pointed out by Jones.

(II) If the surface has *zero* camber, i.e., $\alpha = \alpha(y)$, and if the upwash is prescribed *symmetrically* with respect to the midspan, i.e., $\alpha = +\alpha(-y)$, the *spanwise distribution* in the *pressure difference* ($\Delta p \approx -\rho U\Delta\partial\varphi/\partial x$) will be found the same as over a *flat plate* at angle of attack, which is given by the first term of the right-hand member of Eq. (8). If, instead, the upwash distribution is prescribed *antisymmetrically* with respect to the midspan, i.e., $\alpha(y) = -\alpha(-y)$, the spanwise distribution in the pressure difference will then be found the same as for a *plate in rolling*, which is given by the second term of the right-hand member of Eq. (8).

It is of interest to note that the "zero cambered" airfoils mentioned above include not only the case of symmetrically linear twist as well as the case of differentially deflected triangular plate, but cases of control surface deflections in general, provided the "gaps" between the surfaces are of zero width and run across the wing's plane from the leading edge to the trailing edge in the *streamwise* direction.

In arriving at the above conclusions, it has also been assumed that the flow around the leading edge is "nonseparated" and that the planform is symmetrical, whose shape is, however, arbitrary. It is worth noticing that when the airfoil becomes *not-so-slender* in the sense of reference 3, the first conclusion stated above can be shown still valid, while the second is no longer true.

In a private communication, H. R. Lawrence of Cornell Aeronautical Laboratory kindly informs the writer that he has also arrived at the same result of Eq. (8) in a different manner.

References

[1] Jones, R. T., *Properties of Low Aspect-Ratio Wings at Speed Below and Above the Speed of Sound*, NACA TN 1032, 1946.

[2] Cheng, H. K., and Rott, N., *Generalization of the Inversion Formula of Thin Airfoil Theory*, Journal of Rational Mechanics and Analysis, Vol. 3, No. 3, May, 1954.

[3] Adams, M. C., and Sears, W. R., *Slender-Body Theory—Review and Extension*, Journal of Aeronautical Sciences, Vol. 20, No. 2, p. 85, February, 1953.

A Semiempirical Method for Determining Delta-Wing Pressure Distributions in an Incompressible Flow

William R. Laidlaw and P. T. Hsu
Massachusetts Institute of Technology, Cambridge, Mass.

August 4, 1954

Symbols

b	=	root semichord
c	=	root chord
$F(x/c)$	=	pressure correction function
$k = (\omega b/U)$	=	reduced frequency of oscillation
$\Delta p(x, y, t)$	=	lift per unit area
$s(x)$	=	local semispan
U	=	airspeed

$W_a(x, y, t)$ = downwash at camber surface
x = chordwise coordinate (measured aft from vertex)
y, η = spanwise coordinate
z = vertical coordinate
$Z_a(x, y, t)$ = vertical deflection of camber surface
ρ = air density
$\varphi(x, y, t)$ = perturbation potential in plane $z = 0$
ω = circular frequency of oscillation

Discussion

With the ever-increasing popularity of the delta wing in the design of modern high-speed aircraft, there has come a demand for methods of analysis which are sufficiently rapid for use in the design office but at the same time may be relied upon to give aerodynamic information of reasonable accuracy.

The delta-wing problem is by no means a new one. In the past, Jones[1] has considered the case of an extremely slender wing in a steady incompressible flow, whereas Garrick[2] and Voss[3] have extended this work to cover the unsteady case. Lawrence[4] and Lawrence and Gerber[5] have made worth-while improvements on the slender-wing theory to cover delta wings in a wide range of aspect ratio. The latter theory is, however, considerably more complicated than the previous slender-wing analysis; and, at the same time, it is no longer possible to obtain the pressure distribution.

The object of the present discussion is, therefore, to propose a semiempirical approach to the problem, which retains the simplicity of the slender-wing theory and yet gives results comparable to those of Lawrence and Gerber.

In general, the lift per unit area at any point on a thin lifting surface may be written:

$$\Delta p(x, y, t) = 2\rho \left[\frac{\partial \varphi}{\partial t}(x, y, t) + U \frac{\partial \varphi}{\partial x}(x, y, t) \right] \tag{1}$$

According to the theory of Garrick[2] and Voss,[3] the velocity potential $\varphi(x, y, t)$ is given by the relation:

$$\frac{\partial \varphi}{\partial y}(x, y, t) = \frac{1}{\pi \sqrt{s(x)^2 - y^2}} \oint_{-s}^{s} \frac{W_a(x, \eta, t)\sqrt{(x)^2 - \eta^2}}{y - \eta} \, d\eta \tag{2}$$

where the downwash $W_a(x, y, t)$ is prescribed in terms of the wing motion $Z_a(x, y, t)$ by the expression:

$$W_a(x, y, t) = \frac{\partial Z_a}{\partial t}(x, y, t) + U \frac{\partial Z_a}{\partial x}(x, y, t) \tag{3}$$

Eq. (2) is valid for any arbitrary motion of the wing camber surface, and therefore includes, as a special case, the steady flow. The only requirement attached to the above expression for $\varphi(x, y, t)$ is that the ratio of wing span to wing chord be very small. In the past, there has been much conjecture concerning the consequences of this aspect ratio limitation when applying the theory to practical problems, and further studies were definitely indicated.

Tests and calculations were conducted at M.I.T.[6] to determine pressure distributions on two rigid oscillating delta wings of aspect ratios 1.07 and 2.31, and the following conclusions have been stated:

(1) The main fault of the slender-wing theory is that it fails to provide for the Kutta condition of zero pressure at the trailing edge. This causes an overestimation of the pressures on the rear portion of the wing, and gives rise to extremely large errors in lift and pitching moment even for the relatively slender aspect ratio 1.07 wing.

(2) The slender-wing theory predicts pressures near the vertex with good accuracy for both delta wings.

(3) The shapes of the theoretical spanwise pressure distributions at fixed chordwise stations are in good qualitative agreement with the experimental results, although errors in "scale" exist which increase as the trailing edge is approached.

(4) The pressure phase angles, in all cases, are in good agreement with experiment over the complete plan form.

In view of the above statements, a possible means of improving the theory immediately presents itself: namely, the use of a multiplicative function which will permit a more realistic representation of pressures near the trailing edge, and at the same time leave the theoretical results unaltered in all other respects.

For this purpose, the function:

$$F(x/c) = \sqrt{1 - (x/c)^2}$$

is suggested. It will be noted that $F(x/c)$ is a real function of only the chordwise variable; hence, although it alters the pressure amplitudes, it leaves the pressure-phase angles and the spanwise shape of the pressure distribution unchanged. Furthermore, conditions in the vicinity of the vertex remain identical to those of the unmodified theory; whereas at the trailing edge, it provides for the Kutta condition and gives the pressure distribution a slope singularity resembling that of two-dimensional thin airfoil theory.

If we then denote Δp_u as the pressure at a point (x, y) as computed from the slender-wing theory of Jones, Garrick, and Voss, the modified pressure Δp_m at the same point is given by the relation:

$$\Delta p_m(x, y) = \sqrt{1 - (x/c)^2}\,\Delta p_u(x, y) \tag{4}$$

Eq. (4) was used to compute pressure distributions for the two delta wings described above. Comparisons were then made with the previous experimental and theoretical results. Excellent agreement with the experimental data was obtained for a wide range of reduced frequency $[k = (\omega b/U)]$ for both rigid body pitching and vertical translation motions. This was shown not only by the pressure distributions, but also by the chordwise lift distributions and the total lift and pitching moments. Complete theoretical and experimental comparisons may be found in reference 6.

In order to determine the validity of this pressure correction function when applied to the air forces which are exerted on a wing performing higher order elastic motions, a flutter calculation was carried out on a delta wing which had previously been tested at M.I.T. The details of this wing, the flutter tests, and the previous slender-wing flutter calculations are thoroughly described in reference 7. Briefly, the flutter model consisted of a delta wing of 25.75° vertex angle (aspect ratio 0.915), fabricated of "rigid" spanwise segments but free to deform in the chordwise direction. The model was restrained in the wind tunnel by a simple support located at 32.15% of the root chord. The observed flutter speed and frequency respectively are given in Table 1.

The original flutter calculations employed an "assumed mode" technique, which incorporated rigid body pitching about the support point, and the first two still air elastic modes, in the flutter mode.

The calculations of reference 7 included a very accurate analysis of the inertial and elastic parameters of the wing, and hence the large errors which appear in the flutter speed and frequency (Table 1) may be attributed primarily to the inadequacy of the unmodified slender-wing theory to provide a satisfactory representation of the aerodynamic forces

Table 1
Theoretical and Experimental Flutter Data—Aspect Ratio 0.915 Delta Wing

Case	Flutter Speed, U_F (M.P.H.)	Flutter Frequency, ω_F (Rad./Sec.)	Reduced Frequency, $k_F = (\omega_F \cdot b)/U_F$
Experiment	39.1	14.6	0.557
Unmodified slender wing theory	65.7	22.0	0.500
Modified slender wing theory	33.5	11.5	0.512

The new set of flutter calculations, which have recently been completed, utilize the original structural analysis, but incorporate aerodynamic forces modified according to Eq. (4). Specifically, this amounted to a re-evaluation of the integrals which lead to the generalized forces in the flutter equations. The results of the revised analysis are presented in Table 1, and show a remarkable improvement over the previous theoretical speed and frequency.

The improvements resulting from the use of this empirical correction function, may be attributed to the following two factors.

First, it provides a means of satisfying the Kutta condition, thus giving a more realistic representation of the pressures in the vicinity of the trailing edge.

Secondly, it has been observed that, according to the unmodified theory, the pressure distribution on a delta wing is affected strongly by the slope and curvature of the camber surface. Flutter results, therefore, become extremely sensitive to the shape of the wing, and since pressures near the trailing edge are greatly overestimated, this region assumes a high degree of importance. When these trailing edge pressures are adequately represented, the accuracy of a given flutter calculation becomes less dependent on the nature of the assumed modes.

With the experimental evidence of references 6 and 7 as a basis, we may conclude that the semiempirical technique described above, for obtaining delta-wing pressure distributions, is satisfactory. It should be noted, however, that since the procedure is based essentially on a combination of experimental observations and physical reasoning, it should be used with discretion when applied to delta wings of large aspect ratio or to other than triangular wings.

The method does, however, yield results which compare favorably with the more exact Lawrence and Gerber theory, and at the same time it retains the simplicity of the slender-wing analysis. These features should give it much appeal from the engineering point of view, particularly since it is valid for both the steady and unsteady cases regardless of the shape of the camber surface or the complexity of the oscillation mode.

References

[1] Jones, R. T., *Properties of Low Aspect Ratio Pointed Wings at Speeds Below and Above the Speed of Sound*, NACA Technical Report 835, 1946.

[2] Garrick, I. E., *Some Research on High Speed Flutter*, Proceedings of the Third Anglo-American Aeronautical Conference, Appendix B, R.Ae.S.-I.A.S., 1951.

[3] Voss, H. M., *Flutter of Low Aspect Ratio Lifting Surfaces*, S.M. Thesis, Massachusetts Institute of Technology, May, 1951.

[4] Lawrence, H. R., *The Lift Distribution on Low Aspect Ratio Wings at Subsonic Speeds*, Journal of the Aeronautical Sciences, Vol. 18, No. 10, p. 683, Oct., 1951.

[5] Lawrence, H. R., and Gerber, E. H., *The Aerodynamic Forces on Low Aspect Ratio Wings Oscillating in an Incompressible Flow*, Journal of the Aeronautical Sciences, Vol. 19, No. 11, p. 769, Nov. 1952.

[6] Laidlaw, W. R., *Theoretical and Experimental Pressure Distributions on Oscillating Low Aspect Ratio Wings*, Sc.D. Thesis, Massachusetts Institute of Technology, May, 1954.

[7] Voss, H. M., Zartarian, G., and Hsu, P. T., *Theoretical and Experimental Investigation of the Aeroelastic Behaviour of Low-Aspect-Ratio Wings*, M.I.T. Aeroelastic and Structures Research Laboratory, Contract NOa(s) 51-109-c, June, 1953.

Addendum—"Characteristic Solution for Axially Symmetric Transonic Flow"[1]

Erik Mollo-Christensen

Research Engineer, Department of Aeronautical Engineering, Massachusetts Institute of Technology, Cambridge, Mass.

August 4, 1954

In a letter from Kelsey Walker, Jr., Project Engineer, Municipal University of Wichita, Kansas, he points out that the solution of the transonic equation given by me[1] had previously been found by E. W. Graham in 1949.[2]

At the same time, Prof. Leon Trilling, M.I.T., found that it is included as a special case in a solution given by G. Guderley.[3]

References

[1] Journal of the Aeronautical Sciences, Vol. 21, No. 7, p. 501, July, 1954.

[2] Graham, E. W., *Solution of a Non-Linear Equation for Transonic Flow with Rotational Symmetry*, Douglas Aircraft Report SM-13677, 1949.

[3] Guderley, G., and Yoshihara, H., *Axial-Symmetric Transonic Flow*, Air Force Technical Report 5797, September, 1949.

Shock-Wave Yaw for 9 ½° Semiapex Cone

Eugene D. Boyer

Ballistics Research Laboratories, Aberdeen Proving Ground, Maryland

August 5, 1954

The semiapex angle of the shock wave and the ratio of the shock-wave yaw to the yaw of a projectile for small yaw is theoretically predicted by A. H. Stone.[1] Wind-tunnel verification of this theory is described in reference 6. An experimental verification of the theory has also been obtained from cones and cone cylinders[5] fired in the Free Flight Aerodynamics Range of the Ballistic Research Laboratories. (See Figs. 1 and 2.)

The theoretical values as predicted by Stone are obtained directly from Kopal's tables.[2, 3] In order to determine these values for a cone, semiapex angle θ_s of $9\frac{1}{2}°$, we must first determine the surface velocity component U_s, in terms of the Mach Number M. Knowing U_s, we can then obtain the shock-to-

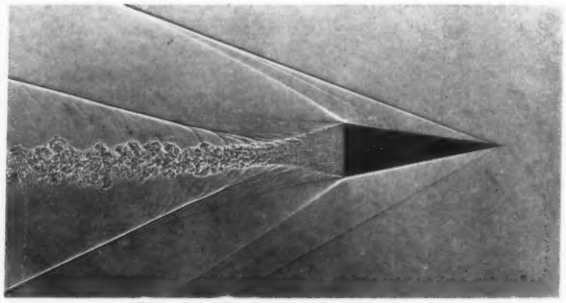

Fig. 1. Shadowgraph pure cone.

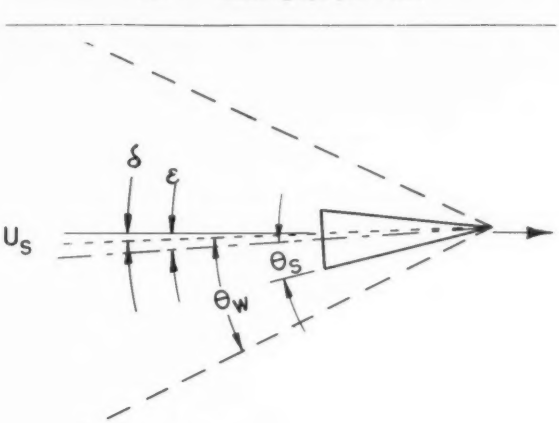

Fig. 2. Yawing cone.

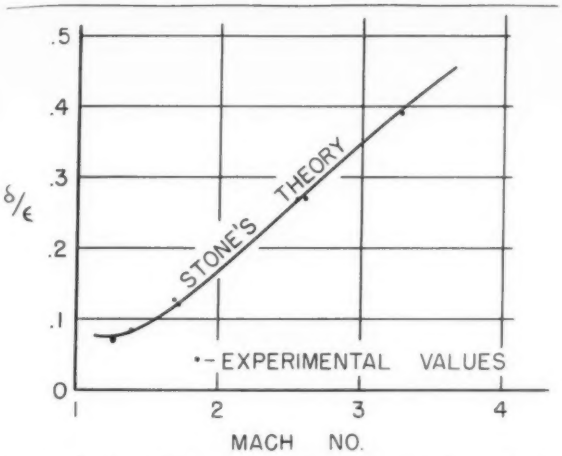

FIG. 3. Ratio of shock-wave yaw to yaw of projectile vs. Mach Number.

cone-yaw ratio δ/ϵ, by two-way linear interpolation. Fig. 3 shows the predicted behavior of the ratio δ/ϵ for various Mach Numbers.

For the empirical values a number of rounds with different Mach Numbers were selected for a distribution of points on the δ/ϵ vs. M curve. Since the change in M is less than 0.16 through the range, each round is considered to have a constant Mach Number. The yaws were measured only in one plane, vertical or horizontal. Only those stations were selected for which the yaw in one plane was very small, less than $^1/_2°$, and the yaw in the measured plane was fairly large, at least six times as great.

The projected angular positions δ^* and ϵ^* were measured on a grid. From these measured angles the true yaw is obtained.[4]

Since we are considering a body of revolution it is reasonable to assume that for zero yaw the yaw of the shock wave is also zero. The ratio of the two yaws can then be determined by fitting the function $\delta = b\epsilon$, by least squares, to the yaw angle data. These values along with the theoretical values are seen in Fig. 3 plotted against Mach Number. The agreement is good with the differences of the experimental and theoretical values being less than the statistical error of the experimental values.

REFERENCES

[1] Stone, A. H., *On Supersonic Flow Past a Slightly Yawing Cone*, Journal of Mathematics and Physics, 30, pp. 67–80, 1952.

[2] Kopal, Z., *Tables of Supersonic Flow Around Cones*, M.I.T. Technical Rept. 1, 1947.

[3] Kopal, Z., *Tables of Supersonic Flow Around Cones*, M.I.T. Technical Rept. 3, 1947.

[4] Murphy, C. H., *Data Reduction for the Free Flight Ranges*, B.R.L. Rept. 900, 1954.

[5] Boyer, E. D., *Shock-Wave Yaw for 9¹/₂° Semi-Apex Cone*, B.R.L. Technical Note 887, 1954.

[6] Cronvich, L. L., *Results of Experimental Studies of Pressure Distribution on Cones at Supersonic Velocities*, APL/JHU TG-91, 1950.

Effect of Spin in Aerodynamic Properties of Bodies of Revolution

L. E. Schmidt and C. H. Murphy

Ballistics Research Laboratories, Aberdeen Proving Ground, Maryland

August 6, 1954

LEHNERT AND HASTINGS[1, 2] have measured the effect of spin on base pressure of cone-cylinders at a Mach Number of 2.86 and for Reynolds Numbers from 2.5×10^6 to 4.5×10^6. They found that the character of the boundary layer at the base was an important factor. An increase in spin would cause either a considerable decrease in base pressure if the flow was laminar or a slight increase if it was turbulent. Recent firings[3] in one of BRL's spark ranges indicate a different situation at $R_e = 3.0 \times 10^6$ and $M = 1.3$.

The primary purpose of these firings was to study the effect of spin on the aerodynamic coefficients of spin-stabilized missiles. The model was a 5-caliber long body of revolution with 2-caliber secant ogival nose and a cylindrical body. The radius of the ogive was 8.5 calibers. Measurements[4] were made of total drag, C_D, normal force, C_{N_α}, overturning moment, C_{M_α}, damping moment, $C_{M_q} + C_{M_{\dot\alpha}}$, Magnus moment, $C_{M_{p\alpha}}$, and spin decelerating moment, C_{l_p}, coefficients at different values of spin $pd/2V$, between 0.079 and 0.323 (d is model diameter). Since C_D is quite sensitive to the magnitude of yaw, only those rounds with less than 3° of yaw were considered for drag determination. Only the total drag and the Magnus moment coefficients showed a measurable variation with spin.

In reference 5 it is shown that for configurations possessing a plane of mirror symmetry the coefficients are even functions of spin. For this reason C_D and $C_{M_{p\alpha}}$ were plotted against $(pd/2V)^2$. A linear relationship in spin squared was assumed and fitted by least squares to the C_D and $C_{M_{p\alpha}}$ data (see Figs. 1 and 2). The slopes, C_D', $C_{M_{p\alpha}}'$, and intercepts $C_D(0)$, $C_{M_{p\alpha}}(0)$ were computed to be:

$$C_D(0) = 0.415 \pm 0.002 \qquad C_{M_{p\alpha}}(0) = 0.64 \pm 0.05$$
$$C_D' = 0.20 \pm 0.02 \qquad C_{M_{p\alpha}}' = -5.1 \pm 0.8$$

Although $C_{M_{p\alpha}}'$ is poorly determined, the trend is statistically significant.

In all firings the boundary layer at the base was turbulent and transition occurred between one and two calibers forward of the base. An upper bound to the contribution of the skin friction variation with spin to C_D was estimated[3] to be 0.05. The difference of 0.15 must then be caused by a *decrease* in base pressure for increasing spin. For comparison purposes C_D for base pressure variation was computed from the Lehnert and Hastings data. For laminar flow at $R_e = 3.0 \times 10^6$, $C_D' = 0.44$ and for

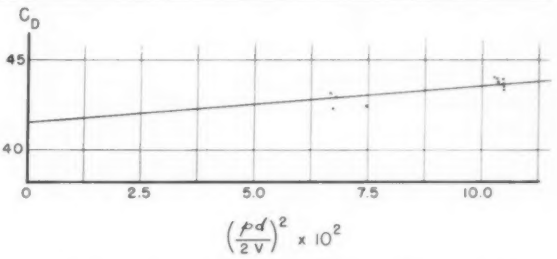

FIG. 1. Zero-yaw drag coefficient vs. spin squared.

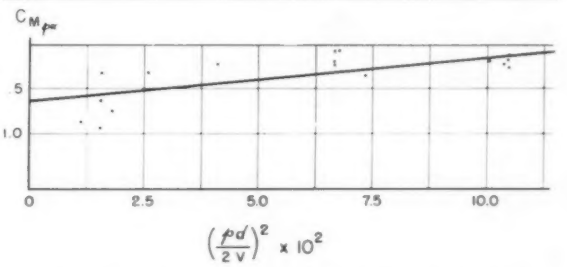

FIG. 2. Magnus moment coefficient vs. spin squared

turbulent flow of about two calibers extent, forward of the base, at $R_s = 3.8 \times 10^6$, $C_D' = -0.14$.

References

[1] Lehnert, R., and Hastings, S. M., *Spin Effect on Base Pressure of Cone-Cylinders*, Readers' Forum, Journal of the Aeronautical Sciences, Vol. 21, No. 4, pp. 286–287, April, 1954.

[2] Lehnert, R., and Hastings, S. M., *Spin Effects on Base Pressure of Cone-Cylinders at M = 2.86*, NAVORD Rept. 2956, Oct., 1953.

[3] Schmidt, L. E., and Murphy, C. H., *Effect of Spin on Aerodynamic Properties of Bodies of Revolution*, Ballistic Research Laboratories Memorandum Rept., 715, Aug., 1953.

[4] Murphy, C. H., *Data Reduction for the Free Flight Spark Ranges*, Ballistic Research Laboratories Rept. 900, Feb., 1954.

[5] Maple, C. G., and Synge, J. L., *Aerodynamic Symmetry of Projectiles*, Q.A.M. Vol. VI, No. 4, pp. 345–366, Jan., 1949.

Tip or Leading-Edge Temperatures on Pointed Heat Conducting Bodies at High Supersonic Speeds*

M. Richard Denison
North American Aviation, Inc., Downey, Calif.

August 8, 1954

Symbols

A	=	cross-sectional area at distance x
A_L	=	cross-sectional area at distance L
F	=	$32h_LS_LL/kA_L$ dimensionless parameter for cone
G	=	$16h_LS_LL/kA_L$, dimensionless parameter for wedge
h	=	heat-transfer coefficient at distance x
h_L	=	heat-transfer coefficient at distance L
I_ν	=	modified Bessel function of first kind
k	=	thermal conductivity
K_ν	=	modified Bessel function of second kind
L	=	distance from tip or leading edge to base
Q	=	heat absorbed by sink
S	=	surface area from tip to distance x
S_L	=	surface area from tip to distance L
T	=	body temperature at distance x
T_{iw}	=	insulated wall or recovery temperature
T_0	=	tip or leading edge temperature
u	=	$(phLSLL/\lambda^2kA_L)^{1/2}(x/L)^\lambda$, dimensionless variable
x	=	distance from tip or leading edge
θ	=	$T_{iw} - T$

Discussion

If a body were to move through the atmosphere at a fast enough speed, recovery temperatures high enough to melt any known material could be reached. It is known that over most portions of the body surface temperatures could be reduced by cooling the boundary layer, but there seems to be widespread belief that the temperature at the leading edge or tip of a structure must necessarily be at the recovery temperature. For example, see references 1 and 2. This belief probably arises because in these regions the boundary layer is so thin that the local heat-transfer coefficient becomes very large.

At the suggestion of Dr. E. R. Van Driest of North American Aviation's Aerophysics Department, the following study was carried out to determine the validity of the above concept. The results show that the concept is overconservative even with a heat transfer coefficient that approaches infinity at the leading edge.

Consider steady-state heat conduction in a solid pointed body at zero angle of attack with a heat sink at the base. Included among such bodies are cones and wedges which are important shapes for aircraft design. It will be shown that for both the cone and wedge with a heat sink, the tip or leading edge temperature is less than the recovery temperature. If it is true in these simple cases, then it must also be true in more complex cases that the tip or leading edge temperature depends on the particular heat conduction conditions which exist.

Assume that the body is sufficiently thin so that the internal temperature gradients normal to the surface are negligible. Thus the body temperature is a function of the distance from the tip only. This will be designated the x direction. Assume, also, that the cross section of the body changes with a power of x, and neglect radiation from the surface.

A heat balance for an element gives, neglecting higher order terms,

$$kA\frac{d^2T}{dx^2} + k\frac{dA}{dx}\frac{dT}{dx} + h\frac{dS}{dx}(T_{iw} - T) = 0 \tag{1}$$

Let $\theta = T_{iw} - T$. Then

$$kA\frac{d^2\theta}{dx^2} + k\frac{dA}{dx}\frac{d\theta}{dx} - h\frac{dS}{dx}\theta = 0 \tag{2}$$

Assume that A, S, and h are power functions of x and express them in terms of their values at the base of the body, $x = L$.†

For convenience in the final result introduce constants λ and ν in the powers of x such that

$$A = A_L(x/L)^{1-2\lambda\nu} \tag{2a}$$

Hence,

$$\frac{1}{A}\frac{dA}{dx} = (1 - 2\lambda\nu)x^{-1} \tag{2b}$$

Also let

$$h\frac{dS}{dx} = \frac{phLS_L}{L}\left(\frac{x}{L}\right)^{2\lambda(1-\nu)-1} \tag{2c}$$

where p is another constant. When Eqs. (2b) and (2c) are substituted, Eq. (2) becomes

$$\frac{d^2\theta}{dx^2} + (1 - 2\lambda\nu)x^{-1}\frac{d\theta}{dx} - \left(\frac{phLS_L}{kA_LL^{2\lambda-1}}\right)x^{2(\lambda-1)}\theta = 0 \tag{3}$$

Let

$$u = \left(\frac{phLS_LL}{kA_L\lambda^2}\right)^{1/2}\left(\frac{x}{L}\right)^\lambda$$

In terms of u, Eq. (3) can be written as

$$\frac{d^2\theta}{du^2} + \frac{(1 - 2\nu)}{u}\frac{d\theta}{du} - \theta = 0 \tag{4}$$

The solution of Eq. (4) is

$$\theta = u^\nu[c_1I_\nu(u) + c_2K_\nu(u)] \tag{5}$$

where I_ν and K_ν are modified Bessel functions of the first and second kind respectively.

Solution for Cone

The cross-sectional area of a cone is proportional to x^2. Hence

$$A = A_L(x/L)^2$$

Comparison of this with Eq. (2a) gives

$$2 = 1 - 2\lambda\nu \tag{6}$$

The surface area is also proportional to x^2 so that

$$S = S_L(x/L)^2$$

and

$$dS/dx = 2S_L/L(x/L)$$

For compressible laminar flow with constant-wall temperature and static pressure, Crocco[4] has shown that

* The author wishes to thank Dr. J. L. Fox of the Aerophysics Department for his advice in this study.

† Gardner[2] has solved this equation with h constant, A and S power functions of x. He also used different boundary conditions than will be used here.

$$h = h_L(x/L)^{-1/2}$$

Although the temperature gradient will be large and the Prandtl boundary layer equations are not applicable in the vicinity of the cone tip, this relationship will be used for the entire region. Then

$$h\frac{dS}{dx} = \frac{2S_L h_L}{L}\left(\frac{x}{L}\right)^{1/2}$$

Comparison of this with Eq. (2c) gives $p = 2$ and

$$1/2 = 2\lambda(1 - \nu) - 1 \tag{7}$$

Simultaneous solution of Eq. (6) and Eq. (7) gives

$$\nu = -2, \qquad \lambda = 1/4$$

Therefore, the solution for a cone is by Eq. (5)

$$\theta = u^{-2}[c_1 I_{-2}(u) + c_2 K_{-2}(u)] \tag{8}$$

where

$$u = \left(\frac{32h_L S_L L}{kA_L}\right)^{1/2}\left(\frac{x}{L}\right)^{1/4}$$

Let $F = 32h_L S_L L/kA_L$. Then $u = F^{1/2}(x/L)^{1/4}$. Now the boundary conditions must be satisfied. These are:

$$\text{at } x = 0 \text{ or } u = 0, \qquad \theta \text{ is finite}$$

$$\text{at } x = L \text{ or } u = F^{1/2}, \qquad kA_L\left(\frac{d\theta}{dx}\right)_L = Q$$

where Q is the amount of heat absorbed by the heat sink at the base of the cone.

Since $K_{-2}(0) = \infty$ the first boundary condition gives $c_2 = 0$. In order to find c_1, $d\theta/dx$ must be obtained.

From Eq. (8)

$$\frac{d\theta}{du} = c_1\left[-2u^{-3}I_{-2} + u^{-2}\frac{dI_{-2}}{du}\right]$$

$$= c_1 u^{-2}[uI_{-3}]^*$$

Hence

$$\frac{d\theta}{dx} = c_1\frac{F^2}{4L}u^{-5}I_{-3}(u) \tag{9}$$

At $x = L$ or $u = F^{1/2}$ Eq. (9) and the second boundary condition give

$$c_1 = \frac{4QL}{kA_L}\frac{F^{1/2}}{I_{-3}(F^{1/2})} \tag{10}$$

Finally

$$\theta = T_{iw} - T = \frac{4QL}{kA_L}\frac{F^{1/2}}{I_{-3}(F^{1/2})}u^{-2}I_{-2}(u) \tag{11}$$

From the properties of Bessel functions

$$I_{-\nu}(u) = I_\nu(u) = \sum_{m=0}^{\infty}\frac{(1/2u)^{\nu+2m}}{m!\Gamma(\nu + m + 1)}$$

Hence from Eq. (8)

$$T_{iw} - T = \frac{c_1}{4}\sum_{m=0}^{\infty}\frac{(1/2u)^{2m}}{m!\Gamma(3 + m)} \tag{12}$$

At $x = 0$ or $u = 0$

$$T_{iw} - T_0 = c_1/4 \times 1/2$$

so that

$$T_0 = T_{iw} - \frac{QL}{2kA_L}\frac{F^{1/2}}{I_3(F^{1/2})} \tag{13}$$

From Eq. (13) it can be seen that if Q is positive, that is, if heat flows from the base to the heat sink, the cone tip temperature, T_0, is less than T_{iw}. Also from Eq. (12), since $u^2 = \text{const.}\ x^{1/2}$, it can be seen that the temperature gradient dT/dx goes to infinity at the origin as $x^{-1/2}$.

* See reference 5 for properties of Bessel functions.

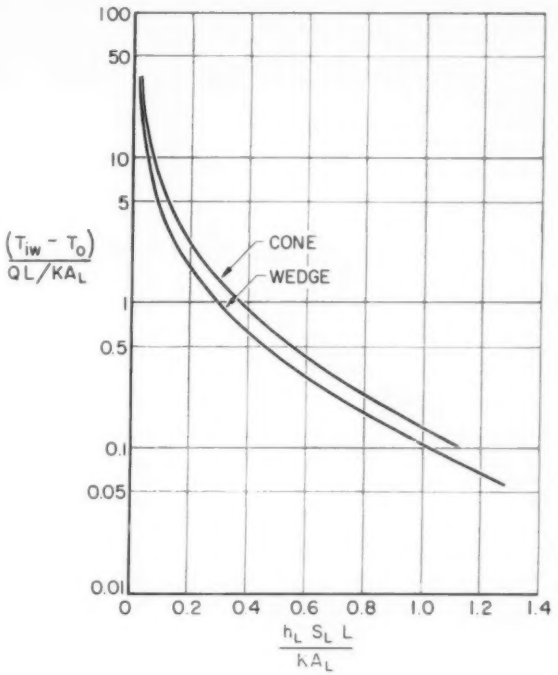

FIG. 1. Tip or leading-edge temperatures for cones and wedges with a heat sink at the base.

WEDGE SOLUTION

For a wedge of infinite span a similar procedure gives

$$\nu = 0, \quad \lambda = 1/4, \quad p = 1$$

From Eq. (5) the solution for the wedge is

$$\theta = c_1' I_0(u) + c_2' K_0(u) \tag{14}$$

with

$$u = \left(\frac{16h_L S_L L}{kA_L}\right)^{1/2}\left(\frac{x}{L}\right)^{1/4}$$

Let $G = 16h_L S_L L/kA_L$. Then with the same boundary conditions as for the cone

$$c_2' = 0$$

$$c_1' = \frac{4QL}{kA_L}\frac{1}{G^{1/2}I_1(G^{1/2})}$$

Since $I_0(0) = 1$

$$T_0 = T_{iw} - \frac{4QL}{kA_L}\frac{1}{G^{1/2}I_1(G^{1/2})} \tag{15}$$

Therefore, the leading edge temperature for the wedge is also less than T_{iw} if Q is positive. It again turns out that dT/dx goes to infinity at the leading edge as $x^{-1/2}$.

The tip or leading edge temperatures for cones and wedges with a heat sink at the base are presented graphically in dimensionless form in Fig. 1.

REFERENCES

[1] Kaye, J., *The Transient Temperature Distribution in a Wing Flying at Supersonic Speeds*, Journal of the Aeronautical Sciences, Vol. 17, No. 12, p. 787, Dec., 1950.

[2] Bryson, A. E., and Edwards, R. H., *The Effect of Nonuniform Surface Temperature on the Transient Aerodynamic Heating of Thin-Skinned Bodies*, Journal of the Aeronautical Sciences, Vol. 19, No. 7, pp. 471–475, July, 1952.

[3] Gardner, K. A., *Efficiency of Extended Surface*, Trans. ASME, Vol. 67, p. 621, Nov., 1945.

[4] Crocco, L., *Lo Strato Limite Laminare nei Gas*, Monografie Scientifiche di Aeronautica, No. 3, Ministero della Difesa-Aeronautica, Roma, Dec., 1946. (Trans. in North American Aviation Aerophysics Lab., Rep. AL-684, July 15, 1948.)

[5] Watson, G. N., *A Treatise on the Theory of Bessel Functions*, 2nd Edition, Cambridge University Press, Cambridge, England, 1952.

On Panel Flutter in Supersonic Flow

W. C. Randels

Lockheed Aircraft Corporation, Burbank, Calif.

August 9, 1954

THE WORK IN reference 1 analyzes the possiblity of flutter of panels with multiple simple supports. The authors seem disturbed by the results which do not offer guide lines for the design of skins for supersonic vehicles. It is suggested that this may be due to the inapplicability of the model used. In reference 2 the more plausible model of a panel clamped at both ends is analyzed giving a criterion for design.

References

[1] Hedgepeth, J. M., Budiansky, B., and Leonard, R. W., *Analysis of Flutter in Compressible Flow of a Panel on Many Supports*, Journal of the Aeronautical Sciences, Vol. 21, p. 475, 1954.

[2] Isaacs, R. P., *Translability Flutter of Supersonic Aircraft Panels*, RAND Paper, p. 101, 1949.

Throat Station Concept in Transonic Flow over Two-Dimensional Wedges

Robert Wesley Truitt

Professor of Aeronautical Engineering, Virginia Polytechnic Institute, Blacksburg, Va.

August 11, 1954

THE FLOW OVER THE front surface of a wedge at zero angle of attack is particularly adaptable to the concept of the convergent portion of a de Laval nozzle. The existence of a stagnation point at the leading edge of the wedge serves as the "reservoir." The favorable pressure gradient over the front surface accelerates the flow from zero speed at the leading edge "reservoir" to a maximum speed at the wedge shoulder (throat station). Under the assumption of isentropic flow along the front wedge surface, the area-pressure relation may be written as:[1]

$$\left(\frac{A_L}{A_T}\right)^2 = \frac{\gamma - 1}{2} \frac{\left(\frac{2}{\gamma + 1}\right)^{(\gamma + 1)/(\gamma - 1)}}{\left(\frac{p_L}{p_0}\right)^{2/\gamma}\left[1 - \left(\frac{p_L}{p_0}\right)^{[(\gamma - 1)/\gamma]}\right]} \qquad (1)$$

where A_L is the local cross-sectional area of the stream-tube corresponding to the local static pressure p_L; A_T is the cross-sectional area of the stream-tube at the minimum throat (wedge shoulder); p_0 is the pressure in the "reservoir" (stagnation point).

Experimental pressure distributions for a 10 per cent thick diamond airfoil[2] in the form of p_L/p_t have been used in Eq. (1) and the results plotted in Fig. 1. It is seen that in the subcritical flow range—i.e., where $A_L/A_T > 1.0$ at $x/c = 1.0$, the area ratio at each x/c-station decreases with increasing free-stream Mach Number. However, at the critical Mach Number—i.e., when $A_L/A_T = A_L/A^* = 1$ at $x/c \doteq 1.0$, any further increase in free-stream Mach Number results in practically no change in the area ratio at a given x/c-station. In a fixed-wall two-dimensional converging channel, if the Mach Number reaches 1.0 in the throat, the local Mach Number at all other sections becomes fixed at a definite subsonic value. This is evident from Eq. (1) since, for isentropic flow,

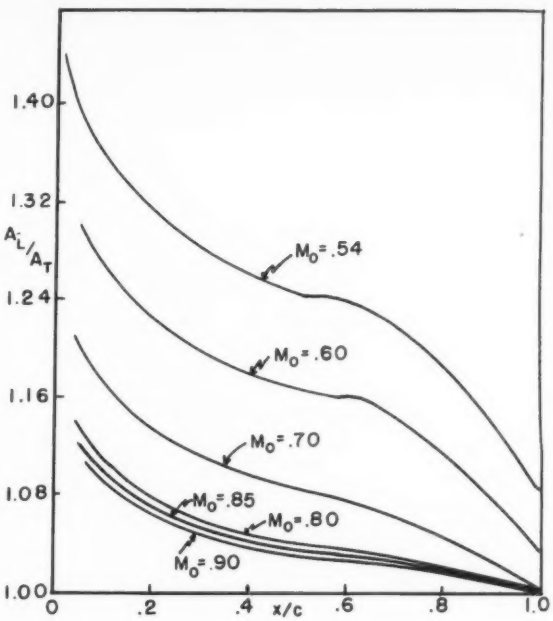

FIGURE 1

$$\frac{p_L}{p_0} = \left(1 + \frac{\gamma - 1}{2} M_L^2\right)^{-[\gamma/(\gamma - 1)]} \qquad (2)$$

where M_L is the local Mach Number. This throat station concept was used previously by Tsien and Fejer.[3] The advantage of the present application is that the throat station is known to occur near the wedge shoulder, whereas, in reference 3, its location necessitated a trial-and-error method for a conventional subsonic airfoil.

Constant Local Mach Number Range

From the above, the beginning of the constant local Mach Number distribution can be found approximately by a compressibility correction method. For example, applying the Kármán-Tsien method to low-speed experimental data for a wedge of semiangle 7.5°, the critical Mach Number corresponding to the peak negative pressure near the shoulder was found to be $M_{0_{crit.}} = 0.815$. Thus, in transonic similarity notation, the lower limit of the constant local Mach Number range is approximately

$$\xi_{0_{crit.}} = \frac{M_{0_{crit.}}^2 - 1}{[(\gamma + 1)\theta]^{2/3}} \doteq -0.72 \qquad (3)$$

Due to "symmetry" about free-stream Mach Number one, the approximate upper limit of the constant local Mach Number range can be found from the exact normal shock relation:[1]

$$M_2^2 = \frac{1 + [(\gamma - 1)/2] M_1^2}{\gamma M_1^2 - [(\gamma - 1)/2]} \qquad (4)$$

where M_1 and M_2 are the Mach Numbers before and after the normal shock, respectively. The upper limit Mach Number, $M_{0_{U.L.}} = M_1$, is found from Ep. (4) by substituting $M_2 = M_{0_{crit.}} = 0.815$. This gives $M_{0_{U.L.}} = M_1 = 1{,}246$, which corresponds to the upper limit reduced free-stream Mach Numbers:

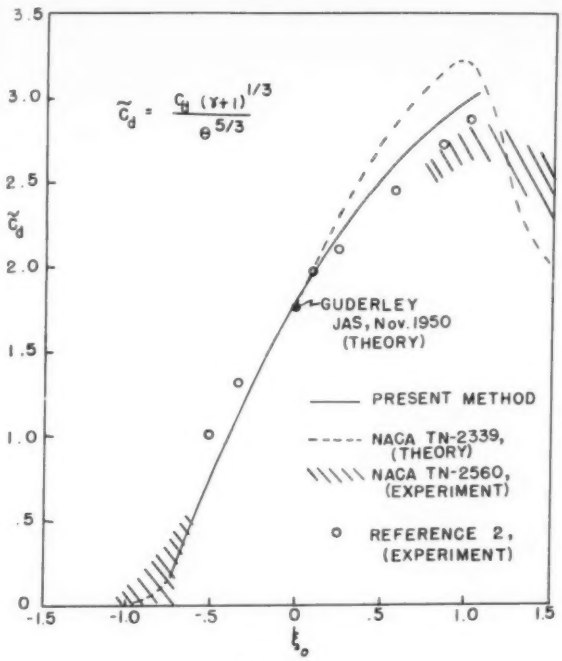

FIGURE 2

$$\xi_{W.L.} = \frac{M_0^2{}_{t.L.} - 1}{[(\gamma+1)\theta]^{2/3}} = 1.2$$

It is assumed that the detached shock is approximately a normal one. It is known, of course, that for $\xi_{W.L.} = 1.2$ it is somewhat curved and, as such, the flow behind the shock is slightly nonuniform. However, neglecting shock curvature, the local Mach Number distribution is approximately constant in the range $-0.72 \leq \xi_0 \leq 1.2$

Pressure Drag

The pressure distribution and hence the pressure drag can be found by applying, say, the Kármán-Tsien method to low-speed, ($M_0 \approx 0$) experimental pressure data for a wedge up to and including the critical Mach Number—i.e., $\xi_{0crit.} = -0.72$. Now the local Mach Number distribution, corresponding to the Kármán-Tsien solution at $\xi_{crit.} = -0.72$, will remain virtually constant in the range $-0.72 \leq \xi_0 \leq 1.2$. Using a method similar to that used first by Maccoll and Codd[4] and later by Griffith,[5] it is a simple matter to find the pressure distribution and pressure drag through the transonic range $-0.72 \leq \xi_0 \leq 1.2$.

As described, the Kármán-Tsien method was applied to low-speed experimental data for a 7.5° semiangle wedge with straight afterbody. The results are plotted in transonic similarity form along with previous experimental and theoretical data in Fig. 2. The agreement of the present method with other findings is evident.

References

[1] Liepmann, H. W., and Puckett, A. E., *Aerodynamics of a Compressible Fluid*, John Wiley & Sons, Inc., 1947.

[2] Nelson, W. J., and Bloetscher, F., *An Experimental Investigation of the Zero-Lift Pressure Distribution Over a Wedge Airfoil in Closed, Slotted, and Open-Throat Tunnels at Transonic Mach Numbers*, NACA RM L52C18, June 16, 1952.

[3] Tsien, H. S., and Fejer, A., *A Method for Predicting the Transonic Flow Over Airfoils and Similar Bodies from Data Obtained at Small Mach Numbers*, GALCIT, December, 1944.

[4] Maccoll, J. W., and Codd, J., *Theoretical Investigations of the Flow Around Various Bodies in the Sonic Region of Velocities*, Ministry of Supply, Armament Research Dept., September, 1954.

[5] Griffith, W., *Shock-Tube Studies of Transonic Flow Over Wedge Profiles*, Journal of the Aeronautical Sciences, Vol. 19, No. 4, pp. 249–257 (April, 1952).

Effect of Helicopter Blade Stall on Blade Flapping

K. H. Hohenemser
McDonnell Aircraft Corporation, St. Louis, Mo.
August 9, 1954

In reference 1 an equation is derived giving the flapping angle of a helicopter blade between azimuth π and 2π under the assumption that the blade is completely stalled and that its lift coefficient is constant in this azimuth angle range. Assuming further zero flapping velocity at azimuth π the flapping angle at 2π becomes a function of the flapping angle at π. For a typical numerical example the flapping angle at 2π (downwind) is downward when the up flapping angle at π (upwind) is more than 10°.

The same concept as to region of blade stall had already been used in reference 2 to derive a complete solution of the problem of blade flapping in conditions of extreme blade stall which is free of specific assumptions as to flapping angle and flapping velocity at the boundary of the stalled region. Reference 2 theory was checked against results of wind tunnel tests with a 10-ft. intermeshing rotor model, conducted in 1939, and was found satisfactory in the applicable region. These tests included nose-up conditions of extreme blade stall, leading to very large flapping angles. The droop stop of −3° did not prevent the blade tips from assuming downwind positions corresponding to down flapping angles of much more than −3°.

These tests, in agreement with reference 2 theory, have shown that large clearances between blades and fuselage or boom are necessary (in spite of limiting droop stops) in order to avoid blade-fuselage or blade-boom interference in conditions of high nose-up altitudes producing severe blade stall.

References

[1] Stepniewski, W. Z., *On Down Flapping of a Stalled Helicopter Blade*, Journal of the Aeronautical Sciences, Vol. 21, No. 6, p. 428, June, 1954.

[2] Sissingh, G., *Ein Verfahren zur direkten Bestimmung der Schlagbewegung von Flugzustaenden mit hohen Blattbelastungen*, Jahrbuch, 1941, der deutschen Luftfahrtforschung, I 364.

Index to Volume 21

Journal of the Aeronautical Sciences

Numbers 1–12, January–December, 1954

No. 1, January, 1954, pages 1–72
No. 2, February, 1954, pages 73–144
No. 3, March, 1954, pages 145–216
No. 4, April, 1954, pages 217–288
No. 5, May, 1954, pages 289–360
No. 6, June, 1954, pages 361–432
No. 7, July, 1954, pages 433–504
No. 8, August, 1954, pages 505–576
No. 9, September, 1954, pages 577–648
No. 10, October, 1954, pages 649–720
No. 11, November, 1954, pages 721–792
No. 12, December, 1954, pages 793–872

The material has been indexed under a general subject heading and by author and has been further cross-indexed under various subheadings.

*—An asterisk following an item identifies it as having appeared in the Readers' Forum section.

ABZUG, MALCOLM J. Effects of Certain Steady Motions on Small-Disturbance Airplane Dynamics 749

Aerodynamics—

Addendum—"Characteristic Solution for Axially Symmetric Transonic Flow," Erik Mollo-Christensen* 856
The Aerodynamic Forces on a Slender Low (or High) Wing, Circular Body, Vertical Tail Configuration, Arthur E. Bryson, Jr.* 574
Applications of Hypersonic Small-Disturbance Theory, Milton D. Van Dyke 179
Calculated Amplified Oscillations in the Plane Poiseuille and Blasius Flows, S. F. Shen* 62
Characteristic Solution for Axially Symmetric Transonic Flow, Erik Mollo-Christensen* 501
The Distributions of Concentration and Temperature in a Laminar Jet Diffusion Flame, James A. Fay 681
Errata—"Quadruple Velocity Correlations and Pressure Fluctuations in Isotropic Turbulence," M. S. Uberoi* 142
Further Remarks Concerning Integral Transforms of the Wave Equation, Max. A. Heaslet and Harvard Lomax* 142
The Interaction of Two Similarly Facing Shock Waves, G. V. Bull, L. R. Fowell, and D. H. Henshaw* 210
The Method of Superposition of Planar Wave Systems, Wallace D. Hayes* 282
Note on the Propagation of Infinitesimal Disturbances in Gases According to the Navier-Stokes Equations, M. Lessen* 849
The Numerical Solution of Certain Nonlinear Supersonic Flow Problems on the IBM Card Programmed Calculator, R. E. Bower and J. H. Higman* 205
On a Perturbation Theory Based on the Method of Characteristics, C. C. Lin* 202
On a Result of Nikolskii and Taganov Concerning Transonic Flow, Marvin Stern* 133
On the Stability of a Vortex Sheet in an Inviscid Compressible Fluid, Shih-I Pai 325
Pseudotransonic Similitude and First-Order Wave Structure, Wallace D. Hayes 721
Second-Order Methods in Inviscid Supersonic Theory, J. Fell and D. C. M. Leslie* 851
The Secondary Flow About Struts and Airfoils, W. R. Hawthorne 588
The Shock Strength in the Regular Reflection of Weak Shock Waves, William Chester* 347
Some Interference Effects Between Two Flat Surfaces Planing Parallel to Each Other at High Speed, Daniel Savitsky and David A. Dingee* 419
Three-Dimensional Study of a Jet Penetrating a Stream at Right Angles, J. P. Fraser* 59

Aerodynamics, Bodies—

Comments on Location of Detached Shocks and Truitt's Dilemma, E. V. Laitone* 64
Concluding Remarks on Detached Shock Waves, Robert Wesley Truitt* 496
Effect of Spin in Aerodynamic Properties of Bodies of Revolution, L. E. Schmidt and C. H. Murphy* 857
Effects of Afterbody Configuration on the Pressure Distribution over the Nose of Two-Dimensional Wedges, R. W. Truitt and F. W. Martin* 567
The Estimation of Normal-Force, Drag, and Pitching-Moment Coefficients for Blunt-Based Bodies of Revolution at Large Angles of Attack, Howard R. Kelly 549
Evaluation of the Inertia Coefficients of the Cross Section of a Slender Body, Arthur E. Bryson, Jr.* 424
The Flow on a Rotating Body of Revolution in Axial Flow, H. Schlichting and E. Truckenbrodt* 417
Gap Effect on Slender Wing-Body Interference, Duane W. Dugan* 57
A Guide to the Use of the M.I.T. Cone Tables, Richard C. Roberts and James D. Riley 336
An Integral Equation Occurring in the Theory of a Slender Quasi-Axisymmetrical Body, Paul F. Byrd* 351
Nose Shapes for Minimum Pressure Drag at Supersonic Mach Numbers, Leland H. Jorgensen* 276
On the Curved Shock Wave Due to an Infinite Wedge, Kinzo Hida* 214
On the Interaction of a Plane Shock Wave with a Wedge, Ken-iti Munakata* 501
On Motion of Submerged Cylinder, H. S. Tan* 848
On Slender-Body Theory and Apparent Mass, Alvin H. Sacks* 713
On "Supersonic Flow About Slender Bodies of Elliptic Cross Section," C. H. E. Warren* 57
On the Transonic Drag of Accelerated Bodies, John W. Miles* 644
Results of Some Base Pressure Experiments at Intermediate Reynolds Numbers with $M = 2.84$, L. L. Kavanau 257
Shock-Wave Yaw for $9\frac{1}{2}°$ Semiapex Cone, Eugene D. Boyer* 856

Aerodynamics, Bodies (*Continued*)

Slender Bodies of Minimum Wave Drag, W. T. Lord and E. Eminton* ... 569
Spin Effect on Base Pressure of Cone-Cylinders, R. Lehnert and S. M. Hastings* ... 286
Throat Station Concept in Transonic Flow over Two-Dimensional Wedges, Robert Wesley Truitt* ... 860
Wing-Body Interference at Subsonic and Supersonic Speeds—Survey and New Developments, H. R. Lawrence and A. H. Flax ... 289

Aerodynamics, Boundary Layer & Skin Friction—

Addendum—"Effect of Diffusion Fields on the Laminar Boundary Layer," John W. Smith ... 640
The Calculation of Wall Shearing Stress from Heat-Transfer Measurements in Compressible Flows, Nick S. Diaconis* ... 201
Comments on "The Effect of Boundary Layer on Sonic Flow Through an Abrupt Cross-Sectional Area Change," Helmut H. Korst* ... 568
The Compressible Laminar Boundary Layer, Deane N. Morris* ... 418
The Compressible Laminar Boundary Layer on a Rotating Body of Revolution, Sheng To Chu and A. N. Tifford* ... 345
Effect of Diffusion Fields on the Laminar Boundary Layer, John W. Smith ... 154
The Effect of Heat Transfer on the Behavior of a Compressible Laminar Boundary Layer Under Favorable and Adverse Pressure Gradients, Ting-Yi Li and H. T. Nagamatsu* ... 850
Effect of Large Temperature Changes (Including Viscous Heating) upon Laminar Boundary Layers with Variable Free-Stream Velocity, Solomon Levy ... 459
The Effect of Leading-Edge Bluntness on a Laminar Supersonic Boundary Layer, W. S. Bradfield, D. G. DeCoursin, and C. B. Blumer ... 373
The Effect of Mass Transfer on the Compressible Turbulent Boundary-Layer Skin Friction and Heat Transfer, William H. Dorrance and Frank J. Dore ... 404
An Empirical Method for Calculation of the Growth of a Turbulent Boundary Layer, Donald Ross and J. M. Robertson* ... 355
Further Remarks on "Interactions Between Wholly Laminar or Wholly Turbulent Boundary Layers and Shock Waves Strong Enough to Cause Separation," G. E. Gadd and D. W. Holder* ... 571
Laminar Boundary-Layer Temperature Recovery Factor on a Cone at Nominal Mach Number Six, Douglas S. Mackay and Henry T. Nagamatsu* ... 65
Measurements of Turbulent Friction on a Smooth Flat Plate in Supersonic Flow, Donald Coles ... 433
A Method for Analyzing the Heat Insulating Properties of the Laminar Compressible Boundary Layer, Paul A. Libby and Adrian Pallone ... 825
Note on Boundary-Layer Transition in Supersonic Flow, A. H. Lange and R. E. Lee* ... 58
Note on "Calculation Method for Three-Dimensional Rotationally Symmetrical Laminar Boundary Layers with Arbitrary Free-Stream Velocity . . .," J. C. Cooke* 141
Note on an Interaction Between the Boundary Layer and the Inviscid Flow, Antonio Ferri and Paul A. Libby* ... 130
A Note on the Laminar Boundary Layer on a Circular Cylinder in Axial Incompressible Flow, Howard R. Kelly* ... 634
On the Approximate Solution of the Laminar Boundary-Layer Equations, Itiro Tani ... 487
On the Calculation of Laminar Boundary-Layer Stability, Martin Bloom* ... 207
On a Differential Equation Occurring in the Theory of Heat Flow in Boundary Layers with Hartree's Velocity Profiles, Henry E. Fettis* ... 132
On Heat Transfer in a Compressible Laminar Boundary Layer, Alfred H. Silver* ... 352
Probe Interference in Measurements in Supersonic Laminar Boundary Layers, M. V. Morkovin and W. S. Bradfield* ... 785
Propagation of Turbulence from an Instantaneous Point Disturbance, Morton Mitchner* ... 350
Remarks on "Interactions Between Wholly Laminar or Wholly Turbulent Boundary Layers and Shock Waves Strong Enough to Cause Separation," Seymour M. Bogdonoff* ... 138
Similar Solutions of Compressible Laminar Boundary-Layer Equations, Clarence B. Cohen* ... 281
Simplified Analysis of Turbulent Boundary-Layer Development Along Cylindrical Surfaces with Variable Free-Stream Mach Number, Hans U. Eckert ... 695
Skin Friction in Slip Flow, S. A. Schaaf and F. S. Sherman 85
A Theory of Shock-Wave Boundary-Layer Interaction, Theodore R. Goodman* ... 715
Three-Dimensional Laminar Boundary Layer with Small Cross-Flow, Artur Mager ... 835
Transition-Point Fluctuations in Supersonic Flow, John C. Evvard, Maurice Tucker, and Warren C. Burgess, Jr. 731
Transport of the Bounary Layer in Secondary Flow, F. F. Ehrich and R. W. Detra* ... 136
Turbulent Boundary Layers in Adverse Pressure Gradients, Francis H. Clauser ... 91

Aerodynamics, Heat Transfer—

Approximate Solutions for Heat Transfer with Convection Flows, M. Herbeck* ... 142
The Effect of Mass Transfer on the Compressible Turbulent Boundary-Layer Skin Friction and Heat Transfer, William H. Dorrance and Frank J. Dore ... 404
Errata to "The Calculation of Wall Shearing Stress from Heat-Transfer Measurements in Compressible Flows," Nick S. Diaconis* ... 499
Forced Convection from Surfaces at Nonuniform Temperatures, Morton Finston* ... 779
Survey of Friction Coefficients, Recovery Factors, and Heat-Transfer Coefficients for Supersonic Flow, Joseph Kaye ... 117
Temperature Distribution in Laminar Stagnation-Point Flow with Axisymmetry, Chia-Shun Yih ... 37
Tip or Leading-Edge Temperatures on Pointed Heat Conducting Bodies at High Supersonic Speeds, M. Richard Denison* ... 858

Aerodynamics, Internal Flow—

Design and Performance of an Adjustable Two-Dimensional Nozzle with Boundary-Layer Correction, G. H. Backer ... 50
Experimental Velocity Profiles for Adiabatic Supersonic Flow of Air in a Tube, Joseph Kaye, George A. Brown, and John J. Dieckmann* ... 203
Flow Between Nozzles in Series with an Isentropic Work Change, Charles A. MacGregor* ... 423
A Mach 3.106 Two-Dimensional Adjustable Nozzle for Low-Density Flow, Lawrence Talbot* ... 708
Stability of a Semiflexible Duct System, A. L. Guess* ... 570
A Theoretical and Experimental Study of Finite Amplitude Wave Interactions with Channels of Varying Area, A. Kahane, W. R. Warren, W. C. Griffith, and A. A. Marino ... 505

Aerodynamics, Turbines & Compressors—

Calculation of Compressible Cascade Flow by the Method of Flux Analysis, Shigeo Uchida ... 237
Problems and Results of Investigations on Cascade Flow, Hermann Schlichting ... 163
Secondary Flow Losses in Turbine Cascades, N. Scholz* ... 707
Single Degree of Freedom Flutter of Compressor Blades in Separated Flow, Jan R. Schnittger ... 27
Stall Propagation in Cascades of Airfoils, Alan H. Stenning* ... 711

Aerodynamics, Wings & Airfoils—

Applicability of Piston Theory to the Flow Around Wings in Unsteady Motion, Erik Mollo-Christensen and Holt Ashley* ... 779
Effect of Leading-Edge Separation on the Lift of a Delta Wing, C. E. Brown and W. H. Michael, Jr. ... 690
An Empirical Method for Correction of a Wing Downwash Field for the Rolling Up of the Trailing Vortex Sheet in Incompressible Flow, S. J. Deitchman* ... 67
Errata on Alternative Forms for the Basic Equations of Transonic Flow Theory, John R. Spreiter* ... 360
An Experimental Determination of Flat Plate Recovery Factors for Mach Numbers Between 1.90 and 3.14, R. H. Shoulberg, J. A. F. Hill, and M. A. Rivas, Jr. ... 763
The Flow over a Flat Plate with a Small Angle of Attack at Mach Number 1, Gottfried Guderley ... 261
An Investigation of the Aerodynamics of Sharp Leading-Edge Swept Wings at Low Speeds, C. E. Pappas and A. E. Kunen ... 649
Leading-Edge Separation from Delta Wings, R. H. Edwards* ... 134
Lift Distribution on Supersonic Wings with Subsonic Leading Edges and Arbitrary Angle of Attack Distribution, Bernard Etkin and Frank A. Woodward* ... 783
Load Distributions of Some Twisted and Cambered Delta Wings with Supersonic Leading and Trailing Edges, H. K. Zienkiewicz* ... 421
On Alternative Forms for the Basic Equations of Transonic Flow Theory, John R. Spreiter* ... 70
On Jones's Criterion for Thin Wings of Minimum Drag, R. Sedney* ... 639
On Solving Subsonic Unsteady Flow Lifting Surface Problems by Separating Variables, J. W. Miles* ... 427
Prediction of the Characteristics of Two-Dimensional Airfoils, D. A. Spence ... 577
Pressure Distribution at Mach Number One over a Flat Plate at Angle of Attack, Robert Wesley Truitt* ... 713
Remarks on Nonlinear Lift and Vortex Separation, Hsien K. Cheng* ... 212
A Reply—Load Distributions on Delta Wings at Supersonic Speeds, Julian H. Kainer* ... 792
The Second-Order Compressibility Rule for Airfoils, Milton D. Van Dyke* ... 647
A Semiempirical Method for Determining Delta-Wing Pressure Distributions in an Incompressible Flow, William R. Laidlaw and P. T. Hsu* ... 854
Some Aerodynamic Effects of Streamwise Gaps in Low Aspect Ratio Lifting Surfaces at Supersonic Speeds, Z. O. Bleviss and R. A. Struble ... 665
A Supplementary Note on the Spanwise Loadings over Slender Airfoils, Hsien K. Cheng* ... 853
Theorems Concerning the Drag Reduction of Wings of Fixed Plan Form, A. M. Rodriguez, P. A. Lagerstrom, and E. W. Graham ... 1
Theoretical and Experimental Investigations on Swept and Delta Wings in Incompressible Flow, E. Truckenbrodt* ... 637
Transonic Flow Past Wedge Profiles by Hydraulic Analogy, E. V. Laitone and Helmer Nielsen* ... 498
Viscous and Leading-Edge Thickness Effects on the Pressures on the Surface of a Flat Plate in Hypersonic Flow, Mitchel H. Bertram* ... 430

Aeroelasticity—

Aerodynamic Coefficients of an Oscillating Airfoil in Two-Dimensional Subsonic Flow, R. Timman, A. I. van de Vooren, and J. H. Greidanus* ... 499
Aerodynamic Flutter Coefficients for an Airfoil with Leading- and Trailing-Edge Flaps in Two-Dimensional Supersonic Flow, Hermann J. Hassig* ... 131
Analysis of Flutter in Compressible Flow of a Panel on Many Supports, John M. Hedgepeth, Bernard Budiansky, and Robert W. Leonard ... 475
Application of Volterra Linear Integral Equations to the Numerical Solution of Vibration Problems—II, J. L. Bogdanoff, J. E. Goldberg, and Hsu Lo ... 383
An Approximate Method for Determining the Effects of Wing Twist on Airplane Gust Loads, Frederic M. Hoblit* ... 641
Corrections and Additions to "A Modification of the Holzer Method for Computing Uncoupled Torsion and Bending Modes," Henry E. Fettis* ... 359
Design of Tubes for Maximum Torsional Frequency, P. Cicala* ... 646
Development of Charts for Downwash Coefficients of Oscillating Wings of Finite Span and Arbitrary Plan Form, Max A. Dengler ... 809
The Effect of Tip Removal on the Natural Vibrations of Uniform Cantilevered Triangular Plates, P. N. Gustafson, W. F. Stokey, and C. F. Zorowski ... 621
Errata to "The Aerodynamic Forces on Low Aspect Ratio Wings Oscillating in an Incompressible Flow," H. R. Lawrence and E. H. Gerber* ... 141
An Exact Solution for Two-Dimensional Linear Panel Flutter at Supersonic Speeds, Martin Goland and Yudell L. Luke* ... 275
Extreme Values in Aeronautics, Emil J. Gumbel and Philip G. Carlson ... 389
A General Method for Solving Problems of the Unsteady Lifting Surface Theory in the Subsonic Range, H. G. Kuessner ... 17
Generalized Aerodynamic Forces on the Delta Wing with Supersonic Leading Edges, J. Walsh, G. Zartarian, and H. M. Voss ... 739
The Kernel Function of the Integral Equation Relating the Lift and Downwash Distributions of Oscillating Finite Wings in Subsonic Flow, G. N. Lance* ... 635
Linearized Theory of the Oscillating Airfoil in Compressible Subsonic Flow, R. Timman ... 230
A Note Concerning the Effect of Wing Twist on the Response of a Wing to a Sharp-Edged Gust, Franklin W. Diederich* ... 636
On the Excitation of Pure Natural Modes, Ernst Schultze* 566
On the Nonlinear Thickness Effect for a Supersonic Oscillating Airfoil, John W. Miles* ... 714
On Panel Flutter in Supersonic Flow, W. C. Randels* ... 860
On Structural Fatigue Under Random Loading, John W. Miles ... 753
On Use of the Reverse Flow Theorem in the Problem of Aeroelastic Deflections, H. M. Voss* ... 569
Stability and Free Vibration of Nonuniform Beams Continuous Across Flexible Supports, H. L. Cox and P. H. Denke* ... 572
The Static Stability of a Two-Dimensional Curved Panel in a Supersonic Flow, with an Application to Panel Flutter, Y. C. Fung ... 556
The Story of Shimmy, William J. Moreland ... 793

Aeroelasticity (*Continued*)
A Theoretical Investigation of the Oscillating Control Surface Frequency Response Technique of Flight Flutter Testing, R. A. Pepping ... 533

Aluminum-alloy formed structural shapes in compression, the ultimate strength of ... 217
ANDREW, G. M. Controlled Motion with Time Lag in Autopilot* ... 346
ASHLEY, HOLT, AND ERIK MOLLO-CHRISTENSEN. Applicability of Piston Theory to the Flow Around Wings in Unsteady Motion* ... 779

BACKER, G. H. Design and Performance of an Adjustable Two-Dimensional Nozzle with Boundary-Layer Correction ... 50
Base pressure experiments at intermediate Reynolds Numbers with $M = 2.84$, results of some ... 257
BEHARRELL, JACK L., AND HANS R. FRIEDRICH. The Transfer Function of a Rocket-Type Guided Missile with Consideration of Its Structural Elasticity ... 454
BERTRAM, MITCHEL H. Viscous and Leading-Edge Thickness Effects on the Pressures on the Surface of a Flat Plate in Hypersonic Flow* ... 430
BIJLAARD, P. P. Buckling Stress of Thin Cylindrical Clamped Shells Subject to Hydrostatic Pressure* ... 852
Blades, compressor, in separated flow, single degree of freedom flutter of ... 27
BLEVISS, Z. O., AND R. A. STRUBLE. Some Aerodynamic Effects of Streamwise Gaps in Low Aspect Ratio Lifting Surfaces at Supersonic Speeds ... 665
BLOOM, MARTIN. On the Calculation of Laminar Boundary-Layer Stability* ... 207
BLUMER, C. B., W. S. BRADFIELD, AND D. G. DECOURSIN. The Effect of Leading-Edge Bluntness on a Laminar Supersonic Boundary Layer ... 373
Blunt-based bodies of revolution at large angles of attack, the estimation of normal-force, drag, and pitching-moment coefficients for ... 549
BOGDANOFF, J. L., J. E. GOLDBERG, AND HSU LO. Application of Volterra Linear Integral Equations to the Numerical Solution of Vibration Problems—II ... 383
BOGDONOFF, SEYMOUR M. Remarks on "Interactions Between Wholly Laminar or Wholly Turbulent Boundary Layers and Shock Waves Strong Enough to Cause Separation"* ... 138
BOWER, R. E., AND J. H. HIGMAN. The Numerical Solution of Certain Nonlinear Supersonic Flow Problems on the IBM Card Programmed Calculator* ... 205
BOYER, EUGENE D. Shock-Wave Yaw for $9\frac{1}{2}°$ Semiapex Cone* ... 856
BRADFIELD, W. S., D. G. DECOURSIN, AND C. B. BLUMER. The Effect of Leading-Edge Bluntness on a Laminar Supersonic Boundary Layer ... 373
BRADFIELD, W. S., AND M. V. MORKOVIN. Probe Interference in Measurements in Supersonic Laminar Boundary Layers* ... 785
BREUER, D. W., AND B. E. GATEWOOD. Allowable Stresses for Channels and Zees in Bending* ... 349
BROWN, C. E., AND W. H. MICHAEL, JR. Effect of Leading-Edge Separation on the Lift of a Delta Wing ... 690
BROWN, GEORGE A., JOSEPH KAYE, AND JOHN J. DIECKMANN. Experimental Velocity Profiles for Adiabatic Supersonic Flow of Air in a Tube* ... 203
BRYSON, ARTHUR E., JR. The Aerodynamic Forces on a Slender Low (or High) Wing, Circular Body, Vertical Tail Configuration* ... 574
BRYSON, ARTHUR E., JR. Comment on the Stability Derivatives of a Wing-Body-Vertical Tail Configuration* ... 59
BRYSON, ARTHUR E., JR. Evaluation of the Inertia Coefficients of the Cross Section of a Slender Body* ... 424
BUDIANSKY, BERNARD, JOHN M. HEDGEPETH, AND ROBERT W. LEONARD. Analysis of Flutter in Compressible Flow of a Panel on Many Supports ... 475
BULL, G. V., L. R. FOWELL, AND D. H. HENSHAW. The Interaction of Two Similarly Facing Shock Waves* ... 210
BURGESS, WARREN C., JR., MAURICE TUCKER, AND JOHN C. EVVARD. Transition-Point Fluctuations in Supersonic Flow ... 731
BYRD, PAUL F. An Integral Equation Occurring in the Theory of a Slender Quasi-Axisymmetrical Body* ... 351

CAMPBELL, GEORGE S. A Note on Rolling Pull-Out Calculations* ... 789
CARLSON, PHILIP G., AND EMIL J. GUMBEL. Extreme Values in Aeronautics ... 389
Cascade flow, compressible, by the method of flux analysis, calculation of ... 237
Cascade flow, problems and results of investigations on ... 163
CHENG, HSIEN K. Remarks on Nonlinear Lift and Vortex Separation* ... 212
CHENG, HSIEN K. A Supplementary Note on the Spanwise Loadings over Slender Airfoils* ... 853
CHESTER, WILLIAM. The Shock Strength in the Regular Reflection of Weak Shock Waves* ... 347
CHU, SHENG TO, AND A. N. TIFFORD. The Compressible Laminar Boundary Layer on a Rotating Body of Revolution* ... 345
CICALA, P. Design of Tubes for Maximum Torsional Frequency* ... 646
CLAUSER, FRANCIS H. Turbulent Boundary Layers in Adverse Pressure Gradients ... 91
COHEN, CLARENCE B. Similar Solutions of Compressible Laminar Boundary-Layer Equations* ... 281
COLES, DONALD. Measurements of Turbulent Friction on a Smooth Flat Plate in Supersonic Flow ... 433
Columns, limit design of ... 43
Columns with hat sections, charts for the calculation of the critical compressive stress for local instability of ... 399
Cone tables, M.I.T., a guide to the use of the ... 336
COOKE, J. C. Note on "Calculation Method for Three-Dimensional Rotationally Symmetrical Laminar Boundary Layers with Arbitrary Free-Stream Velocity . . ."* ... 141
COX, HUGH L., AND P. H. DENKE. Stability and Free Vibration of Nonuniform Beams Continuous Across Flexible Supports* ... 572
COX, HUGH L., AND BERTRAM KLEIN. Approximate Structural Analysis by the Method of Collocation* ... 719

DECOURSIN, D. G., W. S. BRADFIELD, AND C. B. BLUMER The Effect of Leading-Edge Bluntness of a Laminar Supersonic Boundary Layer ... 373
DEITCHMAN, S. J. An Empirical Method for Correction of a Wing Downwash Field for the Rolling Up of the Trailing Vortex Sheet in Incompressible Flow* ... 67
DENGLER, MAX A. Development of Charts for Downwash Coefficients of Oscillating Wings of Finite Span and Arbitrary Plan Form ... 809
DENISON, M. RICHARD. Tip or Leading-Edge Temperatures on Pointed Heat Conducting Bodies at High Supersonic Speeds* ... 858
DENKE, P. H., AND H. L. COX. Stability and Free Vibration of Nonuniform Beams Continuous Across Flexible Supports* ... 572

De Santo, Daniel F., and Chi-Teh Wang. Errata "Differentiation of Experimental Data by Means of Higher Order Finite-Difference Formulas"* 789

Design—

Errata—"A Method of Estimating Wing Weights," Abraham Hyatt* 720

The First Half-Century of Flight in America (The Seventeenth Wright Brothers Lecture), Glenn L. Martin 73

A Method for Estimating Wing Weights, Abraham Hyatt 363

Detra, R. W., and F. F. Ehrich. Transport of the Boundary Layer in Secondary Flow* 136

Diaconis, Nick S. The Calculation of Wall Shearing Stress from Heat-Transfer Measurements in Compressible Flows* 201

Diaconis, Nick S. Errata to "The Calculation of Wall Shearing Stress from Heat-Transfer Measurements in Compressible Flows* 499

Dieckmann, John J., Joseph Kaye, and George A. Brown. Experimental Velocity Profiles for Adiabatic Supersonic Flow of Air in a Tube* 203

Diederich, Franklin W. A Note Concerning the Effect of Wing Twist on the Response of a Wing to a Sharp-Edged Gust* 636

Dingee, David A., and Daniel Savitsky. Some Interference Effects Between Two Flat Surfaces Planing Parallel to Each Other at High Speed* 419

Dore, Frank J., and William H. Dorrance. The Effect of Mass Transfer on the Compressible Turbulent Boundary-Layer Skin Friction and Heat Transfer 404

Dorrance, William H., and Frank J. Dore. The Effect of Mass Transfer on the Compressible Turbulent Boundary-Layer Skin Friction and Heat Transfer 404

Drucker, D. C., and E. T. Onat. On the Concept of Stability of Inelastic Systems 543

Dugan, Duane W. Gap Effect on Slender Wing-Body Interference* 57

Eckert, Hans U. Simplified Analysis of Turbulent Boundary-Layer Development Along Cylindrical Surfaces with Variable Free-Stream Mach Number 695

Edwards, R. H. Leading-Edge Separation from Delta Wings* 134

Ehrich, F. F., and R. W. Detra. Transport of the Boundary Layer in Secondary Flow* 136

Eminton, E., and W. T. Lord. Slender Bodies of Minimum Wave Drag* 569

Ensrud, A. F., and M. A. Melcon. Erratum—"Analysis of Stiffened Curved Panels Under Shear and Compression"* 427

Etkin, Bernard, and Frank A. Woodward. Lift Distribution on Supersonic Wings with Subsonic Leading Edges and Arbitrary Angle of Attack Distribution* 783

Evvard, John C., Maurice Tucker, and Warren C. Burgess, Jr. Transition-Point Fluctuations in Supersonic Flow 731

Extreme values in aeronautics 389

Fatigue, structural, under random loading 753

Fay, James A. The Distributions of Concentration and Temperature in a Laminar Jet Diffusion Flame 681

Fell, J., and D. C. M. Leslie. Second-Order Methods in Inviscid Supersonic Theory* 851

Ferri, Antonio, and Paul A. Libby. Note on an Interaction Between the Boundary Layer and the Inviscid Flow* 130

Fettis, Henry E. Corrections and Additions to "A Modification of the Holzer Method for Computing Uncoupled Torsion and Bending Modes"* 359

Fettis, Henry E. On a Differential Equation Occurring in the Theory of Heat Flow in Boundary Layers with Hartree's Velocity Profiles* 132

Finston, Morton. Forced Convection from Surfaces at Nonuniform Temperatures* 779

First half-century of flight in America (The Seventeenth Wright Brothers Lecture) 73

Flax, A. H., and H. R. Lawrence. Wing-Body Interference at Subsonic and Supersonic Speeds—Survey and New Developments 289

Flight flutter testing, a theoretical investigation of the oscillating control surface frequency response technique of 533

Flight Propulsion—

Aerodynamic Determination of Flame Speed, Robert A. Gross* 139

Some Properties of Intense Sound Waves in Relation to Combustion, J. C. Truman 69

Flow over a flat plate with a small angle of attack at Mach Number 1 261

Flow, supersonic, transition-point fluctuations in 731

Flutter in compressible flow of a panel on many supports, analysis of 475

Fowell, L. R., G. V. Bull, and D. H. Henshaw. The Interaction of Two Similarly Facing Shock Waves* 210

Frames, indeterminate, optimum design of 615

Frankland, J. M., and R. E. Roach. Strength Under Combined Tension and Bending in the Plastic Range 449

Fraser, J. P. Three-Dimensional Study of a Jet Penetrating a Stream at Right Angles* 59

Freudenthal, Alfred M. On Inelastic Thermal Stresses in Flight Structures 772

Friedrich, Hans R., and Jack L. Beharrell. The Transfer Function of a Rocket-Type Guided Missile with Consideration of Its Structural Elasticity 454

Frost, Richard C. Supersonic Flap Lift Effectiveness for Some General Plan Forms 609

Fung, Y. C. The Static Stability of a Two-Dimensional Curved Panel in a Supersonic Flow, with an Application to Panel Flutter 556

Gadd, G. E., and D. W. Holder. Further Remarks on "Interactions Between Wholly Laminar or Wholly Turbulent Boundary Layers and Shock Waves Strong Enough to Cause Separation"* 571

Gatewood, B. E. Buckling Loads for Columns of Variable Cross Section* 287

Gatewood, B. E. Thermal Loads on Joints* 645

Gatewood, B. E., and D. W. Breuer. Allowable Stresses for Channels and Zees in Bending* 349

Gerard, George. Life Expectancy of Aircraft Under Thermal Flight Conditions 675

Gerard, George, and Ralph Papirno. Note on Photoelastic Study of a Swept-Wing Model* 846

Gerber, E. H., and H. R. Lawrence. Errata to "The Aerodynamic Forces on Low Aspect Ratio Wings Oscillating in an Incompressible Flow"* 141

Goland, Martin, and Yudell L. Luke. An Exact Solution for Two-Dimensional Linear Panel Flutter at Supersonic Speeds* 275

GOLDBERG, J. E., J. L. BOGDANOFF, AND HSU LO. Application of Volterra Linear Integral Equations to the Numerical Solution of Vibration Problems—II ... 383
GOODIER, J. N., AND C. S. HSU. Nonsinusoidal Buckling Modes of Sandwich Plates ... 525
GOODMAN, THEODORE R. A Theory of Shock-Wave Boundary-Layer Interaction* ... 715
GRAHAM, E. W., A. M. RODRIGUEZ, AND P. A. LAGERSTROM. Theorems Concerning the Drag Reduction of Wings of Fixed Plan Form ... 1
GREIDANUS, J. H., R. TIMMAN, AND A. I. VAN DE VOOREN. Aerodynamic Coefficients of an Oscillating Airfoil in Two-Dimensional Subsonic Flow* ... 499
GRIFFITH, W. C., W. R. WARREN, A. KAHANE, AND A. A. MARINO. A Theoretical and Experimental Study of Finite Amplitude Wave Interactions with Channels of Varying Area ... 505
GROSS, ROBERT A. Aerodynamic Determination of Flame Speed* ... 139
GUDERLEY, GOTTFRIED. The Flow over a Flat Plate with a Small Angle of Attack at Mach Number 1 ... 261
GUESS, A. L. Stability of a Semiflexible Duct System* ... 570
GUMBEL, EMIL J., AND PHILIP G. CARLSON. Extreme Values in Aeronautics ... 389
GUSTAFSON, P. N., W. F. STOKEY, AND C. F. ZOROWSKI. The Effect of Tip Removal on the Natural Vibrations of Uniform Cantilevered Triangular Plates ... 621

HASEGAWA, M. On Buckling of a Clamped Rhombic Thin Plate in Shear* ... 720
HASSIG, HERMANN J. Aerodynamic Flutter Coefficients for an Airfoil with Leading- and Trailing-Edge Flaps in Two-Dimensional Supersonic Flow* ... 131
HASTINGS, S. M., AND R. LEHNERT. Spin Effect on Base Pressure of Cone-Cylinders* ... 286
HAWTHORNE, W. R. The Secondary Flow About Struts and Airfoils ... 588
HAYES, WALLACE D. The Method of Superposition of Planar Wave Systems* ... 282
HAYES, WALLACE D. Pseudotransonic Similitude and First-Order Wave Structure ... 721
HEASLET, MAX. A., AND HARVARD LOMAX. Further Remarks Concerning Integral Transforms of the Wave Equation* ... 142
Heat insulating properties of the laminar compressible boundary layer, a method for analyzing the ... 825
HEDGEPETH, JOHN M., BERNARD BUDIANSKY, AND ROBERT W. LEONARD. Analysis of Flutter in Compressible Flow of a Panel on Many Supports ... 475
HENSHAW, D. H., G. V. BULL, AND L. R. FOWELL. The Interaction of Two Similarly Facing Shock Waves* ... 210
HERBECK, M. Approximate Solutions for Heat Transfer with Convection Flows* ... 142
HIDA, KINZO. On the Curved Shock Wave Due to an Infinite Wedge* ... 214
HIGMAN, J. H., AND R. E. BOWER. The Numerical Solution of Certain Nonlinear Supersonic Flow Problems on the IBM Card Programmed Calculator* ... 205
HILL, J. A. F., R. H. SHOULBERG, AND M. A. RIVAS, JR. An Experimental Determination of Flat Plate Recovery Factors for Mach Numbers Between 1.90 and 3.14 ... 763
HOBLIT, FREDERIC M. An Approximate Method for Determining the Effects of Wing Twist on Airplane Gust Loads* ... 641
HOHENEMSER, K. H. Effect of Helicopter Blade Stall on Blade Flapping* ... 861
HOLDER, D. W., AND G. E. GADD. Further Remarks on "Interactions Between Wholly Laminar or Wholly Turbulent Boundary Layers and Shock Waves Strong Enough to Cause Separation"* ... 571
HSU, C. S., AND J. N. GOODIER. Nonsinusoidal Buckling Modes of Sandwich Plates ... 525
HSU, P. T., AND WILLIAM R. LAIDLAW. A Semiempirical Method for Determining Delta-Wing Pressure Distributions in an Incompressible Flow* ... 854
HYATT, ABRAHAM. Errata—"A Method of Estimating Wing Weights"* ... 720
HYATT, ABRAHAM. A Method for Estimating Wing Weights ... 363
Hypersonic small-disturbance theory, applications of ... 179

Inelastic systems, on the concept of stability of ... 543
Inelastic thermal stresses in flight structures ... 772
Interference, wing-body, at subsonic and supersonic speeds—survey and new developments ... 289
IRVING, J., AND N. MULLINEUX. Rectangular Plates with Stringers and Ribs* ... 847

JOHNSON, JAMES H., JR. Critical Buckling Stresses of Simply Supported Flat Rectangular Plates Under Combined Longitudinal Compression, Transverse Compression, and Shear ... 411
JORDAN, PETER F. Differentiation of Experimental Data* ... 417
JORGENSEN, LELAND H. Nose Shapes for Minimum Pressure Drag at Supersonic Mach Numbers* ... 276

KAHANE, A., W. R. WARREN, W. C. GRIFFITH, AND A. A. MARINO. A Theoretical and Experimental Study of Finite Amplitude Wave Interactions with Channels of Varying Area ... 505
KAINER, JULIAN H. A Reply—Load Distributions on Delta Wings at Supersonic Speeds* ... 792
KAVANAU, L. L. Results of Some Base Pressure Experiments at Intermediate Reynolds Numbers with $M = 2.84$ ... 257
KAYE, JOSEPH. Survey of Friction Coefficients, Recovery Factors, and Heat-Transfer Coefficients for Supersonic Flow ... 117
KAYE, JOSEPH, GEORGE A. BROWN, AND JOHN J. DIECKMANN. Experimental Velocity Profiles for Adiabatic Supersonic Flow of Air in a Tube* ... 203
KELLY, HOWARD R. The Estimation of Normal-Force, Drag, and Pitching-Moment Coefficients for Blunt-Based Bodies of Revolution at Large Angles of Attack ... 549
KELLY, HOWARD R. A Note on the Laminar Boundary Layer on a Circular Cylinder in Axial Incompressible Flow* ... 634
KEMPNER, JOSEPH. Postbuckling Behavior of Axially Compressed Circular Cylindrical Shells ... 329
KLEIN, BERTRAM, AND HUGH L. COX. Approximate Structural Analysis by the Method of Collocation* ... 719
KORST, HELMUT H. Comments on "The Effect of Boundary Layer on Sonic Flow Through an Abrupt Cross-Sectional Area Change"* ... 568
KOSKO, E. Effect of Local Modifications in Redundant Structures* ... 206
KRZYWOBLOCKI, M. Z. v. Remarks on "Subsonic Compressibility Corrections for Propellers and Helicopter Rotors"* ... 214
KUESSNER, H. G. A General Method for Solving Problems of the Unsteady Lifting Surface Theory in the Subsonic Range ... 17
KUNEN, A. E., AND C. E. PAPPAS. An Investigation of the Aerodynamics of Sharp Leading-Edge Swept Wings at Low Speeds ... 649

LAGERSTROM, P. A., A. M. RODRIGUEZ, AND E. W. GRAHAM. Theorems Concerning the Drag Reduction of Wings of Fixed Plan Form ... 1
LAIDLAW, WILLIAM R., AND P. T. HSU. A Semiempirical Method for Determining Delta-Wing Pressure Distributions in an Incompressible Flow* ... 854
LAITONE, E. V. Comments on Location of Detached Shocks and Truitt's Dilemma* ... 64
LAITONE, E. V., AND HELMER NIELSEN. Transonic Flow Past Wedge Profiles by Hydraulic Analogy* ... 498
LAITONE, E. V., AND LAWRENCE TALBOT. Remarks on Compressible Flow Actuator Disc Theory ... 638
Laminar jet diffusion flame, the distributions of concentration and temperature in a ... 681
Laminar stagnation-point flow with axisymmetry, temperature distribution in ... 37
LANCE, G. N. The Kernel Function of the Integral Equation Relating the Lift and Downwash Distributions of Oscillating Finite Wings in Subsonic Flow* ... 635
LANGE, A. H., AND R. E. LEE. Note on Boundary-Layer Transition in Supersonic Flow* ... 58
Lateral stability, dynamic, of aircraft, a vector method approach to the analysis of the ... 251
LAUFER, JOHN. Factors Affecting Transition Reynolds Numbers on Models in Supersonic Wind Tunnels* ... 497
LAWRENCE, H. R., AND A. H. FLAX. Wing-Body Interference at Subsonic and Supersonic Speeds—Survey and New Developments ... 289
LAWRENCE, H. R., AND E. H. GERBER. Errata to "The Aerodynamic Forces on Low Aspect Ratio Wings Oscillating in an Incompressible Flow"* ... 141
Leading-edge bluntness on a laminar supersonic boundary layer, effect of ... 373
LEE, R. E., AND A. H. LANGE. Note on Boundary-Layer Transition in Supersonic Flow* ... 58
LEHNERT, R., AND S. M. HASTINGS. Spin Effect on Base Pressure of Cone-Cylinders* ... 286
LEONARD, ROBERT W., JOHN M. HEDGEPETH, AND BERNARD BUDIANSKY. Analysis of Flutter in Compressible Flow of a Panel on Many Supports ... 475
LESLIE, D. C. M., AND J. FELL. Second-Order Methods in Inviscid Supersonic Theory* ... 851
LESSEN, M. Note on the Propagation of Infinitesimal Disturbances in Gases According to the Navier-Stokes Equations* ... 849
LEVY, SAMUEL. Determination of Loads in the Presence of Thermal Stresses ... 659
LEVY, SOLOMON. Effect of Large Temperature Changes (Including Viscous Heating) upon Laminar Boundary Layers with Variable Free-Stream Velocity ... 459
LI, TING-YI, AND H. T. NAGAMATSU. The Effect of Heat Transfer on the Behavior of a Compressible Laminar Boundary Layer Under Favorable and Adverse Pressure Gradients* ... 850
LIBBY, PAUL A., AND ANTONIO FERRI. Note on an Interaction Between the Boundary Layer and the Inviscid Flow* ... 130
LIBBY, PAUL A., AND ADRIAN PALLONE. A Method for Analyzing the Heat Insulating Properties of the Laminar Compressible Boundary Layer ... 825
Life expectancy of aircraft under thermal flight conditions ... 675
Lift of a delta wing, effect of leading-edge separation on the ... 690
Lifting surfaces, low aspect ratio, at supersonic speeds, some aerodynamic effects of streamwise gaps in ... 665
LIN, C. C. On a Perturbation Theory Based on the Method of Characteristics* ... 202
LIVESEY, J. L. Design of Total Pressure Probes for Minimum Interference with Measured Flow* ... 641
LO, HSU, J. L. BOGDANOFF, AND J. E. GOLDBERG. Application of Volterra Linear Integral Equations to the Numerical Solution of Vibration Problems—II ... 383
Loads in the presence of thermal stresses, determination of ... 659
LOMAX, HARVARD, AND MAX. A. HEASLET. Further Remarks Concerning Integral Transforms of the Wave Equation* ... 142
LORD, W. T., AND E. EMINTON. Slender Bodies of Minimum Wave Drag* ... 569
LUKE, YUDELL L., AND MARTIN GOLAND. An Exact Solution for Two-Dimensional Linear Panel Flutter at Supersonic Speeds* ... 275

MACGREGOR, CHARLES A. Flow Between Nozzles in Series with an Isentropic Work Change* ... 423
MACKAY, DOUGLAS S., AND HENRY T. NAGAMATSU. Laminar Boundary-Layer Temperature Recovery Factor on a Cone at Nominal Mach Number Six* ... 65
MAGER, ARTUR. Three-Dimensional Laminar Boundary Layer with Small Cross-Flow ... 835
MARINO, A. A., W. C. GRIFFITH, W. R. WARREN, AND A. KAHANE. A Theoretical and Experimental Study of Finite Amplitude Wave Interactions with Channels of Varying Area ... 505
MARTIN, F. W., AND R. W. TRUITT. Effects of Afterbody Configuration on the Pressure Distribution over the Nose of Two-Dimensional Wedges* ... 567
MARTIN, GLENN L. The First Half-Century of Flight in America (The Seventeenth Wright Brothers Lecture) ... 73

Mathematics—
Differentiation of Experimental Data, Peter F. Jordan* ... 417
Errata—"Differentiation of Experimental Data by Means of Higher Order Finite-Difference Formulas," Chi-Teh Wang and Daniel F. De Santo* ... 789
Methods for Determining the First and Second Derivatives of Experimental Data, Ernest E. H. Schurmann and Theron L. Smith* ... 420

MAZELSKY, BERNARD. Extension of Power Spectral Methods of Generalized Harmonic Analysis to Determine Non-Gaussian Probability Functions of Random Input Disturbances and Output Responses of Linear Systems ... 145
MCCOMB, HARVEY G., JR. Errata—"Stress Analysis of Sheet-Stringer Panels with Cutouts"* ... 58
MELCON, M. A., AND A. F. ENSRUD. Erratum—"Analysis of Stiffened Curved Panels Under Shear and Compression"* ... 427
MICHAEL, W. H., JR., AND C. E. BROWN. Effect of Leading-Edge Separation on the Lift of a Delta Wing ... 690
MIELE, ANGELO. On the Nonsteady Climb of Turbojet Aircraft* ... 781
MILES, JOHN W. On the Nonlinear Thickness Effect for a Supersonic Oscillating Airfoil* ... 714
MILES, JOHN W. On Solving Subsonic Unsteady Flow Lifting Surface Problems by Separating Variables* ... 427
MILES, JOHN W. On Structural Fatigue Under Random Loading ... 753
MILES, JOHN W. On the Transonic Drag of Accelerated Bodies* ... 644
MITCHNER, MORTON. Propagation of Turbulence from an Instantaneous Point Disturbance* ... 350
MOLLO-CHRISTENSEN, ERIK. Addendum—"Characteristic Solution for Axially Symmetric Transonic Flow"* ... 856
MOLLO-CHRISTENSEN, ERIK. Characteristic Solution for Axially Symmetric Transonic Flow* ... 501
MOLLO-CHRISTENSEN, ERIK, AND HOLT ASHLEY. Applicability of Piston Theory to the Flow Around Wings in Unsteady Motion* ... 779

MORELAND, WILLIAM J. The Story of Shimmy 793

MORKOVIN, M. V., AND W. S. BRADFIELD. Probe Interference in Measurements in Supersonic Laminar Boundary Layers* 785

MORRIS, DEANE N. The Compressible Laminar Boundary Layer* 418

MULLINEUX, N., AND J. IRVING. Rectangular Plates with Stringers and Ribs* 847

MUNAKATA, KEN-ITI. On the Interaction of a Plane Shock Wave with a Wedge* 501

MURPHY, C. H. Effect of Roll on Dynamic Instability of Symmetric Missiles* 643

MURPHY, C. H., AND L. E. SCHMIDT. Effect of Spin in Aerodynamic Properties of Bodies of Revolution* 857

NAGAMATSU, HENRY T., AND TING-YI LI. The Effect of Heat Transfer on the Behavior of a Compressible Laminar Boundary Layer Under Favorable and Adverse Pressure Gradients* 850

NAGAMATSU, HENRY T., AND DOUGLAS S. MACKAY. Laminar Boundary-Layer Temperature Recovery Factor on a Cone at Nominal Mach Number Six* 65

NASH, WILLIAM A. Buckling of Thin Cylindrical Shells Subject to Hydrostatic Pressure* 354

NEEDHAM, ROBERT A. The Ultimate Strength of Aluminum-Alloy Formed Structural Shapes in Compression 217

NIELSEN, HELMER, AND E. V. LAITONE. Transonic Flow Past Wedge Profiles by Hydraulic Analogy* 498

Nozzle, adjustable two-dimensional, with boundary-layer correction, design and performance of 50

OLIVER, HENRY, AND FREDERICK V. POHLE. Temperature Distribution and Thermal Stresses in a Model of a Supersonic Wing 8

ONAT, E. T., AND D. C. DRUCKER. On the Concept of Stability of Inelastic Systems 543

OPPENHEIM, A. K., AND L. TALBOT. On the Propeller Discontinuity* 61

PAI, SHIH-I. On the Stability of a Vortex Sheet in an Inviscid Compressible Fluid 325

PALLONE, ADRIAN, AND PAUL A. LIBBY. A Method for Analyzing the Heat Insulating Properties of the Laminar Compressible Boundary Layer 825

Panel flutter, the static stability of a two-dimensional curved panel in a supersonic flow, with an application to 556

PAPIRNO, RALPH, AND GEORGE GERARD. Note on Photoelastic Study of a Swept-Wing Model* 846

PAPPAS, C. E., AND A. E. KUNEN. An Investigation of the Aerodynamics of Sharp Leading-Edge Swept Wings at Low Speeds 649

PARIS, PAUL C. Limit Design of Columns 43

PEPPING, R. A. A Theoretical Investigation of the Oscillating Control Surface Frequency Response Technique of Flight Flutter Testing 533

Performance

Airplane Stopping Distance, B. Saelman* 790

Energy Approach to the General Aircraft Performance Problem, Edward S. Rutowski 187

On the Nonsteady Climb of Turbojet Aircraft, Angelo Miele* 781

Plastic disc, rotating, the bursting speed of a 196

Plastic solids, work-hardening elastic-, thermal and creep effects in 343

Plate, flat, recovery factors for Mach Numbers between 1.90 and 3.14, an experimental determination of 763

Plate, smooth flat, in supersonic flow, measurements of turbulent friction on a 433

Plates, sandwich, nonsinusoidal buckling modes of 525

Plates, simply supported flat rectangular, under combined longitudinal compression, transverse compression, and shear, critical buckling stresses of 411

Plates, simply supported rectangular, general instability of 109

Plates, uniform cantilevered triangular, the effect of tip removal on the natural vibrations of 621

POHLE, FREDERICK V., AND HENRY OLIVER. Temperature Distribution and Thermal Stresses in a Model of a Supersonic Wing 8

POPE, ALAN. Effect of Cable Model Mounting on Wind-Tunnel Static Pressures at High Speeds* 716

POPE, ALAN. Streamline Curvature Effects for Finite Wings in Wind Tunnels* 279

POPE, ALAN. Wind-Tunnel Model Position for Transonic Testing* 280

PRAGER, WILLIAM, AND ALEXANDER J. WANG. Thermal and Creep Effects in Work-Hardening Elastic-Plastic Solids 343

PRAGER, WILLIAM, AND H. J. WEISS. The Bursting Speed of a Rotating Plastic Disc 196

Propellers

On the Propeller Discontinuity, L. Talbot and A. K. Oppenheim* 61

Remarks on Compressible Flow Actuator Disc Theory, Lawrence Talbot and E. V. Laitone* 638

Remarks on "Subsonic Compressibility Corrections for Propellers and Helicopter Rotors," M. Z. v. Krzywoblocki 214

RADOK, J. R. M. General Instability of Simply Supported Rectangular Plates 109

RANDELS, W. C. On Panel Flutter in Supersonic Flow* 860

READEY, WILLIAM B. Optimum Design of Indeterminate Frames 615

RILEY, JAMES D., AND RICHARD C. ROBERTS. A Guide to the Use of the M.I.T. Cone Tables 336

RIPARBELLI, C. A Paradox in the Theory of Impact* 429

RIVAS, M. A., JR., J. A. F. HILL, AND R. H. SHOULBERG. An Experimental Determination of Flat Plate Recovery Factors for Mach Numbers Between 1.90 and 3.14 763

ROACH, R. E., AND J. M. FRANKLAND. Strength Under Combined Tension and Bending in the Plastic Range 449

ROBERTS, RICHARD C., AND JAMES D. RILEY. A Guide to the Use of the M.I.T. Cone Tables 336

ROBERTSON, J. M., AND DONALD ROSS. An Empirical Method for Calculation of the Growth of a Turbulent Boundary Layer* 355

Rocket-type guided missile with consideration of its structural elasticity, the transfer function of a 454

RODRIGUEZ, A. M., P. A. LAGERSTROM, AND E. W. GRAHAM. Theorems Concerning the Drag Reduction of Wings of Fixed Plan Form 1

ROSS, DONALD, AND J. M. ROBERTSON. An Empirical Method for Calculation of the Growth of a Turbulent Boundary Layer* 355

Rotating Wing Aircraft

Effect of Helicopter Blade Stall on Blade Flapping, K. H. Hohenemser* 861

Rotating Wing Aircraft *(Continued)*
On Down Flapping of a Stalled Helicopter Blade, W. Z. Stepniewski* ... 428
Remarks on "Subsonic Compressibility Corrections for Propellers and Helicopter Rotors," M. Z. v. Krzywoblocki* ... 214

Rutowski, Edward S. Energy Approach to the General Aircraft Performance Problem ... 187

Sacks, Alvin H. On Slender-Body Theory and Apparent Mass* ... 713
Saelman, B. Airplane Stopping Distance* ... 790
Savitsky, Daniel, and David A. Dingee. Some Interference Effects Between Two Flat Surfaces Planing Parallel to Each Other at High Speed* ... 419
Scanlan, R. H. Electrical Resistance Networks for Beam and Column Problems* ... 787
Schaaf, S. A., and F. S. Sherman. Skin Friction in Slip Flow ... 85
Schlichting, Hermann. Problems and Results of Investigations on Cascade Flow ... 163
Schlichting, Hermann, and E. Truckenbrodt. The Flow on a Rotating Body of Revolution in Axial Flow* ... 417
Schmidt, L. E., and C. H. Murphy. Effect of Spin in Aerodynamic Properties of Bodies of Revolution* ... 857
Schnittger, Jan R. Single Degree of Freedom Flutter of Compressor Blades in Separated Flow ... 27
Scholz, N. Secondary Flow Losses in Turbine Cascades* ... 707
Schuh, H. On the Calculation of Temperature Distribution and Thermal Stresses in Parts of Aircraft Structures at Supersonic Speeds* ... 575
Schultze, Ernst. On the Excitation of Pure Natural Modes* ... 566
Schurmann, Ernest E. H., and Theron L. Smith. Methods for Determining the First and Second Derivatives of Experimental Data* ... 420
Sedney, R. On Jones's Criterion for Thin Wings of Minimum Drag* ... 639
Seide, Paul. Comments on "Ripple-Type Buckling of Sandwich Columns"* ... 282
Shells, axially compressed circular cylindrical, postbuckling behavior of ... 329
Shen, S. F. Calculated Amplified Oscillations in the Plane Poiseuille and Blasius Flows* ... 62
Sherman, F. S., and S. A. Schaaf. Skin Friction in Slip Flow ... 85
Shimmy, the story of ... 793
Shoulberg, R. H., J. A. F. Hill, and M. A. Rivas, Jr. An Experimental Determination of Flat Plate Recovery Factors for Mach Numbers Between 1.90 and 3.14 ... 763
Silver, Alfred H. On Heat Transfer in a Compressible Laminar Boundary Layer* ... 352
Smith, John W. Addendum—"Effect of Diffusion Fields on the Laminar Boundary Layer"* ... 640
Smith, John W. Effect of Diffusion Fields on the Laminar Boundary Layer ... 154
Smith, Theron L., and Ernest E. H. Schurmann. Methods for Determining the First and Second Derivatives of Experimental Data* ... 420
Spence, D. A. Prediction of the Characteristics of Two-Dimensional Airfoils ... 577
Spreiter, John R. Errata on Alternative Forms for the Basic Equations of Transonic Flow Theory* ... 360
Spreiter, John R. On Alternative Forms for the Basic Equations of Transonic Flow Theory* ... 70

Stability & Control—
Comment on the Stability Derivatives of a Wing-Body-Vertical Tail Configuration, Arthur E. Bryson, Jr.* ... 59
Controlled Motion with Time Lag in Autopilot, G. M. Andrew* ... 346
Effect of Roll on Dynamic Instability of Symmetric Missiles, C. H. Murphy* ... 643
Effects of Certain Steady Motions on Small-Disturbance Airplane Dynamics, Malcolm J. Abzug ... 749
Extension of Power Spectral Methods of Generalized Harmonic Analysis to Determine Non-Gaussian Probability Functions of Random Input Disturbances and Output Responses of Linear Systems, Bernard Mazelsky ... 145
A Note About the Effects of Product of Inertia on Lateral Stability, C. N. Tsu* ... 496
A Note on Rolling Pull-Out Calculations, George S. Campbell* ... 789
Supersonic Flap Lift Effectiveness for Some General Plan Forms, Richard C. Frost ... 609
The Transfer Function of a Rocket-Type Guided Missile with Consideration of Its Structural Elasticity, Jack L. Beharrell and Hans R. Friedrich ... 454
A Vector Method Approach to the Analysis of the Dynamic Lateral Stability of Aircraft, L. Sternfield ... 251

Stability of a vortex sheet in an inviscid compressible fluid ... 325
Stenning, Alan H. Stall Propagation in Cascades of Airfoils* ... 711
Stepniewski, W. Z. On Down Flapping of a Stalled Helicopter Blade* ... 428
Stern, Marvin. On a Result of Nikolskii and Taganov Concerning Transonic Flow* ... 133
Sternfield, L. A Vector Method Approach to the Analysis of the Dynamic Lateral Stability of Aircraft ... 251
Stokey, W. F., P. N. Gustafson, and C. F. Zorowski. The Effect of Tip Removal on the Natural Vibration of Uniform Cantilevered Triangular Plates ... 621

Stress Analysis & Structures—
Allowable Stresses for Channels and Zees in Bending, B. E. Gatewood and D. W. Breuer* ... 349
Approximate Structural Analysis by the Method of Collocation, Bertram Klein and Hugh L. Cox* ... 719
Buckling Loads for Columns of Variable Cross Section, B. E. Gatewood* ... 287
Buckling Stress of Thin Cylindrical Clamped Shells Subject to Hydrostatic Pressure, P. P. Bijlaard* ... 852
Buckling of Thin Cylindrical Shells Subject to Hydrostatic Pressure, William A. Nash* ... 354
The Bursting Speed of a Rotating Plastic Disc, H. J. Weiss and W. Prager ... 196
Charts for the Calculation of the Critical Compressive Stress for Local Instability of Columns with Hat Sections, Christian J. Van Der Maas ... 399
Comments on "Ripple-Type Buckling of Sandwich Columns," Paul Seide* ... 282
Critical Buckling Stresses of Simply Supported Flat Rectangular Plates Under Combined Longitudinal Compression, Transverse Compression, and Shear, James H. Johnson, Jr. ... 411
Determination of Loads in the Presence of Thermal Stresses, Samuel Levy ... 659
Effect of Local Modifications in Redundant Structures, E. Kosko* ... 206
Electrical Resistance Networks for Beam and Column Problems, R. H. Scanlan* ... 787
Errata—"Stress Analysis of Sheet-Stringer Panels with Cutouts," Harvey G. McComb, Jr.* ... 58

Stress Analysis & Structures *(Continued)*

Erratum—"Analysis of Stiffened Curved Panels Under Shear and Compression," M. A. Melcon and A. F. Ensrud* ... 427
General Instability of Simply Supported Rectangular Plates, J. R. M. Radok ... 109
Life Expectancy of Aircraft Under Thermal Flight Conditions, George Gerard ... 675
Limit Design of Columns, Paul C. Paris ... 43
Nonsinusoidal Buckling Modes of Sandwich Plates, J. N. Goodier and C. S. Hsu ... 525
Note on Photoelastic Study of a Swept-Wing Model, George Gerard and Ralph Papirno* ... 846
On Buckling of a Clamped Rhombic Thin Plate in Shear, M. Hasegawa* ... 720
On the Calculation of Temperature Distribution and Thermal Stresses in Parts of Aircraft Structures at Supersonic Speeds, H. Schuh* ... 575
On the Concept of Stability of Inelastic Systems, D. C. Drucker and E. T. Onat ... 543
On Inelastic Thermal Stresses in Flight Structures, Alfred M. Freudenthal ... 772
Optimum Design of Indeterminate Frames, William B. Readey ... 615
A Paradox in the Theory of Impact, C. Riparbelli* ... 429
Postbuckling Behavior of Axially Compressed Circular Cylindrical Shells, Joseph Kempner ... 329
Rectangular Plates with Stringers and Ribs, J. Irving and N. Mullineux* ... 847
Strength Under Combined Tension and Bending in the Plastic Range, J. M. Frankland and R. E. Roach ... 449
Temperature Distribution and Thermal Stresses in a Model of a Supersonic Wing, Frederick V. Pohle and Henry Oliver ... 8
Thermal and Creep Effects in Work-Hardening Elastic-Plastic Solids, Alexander J. Wang and William Prager ... 343
Thermal Loads on Joints, B. E. Gatewood* ... 645
The Ultimate Strength of Aluminum-Alloy Formed Structural Shapes in Compression, Robert A. Needham ... 217

Struble, R. A., and Z. O. Bleviss. Some Aerodynamic Effects of Streamwise Gaps in Low Aspect Ratio Lifting Surfaces at Supersonic Speed ... 665
Struts and airfoils, secondary flow about ... 588
Supersonic flap lift effectiveness for some general plan forms ... 609
Supersonic flow, survey of friction coefficients, recovery factors, and heat-transfer coefficients for ... 117
Swept wings, sharp leading-edge, at low speeds, an investigation of the aerodynamics of ... 649

Talbot, Lawrence. A Mach 3.106 Two-Dimensional Adjustable Nozzle for Low-Density Flow* ... 708
Talbot, Lawrence, and E. V. Laitone. Remarks on Compressible Flow Actuator Disc Theory* ... 638
Talbot, Lawrence, and A. K. Oppenheim. On the Propeller Discontinuity* ... 61
Tan, H. S. On Motion of Submerged Cylinder* ... 846
Tani, Itiro. On the Approximate Solution of the Laminar Boundary-Layer Equations ... 487
Temperature changes (including viscous heating) upon laminar boundary layers with variable free-stream velocity, effect of large ... 459
Tifford, A. N., and Sheng To Chu. The Compressible Laminar Boundary Layer on a Rotating Body of Revolution* ... 345
Timman, R. Linearized Theory of the Oscillating Airfoil in Compressible Subsonic Flow ... 230
Timman, R., A. I. van de Vooren, and J. H. Greidanus. Aerodynamic Coefficients of an Oscillating Airfoil in Two-Dimensional Subsonic Flow* ... 499
Truckenbrodt, E. Theoretical and Experimental Investigations on Swept and Delta Wings in Incompressible Flow* ... 637
Truckenbrodt, E., and H. Schlichting. The Flow on a Rotating Body of Revolution in Axial Flow* ... 417
Truitt, Robert Wesley. Concluding Remarks on Detached Shock Waves* ... 496
Truitt, Robert Wesley. Pressure Distribution at Mach Number One over a Flat Plate at Angle of Attack* ... 713
Truitt, Robert Wesley. Throat Station Concept in Transonic Flow over Two-Dimensional Wedges* ... 860
Truitt, Robert Wesley, and F. W. Martin. Effects of Afterbody Configuration on the Pressure Distribution over the Nose of Two-Dimensional Wedges* ... 567
Truman, J. C. Some Properties of Intense Sound Waves in Relation to Combustion* ... 69
Tsu, C. N. A Note About the Effects of Product of Inertia on Lateral Stability* ... 496
Tucker, Maurice, John C. Evvard, and Warren C. Burgess Jr. Transition-Point Fluctuations in Supersonic Flow ... 731
Turbulent boundary-layer development along cylindrical surfaces with variable free-stream Mach Number, simplified analysis of ... 695
Turbulent boundary layers in adverse pressure gradients ... 91

Uberoi, M. S. Errata—"Quadruple Velocity Correlations and Pressure Fluctuations in Isotropic Turbulence"* 142
Uchida, Shigeo. Calculation of Compressible Cascade Flow by the Method of Flux Analysis ... 237

Van Der Maas, Christian J. Charts for the Calculation of the Critical Compressive Stress for Local Instability of Columns with Hat Sections ... 399
Van de Vooren, A. I., R. Timman, and J. H. Greidanus. Aerodynamic Coefficients of an Oscillating Airfoil in Two-Dimensional Subsonic Flow* ... 499
Van Dyke, Milton D. Applications of Hypersonic Small-Disturbance Theory ... 179
Van Dyke, Milton D. The Second-Order Compressibility Rule for Airfoils* ... 647
Vibration problems—II, application of Volterra linear integral equations to the numerical solution of ... 383
Voss, H. M. On Use of the Reverse Flow Theorem in the Problem of Aeroelastic Deflections* ... 569
Voss, H. M., G. Zartarian, and J. Walsh. Generalized Aerodynamic Forces on the Delta Wing with Supersonic Leading Edges ... 739

Walsh, J., G. Zartarian, and H. M. Voss. Generalized Aerodynamic Forces on the Delta Wing with Supersonic Leading Edges ... 739
Wang, Alexander J., and William Prager. Thermal and Creep Effects in Work-Hardening Elastic-Plastic Solids ... 343
Wang, Chi-Teh, and Daniel F. De Santo. Errata—"Differentiation of Experimental Data by Means of Higher Order Finite-Difference Formulas"* ... 789
Warren, C. H. E. On "Supersonic Flow About Slender Bodies of Elliptic Cross Section"* ... 57
Warren, W. R., A. Kahane, W. C. Griffith, and A. A. Marino. A Theoretical and Experimental Study of Finite Amplitude Wave Interactions with Channels of Varying Area ... 505

Wave structure, first-order, pseudotransonic similitude and 721
WEISS, H. J., AND W. PRAGER. The Bursting Speed of a Rotating Plastic Disc 196

Wind Tunnels—
Calculation of Compressible Cascade Flow by the Method of Flux Analysis, Shigeo Uchida 237
Design of Total Pressure Probes for Minimum Interference with Measured Flow, J. L. Livesey* 641
Effect of Cable Model Mounting on Wind-Tunnel Static Pressures at High Speeds, Alan Pope* 716
Factors Affecting Transition Reynolds Numbers on Models in Supersonic Wind Tunnels, John Laufer* 497
Streamline Curvature Effects for Finite Wings in Wind Tunnels, Alan Pope* 279
Wind-Tunnel Model Position for Transonic Testing, Alan Pope* 280

Wing, delta, with supersonic leading edges, generalized aerodynamic forces on 739
Wing, supersonic, temperature distribution and thermal stresses in a model of a 8
Wing weights, a method for estimating 363
Wings of fixed plan form, theorems concerning the drag reduction of 1
Wings, oscillating, of finite span and arbitrary plan form, development of charts for downwash coefficients of 809
WOODWARD, FRANK A., AND BERNARD ETKIN. Lift Distribution on Supersonic Wings with Subsonic Leading Edges and Arbitrary Angle of Attack Distribution* 783

YIH, CHIA-SHUN. Temperature Distribution in Laminar Stagnation-Point Flow with Axisymmetry 37

ZARTARIAN, G., J. WALSH, AND H. M. VOSS. Generalized Aerodynamic Forces on the Delta Wing with Supersonic Leading Edges 739
ZIENKIEWICZ, H. K. Load Distributions on Some Twisted and Cambered Delta Wings with Supersonic Leading and Trailing Edges* 421
ZOROWSKI, C. F., P. N. GUSTAFSON, AND W. F. STOKEY. The Effect of Tip Removal on the Natural Vibrations of Uniform Cantilevered Triangular Plates 621

ST. LOUIS PUBLIC LIBRARY
JAN
9
1956

Third U.S. National Congress of Applied Mechanics

Preliminary Announcement

The Third U.S. National Congress of Applied Mechanics will be held at Brown University, Providence, R.I., during June 11–14, 1958. It is hoped that the scheduling of conflicting meetings can be avoided by this early announcement of the date chosen for the Congress. Further announcements concerning the preparation of papers will be made as the Congress draws nearer.

Inquiries regarding the Congress should be addressed to one of the following members of the Organizing Committee at Brown University, Providence 12, R.I.: Prof. D. C. Drucker, Secretary; Prof. E. H. Lee, Treasurer; or Prof. W. Prager, Chairman.

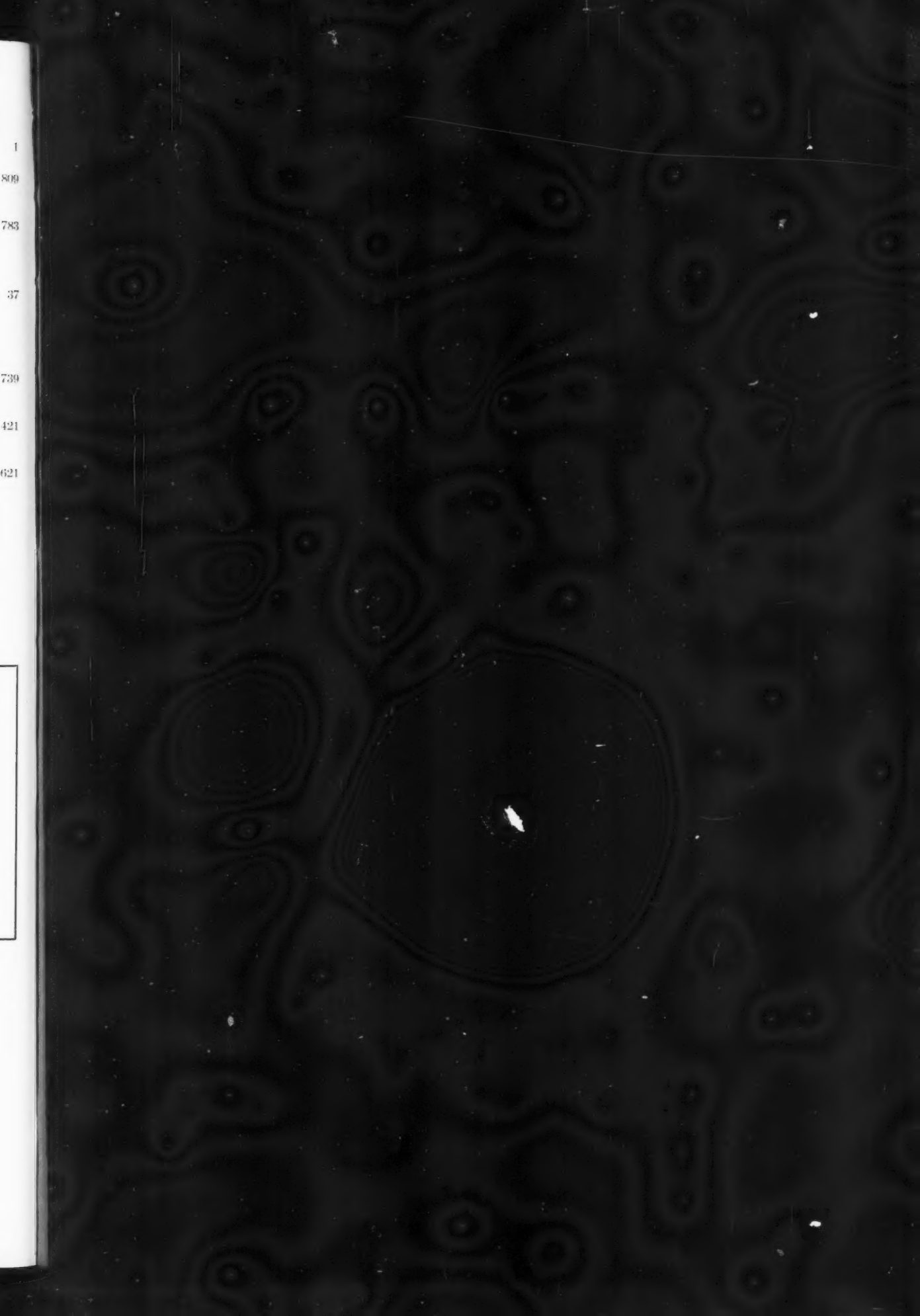

MA
desire
consec
allow
chang
is, the
Typog
wish t
mailin
flat.
protec
Scienc
scripts
Editor
the pa

TIT
and in
use of
quent
makes
partic
service
name
should
which
author

SUM
beginn
as an
major
stitute
referen
cially
papers
the ma
contain
paper.

SUB
at freq
simplif

MA
of littl
practic
tables
materia
that pr

REF
footnot
the end
lows.
Ed., V
zines:
Some
nomeno
Please

SUGGESTIONS *for* CONTRIBUTORS

to the Publications of the

INSTITUTE *of the* AERONAUTICAL SCIENCES

The Institute of the Aeronautical Sciences invites both members and nonmembers from any country to submit papers for publication in the JOURNAL OF THE AERONAUTICAL SCIENCES and the AERONAUTICAL ENGINEERING REVIEW. The Institute, following the practice of other societies, does not pay for contributions.

The following directions for the preparation of papers, if followed by authors, will save correspondence, avoid the return of papers for changes, minimize the work of preparation for the printer, and save the expense due to the charges made for "author's corrections."

MANUSCRIPTS: The original typewritten copy of the paper is desired, double or triple spaced on one side of white paper sheets, consecutively numbered. There should be wide margins to allow for the marking of directions to the printer. Correcting, changing, or adding to papers after they are in type is costly. It is, therefore, imperative that papers submitted be in final form. Typographical errors may be corrected on proofs, but if authors wish to add material, they may do so at their own expense. In mailing, drawings may be rolled but manuscripts should be sent flat. Send by first-class mail (register if you wish for your own protection) to the Editorial Office, Institute of the Aeronautical Sciences, 2 East 64th Street, New York 21, N.Y. All manuscripts will be examined by the Editorial Committee and by the Editor. Authors will be advised as promptly as possible whether the paper is acceptable for publication.

TITLES: The title of the paper should be brief. The name and initials of the author should be written as he prefers. The use of the full name of an author is advocated because of the frequent duplication of initials and surnames which sometimes makes it difficult to establish the identity of the author. This is particularly important for large annual indexing and abstracting services. All titles and degrees or honors are omitted. The name of the organization with which the author is associated should be placed after his name on a separate line. The date on which the paper is received will be inserted by the Editor. The author's title should be indicated in a footnote.

SUMMARIES OR ABSTRACTS: An abstract to be printed at the beginning should accompany each article. It should be adequate as an *index* and as a *summary*. It should contain a statement of major conclusions reached, since summaries in many cases constitute the only source of information used in compiling scientific reference indexes. Abstracts printed in other journals, especially foreign, in most cases, consist of summaries from printed papers. The summary should explain as adequately as possible the major conclusions to a nonspecialist in the subject and should contain from 100 to 300 words, depending on the length of the paper.

SUBHEADINGS: Subheadings should be inserted by the author at frequent intervals. The work of editorial preparation will be simplified by the author's provision of many subheadings.

MATTER USUALLY DELETED: Photographs or illustrations of little technical interest and not showing advances in general practice. Too detailed tabular matter (general results of such tables may be included in the text). Lengthy descriptions of materials or processes or of preliminary experiments or theories that preceded final results; salient features only are of interest.

REFERENCES AND FOOTNOTES: References should appear as footnotes only, numbered consecutively and grouped together at the end of the manuscript. The arrangement should be as follows. For books: [1] Durand, W. F., *Aerodynamic Theory*, 1st Ed., Vol. 1, p. 23; Julius Springer, Berlin, 1934. For magazines: [1] England, C. R., Crawford, A. B., and Mumford, W. W., *Some Results of a Study of Ultra-Short-Wave Transmission Phenomenon*, Proc. I.R.E., Vol. 20, No. 12, pp. 481–482, March, 1933. Please give author, title, edition, volume, page, publisher, and date of publication as indicated. Omission of one required fact causes much extra editorial work and possible inaccuracies.

ILLUSTRATIONS: Illustrations should accompany manuscripts, and each should always be referred to in the text by number. Drawings or graphs should not be larger than 12 × 16 inches, and must be made with jet black India ink on white paper or tracing cloth, the latter being preferred. *Do not use typewriter for lettering.* The smallest lettering on 8 × 10-inch figures should be no less than $1/4$ inch high. Cross-section paper (white with black lines) may be used but it should not have more than 4 lines per inch. If finer ruled paper is used, the major division lines should be drawn in with black ink, omitting the finer divisions. In the case of finely ruled paper, only blue-lined paper can be accepted. *Tracing paper and blueprints* are not acceptable. Lettering and all markings must be large enough to be readable after reduction. Mail rolled or flat; never fold. Drawings that cannot be reproduced (including pencil drawings) will be returned to the author for redrawing thus delaying publication of the paper. Photographs should be distinct and show clear black and white contrasts. They must be on glossy white paper. Avoid round and oval photographs.

CAPTIONS AND LEGENDS: Legends or captions must accompany each drawing or photograph submitted. If written on the drawing or photograph, they should be placed below and well outside the part to be reproduced. Each table should have a caption such as Table 1, Table 2, Table 3, etc. Captions should be complete in themselves so as to make the data intelligible to the reader without reference to the text. A duplicate list of captions for figures should be included as the last page of the manuscript. Use "Fig. 1" (not Figure 1), "Figs. 3 and 4," etc., in both the text and the numbering of illustrations. In the text, "Eq. (1)" or "Eqs. (1) and (2)" is used, not "Equation (1)." In captions and legends, except for "Fig." and "Eq.," and in table headings write all words in full; do not abbreviate.

MATHEMATICAL WORK: Only the simplest formulas should be typewritten; all others should be carefully written in pen and ink, the writing to be large enough so that ample room is provided to mark mathematical matter for the printer. A considerable spacing for marking should be allowed above and below all equations. All complicated equations should be repeated on separate sheets with plenty of space left for marking. The solidus should be used for simple fractions appearing within the text. Make all expressions clear to the typesetter. Greek letters used in formulas should be clearly designated by name on the margin of the manuscript. All symbols should be clearly written and carefully checked. The difference between capital and lower-case letters should be clearly distinguished and care taken to avoid confusion between zero (0) and the letter (o), between the numeral (one) and the letter (ell) and the prime (′), between alpha and a, kappa and k, u and mu, v and nu, n and eta. All subscripts and exponents should be clearly marked, and dots and bars over letters or mathematical expressions should be avoided. Avoid complicated exponents and subscripts. When it is necessary to repeat a complicated expression, it should be represented by some convenient symbol.

NOMENCLATURE AND ABBREVIATIONS: Standard abbreviations should be used, and it should be noted that most abbreviations are lower case such as m.p.h., b.m.e.p., i.h.p., b.hp., hp., . . . etc.

CORPORATE MEMBERS

OF THE

INSTITUTE OF THE AERONAUTICAL SCIENCES

ACADEMY OF AERONAUTICS, INC.
ADAMS RITE MANUFACTURING COMPANY
AEROJET-GENERAL CORPORATION, SUBSIDIARY OF THE GENERAL TIRE & RUBBER COMPANY
AEROLAB DEVELOPMENT COMPANY
AERONCA MANUFACTURING CORPORATION
AEROQUIP CORPORATION
AGAWAM AIRCRAFT PRODUCTS, INC.
AIR ASSOCIATES, INC.
AIRBORNE ACCESSORIES CORPORATION
AIRBORNE INSTRUMENTS LABORATORY, INC.
AIRCRAFT RADIO CORPORATION
ALLIS-CHALMERS MANUFACTURING COMPANY
ALLISON DIVISION, GENERAL MOTORS CORPORATION
ALUMINUM COMPANY OF AMERICA
AMERICAN AIRLINES, INC.
AMERICAN BOSCH ARMA CORPORATION
AMERICAN NON-GRAN BRONZE COMPANY
AMERICAN PHENOLIC CORPORATION
AMERICAN STEEL & WIRE DIVISION, UNITED STATES STEEL CORPORATION
ANDERSON, GREENWOOD & CO.
ARDE ASSOCIATES
ASSOCIATED AVIATION UNDERWRITERS
AVIEN, INC.
  CONTROL LABORATORIES INC.
BAKER STEEL & TUBE COMPANY
BEECH AIRCRAFT CORPORATION
BELL AIRCRAFT CORPORATION
BENDIX AVIATION CORPORATION
  BENDIX INTERNATIONAL DIVISION
  BENDIX PRODUCTS DIVISION
  BENDIX RADIO DIVISION
  ECLIPSE-PIONEER DIVISION
  FRIEZ INSTRUMENT DIVISION
  PACIFIC DIVISION
  SCINTILLA DIVISION
THE BG CORPORATION
BOEING AIRPLANE COMPANY
  SEATTLE DIVISION
  WICHITA DIVISION
BOOZ, ALLEN & HAMILTON
BRANDT MANUFACTURING COMPANY
THE BRISTOL AEROPLANE COMPANY OF CANADA LIMITED
CAL-AERO TECHNICAL INSTITUTE
CALIFORNIA PANEL & VENEER COMPANY
CANADAIR LIMITED
THE CESSNA AIRCRAFT COMPANY
CHANCE VOUGHT AIRCRAFT, INCORPORATED
THE CHASE NATIONAL BANK OF THE CITY OF NEW YORK
CIBA COMPANY, INC.
THE CLEVELAND PNEUMATIC TOOL COMPANY
CLIFFORD MANUFACTURING COMPANY, DIVISION OF STANDARD-THOMPSON CORPORATION
CONSULTANTS & DESIGNERS, INC.
CONTINENTAL MOTORS CORPORATION
CONVAIR DIVISION OF GENERAL DYNAMICS CORPORATION
COOPER PRECISION PRODUCTS
CORNELL AERONAUTICAL LABORATORY, INC.
CORYDON M. JOHNSON CO., INC.
CURTISS-WRIGHT CORPORATION
  ELECTRONICS DIVISION
  MARQUETTE METAL PRODUCTS COMPANY
  PROPELLER DIVISION
  WRIGHT AERONAUTICAL DIVISION
DECKER AVIATION CORPORATION
DOAK AIRCRAFT COMPANY, INC.
DOELCAM CORPORATION
DOUGLAS AIRCRAFT COMPANY, INC.
  EL SEGUNDO DIVISION
  LONG BEACH DIVISION
  SANTA MONICA DIVISION
  TULSA DIVISION
THE DOW CHEMICAL COMPANY, MAGNESIUM DEPARTMENT
DZUS FASTENER COMPANY, INC.
EASTERN AIR LINES, INC.
EATON MANUFACTURING COMPANY
EDO CORPORATION
ELASTIC STOP NUT CORPORATION OF AMERICA
ELECTROL INCORPORATED
ESSO STANDARD OIL COMPANY
ETHYL CORPORATION
FAIRCHILD CAMERA AND INSTRUMENT CORPORATION
  FAIRCHILD AERIAL SURVEYS
FAIRCHILD ENGINE AND AIRPLANE CORPORATION
  AMERICAN HELICOPTER DIVISION
  FAIRCHILD AIRCRAFT DIVISION
  FAIRCHILD ENGINE DIVISION
  FAIRCHILD GUIDED MISSILES DIVISION
  STRATOS DIVISION
FEDERAL TELECOMMUNICATION LABORATORIES, DIVISION OF INTERNATIONAL TELEPHONE AND TELEGRAPH CORPORATION
FIRESTONE TIRE & RUBBER COMPANY
FLETCHER AVIATION CORPORATION
FLIGHT REFUELING INC.
THE GARRETT CORPORATION
  AIRESEARCH MANUFACTURING CO.
GENERAL ELECTRIC COMPANY
  AIRCRAFT GAS TURBINE DIVISION
  AVIATION DIVISIONS
G. M. GIANNINI & CO., INC.
THE B. F. GOODRICH COMPANY
THE GOODYEAR TIRE & RUBBER COMPANY, INC.
GRUMMAN AIRCRAFT ENGINEERING CORPORATION
HARVEY MACHINE CO., INC.
ROBERT HEWITT ASSOCIATES
INDUSTRIAL SOUND CONTROL, INC.
INSURANCE COMPANY OF NORTH AMERICA COMPANIES
THE INTERNATIONAL NICKEL COMPANY, INC.
JACK & HEINTZ, INC.
JOHNS-MANVILLE SALES CORPORATION
EARLE M. JORGENSEN COMPANY
KEARFOTT COMPANY, INC., DIVISION OF GENERAL PRECISION EQUIPMENT CORPORATION
WALTER KIDDE & COMPANY, INC.
KOLLSMAN INSTRUMENT CORPORATION, SUBSIDIARY OF STANDARD COIL PRODUCTS CO., INC.
LAVELLE AIRCRAFT CORPORATION
LEAR, INCORPORATED
THE LIQUIDOMETER CORPORATION
LOCKHEED AIRCRAFT CORPORATION
  CALIFORNIA DIVISION
  GEORGIA DIVISION
  MISSILE SYSTEMS DIVISION
LOEWY CONSTRUCTION COMPANY, INC., SUBSIDIARY OF HYDROPRESS, INC.
LONGINES-WITTNAUER WATCH COMPANY, INC.
LONGREN AIRCRAFT COMPANY
MARQUARDT AIRCRAFT COMPANY
THE GLENN L. MARTIN COMPANY
McDONNELL AIRCRAFT CORPORATION
MELETRON CORPORATION
MINNEAPOLIS-HONEYWELL REGULATOR COMPANY AERONAUTICAL DIVISION
NATIONAL CREDIT OFFICE, INC.
NORTH AMERICAN AVIATION, INC.
NORTHROP AIRCRAFT, INC.
NUCLEAR DEVELOPMENT ASSOCIATES, INC.
PAN AMERICAN WORLD AIRWAYS, INC.
THE PARKER APPLIANCE COMPANY
PESCO PRODUCTS DIVISION, BORG-WARNER CORPORATION
PHILLIPS PETROLEUM COMPANY
PIASECKI HELICOPTER CORPORATION
THE PURE OIL COMPANY
RADIOPLANE COMPANY
J. B. REA COMPANY, INC.
REACTION MOTORS, INC.
REPUBLIC AVIATION CORPORATION
E. V. ROBERTS AND ASSOCIATES
A. V. ROE CANADA LIMITED
JOHN A. ROEBLING'S SONS CORPORATION
ROHR AIRCRAFT CORPORATION
PAUL ROSENBERG ASSOCIATES
RYAN AERONAUTICAL COMPANY
SCHRILLO AERO TOOL ENGINEERING COMPANY
SEABOARD & WESTERN AIRLINES, INC.
SHELL OIL COMPANY
SIMMONDS AEROCESSORIES, INC.
SOCONY-VACUUM OIL COMPANY, INC.
SOLAR AIRCRAFT COMPANY
R. DIXON SPEAS
SPERRY GYROSCOPE COMPANY DIVISION OF THE SPERRY CORPORATION
STANDARD OIL COMPANY OF CALIFORNIA
STANDARD OIL COMPANY (INDIANA)
STANLEY AVIATION CORPORATION
THE STEEL PRODUCTS ENGINEERING COMPANY
STROUKOFF AIRCRAFT CORPORATION
STURGESS, INC.
SUMMERS GYROSCOPE COMPANY
THE H. I. THOMPSON FIBER GLASS COMPANY
THOMPSON PRODUCTS, INC.
TOOLKO ENGINEERING COMPANY
TRANS WORLD AIRLINES, INC.
TURBO PRODUCTS, INC.
UNION CARBIDE AND CARBON CORPORATION
  BAKELITE COMPANY
  ELECTRO METALLURGICAL COMPANY
  HAYNES STELLITE COMPANY
  LINDE AIR PRODUCTS COMPANY
  NATIONAL CARBON COMPANY
UNITED AIR LINES, INC.
UNITED AIRCRAFT CORPORATION
  HAMILTON STANDARD DIVISION
  PRATT & WHITNEY AIRCRAFT DIVISION
  SIKORSKY AIRCRAFT DIVISION
  UNITED AIRCRAFT EXPORT CORPORATION
  UNITED AIRCRAFT SERVICE CORPORATION
UNITED STATES AVIATION UNDERWRITERS, INC.
UNITED STATES RUBBER COMPANY
VARD, INC.
VICKERS INCORPORATED, DIVISION OF THE SPERRY CORPORATION
WESTERN GEAR WORKS
WESTINGHOUSE ELECTRIC CORPORATION
  AIR ARM DIVISION
  AVIATION GAS TURBINE DIVISION
  INDUSTRIAL ELECTRONICS DIVISION
  SMALL MOTOR DIVISION, AIRCRAFT DEPARTMENT
WESTON ELECTRICAL INSTRUMENT CORPORATION
WYMAN-GORDON COMPANY
YOUNG RADIATOR COMPANY